Hydraulic Roughness of Armoured Gravel Beds: the Role of Grain Protrusion

by

VIOLETA MARTIN

B.Sc., Civil Engineering, University of Novi Sad, Yugoslavia, 1989
M.A.Sc., Civil Engineering, University of British Columbia, 1996

A THESIS SUBMITTED IN PARTIAL FULFILMENT OF THE REQUIREMENTS FOR THE DEGREE OF

DOCTOR OF PHILOSOPHY

IN THE FACULTY OF GRADUATE STUDIES

(DEPARTMENT OF CIVIL ENGINEERING)

We accept this thesis as conforming
to the required standard

UNIVERSITY OF BRITISH COLUMBIA

January, 2003

In presenting this thesis in partial fulfilment of the requirements for an advanced degree at the University of British Columbia, I agree that the Library shall make it freely available for reference and study. I further agree that permission for extensive copying of this thesis for scholarly purposes may be granted by the head of my department or by his or her representatives. It is understood that copying or publication of this thesis for financial gain shall not be allowed without my written permission.

Department of Civil Engineering

The University of British Columbia
Vancouver, Canada

Date Feb. 27, 2003.

ABSTRACT

A new theoretical analysis was developed that accounts for variable grain protrusion within self-formed, stable gravel armour layers. A key feature of the analysis is accounting for the variation in drag coefficient, drag force and critical dimensionless shear stress with grain protrusion above the virtual bed, which is defined here as the elevation at which the extrapolated logarithmic velocity profile becomes equal to zero. The central hypothesis is that self-formed stable armour layers develop through adjustment of grain protrusion such that all grains are at the threshold of motion, at least in a statistical sense. This represents the limiting case of equal mobility. Testing of the analysis using published flume data shows good agreement between observed and predicted roughness height, mean velocity and flow depth.

Experimental work on simulating gravel-bed armouring was carried out to obtain more data and test the assumptions underlying the numerical model. Velocity profiles across and along the flume were measured with an acoustic Doppler velocimeter (ADV). To determine the reliability of ADV measurements in turbulent flows over rough boundaries, a thorough data analysis was undertaken. Shear stresses obtained from the force balance (ρgYS_f), from the velocity profiles, or from the Reynolds stress measurements were compared and showed a reasonable agreement. A unique study on individual grain protrusion was carried out, in which the armoured beds were scanned, digital elevation models (DEM) were developed, and then combined with photographs to obtain the information on protrusions. These measured protrusions are in good agreement with those calculated in the numerical model.

TABLE OF CONTENTS

LIST OF TABLES

LIST OF FIGURES

LIST OF SYMBOLS

A_D	projected grain area normal to the flow above the virtual bed	[m^2]
B	constant of integration	
C	the Chézy coefficient	
C_D	drag coefficient	
C_D^*	grain protrusion drag coefficient	
D	particle diameter	[m]
D_{gi}	geometric mean of the grain size interval	[m]
D_G	geometric mean for the sediment mixture	[m]
D_n	particle size for which n percent of the particles are finer by weight	[m]
f	the Darcy-Weisbach resistance coefficient	
F_D	drag force	[N]
F_i	fraction of grains with diameter D_i present on the bed surface	
Fr	the Froude number	
g	gravitational acceleration	[m/s^2]
H_i	individual grain protrusion height	[m]
k_s	the Nikuradse's equivalent sand roughness, in this thesis referred to as the hydraulic roughness coefficient	[m]
n	the Manning's resistance coefficient	
N_i	random noise in the ADV signal	
q	unit discharge	[m^2/s]
Q	total discharge	[m^3/s]
r	grain radius ($r = 0.5D$)	[m]
R	hydraulic radius	[m]
Re	the Reynolds number ($Re = UY/\nu$)	
S_0	bed slope	
S_f	friction, or energy slope	
S_i	the coherent part of the ADV signal	
S_i'	the ADV return signal from a single pulse	
Sw	water surface slope	
S_s	specific gravity for sediment ($S_s = \rho_s/\rho$)	

u'	longitudinal velocity fluctuation	[m/s]
u_r	reference velocity for calculating the drag force	[m/s]
u_y	flow velocity at elevation y above the bed	[m/s]
u^*	shear velocity	[m/s]
U	mean flow velocity	[m/s]
y	depth	[m]
Y	total depth of flow	[m]
y_r	position of the drag force acting on a grain	[m]
z_i	bed elevation above a datum at cross-section i	[m]
Z_0	coefficient describing the hydraulic roughness of the boundary, height above the datum at which $u = 0$	[m]
w'	vertical velocity fluctuation	[m]
ϕ	particle friction angle	
κ	the von Karman's constant equal to 0.4 for clear water flow	
ν	kinematic viscosity for water	[m^2/s]
θ	is the angle measured from the horizontal plane passing through the grain centre	
ρ	water density	[kg/m^3]
ρ_s	sediment density	[kg/m^3]
σ_G	geometric standard deviation for the sediment mixture	
σ_z	standard deviation of bed surface elevations	
τ_0	average bed shear stress	[N/m^2]
τ_{ci}^*	critical non-dimensional shear stress for the protruding grain	
τ_i'	grain shear stress for grain size i	[N/m^2]
τ'	total grain shear stress ($\tau' = \sum_{i=1}^{n} F_i \tau_i'$)	[N/m^2]

ACKNOWLEDGEMENTS

I would like to express gratitude to my supervisors, Dr. Michael Quick and Dr. Robert Millar for their invaluable assistance, thoughtful suggestions and constructive criticism. Their willingness to contribute their time and knowledge improved the quality of this work and are greatly appreciated. I would also like to thank Mr. Graeme Liebel and Mr. Scott Jackson for their very fine craftsmanship and technical assistance with setting-up the experimental apparatus. My gratitude extends to all the other people in our workshop, who showed interest for my experiments and were always willing to help with last minute modifications. Many thanks to my committee members Dr. Michael Church, Dr. Greg Lawrence, and Dr. Noboru Yonemitsu for their advice throughout the course of this study, and for their reviews of this manuscript.

Special thanks to my colleagues Tim Fisher, Colin Rennie, Daniel Walker and Michael MacLatchy for their friendship, moral and intellectual support, and for providing a hand in the lab. Finally, many thanks to my husband Milan, to my sons Bojan and Boris, my parents and my sister for bearing with me throughout my endeavours, for their understanding, and for making me laugh and continue with my research when it was difficult to see the light at the end of the tunnel.

I spent exceptional years at the University of British Columbia surrounded by great people, learning many new and exciting things, which will enrich the rest of my life. Many thanks to everyone else who I did not mention, but were a big part of this study in some other way.

CHAPTER 1

INTRODUCTION

1.1. Purpose of Present Work

Two parameters of central importance in fluvial hydraulics are the hydraulic roughness and the critical shear stress. These two quantities, or their equivalents, form the basis of most quantitative studies dealing with flow resistance, hydraulic modelling, sediment transport or river morphology. Even the most sophisticated 2-D or 3-D hydrodynamic models require estimates of k_s or Manning's n in order to compute flow characteristics in rivers, particularly in steeper gravel-bed rivers where boundary friction dominates.

Hydraulic roughness is commonly expressed as equivalent sand roughness (k_s), or roughness length (z_0). Critical shear stress is typically formulated in terms of the non-dimensional (or Shields) shear stress, $\tau^* = YS_f / ((S_s-1)D)$, where Y is the depth of flow, S_f is the friction slope, S_s is the specific gravity of sediment particles, and D is some characteristic grain diameter.

In gravel-bed rivers, it is common to estimate hydraulic roughness and critical non-dimensional shear stress using simple empirical relations. Typically, k_s is assumed to be equal to some multiplying factor times a characteristic grain diameter such as $6.8D_{50}$ or $3.5D_{84}$ (Bray, 1980) (where D_{50} is the median bed surface grain diameter and D_{84} is the particle size for which 84% of the particles are finer by weight). In our experiments, k_s accounts for differences in sediment composition, protrusion height and flow parameters, and

in our analysis, the value of k_s will not be assumed, but will be calculated. Similarly, the value of the critical non-dimensional shear stress based on D_{50} (τ_{c50}^*) is usually considered to fall within the range 0.03 to 0.06 with an average value of about 0.045 (Meyer-Peter and Müller, 1948; Gessler, 1971; Miller et al., 1977; Buffington and Montgomery, 1997).

This simplistic approach does not account for, nor explain the wide variation in the observed values of k_s and τ_{c50}^*. Millar (1999) analysed gravel river data compiled from several sources and showed that for bank-full flow, rather than being a constant the ratio of k_s/D_{50} ranged over two orders of magnitude from 0.4 to 55, with no strong central tendency towards any median or mean value. However, in the above analysis k_s values could have contained not only grain roughness, but also form roughness. Variation in the value of τ_{c50}^* outside of the usual range 0.03 to 0.06 is widely acknowledged (see review by Buffington and Montgomery, 1997). Church (1978) and Church et al. (1998) have reported values of τ_{c50}^* up to 0.1.

Despite the fundamental importance of the parameters k_s and τ_{c50}^*, the ability to predict these values in gravel bed rivers is limited. Our knowledge remains largely empirical, although there have been several attempts at deriving theoretical expressions for both hydraulic roughness (Wiberg and Smith, 1991) and critical shear stress (Wiberg and Smith, 1987; Kirchner et al., 1990). None of these studies addressed the relation between hydraulic roughness and bed stability.

In self-formed gravel-bed rivers, Church et al. (1998) recognized two fundamental processes that describe the bed development: (1) textural coarsening or armouring, and (2) development of microbedforms. Textural coarsening occurs because of selective transport and deposition, and results in increased exposure and mobility of the larger, less mobile grains, together with a concomitant reduction in exposure of the smaller, inherently more mobile grains. The terms stable or static armour have been used to describe a special case of gravel-beds that develop in the absence of bed material supply. These beds could typically be found in rivers downstream of a dam, a lake outlet, a sediment trap, or a sediment excavation site.

The term microbedforms is used to describe organized bed structures that include pebble clusters, stone lines, transverse ribs and reticulate stone cells. Microbedforms appear to develop best in widely graded gravel sediments under conditions of low or zero upstream sediment supply (Church et al., 1998). The presence of microbedforms may exert a significant effect on bed stability and hydraulic roughness and account for the large observed range in τ_{c50}^* and k_s values.

This thesis concentrates on the development of static armour layers through textural coarsening. The aim is to relate the hydraulic roughness of the channel flow to the armour layer coarsening, characterised by grain protrusion and roughness coefficient.

1.2. Approach to Analysis and Scope of the Present Work

In this work an analytical model is developed that considers the role of grain protrusion and its effect on both hydraulic roughness and bed stability. The analysis is limited to self-formed armoured gravel beds that develop in clear water flow conditions in the absence of appreciable sediment supply. Therefore, given a certain sediment size distribution, the primary effort of this study is directed toward the issue of how the grain protrusion and hydraulic roughness can adjust, and how the grain protrusion modifies the stability of the bed.

In addition to numerical modelling, eight experiments on gravel-bed channel armouring were carried out in a laboratory setting. The physical modelling was designed to gain better understanding of the processes involved, to attain more data, and to test the underlying assumptions for the numerical model. Special attention was paid to sediment sampling, so that the results for the initial and for the armoured bed samples in this study, and in other reported studies could be compared. ADV measurements were made to establish the nature of the velocity distribution for the channel forming flows and the corresponding relative roughness. Protrusion heights were measured using a laser displacement meter and these data were used to develop digital elevation models (DEMs).

The shear velocities obtained from velocity profiles, from Reynolds stress measurements, or from the depth/slope calculations agreed reasonably well, and indicated that a limiting shear stress exists for a given sediment mixture. Beyond this shear stress, all grain-sizes are set in motion and the bed cannot armour through degradation and minor slope reduction. Rather, a

considerable slope reduction first takes place, until the flow force can be reduced to a value that allows the least mobile particles to become stable.

The numerical model was tested using data from experiments of Proffitt (1980), Saad (1986), and from this research. Reasonable agreement was obtained for the grain protrusion (H), roughness parameter (k_s), depth of flow (Y), and mean velocity (U) for values measured experimentally and calculated using the proposed numerical model.

A review of common concepts for determining the roughness coefficient and the critical shear stress is given in Chapter 2. The analytical approach and the Grain Protrusion Model development are presented in Chapter 3. The model concept and some of the initial results were presented at two conferences (Martin et al., 2000; Martin et al., 2001). The experimental considerations and a detailed data analysis can be found in Chapter 4, parts of which were also presented at a conference (Martin et al., 2002). In Chapter 5, the results obtained through experimentation, comparison with other studies, and the verification of the numerical model are presented. Finally, discussions on results, recommendations and conclusions are given in Chapter 6.

CHAPTER 2

LITERATURE REVIEW

2.1. Armouring Processes

The surface material of a gravel bed stream is typically much coarser than the subsurface material or the bed load material. The surface layer is usually referred to as pavement or mobile armour and is transported downstream within a period of several years. The coarse surface layer is present even when most available sizes are transported (Andrews and Parker, 1987). The development of a coarse mobile armour layer in gravel-bed channels has been explained in terms of self-adjustment of the bed surface to produce a condition of equal mobility of all grain sizes (Parker et al, 1982). Coarsening develops as a consequence of selective transport and deposition, and results in a condition where the transported bed material has a grain size distribution similar to, but slightly finer then the sub-armour sediment.

In alluvial channels with heterogeneous sediment mixtures, if there is no input of sediment from upstream, through a process of selective erosion a so-called static, stable, or degradational armour layer will develop (Sutherland, 1987). Parker and Sutherland (1990) have argued that stable armour represents the limiting state of mobile armour layer development, in which the bed adjusts to vanishing sediment transport. During the late-stage parallel degradation, Parker and Sutherland (1990) demonstrated that a condition of equal mobility develops, in that the size distribution of the transported bed material becomes

approximately equal to that of the sub-armour. Stable or static armour layers develop downstream of a lake, an artificial reservoir, or some other sediment trap, or in irrigation canals. These conditions are relatively easy to reproduce in laboratory flumes (Gessler, 1965; Proffittt, 1980; Chin, 1985; Saad, 1986; Lamberti and Paris, 1992; Gomez, 1993; Church et al., 1998).

Structural modification of the bed surface and formation of pebble clusters, stone lines and stable reticulate structures, or "stone cells", improve the stability of the armour layer. Their formation is the result of smaller stones (though generally larger than D_{84}) accumulating against randomly positioned, larger, structure-forming keystones. The increased bed stability can be interpreted as a direct result of microbedforms taking up a larger proportion of the shear stress, which acts to reduce the background stress applied on the remaining bed surface. The microbedforms have been observed to develop the best under conditions of low or zero upstream sediment supply in both, natural cobble-gravel streambeds, and in flume experiments (Church et al., 1998).

The armour layer will break up and change only if the historical maximum sustained flow is exceeded. After such an event and depending on what is transported from upstream, the surface layer could coarsen further. The armour layer is usually one grain diameter thick and all sediment sizes contained in the subsurface are also usually present in the surface layer, but in different proportions, so that the median diameter of the surface material is typically 2 to 6 times larger than the median diameter of the subsurface material (Andrews and Parker, 1987). The smaller grains contained in an armour layer are hidden and sheltered by larger grains.

The threshold stress for these smaller particles is often exceeded, but because of the complex distribution of applied shear stresses and because of sheltering effects, they remain at rest. Larger grains can protrude higher into the flow and yet still remain stable, because of their larger mass, even though they are exposed to higher applied shear stresses. Gomez (1993) suggested that up to 95% of the total shear stress could be taken by the coarsest 5% of the particles that protrude highest into the flow. Gessler (1990) argued that large grains "are redistributed on the bed surface during the armouring process such that each grain has a maximum exposure to the flow, creating as large a drag as possible."

Depending on the bed material supply and on the flow competence to transport the sediment, the armour layer can form as static or mobile. A hypothetical diagram is proposed to describe the type of armour bed that can form under different bed material supply conditions (Fig. 2.1.). For example, if the amount of bed material entering a river reach is equal to the amount of bed material leaving that reach during some period of time, the transport rate is referred to as an equilibrium transport (Parker, 1990). The bed that would form under these conditions is called a mobile armoured bed. If the transport of bed material was greater or lesser than the equilibrium transport, the bed would aggrade or degrade, respectively. In a case of zero bed material supply, which corresponds to the x-axis in Fig. 2.1, a static armour layer would develop (Sutherland, 1987). Between the static and mobile armour layer zones, a zone of supply limited armour layers exists. These armour layers are formed under conditions of partial sediment transport which results from differences in grain mobility (Wilcock and McArdell, 1993). For all the different types of armour layers that can develop, the armour layer becomes coarser, and more complex with the formation of micro-bed

structures as the imposed shear stress increases, until it reaches a critical or maximum shear stress beyond which no armour can form, as all grains are in motion (Chin et al., 1994).

The above simple approach is further complicated when the flow competence (Wilcock, 1992) is taken into account. For example, the river may be capable of transporting the supply, which is finer than the bed surface. Or it may transport part of the surface material leaving the bed coarser, or deposit part of the sediment that it cannot transport through the reach, or exchange material up to some practical or competence size limit. The imbalance between sediment supply and flow capability to transport the sediment causes size-selective deposition or erosion, and has effects on the armour layer development and on the degree of textural coarsening that occurs in gravel bed rivers. The issue is somewhat simpler in a case of no sediment supply and a static armour layer development, which is examined in this study.

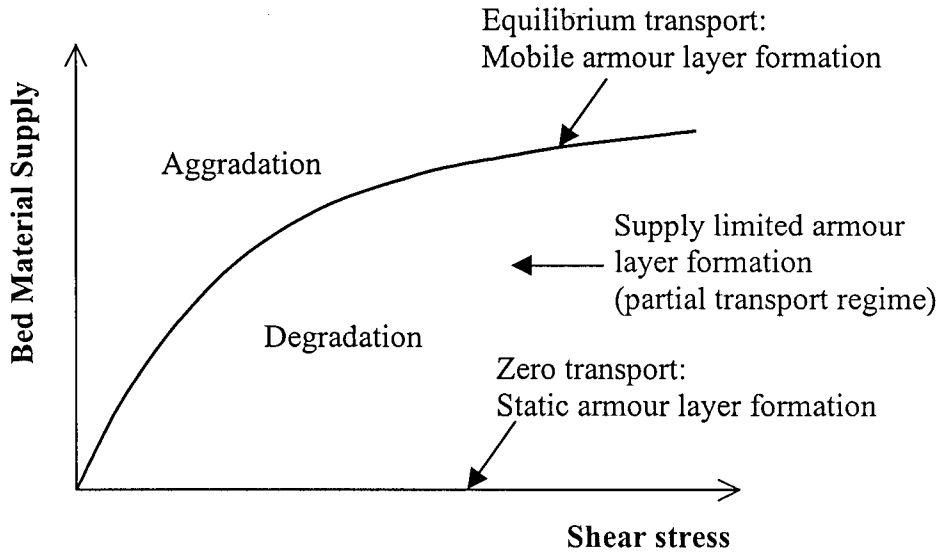

Figure 2.1. *Type of armour layer development depending on bed material supply.*

2.2. Velocity Profile, Virtual Bed Position and Representative Roughness Height

Velocity profile is related to the shear stress distribution in the channel, which in turn is one of the prime factors determining armouring processes and sediment transport. Therefore, the shape of the velocity profile is a very important factor in river hydraulics, but there is still much debate on the topic. In 1926, Prandtl developed the concept of mixing length and laid the foundations for the theory on turbulence. He established for pipe flow that the velocity profile in a turbulent flow regime is logarithmic, which was later modified by his student, Nikuradse (1933), to incorporate the effects of the wall roughness. The logarithmic velocity profile was also confirmed for open channel flow. Gartshore and de Croos (1979), Kironoto and Graf (1994), Gomez (1994), and many others conducted experiments in flumes for flows over rough boundaries, while Smart (1999) conducted measurements in gravel bed rivers, and they all reported logarithmic, or approximately logarithmic velocity profiles extending over much or all of the flow depth. However, Jarrett (1989) reported non-logarithmic velocity profiles measured in steep mountain rivers in Colorado. Simons and Senturk (1992) proposed that physical processes associated with flow resistance are modified when the relative depth (Y/k_s) falls below 4 (i.e. large relative roughness). It is considered that the logarithmic velocity law breaks down at this point, while for intermediate and low relative roughness it may hold. Smart et al. (2002a) suggested that for large relative roughness different power laws may be used to describe the flow resistance, but that the power changes as the roughness increases. Large relative roughness conditions were not investigated in this thesis.

Nikuradse's (1933) logarithmic law-of-the-wall velocity distribution for a fully rough turbulent flow in pipes is described with the following equation:

$$\frac{u_y}{u^*} = \frac{1}{\kappa}\ln\left(\frac{y}{k_s}\right) + B \qquad (2\text{-}1)$$

where u_y is the flow velocity at elevation y above the bed, $u^* = \sqrt{\tau_0 / \rho}$ is the shear velocity, κ is the von Karman constant and is equal to 0.4 for clear water, k_s is the equivalent sand roughness, and B is the constant of integration that is a function of Reynolds number, and is equal to 8.5 for a fully rough turbulent flow. After substituting the values for κ and B, equation 2-1 becomes:

$$\frac{u_y}{u^*} = 2.5\ln\left(\frac{y}{k_s}\right) + 8.5 = 2.5\ln\left(\frac{30y}{k_s}\right) = 5.75\log\left(\frac{30y}{k_s}\right) \qquad (2\text{-}2)$$

which implies that $u_y=0$ for $y=k_s/30$ or, that the velocity becomes zero at a distance $k_s/30$ above the bed.

The mean flow velocity, U, can be determined using the depth-integrated form of the law-of-the-wall:

$$\frac{U}{u^*} = \frac{1}{\kappa}\ln\left(\frac{Y}{k_s}\right) + \overline{B}, \qquad (2\text{-}3)$$

where Y is the total depth of flow, and $\overline{B}$ is equal to 6.0 for a fully rough turbulent flow. After substitution of κ and $\overline{B}$ into 2-3, the following alternate equations are obtained:

$$\frac{U}{u^*} = 2.5\ln\left(\frac{Y}{k_s}\right) + 6.0 = 2.5\ln\left(\frac{11Y}{k_s}\right) = 5.75\log\left(\frac{11Y}{k_s}\right), \qquad (2\text{-}4)$$

Keulegan (1938) extended the log law for a rectangular or a trapezoidal channel of finite width, and for these cases, the constant of integration, $\overline{B}$, in equation 2-3 becomes equal to 6.25, and thus equation 2-4 becomes:

$$\frac{U}{u^*} = 2.5\ln\left(\frac{R}{k_s}\right) + 6.25 = 2.5\ln\left(\frac{12.2R}{k_s}\right) = 5.75\log\left(\frac{12.2R}{k_s}\right), \qquad (2\text{-}5)$$

where R is the hydraulic radius. In this equation, it is assumed that the roughnesses of the bed and the walls are the same.

Another equation similar to equation 2-1, which is commonly used for determining the flow velocity, u_z, at height z above the bed uses coefficient Z_0 to describe the hydraulic roughness of the boundary:

$$\frac{u_z}{u^*} = \frac{1}{\kappa}\ln\left(\frac{z}{Z_0}\right) \qquad (2\text{-}6)$$

In this equation, Z_0 is the height above the datum at which $u = 0$, and therefore $Z_0 = k_s/30$.

The other most commonly used equations for determining the open channel mean flow velocity are the Chezy (2-7), the Darcy-Weisbach (2-8) and the Manning (2-10) formulae.

$$U = C\sqrt{RS_f} \qquad \text{(Chezy, 1775)} \qquad (2\text{-}7)$$

$$\frac{U}{u^*} = \sqrt{\frac{8}{f}} \qquad \text{(Darcy-Weisbach)} \qquad (2\text{-}8)$$

where: C is the Chézy coefficient dependent on the Reynolds number and boundary roughness, but its behaviour was never completely investigated (Henderson, 1966); S_f is the friction, or energy slope; and f is the Darcy-Weisbach resistance coefficient. Systematic

observations made on rivers by the mid nineteenth century revealed that the data could be fitted with an equation in which C varies with $R^{1/6}$ (Gauckler in 1868 and Hagen in 1881). This finding was incorrectly attributed to R. Manning (Henderson, 1966, pp. 96) and equation 2-10 became the very well known and widely used Manning's formula, where n is the Manning's resistance coefficient.

$$C = \frac{R^{1/6}}{n} \qquad \text{or} \qquad (2\text{-}9)$$

$$U = \frac{1}{n} R^{2/3} S_f^{1/2} \qquad \text{(Manning, 1890)} \qquad (2\text{-}10)$$

The most important difference between coefficients k_s and Z_0, and coefficients C, f and n, is that k_s and Z_0 refer to grain roughness and therefore represent the grain resistance, while C, f and n represent the total flow resistance. If the form drag in the channel is negligible and most of the resistance is due to the grain roughness, the two groups of coefficients could be considered similar. A flume study on gravel bed armouring could be considered to fall into this category.

Virtual bed position - For gravel bed rivers the problem arises of how to define the effective position of the riverbed, and how to determine the representative roughness. If the bed material occupies a large fraction of the flow depth, or the bed is mobile, or bed forms are present, the above uncertainties become even more complicated.

The effective location of a rough boundary is difficult to define. Even for uniform spheres, the location depends on the spacing between the roughness elements. Einstein and El Samni

(1949) found zero velocities at *0.2D* below the tops of closely packed hemispheres (where D is the diameter of uniform particles), while Cheng and Clyde (1972) obtained a value of *0.15D* for closely packed spheres placed on top of hemispheres. Chin (1985) summarized the results obtained by several authors for different types of roughness elements, and found that the virtual bed position varied between *0.15D* and *0.35D* below the physical surface, but that values of *0.2D* were most commonly reported. However, if the distance between the roughness elements increases, the bed position is found to be lower. From Chepil's work (1959), the effective bed was defined at approximately *0.45D* below the tops of hemispheres placed three diameters apart. He found that the position of the theoretical bed remained constant for a given surface at all velocities, but varied with the height, shape and arrangement of roughness elements.

Representative roughness height - In gravel-bed rivers, which are made up of mixtures of sediment sizes, grain resistance and the definition of roughness height remain poorly understood. There is much uncertainty on how to define the equivalent or Nikuradse's grain roughness, k_s, which is often assumed to be equal to the median grain diameter, D_{50}. This assumption works reasonably well in more closely graded sand bed rivers, where the size D_{50} could be considered to be a good representative of the grain roughness. However, the issue is further complicated in gravel bed rivers which typically have wider grain size distributions, and contain sediment sizes ranging from sand to gravel, or cobble. For such beds, the mean grain size is often too small to be a good representative of the grain roughness, and there is a range of values proposed for k_s. Various researchers expressed the equivalent roughness height, k_s, as some factor multiplied by the characteristic particle size, D_n, (particle size for

which n percent of the particles are finer by weight), but this proposed roughness height could even exceed the maximum particle size present on the bed (Kamphuis, 1974; Bray,1980; Gessler, 1990). Van Rijn (1982) summarized the available literature and found a range of values from $k_s=D_{90}$ to $k_s=10D_{90}$. It is generally assumed for gravel bed rivers that k_s is equal to $6.8D_{50}$ or $3.5D_{84}$ (after Hey, 1979; Bray, 1980). However, Gomez (1993) reported values as high as $k_s=14.5D_{90}$ from his experiments on self-formed stable armour gravel beds, and these values exceeded even the total depth of flow (this study is further analysed in Chapter 5: there appears to be some error in the original data and the actual maximum k_s value is approximately equal to $3\ D_{90}$).

Figure 2.2.a illustrates the roughness estimate of $k_s = 6.8D_{50}$ vs. the observed k_s values for two sets of experiments on stable armoured gravel beds performed by Proffitt (1980) and Saad (1986), where the observed values of k_s were back-calculated from the measured hydraulic parameters. It was reasonable to expect that the resistance was mainly due to grain roughness and that other forms of roughness were not present in the flume, but even for these conditions of stable armour beds developed in a laboratory, the above estimate of k_s was not very successful. Figure 2.2.a indicates that the hydraulic roughness based on $k_s = 6.8D_{50}$ significantly overestimates the resistance to flow compared to the measured values, while the mean flow velocities are underestimated (Fig. 2.2.b). The predicted mean velocities were calculated using equation 2-5 and assuming $k_s = 6.8D_{50}$.

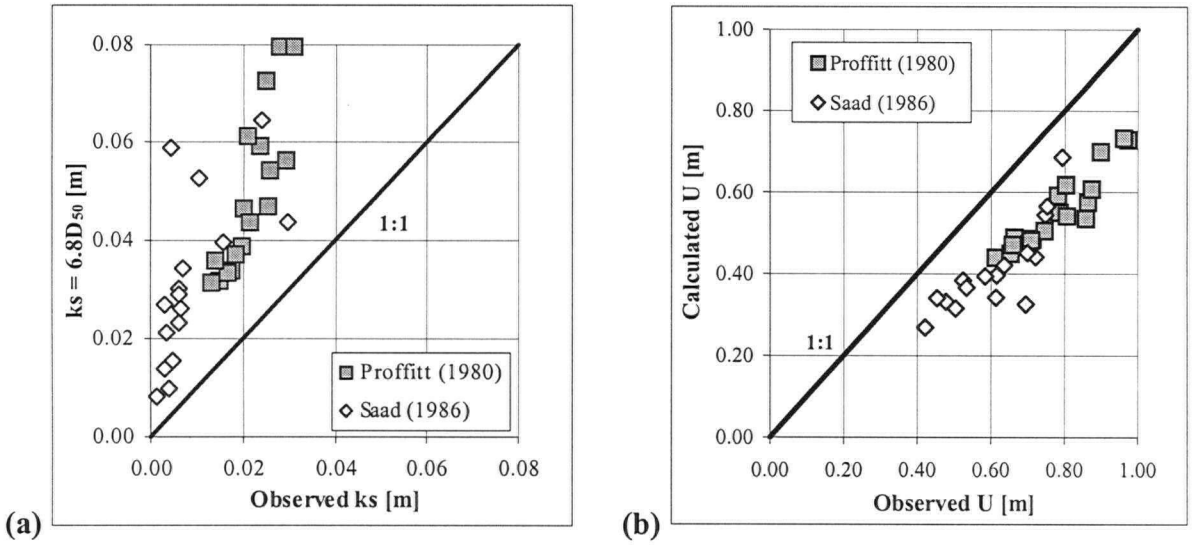

Figure 2.2. *Observed and predicted values of: (a) roughness height, k_s, and (b) mean velocity, U, for experiments of Proffitt (1980) and Saad (1986).*

It would be reasonable to assume that the roughness of natural gravel bed streams could be represented by a single grain size only if we assumed that the particle size distribution, bed arrangement, packing, spacing and sorting, particle size and orientation, clustering or other bed forms were universal and similar for different sites or flow conditions. However, this is not the case, all these different factors being variable. Consequently, many researchers consider that k_s cannot be estimated using a single grain size (Bray, 1985; Hey and Thorne, 1986; Kirchner et al., 1990; Robert, 1990; Carling et al., 1992). The equivalent roughness height, k_s, really represents a characteristic hydraulic friction length for the boundary (Arya, 1975; Smart, 1999). It is a composite parameter dependent not only on the size of the bed material, but also on the spacing and shape of roughness elements and also on bed forms present in the channel (Schlichting, 1968; Gomez, 1993). Nikora et al. (1998) and Smart et al. (2002a) suggested that the roughness properties of gravel bed rivers can be described by three characteristic linear scales, and that k_s is a function of statistical properties of the bed in

the longitudinal, transverse and vertical direction. They found that the standard deviation of bed surface elevations (σ_z) is a reasonable measure of the vertical roughness scale, and that better predictions of flow velocity can be obtained if this parameter is used as a roughness measure than if a characteristic grain size (e.g. D_{84}) or Z_0 are used.

2.3. Relationships Amongst Different Roughness Parameters

Early work of modern fluid dynamics was concerned with pipe roughness and boundary layer roughness, especially for aeronautical drag estimates. This classical boundary layer work defined rough and smooth surfaces in terms of viscous sub-layer thickness. Pioneering work by Nikuradse (1933), Prandtl (1935), and many others laid the fundamentals for analysing turbulent flow and understanding the role of roughness. The work of many researchers was summarized and presented by Schlichting (1968).

The boundary layer work was carried out under closely controlled conditions, which could be defined precisely. In contrast, the present work is concerned with much rougher surfaces, with much more sediment size variation, and perhaps with bedforms and three-dimensional influences. However, we can still make use of the Prandtl-type ideas and try to extend them to this work. A fully rough boundary is defined as a condition in which the roughness projections break through the laminar sub-layer and dominate the flow behaviour. This condition describes the turbulent flow over a gravel bed examined in this study. In this case the flow resistance is entirely due to the form drag on projections, for which the resistance coefficient becomes independent of Reynolds number and dependent only on the ratio R/k_s.

For a flume study on gravel bed armouring, the smooth glass walls offer little resistance to flow compared to the rough armoured bed. In addition, there is very little or no resistance due to different bed forms, so it can be assumed that almost all of the resistance to flow is due to grain roughness. In such case, relationships amongst Chezy C, Manning n, Darcy-Weisbach f, and Nikuradse's equivalent grain roughness k_s can be established. From Nikuradse's experiments and some additional measurements, the relationship for the fully rough flow can be derived from equations 2-5 and 2-8, and by further combining this with equations 2-7 and 2-9, a relationship between the different roughness parameters presented earlier is obtained:

$$\frac{1}{\sqrt{f}} = 2.03\log\left(\frac{12.2R}{k_s}\right) = \frac{C}{\sqrt{8g}} = \frac{R^{1/6}}{8.86n} \qquad (2\text{-}11)$$

The sensitivity of the different roughness parameters is best illustrated with an example. For the assumed values of $n=0.02$ and $R=0.15$ m (typical values from Proffitt's bed armouring experiments), the following values are obtained from equation 2-11: $f=0.004$, $C=36.5$, and $k_s=0.017$ m. If R is kept the same, but n is increased by 10% to a value of 0.022, there is a considerable change in f and k_s, but not in C (i.e. $f=0.005$, $C=33.1$, and $k_s=0.026$ m). Therefore, a 10% increase in n, produced approximately a 50% change in k_s, indicating the high sensitivity of k_s. In reality, values for k_s obtained in Proffitt's experiments ranged from about 0.014 m to over 0.026 m for the two values of n adopted here.

2.4. Critical Shear Stress

The critical shear stress for a gravel bed river is not yet completely understood and defined. The critical shear stress of individual fractions in mixed-size sediments is quite different than that of unisize sediments (Wilcock and Southard, 1988; Wilcock and McArdell, 1993), due to interlocking, hiding, and other effects. There is a range of threshold conditions for individual fractions in an armoured bed. Paintal (1971) argued that there would always be some probability of grain movement, as long as there is any fluid motion, while Neill (1968) defined "lower critical" and "upper critical" conditions, corresponding to the threshold of movement for the middle and the largest fractions, respectively. The upper critical conditions occurred at shear stresses two to three times higher than the lower critical conditions, with armoured beds forming at intermediate stresses.

In contrast, Andrews and Parker (1987) argued that, when bed material motion begins, a whole range of sizes would be involved ("equal mobility" concept), which is due to the varying exposure of particles to fluid forces. Kirchner et al. (1990) showed that the critical shear stress distributions for different grain sizes have the same lower bound, which is consistent with the observation that all grain sizes become mobile at nearly the same mean shear stress. Wilcock and McArdell (1993) and Wilcock et al. (1996) introduced the concept of "partial transport", associated with a region of shear stresses for which the transport rate of some coarser particles is substantially lower than the transport rate of smaller fractions, which results from differences in particle mobility. They showed that on a large gravel-bed river, the range of non-dimensional shear stresses from complete immobility to entrainment

of the entire surface was very narrow (10-15%), with partial transport occurring between the two extremes (Wilcock et al., 1996).

Fenton and Abbott (1977) and Chin (1985) demonstrated the importance of grain protrusion when determining the threshold of motion. The non-dimensional shear stress varied from 0.01 for a fully exposed grain to 0.15 for a grain with no protrusion. Similar values were obtained in other investigations as well. A low value of 0.01 was also calculated from Coleman's experiments (1967) for a sphere placed at an interstice of a hexagonal array of spheres, while values higher than 0.1 were found in some natural riverbeds (Church, 1978; Reid et al., 1985, Buffington et al., 1992). These values are very different from values obtained from the Shields diagram, which gives a constant value of about 0.06 for high grain Reynolds numbers (i.e. zone of fully rough turbulent flow). However, it should be understood that Shields' experiments (1936) were carried out with narrowly graded sediments, which contrasts the conditions found in natural armoured gravel beds.

Fenton and Abbott (1977) demonstrated that the Shields diagram implicitly contained variation with relative protrusion, because the experiments with low Reynolds numbers were carried out with small grains, for which achieving a "truly co-planar bed" was physically impossible. They argued that for smaller grains, total protrusion was inevitable, and thus in the zone of particle Reynolds numbers of up to approximately 10, the variation in critical shear stress would be due to increase in the Reynolds number only. On the contrary, initiation experiments with large Reynolds numbers were carried out with large natural grains (and not spheres) and, even though the grains were of uniform sizes, it would be impossible

to have absolutely zero protrusions due to small natural variations in grain size and laying of the grains, thus the critical shear stresses measured by Shields would be somewhat lower than if protrusions were truly zero. Fenton and Abbott's experiments showed that for Reynolds numbers larger than about 1000, the variation in critical shear stress was due to relative grain protrusion only. In the region of Reynolds numbers between approximately 10 and 1000, the Shields number would vary with both the Reynolds number and the relative grain protrusion.

Another important parameter in initiation of particle motion is the particle friction angle (ϕ), which basically represents the particle's resistance to movement. Pioneering work on this topic was undertaken by White (1940), Bagnold (1941), and Chepil (1959). Chepil showed that the lower bound of friction angles equal to 33° agreed well with Bagnold's angle of repose of a pile of grains, indicating that the two should be similar. Miller and Byrne (1966) established an empirical relationship between the friction angle and D/K (where D is the test grain size, and K is the mean bed particle size). They found that the friction angle decreased with increasing D/K, and that particle shape, packing and sorting also influenced the value of ϕ.

In the work of Wiberg and Smith (1987), Komar and Li (1988), Kirchner et al. (1990), Buffington et al. (1992) and Johnston et al. (1998), the force balance model on individual bed grains was used to estimate the critical shear stress from friction angle values. The grain mobility depends on the particle's friction angle, and on lift and drag forces applied on the particle, which depend on particle's protrusion or exposure to flow, while the balancing force is the particle's immersed weight. They found that the dimensionless critical shear stress was

strongly dependent on grain protrusion, friction angle and grain diameter. However, the critical shear stress, as well as the friction angle, is characterised by a probability distribution and not a single value for a given grain size. Kirchner et al. (1990) and Buffington et al. (1992) showed that the mean friction angles and the mean protrusions were not appropriate values relevant for threshold of motion, because the "average" grains would not be the ones that move first, and therefore the appropriate values should be much less than the mean. Their measurements showed almost no relationship between friction angles and protrusions for individual grains.

The conventionally measured critical shear stress is defined by the most erodible grains. However, the surface topography in water-worked sediments is complex and, thus, the friction angle, grain protrusion and estimated shear velocity may vary widely even for a single grain size on the bed surface. For poorly sorted beds, smaller grains may have lower protrusions and higher friction angles, and therefore higher critical shear stresses and lower erodibility than the larger grains, which is an effect due to hiding and sheltering. Turbulent fluctuations in the flow cause spatial and temporal fluctuations in applied shear stresses, so that particle entrainment will occur during high velocity fluctuations above the mean, which cause short-term shear stress extremes. All of the above considerations about the variability of conditions for natural gravel beds demonstrate that a sharp threshold of motion for the bed as a whole, or for any individual grain size on the bed, does not exist.

CHAPTER 3

NUMERICAL MODEL

3.1. Introduction

Various factors such as particle weight, size and shape, packing and imbrication, or size of surrounding particles determine the resistance of a particle to fluid forces. It is very difficult to take all these factors into account when modelling the particle mobility, as it would make the procedure far too complex. However, the relative grain protrusion (*H/D*) seems to represent a reasonable parameter that can account for differences in applied forces on various grains and can be used in a simplified model to simulate particle mobility. In this model, the force on a grain can be estimated as a function of protrusion provided that the drag and lift coefficients and the velocities can be estimated. However, much uncertainty remains regarding these coefficients, as well as the shape of the velocity profile, and these issues will be addressed later. The analysis presented here was developed by focusing on the roughness parameter, rather than on critical shear stress, as in most of the previous work (Wiberg and Smith, 1987; Kirchner et al., 1990).

3.2. Hypothesis

The fundamental hypothesis in this investigation is that a stable (threshold) armour layer develops such that all grains are at, or near threshold of motion at the "channel forming discharge". It represents the limiting state of equal mobility, i.e. all grains are equally mobile,

in that they are just at the threshold of motion (Parker and Sutherland, 1990). The analysis in the current study is limited to stable or threshold armour layers that develop under condition of zero bed material supply. Protrusion of each grain also represents an adjustment to "equal mobility", in that each grain protrudes just enough to be at the threshold of motion.

3.3. Model Development

An analytical model is developed that accounts for variable grain protrusion under conditions of near zero sediment supply. Protrusion heights of the grains in the armour layer are adjusted until all grains are just at the threshold of motion and the bed has developed the limiting condition of equal mobility (Parker and Sutherland, 1990). This model focuses on the role of grain protrusion and, therefore, it will be referred to as the Grain Protrusion Model.

The model assumes a certain grain size distribution and does not directly consider coarsening that occurs during armour formation. Textural coarsening has been dealt with at length elsewhere (Proffitt, 1980; Parker et al, 1982; Parker and Klingeman, 1982; Dietrich et al., 1989; Parker, 1990; Parker and Sutherland, 1990; Chin et al., 1994). Rather, it is assumed that the grain size distribution for the armour layer is known a priori, and the model is used to calculate grain protrusion and hydraulic roughness so that all grain sizes are exactly at the threshold of motion.

The key components of the Grain Protrusion Model are: (1) calculation of the vertical profile of longitudinal velocities relative to the virtual bed; (2) variation in drag coefficient and drag force

with protrusion above the virtual bed; and (3) variation in critical shear stress with protrusion above the virtual bed. The analysis is based on the assumption of spherical grains and the effects of sheltering are not considered separately, but can be considered incorporated in the particle protrusion.

3.3.1. Velocity profile and location of the virtual bed

In an effort to retain computational simplicity, it is assumed that a logarithmic velocity profile develops over the rough gravel bed for a channel forming discharge. For the Grain Protrusion Model, it is necessary to precisely define the datum or virtual bed elevation from which to calculate the velocity profile and the protrusion heights. In accordance with several previous investigators (Einstein and El Samni, 1949; Chepil, 1959; Cheng and Clyde, 1972), the virtual bed is defined as the elevation at which the extrapolated logarithmic velocity profile becomes equal to zero (Fig. 3.1.). Typically, the virtual bed occurs at some small distance below the actual physical bed surface represented by the top of the grains. The individual grain protrusion height, H_i, is measured from the virtual bed, which is equivalent to the velocity origin (Fig. 3.1.). The depth, y, is measured from $k_s/30$ below the virtual bed (after Nikuradse, 1933), so that $log(30y/k_s)$ in equation 3-3 is zero when $y = k_s/30$, which yields $u_y = 0$ at this point.

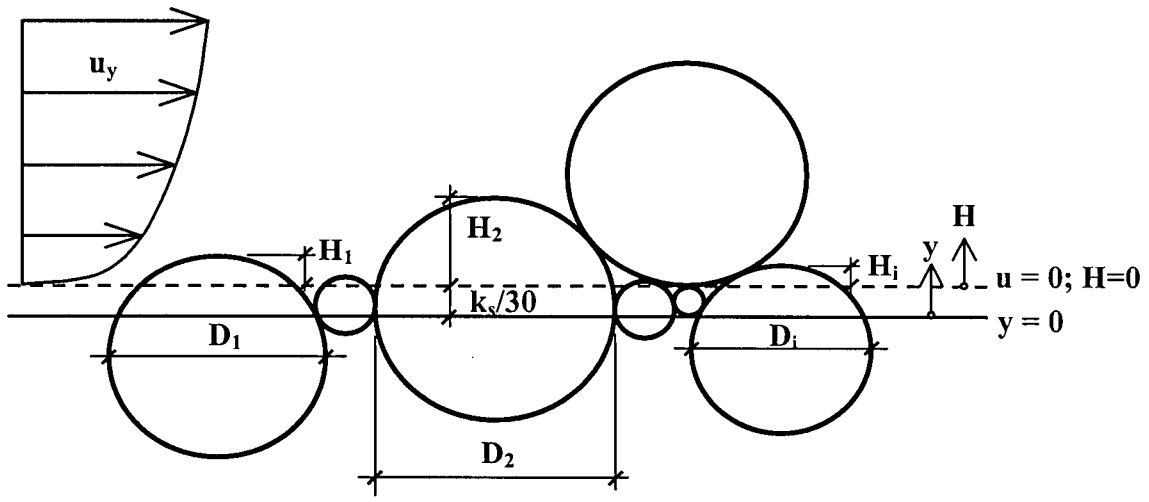

Figure 3.1. *Definition sketch for non-uniform sediment.*

For the theoretical analysis, a logarithmic velocity distribution extending to the water surface is assumed (equivalent to equation 2-1), where the Kuelegan (1938) type equation is used:

$$\frac{u_y}{u^*} = \frac{1}{\kappa}\ln\left(\frac{y}{k_s}\right) + B \qquad (3\text{-}1)$$

where u_y is the time averaged velocity at height y above the bed; κ is the von Karaman constant equal to 0.4; k_s is the equivalent, or Nikuradse's sand roughness height; B is the constant of integration that is a function of Reynolds number (Re), except for fully-rough turbulent flow when it becomes constant at 8.5; and u^* is the shear velocity given by:

$$u^* = \sqrt{\frac{\tau_0}{\rho}} = \sqrt{gRS_f} \qquad (3\text{-}2)$$

Here, τ_0 is the average bed shear stress given by the product ρgYS_f, ρ is the density of water, g is the gravitational acceleration, R is the hydraulic radius, and S_f is the friction slope. After

substituting the values for κ and B, equation 3-1 becomes equivalent to equation 2-2 given in Chapter 2, or:

$$\frac{u_y}{u^*} = 5.75 \log\left(\frac{30y}{k_s}\right) \tag{3-3}$$

3.3.2. Drag force and drag coefficient

The drag force, F_D, acting on a particle on the bed can be expressed as:

$$F_D = C_D A_D \frac{\rho u_r^{\,2}}{2} \tag{3-4}$$

in which C_D is a drag coefficient, A_D is the projected grain area normal to the flow above the virtual bed, and u_r is a reference velocity.

Numerical integration was performed for various grain protrusions to determine the equivalent resultant position (y_r) of the drag force at which the reference velocity (u_r) is estimated (Fig. 3.2.). Assuming that the average drag coefficient (C_D in equation 3-4) is the same as the drag coefficient for each slice (C_D in equation 3-5), the drag force acting on an infinitesimally small section of a protruding particle can be formulated as:

$$dF_D = C_D \frac{1}{2} \rho u_y^2 dA \tag{3-5}$$

where u_y is calculated using equation 3-3, and dA is the section area given by:

$$dA = 2r \cos\theta dy \tag{3-6}$$

in which, r is the grain radius (r=0.5D), θ is the angle measured from the horizontal plane passing through the grain centre, and dy is the slice thickness (see Fig. 3.2.).

Integration of equation 3-5 yields the total drag force acting on a protruding grain, which should be equal to the drag force calculated from equation 3-4, thus, the reference velocity u_r can be calculated. Once u_r is determined from equation 3-4, the drag force position (y_r) can be obtained using equation 3-3.

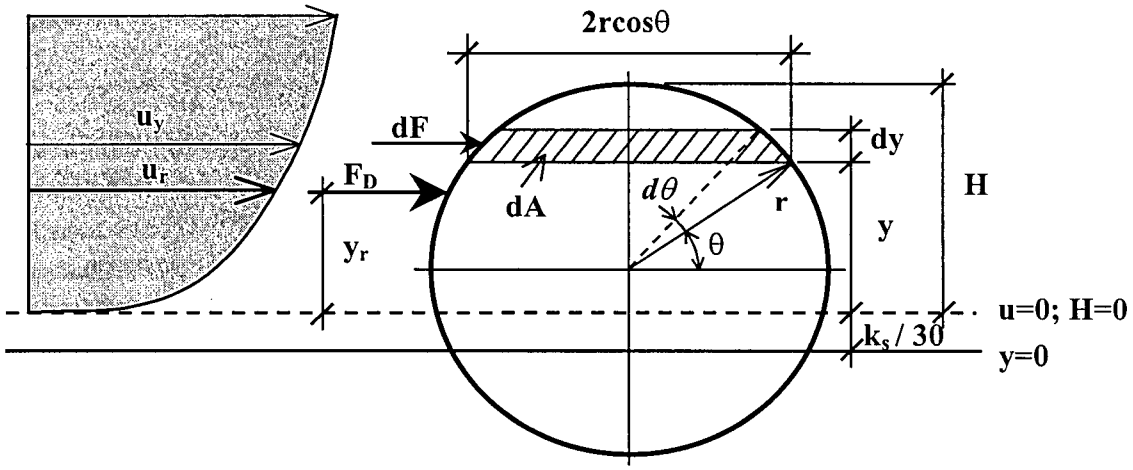

Figure 3.2. *Drag force position on a protruding grain.*

From the above numerical integration, the position of the reference velocity is determined to be approximately at the average height of $y_r = 0.4H$ above the virtual bed and varies only slightly with grain protrusion and the exposed grain area, as shown in Figure 3.3. This analytical result falls between the value determined experimentally by Einstein and El-Samni (1949), $y_r = 0.35H$, and that assumed by Coleman (1967), $y_r = 0.5H$, and thus appears reasonable.

Substituting the reference height $y_r = 0.4H + k_s/30$ into equation 3-3 yields the following expression for u_r:

$$\frac{u_r}{u^*} = 5.75 \log\left(\frac{12H}{k_s} + 1\right) \qquad (3\text{-}7)$$

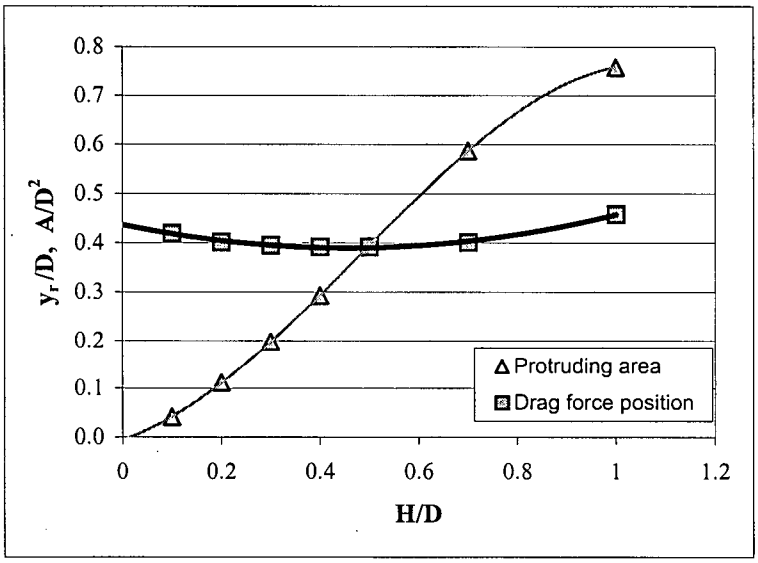

Figure 3.3. *Results of the numerical integration for the drag force position.*

Consideration must also be given to the variation in the drag coefficient with Reynolds number and protrusion height. The value of C_D for spheres has been shown to be a function of particle Reynolds number, $Re = u_r D/\nu$, in which ν is the kinematic viscosity and D is the particle diameter (White, 1986, p. 417). However, little is known about the variation of C_D for a grain within a turbulent boundary layer, particularly for low protrusion heights where both u_r and Re take small values. Because of the intense turbulence in the boundary layer, it is probably reasonable to assume that the drag coefficient will be equal to the fully turbulent case and independent of Reynolds number, and this is the assumption that will be made.

In order to account for the influence of protrusion on the drag force, the force will be written as a function of a variable drag coefficient, C_D^*, multiplied by the particle area and the kinetic energy of the flow:

$$F_D = C_D^* \frac{\pi D^2}{4} \frac{\rho u_r^{\ 2}}{2} \qquad (3\text{-}8)$$

in which C_D^* will now be defined as a function of the relative protrusion (H/D), incorporating variation in the exposed proportion of the grain above the virtual bed. C_D^* will be referred to as the grain protrusion drag coefficient.

It is more convenient in the subsequent analysis to express equation 3-8 in terms of force per unit bed surface area, or shear stress, for each individual grain:

$$\tau' = C_D^* \frac{\rho u_r^{\ 2}}{2} \qquad (3\text{-}9)$$

in which τ' is defined as the grain shear stress. This function is used to account for the variation of C_D^* with relative protrusion above the zero velocity datum. Equation 3-9 does not directly consider the interstitial area between grains, however this is accounted for later in equation 3-16.

Definition of the grain protrusion drag coefficient - Despite the absence of detailed experimental data, it is considered that a reasonable relation that describes the variation of C_D^* with relative protrusion can be assumed (Fig. 3.4.). For $H/D = 0$, the drag on a particle must be equal to zero, and therefore $C_D^* = 0$. For full protrusion when $H/D = 1$, $C_D^* = C_D = 0.5$, where the value of C_D is obtained from Coleman (1967) for a sphere resting on the bed. The value of C_D^* corresponding to $H/D = 0.2$ can be deduced from Nikuradse's data (1933) as follows. Einstein and El Samni (1949) showed that for close-packed uniform grains of diameter D, the virtual bed ($u_y = 0$) is located at a distance of $0.2D$ below the top of the grains. Assuming that the grain shear stress is equal to the boundary shear stress, i.e. $\tau' = \rho u^{*2}$, a value for C_D^* =

0.214 is obtained from equations 3-7 and 3-9 for $H = 0.2D$ and $k_s = D$. These three values of C_D^* are plotted in Figure 3.4., and a smooth curve can be drawn through these points.

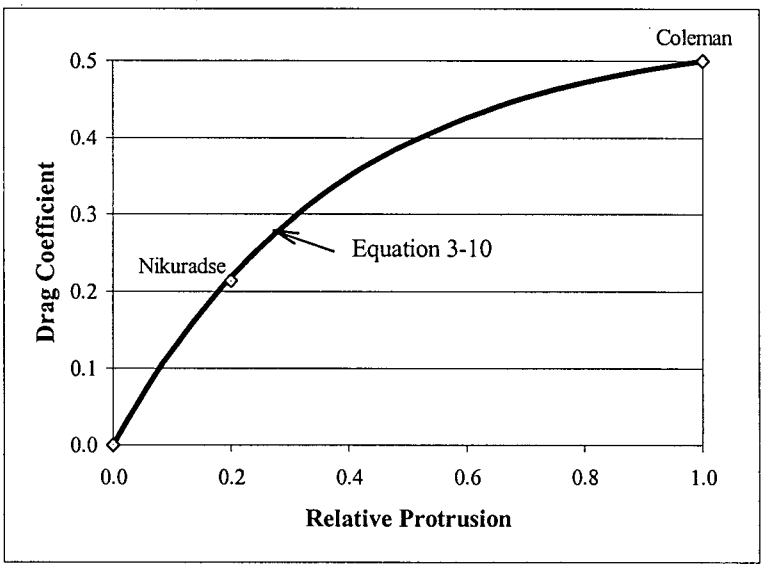

Figure 3.4. *Variation of drag coefficient (C_D^*) with relative protrusion (H/D).*

For computational purposes a simple exponential relation was fitted to the three values of C_D^* (Figure 3.4.):

$$C_D^* = 0.54\left[1 - \exp\left(-2.6\frac{H}{D}\right)\right] \qquad (3\text{-}10)$$

This function is used to account for the variation of C_D^* with relative protrusion above the zero velocity datum in the Grain Protrusion Model.

3.3.3. Variation of critical shear stress with grain protrusion

In the present analysis, the value of the critical non-dimensional shear stress should be calculated for each particle as a function of its exposure, *H/D*. This critical shear stress has

been estimated from published data as follows. Fenton and Abbott (1977) demonstrated the significance of grain protrusion and critical shear stress. Their experiments show that the non-dimensional shear stress varies from 0.01 for a fully exposed grain to 0.15 for a grain with no protrusion. Fenton and Abbott's experiments were slightly modified and repeated by Chin (1985), with similar results.

The combined data sets from Fenton and Abbot (1977) and Chin (1985) were used to redefine the critical non-dimensional shear stress based on our definition of grain protrusion. The original investigators measured protrusion from the top of the surrounding grains. We have recalculated the relative protrusion (*H/D*) from the virtual bed (u_y = 0), by assuming that zero velocity occurs at a distance *0.2D* below the top of the uniformly sized grains used in their experiments.

The following equation defining the lower bound has been fitted to the data (Fig. 3.5.):

$$\tau_c^* = 0.01 + 0.45\exp\left(-11\frac{H}{D}\right) \qquad (3\text{-}11)$$

in which τ_c^* is the critical non-dimensional shear stress for the protruding grain. The lower bound, as opposed to a best-fit, is justified on the grounds that particle stability is determined by the maximum instantaneous shear stress, and not by the time-averaged shear stress (Fenton and Abbott, 1977). For uniform grains for which *H/D = 0.2*, equation 3-11 returns a value for τ_c^* equal to 0.06, which is equivalent to the commonly assumed Shield's value for uniform grains.

Further analysis of the data presented in Figure 3.5. was carried out to examine the influence of lift and drag forces. The lift force was evaluated the same way as the drag force, using the same parameters as given in equation 3-4, and a slightly different lift coefficient ($C_L^* = 0.8\text{-}0.85\ C_D^*$, based on Chepil's work on hemispheres (1959)). The non-dimensional critical shear stress was determined from a force balance for different grain protrusions, and this analysis gave a higher line than the one shown in Figure 3.5, which is reasonable, because average flow parameters were used in the analysis and not the instantaneous maximums, which initiate the movement. The lower bound is considered to be more relevant for this present work, because it is likely to be the maximum instantaneous shear stress, which will dislodge surface particles and result in the final armouring configuration. Therefore, the lift force is inherently incorporated in the initial motion criteria defined by the lower bound critical shear stress.

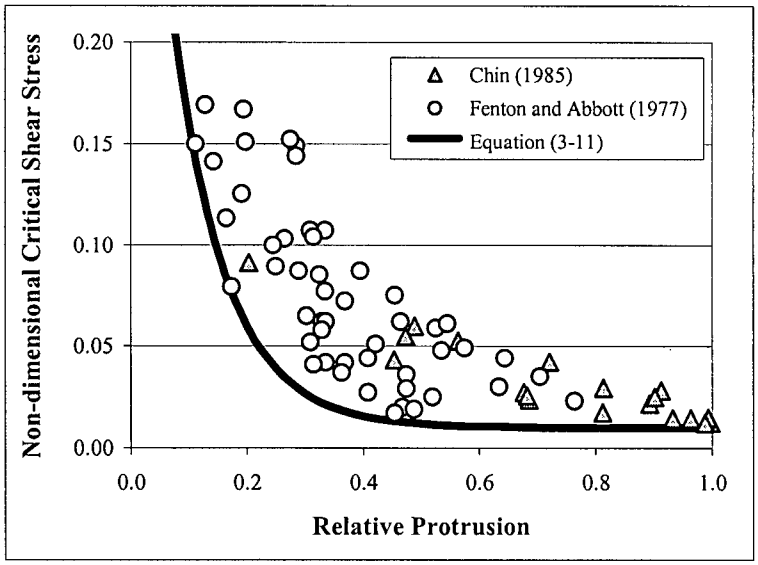

Figure 3.5. *Variation of the non-dimensional critical shear stress (τ_c^*) with relative protrusion (H/D) (after Fenton and Abbott, 1977, and Chin, 1985).*

3.4. Computational Scheme

At the outset of the calculations, the individual grain protrusions are not known and, consequently, the position of the bed level datum and zero velocity are not yet defined. Therefore, the calculation procedure starts by assuming a depth of flow and a roughness coefficient, and then proceeds to estimate a trial set of grain protrusions for each sediment size fraction. Trial calculations then proceed to estimate the total shear stress, which may be found to be greater or less than the total imposed shear stress, ρgYS_f. The iterative procedure is designed so that the trial values are adjusted until agreement is reached. The steps of the procedure are described in detail below.

1. Values for unit discharge (q), friction slope (S_f) and grain size distribution of the armour layer (geometric mean of the grain size interval, D_{gi}, and the corresponding fraction of the bed surface coverage, F_i, where $\Sigma F_i = 1.0$) are prescribed as input to the model (Fig. 3.6.).
2. Computation proceeds in a stepwise iterative manner using a commercially available spreadsheet (e.g. Microsoft® Excel) to solve for equivalent roughness height, k_s, depth, Y, and mean velocity, U. In the first stage, trial values of Y and k_s are assumed.
3. Then, the relative protrusion (H_i/D_i) for each size fraction i is determined by equating the critical non-dimensional shear stress for a grain of size D_{gi} with the non-dimensional shear stress for the same grain size, or:

$$\tau_{ci}^{*} = \tau_{i}^{*} \qquad (3\text{-}12)$$

where

$$\tau_{i}^{*} = \frac{\rho gYS_f}{\rho g(S_s - 1)D_{gi}} \qquad (3\text{-}13)$$

In the above equations τ_i^* is the non-dimensional shear stress for size fraction D_{gi}, and τ_{ci}^* is the corresponding critical value calculated from equation 3-11. Combining equations 3-11, 3-12 and 3-13 yields an expression for the relative protrusion:

$$\frac{H_i}{D_{gi}} = 0.091 \ln\left(\frac{0.45}{\tau_i^* - 0.01}\right) \tag{3-14}$$

For this relative protrusion, the reference velocity (u_{ri}), and the drag coefficient (C_{Di}^*) are calculated using equations 3-7 and 3-10, respectively.

4. The grain shear stress is then calculated using equation 3-9 for each grain size i:

$$\tau_i' = C_{Di}^* \frac{\rho u_{ri}^2}{2} \tag{3-15}$$

5. The total grain shear stress (τ') can be determined by summing the individual grain shear stresses (τ_i') for all i.

$$\tau' = \sum_{i=1}^{n} F_i \tau_i' \tag{3-16}$$

6. Assuming that there are no other sources of roughness than grain protrusion, and if the trial value of k_s is correct, then τ' must be equal to the average bed shear stress given by the product $\rho g Y S_f$. Otherwise, the trial value of k_s has to be updated using an iterative procedure until the condition $\tau' = \rho g Y S_f$ is satisfied. This updating is done using a Goal Seek function in Microsoft® Excel, which is a linear iterative process in which the source cell is increased or decreased at varying rates until a target value is reached. The derived value of k_s is appropriate for the current trial value of Y.

7. The mean velocity, U, is then determined using the depth-integrated form of the law-of-the-wall, in which a wide channel approximation is assumed and u^* is corrected for sidewall effects (equivalent to equation 2-4):

$$\frac{U}{u^*} = 5.75 \log\left(\frac{11Y}{k_s}\right) \tag{3-17}$$

8. The final step is to assess the trial value of Y by comparing the product YU to the input value of unit discharge, q. The trial value of Y is repeatedly updated using a Goal Seek function, which was found to give a convergent solution, until continuity is satisfied, and the model outputs values of k_s, Y, and U. For each trial value of Y, a new value of k_s must be determined (Fig. 3.6.).

Sample calculations are shown in the spreadsheets in Appendix D.

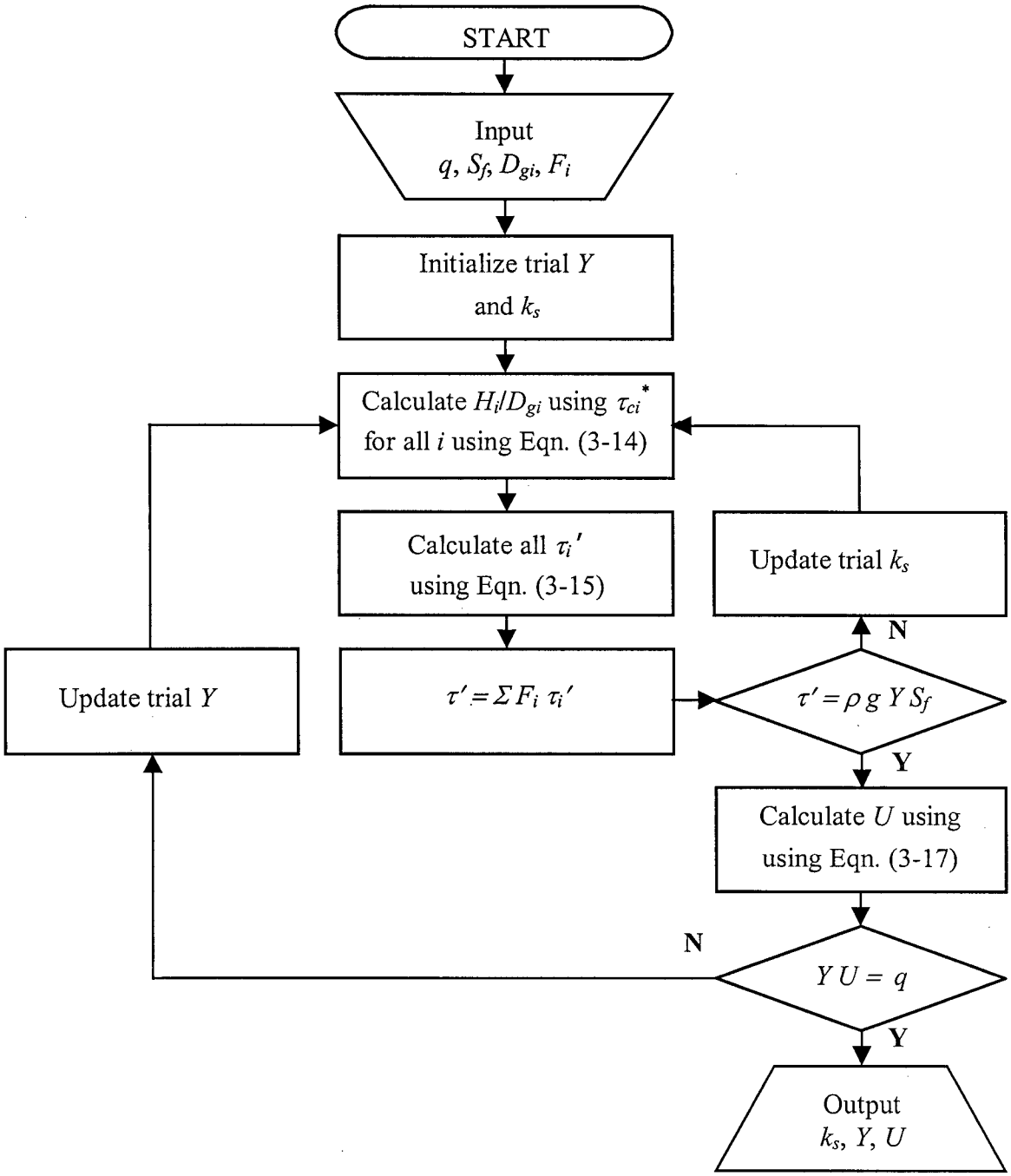

Figure 3.6. *Grain Protrusion Model flow chart.*

3.5. Model Behaviour

Full discussion of the model results will be given in Chapter 5, but some preliminary results will be presented here to illustrate their general nature. Computed variation in relative protrusion height, *H/D*, and cumulative grain shear for different size fractions are shown for Proffitt's run 3-1 (Figures 3.7.a and b). As would be expected, the relative (and absolute) protrusion heights increase with grain size, which is represented by Percent Finer in Figure 3.7.a. Because of their larger mass, larger grains protrude higher into the flow and remain stable, whereas the smaller grains protrude less and remain "hidden" amongst the larger grains.

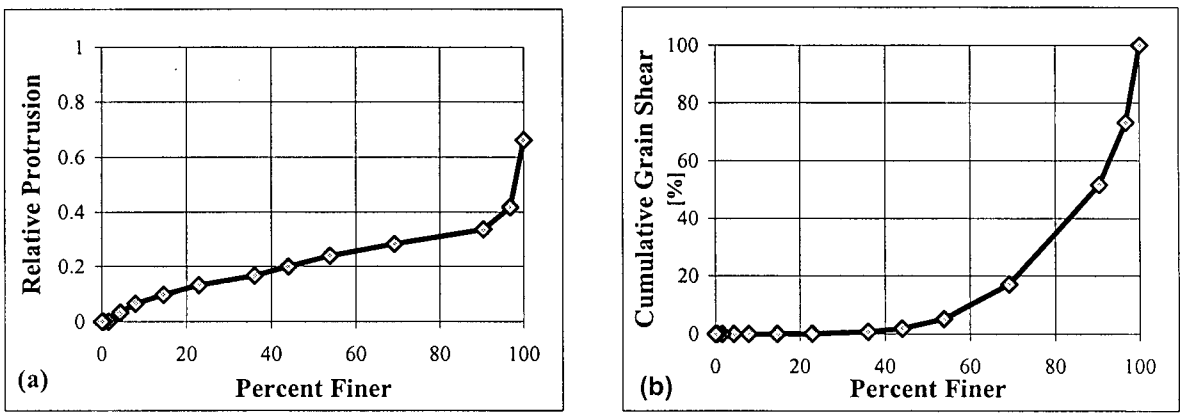

Figure 3.7. *Simulated results for Run 3-1 from Proffitt (1980): (a) Variation in relative protrusion, H/D; (b) Cumulative grain shear stress.*

The shear distribution indicates that most of the shear is accounted for on the largest grains (Fig. 3.7.b). In this example, more than 80% of the total shear is taken up by the coarsest 30% of the bed surface (D_{70} and coarser), and less than 2% of the shear acts on those grains smaller than D_{50}. These results indicate that it is the largest grains in the armour that determine both the stability and the roughness of the armour layer.

The Grain Protrusion Model will be tested in Chapter 5 using hydraulic measurements from some earlier studies on gravel bed armouring (Proffitt, 1980; Saad, 1986), as well as using measurements from this study. However, before the numerical model results are presented, detailed explanation of experiments and hydraulic measurements conducted for this study will be discussed in the following Chapter.

CHAPTER 4

EXPERIMENTAL WORK AND DATA ANALYSIS

4.1. Introduction

Eight experiments were carried out in the Hydraulics Laboratory of the Department of Civil Engineering, The University of British Columbia, Canada. The purpose of the experiments was to develop armoured gravel beds under clear water flow conditions (no sediment feed). The first three experiments were conducted for observational and learning purposes, to determine how the system behaves as a whole, and to test some of the equipment. The bed was not reworked for each consecutive run, but the slope and the discharge were increased, causing a break-up of a previous armour layer and allowing for a new, coarser armour to develop. This was done until the surface was mobile and no armour was developing at a slope of around 1.2%, which was a limiting condition for the given sediment mixture. There were no detailed measurements conducted in these runs.

The following five runs, numbered Run 1 to Run 5, were conducted somewhat differently than described above, with a bed reworked for each run. Detailed measurements were taken and the experiments were designed to test the basic assumptions underlying the theory for the numerical model, i.e.:

- The validity of the logarithmic velocity profile for channel forming flows; and
- The individual grain protrusion heights for different size fractions to confirm the hypothesis on equal mobility.

The experiments provide the following data for testing the numerical model:

- Flow rate;
- Depth;
- Slope;
- Surface grain size distribution;
- Velocity profile distribution; and
- Grain surface elevation data.

The experimental set-up consisted of a 15 m long, 0.5 m wide tilting flume supplied with two pumps having a maximum combined capacity of 0.35 m^3/s (Fig. 4.1.). The supply pipes delivered the water into a large inlet tank, where the flow passed through a set of meshes before entering the flume. The first 6 m of the flume were artificially roughened with large natural cobble and the size was decreased in the downstream direction so that at the beginning of the test section the sizes were between D_{84} and D_{100} of the test sediment mixture. This arrangement ensures that the boundary layer is fully developed before the flow reaches the test section. The test section was 5 m long, followed by another artificially roughened section extending to the end of the flume. A sediment sill was installed at the end of the test section, consisting of 5 mm thick strips, which were removed as the degradation progressed. The tailgate at the end of the flume was used to establish uniform flows at the beginning of each run, and was not readjusted during runs. At the end of the flume, there is an outlet tank fitted with a set of screens, and the finest screen had an opening of 1 mm, which was necessary to capture the finest transported sediments.

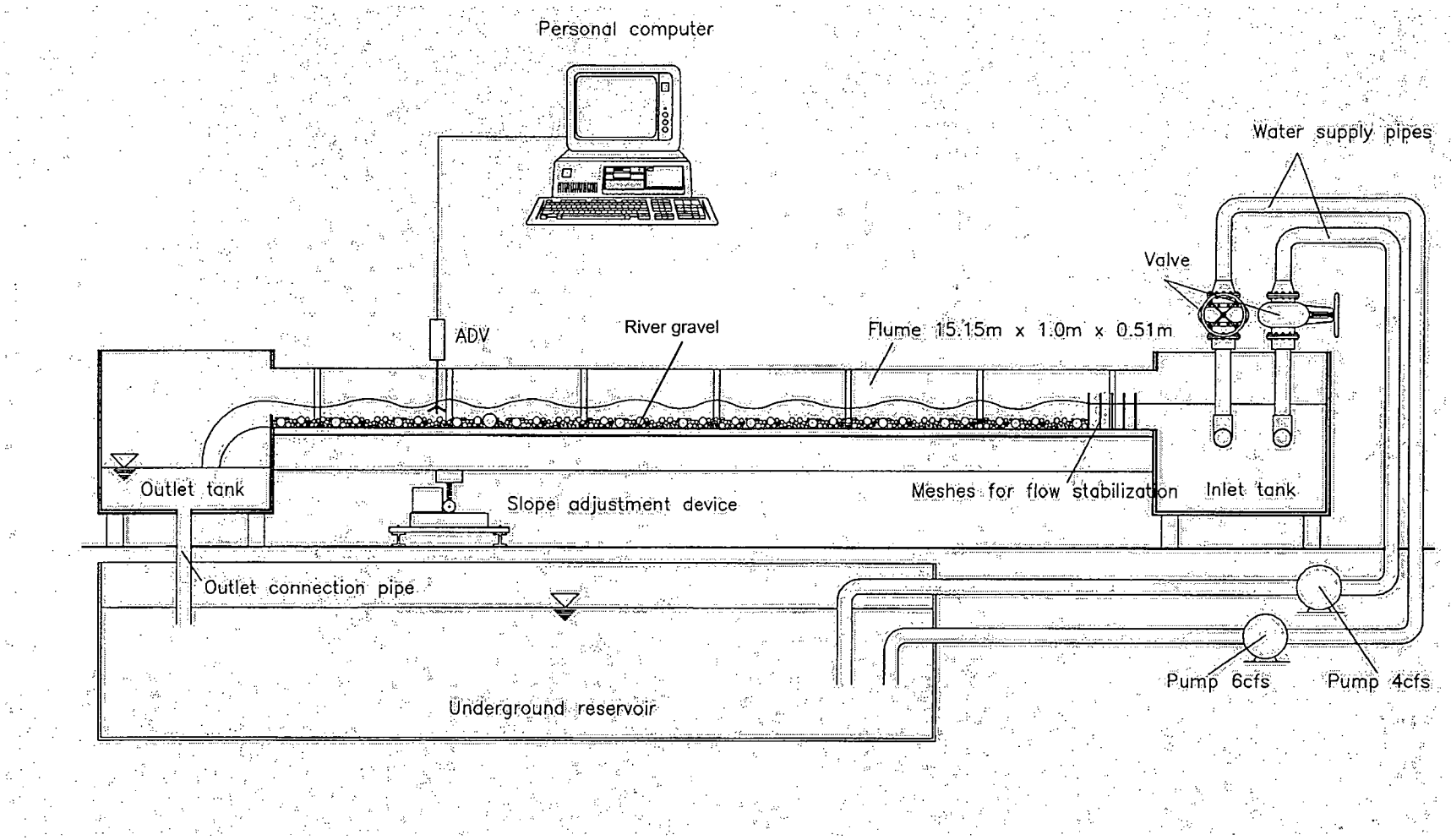

Figure 4.1. *Schema of the experimental apparatus (from Martin, 1996).*

A VersaFLO sonic flow meter was attached to the supply pipe to measure the discharge, and these measurements were used to calculate average velocities in the flume. After the stable armoured beds developed, velocities were also measured using a SonTek Acoustic Doppler Velocimeter (ADV). Several velocity profiles were measured across and along the flume for each run, and these measurements were used to calculate shear velocities and roughness heights. The ADV data were also used to obtain the Reynolds stresses ($-\rho\overline{u'w'}$), which were used to plot the shear stress profiles and to estimate the total shear stresses and the shear velocities on the bed. In addition, a third estimate of the shear stresses was made by using the depth and slope measurements obtained with a point gauge.

The sediment used in these experiments was the same sediment as used in experiments by Church et al. (1998). In their work, the sediment material was scaled to field conditions at Harris Creek, B.C. with a ratio of 1:16. The maximum grain size of 512 mm was scaled down to 32 mm, and the material scaling to less than 0.18 mm was excluded from their experiments. In our work, the sizes smaller than 1 mm were removed from the original mixture, because of problems with trapping the finest sediments. The maximum grain diameter of this new mixture was 32 mm, D_{50} was 2.92 mm and the sorting coefficient, $\sigma_G = \sqrt{D_{84} / D_{16}}$, was 2.57. The coarsest grain sizes were painted in different colours as follows: yellow 8 – 11.3 mm; green 11.3 – 16 mm; red 16 – 22.6 mm; and blue 22.6 – 32 mm. This made it possible to relate grains of different sizes to their protrusion heights by overlaying digital elevation models (DEMs) over coloured photographs. The data for DEMs were obtained by scanning a 900 x 400 mm bed area with a laser displacement meter on a 1 millimetre grid.

Following the experiment, bed surface samples were taken using a piston covered with soft potter's clay (as in Church et al., 1998). To determine the grain size distribution of the armour layer, the areal sample was converted to a volumetric sample using the Kellerhals and Bray method (1971), with a somewhat different conversion coefficient, which was determined for this study.

In this chapter, all measurements, the instrumentation and the data analysis techniques will be discussed. The problems that occurred during the experiments will also be addressed, because these are considered important and useful for similar experimental work in the future. A brief set of conclusions related to the experimental work will be provided at the end of the chapter.

4.2. Hydraulic Parameters –Depth, Slope, Discharge, and Temperature Measurements

Several groups of measurements were undertaken before, during and after the course of experiments. These include water temperature, discharge, bed and water surface elevation measurements, and flume slope measurements. The following Sections will include descriptions of how the measurements were obtained, followed by discussions of the hydraulic parameters that were calculated from these measurements.

4.2.1. Bed and water surface elevation measurements

Bed and water surface elevation measurements were obtained using a point gauge equipped with a Vernier scale having an accuracy of 0.001 ft, or 0.3 mm. The repeatability of reading

the scale when measuring the non-stationary water surface was within 0.004 ft, or 1.2 mm. A small Plexiglas circular plate was installed on the tip of the point gauge, which prevented the gauge sinking into the bed. The point gauge was mounted on an instrument carriage and could be moved across and along the flume, so that measurements could be made at any position in the flume. During the run, measurements were taken on the centreline and at the two quarter points across the flume at every 50 cm to monitor the flow and bed development. In addition to this, the bed was surveyed in more detail before the beginning and after the end of each run, when measurements were carried out at every 25 cm. These measurements were used to obtain water depths, bed and water surface slopes, as well as degradation amounts.

Depth - The flow depth was calculated as a difference between the bed and the water surface elevation. Longitudinal comparison of depth measurements indicated if the flow was uniform. The final average depth (Table 4.1.) was calculated by averaging the measurements from all locations between 2.5 and 4.5 meters of the test section at the end of the run. In addition to point gauge measurements, depth measurements were also obtained by reading the water levels on rulers that were placed every 50 cm along the glass flume walls. These depth measurements were used at the beginning of each run, to help establish uniform flows by adjusting the tailgate opening. The uniform flow had to be established quickly, within 10-15 minutes or even faster for Runs 4 and 5, before considerable amounts of sediment moved, and for this purpose the readings could not be done fast enough with the point gauge.

For all five experiments, uniform flow conditions were established at the beginning of the run. The tailgate was not readjusted during the run, which would ensure that the flow stayed

reasonably uniform throughout the whole run. Closing the tailgate would impose additional shear and additional sediment transport after the bed started armouring. Because of this, the depths and slopes were left to readjust freely to the new roughness conditions in the channel. Comparison of depth measurements during the run suggested that depths increased and flow velocities decreased as a consequence of bed armouring. However, the flows stayed nearly uniform during Runs 1, 2 and 3, but somewhat less so for Runs 4 and 5, where the bed slope readjustment was considerable and will be discussed in more detail in the next Section.

Bed (S_0), water surface (S_w) and friction (S_f) slopes - The initial flume slopes (which were parallel to the initial bed slopes) for each run were measured by using a Leica total station. These slopes were used to convert the different elevations measured with the point gauge relative to a horizontal datum. This was necessary because the instrument carriage was mounted on rails on the top of the flume, which were parallel to the flume bottom and not to the final sediment bed or water surface. The final bed, water surface and friction slopes were obtained by fitting linear least square regression lines through measured elevation data points and calculated energy elevation points, respectively, between 2.5 and 4.5 m of the test section for all runs. The upstream and downstream conditions of the test section could have had an impact on how the bed developed and these areas had to be excluded when determining the slopes. As explained earlier, the bed upstream and downstream of the test section was artificially roughened with gravel material. The upstream section had the same thickness as the sediment in the test section, while the downstream section was somewhat thinner, but an adjustable sediment sill was installed between the test section and the downstream section, such that the evolving degradation in the test section could be accommodated. The

adjustable sediment sill was composed of 5 mm thick metal strips, which were removed as the degradation progressed (Fig. 4.2.).

Figure 4.2. *The adjustable sediment sill at the end of the test section.*

Figures 4.3. and 4.4. contain five graphs in total, which illustrate the point gauge measurements for all five runs separately. In these graphs, the solid black line is the flume bottom, while the solid grey line is the initial bed level, and both lines are also represented with their equations. The two lines were parallel and 10 cm apart for all runs except for Run 2, which will be explained in more detail later. The triangles represent the final bed elevations and were calculated as averages of the three measurements taken across the flume at each location, while the diamonds represent the final water surface elevations, also averaged from the three measurements across the flume. The stars are the final energy levels (E_i) obtained at each location by using the following equation:

$$E_i = z_i + Y_i + \left(\frac{Q^2}{2g(BY_i)^2} \right), \qquad (4\text{-}1)$$

where z_i is the elevation above the datum at cross-section i, Y_i is the average depth across the flume at cross-section i, Q is the flow rate, B is the channel width, and $Q/(BY_i)$ is the average

cross-sectional velocity. Linear trendlines were fitted to these points to obtain the friction slope, S_f, used for the shear stress calculations. Ideally, for uniform flow, S_f should be equal to S_0, but in practice the flow becomes mildly non-uniform. However, the average bed shear stress is still correctly evaluated from the slope of the energy grade line, which yields S_f (Henderson, p. 91, 1966).

Figure 4.3.a represents the different point gauge measurements for Run 1, for which the initial flume and bed slopes were set to 0.2%. The flow conditions for this run were such that there were only minor changes in bed and water surface elevations during the run, which are also confirmed when comparing the initial and final depths and mean velocities shown in Table 4.1. The bed slope changed to 0.1%, but the bed degradation and armouring were not significant and because of this, the bed was not reworked for Run 2 (Fig. 4.3.b). For Run 2, the initial flume slope was set to 0.4%, which was equivalent to the initial bed slope of 0.3%. To have a similar initial depth of flow as in Run 1, the discharge had to be increased to 0.074 m^3/s. This meant a substantial increase in initial velocities, followed by more degradation and stronger armouring. As a consequence of the increased roughness, the average depth increased by almost 4 cm during the run, while the mean velocity decreased by nearly 0.2 m/s (Table 4.1.).

However, it became apparent in Run 2 that the artificial bed upstream of the test section had to be changed for the following experiments, if a substantial scouring at the beginning of the test section was to be avoided. The fixed bed upstream of the test section was 10 cm thick (same thickness as for the test section), and was artificially roughened with relatively uniform gravel grains (D_{50} = 25 mm) glued onto a false floor. As the run progressed, the degradation

increased and the difference in elevations between the artificial section and the test section increased. A scour hole was formed at the beginning of the test section, as the artificial bed "transformed" into a step. Therefore, for the following runs, the bed elevation of the artificial upstream section was lowered to better match the bed elevations of the test section once the degradation occurred. For Run 3, the artificial bed was also composed of fixed gravel grains, but the elevation was lowered by 5 cm, while the test section sediment depth was still left at 10 cm. Unfortunately, this proved to be too low and the influence of such low entrance conditions could be identified in the first 2 m of the test section (Fig. 4.3.c), which was an indication that the upstream conditions needed another modification.

For Runs 4 and 5, the upstream artificial bed section was approximately 7 cm thick, composed of the same uniform gravel grains as in Runs 1 through 3, but now they were not fixed to the floor. The most immediate 1 m preceding the test section was covered with the same sediment as used in the test section, which meant that the top 2 cm of the artificial section was also loose, and the sediment could be transported downstream. The finer material could get transported all the way through the test section, but the larger sizes, as well as the loose artificial roughness elements did not get transported more than about 0.5 m into the test section, which did not represent a problem. The artificial roughness material was of different colour than the test material and it was easy to differentiate the two.

The loose artificial roughness elements placed upstream of the test section seemed to resolve the issue of a scour hole formation at the beginning of the test section. However, the flow conditions and the imposed slopes at the beginning of Runs 4 and 5 were such that

substantial degradation occurred and the bed slopes reduced considerably (Fig. 4.4.a and b). This bed slope reduction is attributed to different mechanisms of bed formation and armouring observed in different runs. In the first three runs (1 to 3), the bed formed through a parallel degradation process. In the initial transport phase, transverse bars were created and finer material (usually $< D_{95}$) was transported downstream in dune-like forms, while the largest grains did not move at all, or moved only short distances and then found a stable position again. The dunes travelled further downstream and out of the test reach, while the bed underneath armoured with larger grains. The bed coarsening caused transport rate to decrease, as less fine material was exposed and thus available for transport. The extent of bed surface coarsening and the amount of transported material depended on the initially imposed hydraulic conditions.

In runs 4 and 5, the sediment transport at the beginning of the experiment was very vigorous and all sizes moved downstream, again in a dune-like pattern. The beginning of the test section was not fed by transported material from upstream, which was the same for all runs, and because of high imposed flows, the degradation here was substantial. However, the material from this part of the test section was feeding the sections further downstream, so the bed slope decreased through time. Therefore, the amount of degradation also decreased in a downstream direction (Fig. 4.4.a and b). The bed in these runs armoured partially through degradation and partially through selective sediment transport. It seems that Runs 4 and 5 required a reduction in shear stress through friction slope adjustment in such a way that the grains could stabilize to accommodate the imposed flow conditions given the material composition on the bed.

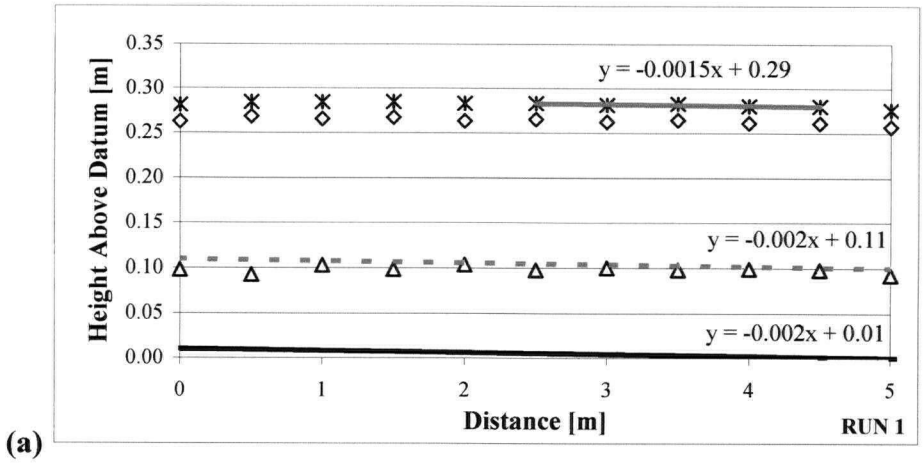

(a)

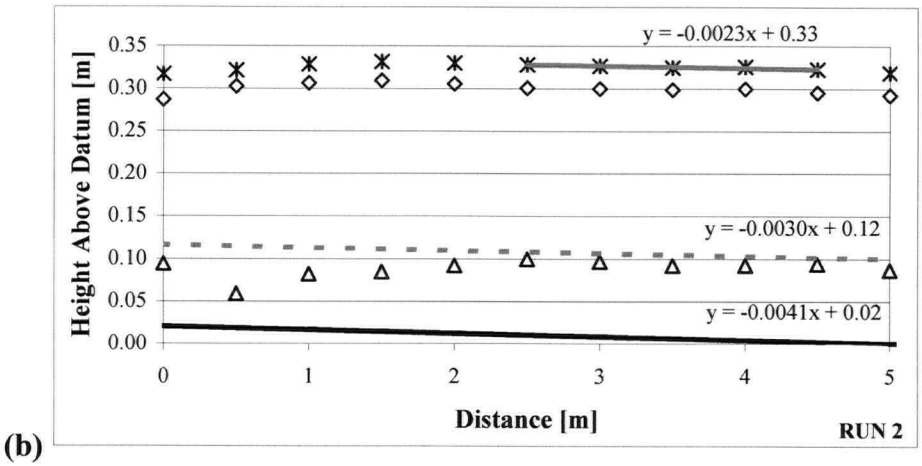

(b)

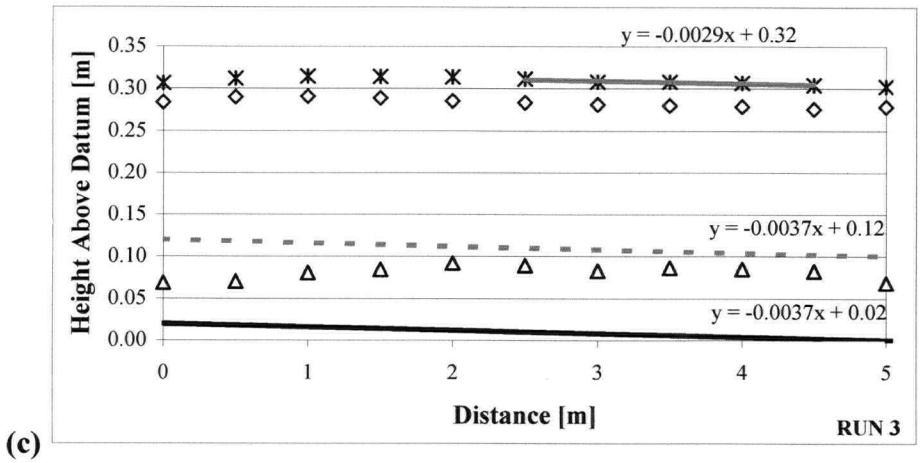

(c)

Figure 4.3. *Bed, water surface and energy slopes for Runs 1 through 3 (Figures a to c), where (—) is the flume bottom, (·····) is the initial bed level, (Δ) are the final bed elevations, (◊) are the final water surface elevations, and (∗) are the calculated energy elevations.*

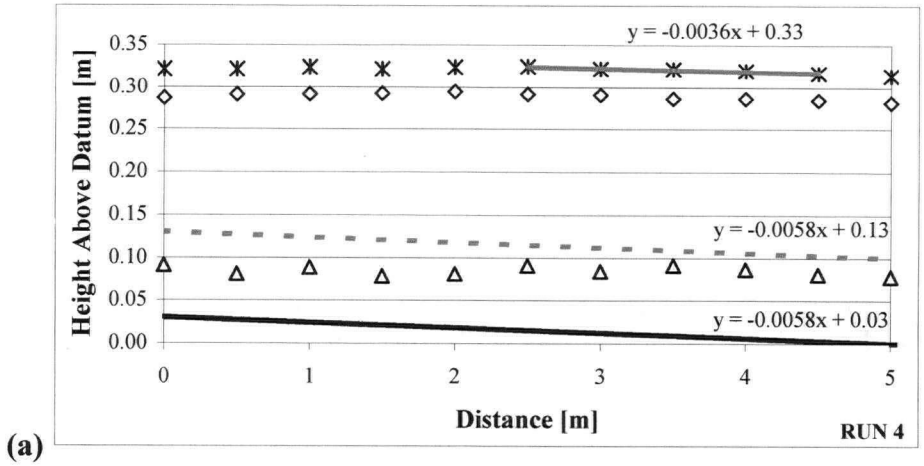

(a)

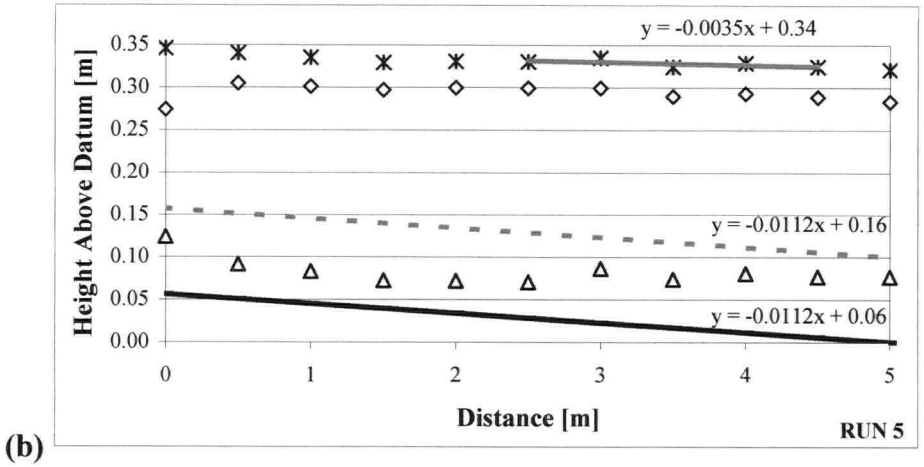

(b)

Figure 4.4. *Bed, water surface and energy slopes for Runs 4 and 5 (Figures a, b), where (—) is the flume bottom, (····) is the initial bed level, (Δ) are the final bed elevations, (◊) are the final water surface elevations, and (∗) are the calculated energy elevations.*

To determine the bed, water and energy slopes, a representative part of the test section had to be identified. Because of a relatively short test section and a small number of points, the slope estimates were very sensitive to which points have been included when fitting the least square regression lines. For this reason, it was important to determine parts of the test section for which the slope estimates were consistent, and where the influence of upstream or downstream conditions was not present. Figure 4.5. illustrates the range of friction slopes

calculated for each run and for different lengths of the test section. In general, the slope determined for the whole length of the test section (i.e. from 0 to 5 m) formed a lower bound, because data from the beginning of the test section were included, and because this part was largely influenced by the upstream conditions and usually experienced more degradation than the rest of the test section (see the bed profiles in Fig. 4.3. and 4.4.). Slopes determined for the section between 3 and 5 m of the test section generally formed the upper bound, because these included the end point of the test section at the 5 meter mark, which was usually somewhat lower and influenced by downstream conditions. The other distances examined for slope determination were between 1.5 and 4.5 m, between 2 and 4 m, between 2.5 and 4.5 m, and between 3 and 4.5 m.

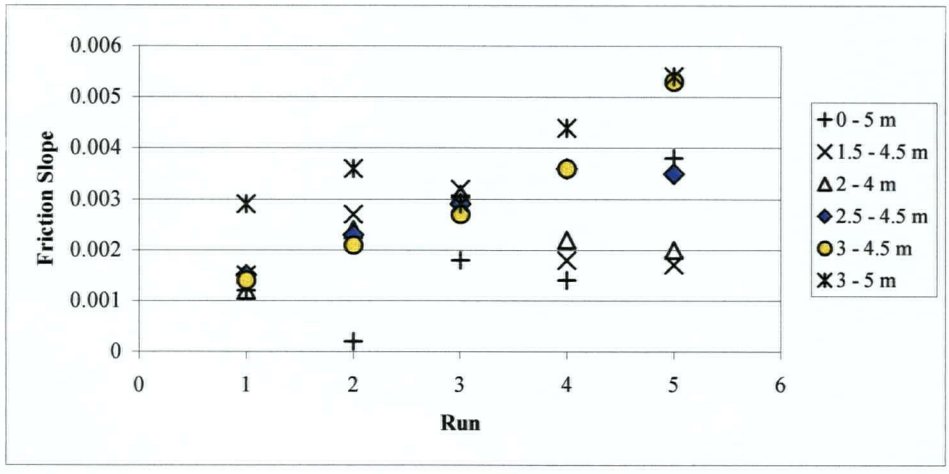

Figure 4.5. *Friction slopes determined for each run for different segments of the test section.*

The scatter in determined slopes is considerable, but for Runs 1 through 4, the channel lengths between 2.5 and 4.5 m, and between 3 and 4.5 m produced consistent friction slopes. These friction slopes increased for each subsequent run, which was consistent with increased

slopes imposed at the beginning of the runs, although the final friction slopes were always somewhat lower than the initial ones. Thus, for these runs the final friction slopes were determined for points between 2.5 and 4.5 meters (values given in Table 4.1.), and these slopes will be used to determine the shear velocities from the depth-slope method in Chapter 5. For Run 5, the points between 3 and 5 m, and 3 and 4.5 m resulted in similar friction slopes, but to make sure that the exit conditions from the test section did not bias the result, it was decided that the friction slope should also be determined for the section between 2.5 and 4.5 meters.

		Initial Conditions:			**Final Conditions:**				
RUN	**Q**	**Y**	**U**	**S_f**	**Y**	**U**	**S_f**	**Fr**	**Re x 10^4**
	[m^3/s]	[m]	[m/s]		[m]	[m/s]			
1	0.05	0.163	0.614	0.0020	0.164	0.61	0.0015	0.48	9.9
2	0.074	0.168	0.882	0.0030	0.204	0.725	0.0023	0.51	14.7
3	0.072	0.161	0.897	0.0037	0.198	0.727	0.0029	0.52	14.3
4	0.081	0.176	0.921	0.0058	0.201	0.806	0.0036	0.57	16.1
5	0.089	0.178	1.002	0.0112	0.216	0.824	0.0035	0.57	17.9

Table 4.1. *Initial and final hydraulic parameters for Runs 1 through 5*

Degradation – The measured bed elevations at different stages during the run made it possible to look at the bed development through time. Figure 4.6. illustrates the degradation through time for a point on the flume centreline 2 m downstream from the beginning of the test section for all five runs. As the imposed initial shear stress increased for each run, the degradation increased as well. Most degradation occurred in the initial phase of the experiment, lasting approximately 200 minutes, after which time it levelled off and the bed elevations did not change significantly.

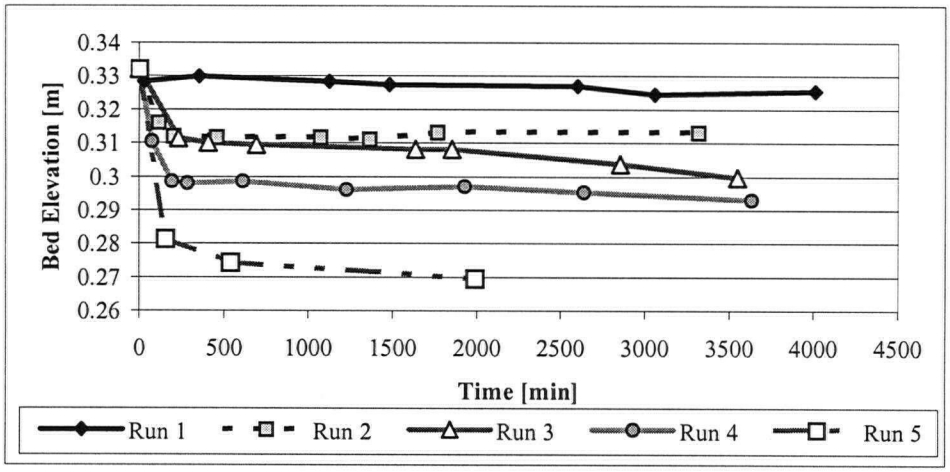

Figure 4.6. *Degradation through time for Runs 1 through 5 for a point on the flume centreline 2 m downstream from the beginning of the test section.*

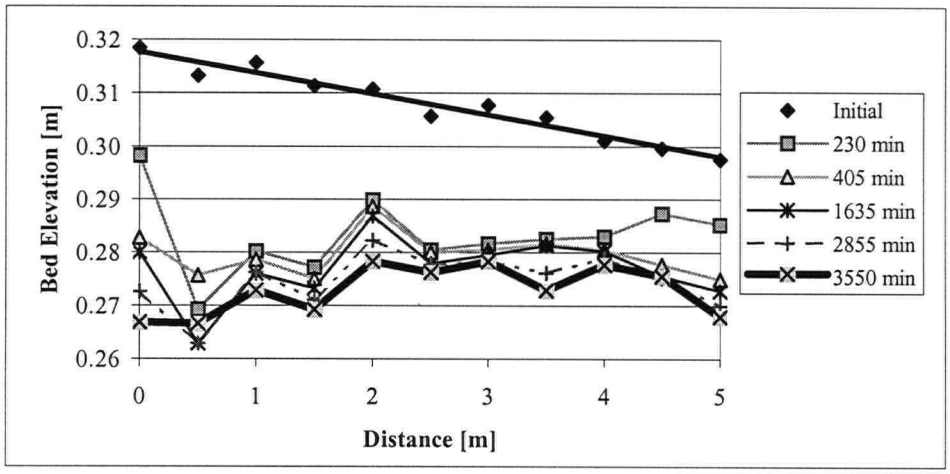

Figure 4.7. *Bed development through time for Run 3 on the flume centreline and along the whole test section (note: vertical scale exaggerated by a factor of 50).*

Figure 4.7. illustrates the bed development for Run 3 for the whole length of the test section at some of the times during the run when the bed was surveyed. Again, it can be seen that most of the degradation occurred during the first 230 minutes. The degradation continued as the experiment progressed, but at a much slower rate. The profile measured at 230 minutes

shows two dunes passing through the channel at about 2 m and 4.5 m downstream from the beginning of the test section. The degradation was more extensive at the beginning of the test section, which was due to the low elevation of the artificial bed upstream of the test section.

The average degradations for the whole test section, as well as for the section for which the final slopes and depths were determined are given in Table 4.2. The degradations for the whole test section (0 to 5 m) were considerably higher than for the section between 2.5 and 4.5 m, also indicating that much more degradation occurred at the beginning of the test section. This was partially due to the entrance conditions and partially to the fact that the most upstream segment of the test section was feeding sediment to the downstream segments.

Run	Average Degradation 0 – 5 m [mm]	Average Degradation 2.5 – 4.5 m [mm]
1	9.4	6.9
2	14.9	7.6
3	31.3	22.0
4	32.2	24.4
5	46.1	34.3

Table 4.2. *Average degradations at the end of Runs 1 through 5.*

4.2.2. Discharge measurements

Continuous discharge measurements were obtained and recorded for all five experiments using a VersaFLO Sonic Flow System by TN Technologies, which was installed on the inlet pipe which supplied water to the experimental flume. This is a non-intrusive flow measuring system, comprised of a multiprocessor transmitter and a pair of transducers, clamped onto the

inlet pipe (Fig. 4.8.). The difference between the reflected and transmitted frequencies, or the Doppler shift, is directly proportional to the linear velocity of the fluid in the pipe, which is then converted into discharge. The typical accuracy of the instrument is ± 2 - 5% of the full scale, which was defined when setting the instrument as 0 to 180 l/s. During experiments, the discharge reading varied slightly and within 1 – 2 l/s. The discharge measurements (Table 4.1.) were used to calculate the mean flow velocity in the flume, and to compare with velocities measured by the ADV.

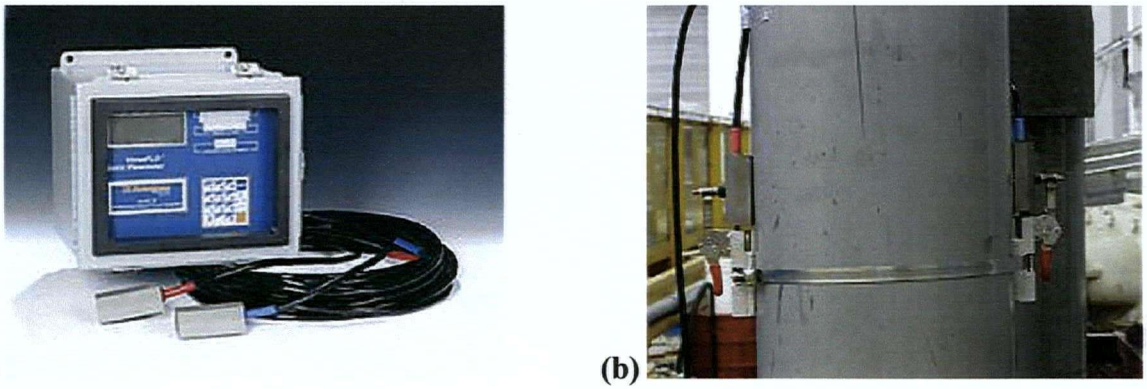

(a) **(b)**

Figure 4.8. *VersaFLO flow meter: (a) The multiprocessor transmitter and a pair of transducers; and (b) The transducers mounted on the inlet pipe (ID 10").*

4.2.3. Temperature measurements

Water temperatures were measured with a reading accuracy of 0.5°C, using a standard glass thermometer at the beginning of experiments, several times during velocity measurements and at the end of experiments. Temperature is an input parameter for the ADV setting, because the instrument calculates the speed of sound, and adjusts the velocity calculation, based on water temperature and salinity (which was zero for these experiments). For instance, for a 5°C change in water temperature, the speed of sound changes by

approximately 1% and the associated change in estimated water velocity is of the same order (SonTek, 1997).

It was observed that, during experiments water temperature increased by approximately 1°C in a day, which means that if an experiment lasted for 3 or 4 days, the temperature would change from the starting 16°C to about 20°C. The variation in water temperature changes the physical properties of water. Variations in water density, or specific weight, are insignificant; and for a change of 5°C, the density would vary only by about 0.10% (Table 4.3.). However, the change in kinematic viscosity is much more significant; and for a change in water temperature of 5°C, the kinematic viscosity changes by over 10%. Viscosity changes are reflected in the Reynolds number ($Re=UY/\nu$). For a rough surface, the fully rough turbulent flow regime starts from $Re > 10^4$ (Henderson, 1966), and the flow resistance is then entirely due to form drag on protruding particles. This condition was an important prerequisite in our experiments, because in our numerical model one of the assumptions is that the total flow resistance is due to the form drag on protruding particles. During all five experiments, the flow was fully rough turbulent flow, irrespective of the water temperature (e.g. Run 1 had the slowest velocities and lowest depths, for which the Reynolds numbers shown in Table 1 were well above 10^4). Viscosity changes can have important effects on the settling velocities of very fine particles. However, this was not a concern because the finest sediment size was 1 mm and this size is not so much influenced by viscosity changes.

Temperature, T	Specific weight, γ	Density, ρ	Kinematic viscosity, ν x 10^{-6}	Reynolds number, Re x 10^4
[°C]	[N/m^3]	[kg/m^3]	[m^2/s]	
15	9801	999.1	1.141	8.8
20	9792	998.2	1.007	9.9
25	9777	997	0.897	11.2

Table 4.3. *Physical properties of water and Reynolds numbers for Run 1.*

4.3. Flow Velocities

Velocity measurements were performed using a SonTek MicroADV (Fig. 4.9.) operating at 50 MHz and analysed using the WinADV software, version 1.845 (Wahl, 2000a). The purpose was to compile velocity profiles from point measurements for different locations in the flume. If the profiles proved to fit the logarithmic distribution, they would be used to determine the shear velocity (u^*) and the equivalent roughness parameter (k_s).

The instrument estimates the velocities by using a technique called pulse coherent Doppler processing, where the ADV measures the change in phase of the return signal from two successive acoustic pulses. The acoustic return is not a reflection from a single target, but a superposition of the reflections from many individual particles contained in the sampling volume. The location of the sampling volume is determined by the geometry of the instrument, and for the MicroADV probe it is located 5 cm below the tip of the probe (Fig. 4.9.b). The standard size for the MicroADV sampling volume is a cylinder of water with a diameter of 4.5 mm and a height of 5.6 mm. The height of the sampling volume determines how close to the boundary the measurements can be made, and it is important that the stationary bed is not included in the sampling volume, because it would decrease the

measured velocity. Extensive explanations on ADV principles of operation can be found in SonTek Operational Manual (1997), Lohrman et al. (1994), Lane et al. (1998), and Voulgaris and Trowbridge (1998).

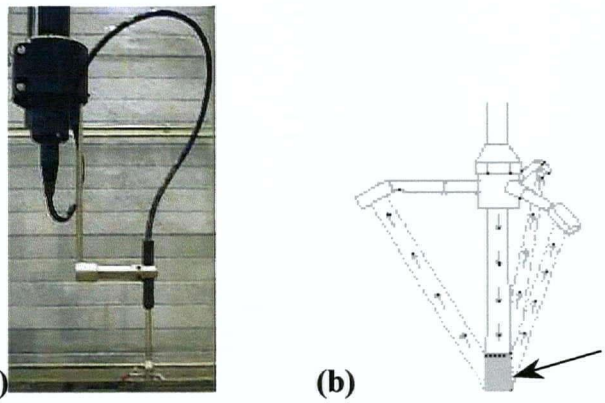

Figure 4.9. *The SonTek MicroADV: (a) The sensor mounted on a flexible cable; and (b) The sampling volume (copied from the SonTek web site).*

4.3.1. Measurements

For each experimental run, velocity measurements were taken at nine locations in the flume. The measurements were taken at three cross-sections that were 3.0 m, 3.5 m and 4.0 m downstream from the beginning of the test section, and were denoted A, B and C, respectively (Fig. 4.10.). For each cross-section, three velocity profiles were taken across the flume (in the middle of the flume and at the two quarter points), and were denoted Centre, Right and Left, looking downstream. The exceptions are Run 1, where profiles at four cross-sections were taken with the first cross-section being located at 2.5 meters from the beginning of the test section and denoted O (12 profiles in total); and Run 2, where only the centreline profiles were measured at 3, 3.5 and 4 meters.

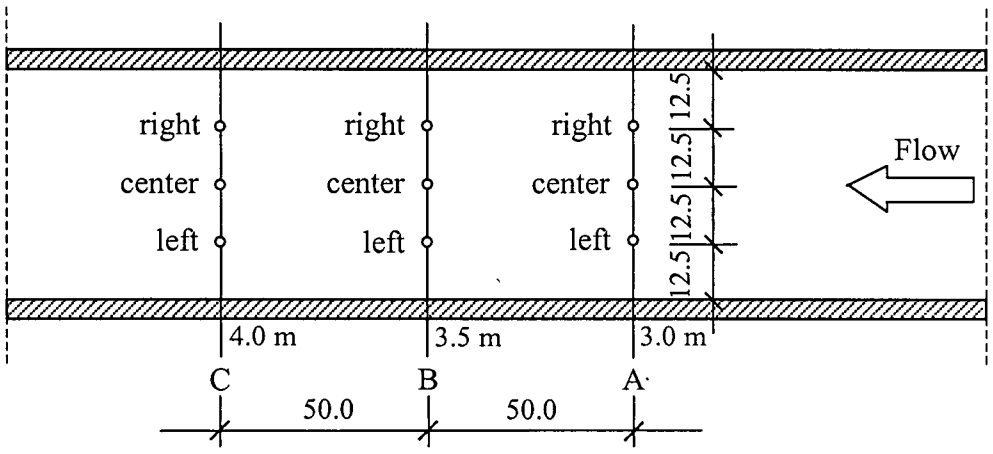

Figure 4.10. *Locations for velocity profile measurements.*

Each velocity profile consisted of measurements taken at ten to fifteen points in the lower half of the flow. The lowest point where measurements were taken was located at 0.5 to 0.7 cm above the bed, which ensured that the ADV sample volume did not include part of the bed. The duration of data acquisition was 60 seconds at each point.

4.3.2. Data analysis

Certain difficulties were encountered when analysing ADV measurements taken during these experiments. These difficulties, together with the guidelines from the equipment manufacturer, and the approach developed for data analysis will be discussed in this section. Some of this work was presented at an international conference on Hydraulic Measurements and Experimental Methods (Martin et al., 2002).

Difficulties - As the boundary becomes rougher, the velocity fluctuations become stronger, thus the ADV signal correlation decreases. Low correlations are associated with highly

turbulent flows, large velocity gradients within the sampling volume, the presence of large individual particles, or interference from the boundary. These influences will be explained in more detail after defining the signal correlation parameter.

Manufacturer guidelines - The ADV operation guidelines from SonTek (1997) recommend setting the velocity range "to the minimum value that covers the range of velocities expected in a given experiment", since the noise in the data increases with increasing velocity range. The velocity range setting will determine the sampling rate of the instrument, where a higher velocity range will result in a faster sampling rate. However, for highly turbulent flows, changing the velocity range to a higher setting may in fact reduce the noise level. The correlation parameter, which is a calculated value displayed during data collection, confirms the data quality and it is recommended that correlation should exceed 70%, while the signal-to-noise ratio (SNR) should consistently be above 15 dB. In the case of highly turbulent flows or highly aerated water, however, the mean velocity measurements can be used even if the correlations are as low as 30% (SonTek, 1997).

ADV signal correlation explained - A detailed analysis of the ADV correlation coefficient can be found in SonTek Technical Notes (1997), which was obtained on personal request, and is not included in the SonTek Operational Manual. A synopsis from this manuscript is given below.

The ADV measures the change in phase of the return signal from two successive acoustic pulses. The return signal is a superposition of the reflections from many individual particles contained in the sampling volume. Phase coherency is achieved if all particles in the

sampling volume maintain their relative positions with respect to each other, in which case the strength and relative phases of individual reflections would not change from one pulse to the next. However, Doppler noise is an inherent part of Doppler-based volume backscatter systems, and there are other sources of noise as well (detailed noise analysis is given in SonTek Technical Notes, 1997; and Voulgaris and Trowbridge, 1998). Thus, the return signal from the second pulse is not a phase-shifted reproduction of the first pulse, but contains a certain amount of noise, which can be added to the coherent part of the return signal:

$$S_1' = S_1 + N_1 \qquad \text{and} \qquad S_2' = S_2 + N_2 \qquad (4\text{-}2)$$

In the above equations, S_1' and S_2' are the return signals from two adjacent pulses, S_1 and S_2 are the coherent parts of the signal, and N_1 and N_2 represent the random noise. The noise adds a random error to the measured phases and to the measured velocities. If the coherent signal power is compared to the total power, i.e. $S_i^2 / (S_i^2 + N_i^2)$, a measure of noise is obtained. It is this ratio that is commonly known as the ADV correlation coefficient and is a direct measure of the Doppler noise in the velocity data.

In practice, the ADV estimates the phase shift between return signals from two successive pulses using a complex auto-correlation function, which has a phase and a magnitude. The phase is proportional to the distance the scatterers have travelled in the time between pulses, and thus to the velocity. The magnitude is a measure of how similar the echoes from two return signals are, and the normalized magnitude gives the correlation coefficient. If the echoes from two neighbouring pulses were identical and only with a phase change, the correlation would be perfect and equal to 100% (i.e. $N = 0$). As the echoes become more dissimilar, the correlation decreases.

In our experiments, the possible reasons for the signal decorrelation are:

- *Turbulent flows* - in such flows it is reasonable to assume that the particles in the sample volume will not maintain their relative positions with respect to each other, thus adding to the Doppler noise of the return signal. This will decorrelate the signal and in this case, low signal correlations will not necessarily mean that the data are bad (see Wahl, 2000b). It is difficult to differentiate between the increased true variability in velocities within the sample volume and the variability in the data due to decorrelation and associated uncertainty in the Doppler noise estimates. In addition, if the turbulent eddies are of the same order as the sample volume or smaller, the noise in velocity measurements will appear to increase, and the correlation will change even more.
- *The presence of large individual particles* - sound being reflected from a number of different points close to the measuring volume confuses the instrument and decorrelates the signal. The occasional saltating grains can be included in this category.
- *Interference from the boundary* – occurs when the return signal from the boundary interferes directly with the return signal from the measuring volume (this problem is more prominent for the downward looking probe), creating a "velocity hole" at particular elevations above the bed, where noise masks the velocity signal (Lane et al., 1998). This effect can be recognized in the ADV output file if the instrument attempts to change the velocity range setting. This deficiency of the instrument can be somewhat corrected by changing the velocity range setting of the instrument, because different settings experience the "velocity hole" at different elevations above the bed. However, in some cases there were regions above the bed where different velocity range settings would not reduce the noise, and those data points had to be rejected. For this instrument and the

given boundary roughness, the velocity hole was experienced at about 1.5 to 3.5 cm above the bed.

- *Large velocity gradients within the sample volume* - the noise due to velocity shear becomes important for elevations close to the boundary, i.e. $y < 0.1Y$, which is equivalent to the bottom 2 cm in our experiments (Lhermitte and Lemmin, 1994). However, the noise values associated with this source are not significant and can be ignored (Voulgaris and Trowbridge, 1998).

It was considered that turbulence and rough bed conditions were the primary reasons for low correlations in these ADV measurements. The SNR values were usually above 15 dB.

Approach to data analysis - In general, for measurements within 5 cm of the bed the correlations were lower than 70% and this was attributed to increase in turbulence. To test this assumption, a set of experiments was designed in which measurements were first performed over a smooth bed (where the turbulence intensity was expected to be low), and then for increasingly turbulent environments for flows over smooth or rough beds. The correlations were high for flows over a smooth bed and decreased considerably for flows over smooth or rough beds as the turbulence increased (Appendix A). A supplementary test was to vary the ADV velocity range setting from 100 cm/s to 250 cm/s to examine how this change affects the correlation. It was confirmed that for highly turbulent flows, a higher velocity setting improved the correlation by about 20%; however, there were cases close to the bed when the correlation decreased (Appendix A). In general, the velocity setting of 100

cm/s provided more consistent results close to the bed (up to 3 cm above the boundary). For distances higher than 3 cm, the ADV velocity range setting of 250 cm/s gave better results.

It is a standard practice to edit and remove bad data points by setting the correlation filter to 70% (SonTek, 1997; Lane et al., 1998; Wahl, 2000a,b). However, given the turbulent nature of flows in these experiments, and thus the low correlation for much of our data, it was necessary to relax this criterion. Since in this study only the average longitudinal velocities at a point were used, while the turbulence structure was not examined in detail, it was essential to determine the variability in average velocities for different degrees of filtering based on correlation. It was found that the average velocities were fairly insensitive to the value of the correlation filter (Appendix A.2.). The filtering criterion could be as low as 30 to 40% correlation with consistent average velocities (within 3%), however there were cases when the differences were as high as 10%. The differences were somewhat higher closer to the bed and decreased as the distance from the bed increased.

The percentage of data retained after applying the correlation filter does not indicate if the velocity value is consistent (Appendix A.2.). However, including more data, even if the correlations are less than 70%, is preferable to using averages based on a very small number of the total data points. Therefore, if there were less than 70% data retained for the analysis after applying the correlation filter, the velocities at that point were excluded.

In summary, the velocity measurements in these experiments were analysed with the correlation filter set to 70% and the average velocities were kept for points for which there

were more than 70% velocity data retained. For points with less than 70% data retained, the analysis was repeated with the filter set to 40% correlation, and again the average velocities were kept if there were more than 70% data retained.

4.3.3. Velocity profiles

For all runs, velocity profiles were measured at various locations across and along the flume (see Fig. 4.10.). These profiles are compared to determine the uniformity of the flow throughout the test section. As a second step in the velocity analysis, the velocity data are plotted on a semi-log graph to test whether they follow a log velocity relationship. If this semi-log plot is good, then the best fit linear relationship is used to determine the coefficients in the log velocity relationship:

$$u_y = 5.75u^* \log\left(\frac{30y}{k_s}\right) \tag{4-3}$$

which can be expanded to:

$$u_y = 5.75u^* \log y + 5.75u^* \log\left(\frac{30}{k_s}\right) \tag{4-4}$$

The slope of the semi-log graph yields the value of $5.75u^*$, and the intercept yields a value from which k_s can be determined.

The variability in the shear stress and the hydraulic roughness, k_s, will be discussed in detail in Chapter 5, while this section will deal with velocities only. Therefore, this assessment will provide more of a qualitative analysis of the profiles, while the analysis of the parameters calculated from the profiles will provide some quantitative answers in the next chapter.

Variations in velocity profiles across the flume – Comparison of velocity profiles across the flume should show whether the flow conditions were uniform across the flume, and if sidewall effects were considerable. The three velocity profiles of each cross section and for each run were plotted on separate graphs, and Figure 4.11. represents the velocity profiles for Run 5, while similar profiles for Runs 1 through 4 can be found in Appendix B (Figures B-1 through B-4). Visual inspection of these figures confirmed that there was some variability observed between the profiles reflected in slower velocities for the profiles near the walls.

The majority of the profiles fit the logarithmic velocity distribution, however, there are several profiles that are clearly segmented (Voulgaris and Trowbridge, 1998), where the velocity profile changes slope at approximately $y = 0.1Y$ (e.g. Run 5 – A Centre and Left (Fig. 4.11.a); Run 5 – B Centre and Right (Fig. 4.11.b), etc.). This can be explained by the flow responding to two different roughness lengths, where the smaller length defines the vertical distribution of velocities near the bed, while the larger length determines the profile above the elevation of about 2 cm (personal communication with M. Church, 2002). Therefore, the lower segment extends only through the lowermost 2 cm of the flow (i.e. $y/Y < 0.1$) and this part of the velocity profile is strongly influenced by the local conditions on the bed. Consequently, for the runs where the bed roughness was higher, more segmented profiles with larger differences in slopes could be identified. The upper segment of the velocity profile, however, is more influenced by the overall resistance to flow and the roughness would be representative of a larger area upstream of the location where the profile was measured. In addition to velocity data, the values of Reynolds stresses were also

determined from ADV measurements, and these Reynolds stress profiles confirmed that there was a break at approximately 2 cm above the bed (see further discussion in Section 4.4.).

The velocity profiles for Runs 1 to 5 compared across the flume, were re-plotted with velocity data from the bottom 2 cm excluded. Figure 4.12. represents the re-plotted velocity profiles for Run 5, while the profiles for the first four runs can be found in Appendix B (Figures B-5 through B-8). The bottom data exclusion resulted in less variability between the profiles within a particular cross section (e.g. compare cross section B for Run 5 in Fig. 4.11.b and Fig. 4.12.b).

This thesis concentrates on the overall flow conditions leading to a formation of armoured beds and, thus, the u^* and k_s values that are representative of a larger area were of primary interest. It was considered that these values would better represent the average flow conditions, and it was decided that velocity data from the bottom 2 cm could be omitted from further analysis. Also, the average shear velocities obtained from such profiles should compare better with the shear velocities obtained from the depth-slope method, which are considered to be the values that represent average conditions in the flume.

The second consideration was to compare the centreline velocity profiles to the profiles measured closer to the flume walls. For most cross sections and for all runs, the velocities were somewhat higher on the centreline of the flume than at the walls. This observation confirmed that the sidewalls affected the velocities near the walls, where the velocities were lower. The differences between the mean centreline and mean quarter point velocities ranged

between 4% and 22%, but the average difference was around 12% except for Run 1, for which the velocities were lower than for the rest of the runs, and the differences averaged at around 6%. The same trend was not confirmed for Run 2, where only the centreline profiles were measured (Figure B-6 in Appendix B.).

After a qualitative comparison of velocity profiles across the flume, it was concluded that the centreline velocities were higher than the velocities measured at the quarter points of the flume, but the conditions developed more or less symmetrically around the centreline, causing similar profiles on the left and right hand side. The reduced velocities for profiles measured at the quarter points could be attributed to the sidewall effects. Otherwise, in terms of the profile slopes, the conditions across the flume were similar, resulting in development of similar velocity profiles and similar shear velocities in each cross section.

Variations in velocity profiles along the flume - Comparing the profiles along the flume should provide information on whether reasonably uniform flow conditions were achieved in the experiment along the test section. Figure 4.13. represents the velocity profiles for Run 5, where the profiles taken along the flume and on the same transverse location in the flume were plotted with data from the bottom 2 cm excluded (see discussion in previous Section). Velocity profiles compared along the flume for Runs 1 through 4 are plotted in Figures B-9 through B-12 in Appendix B.

The examination of Figure 4.13. and Figures B-9 through B-12 in Appendix B, show very little discrepancy between velocity profiles for any of the runs, when compared along the

flume. In Runs 4 and 5, where the roughness and consequently the turbulence were increased, a somewhat higher variability between the profiles was observed than in Runs 1 to 3. However, there was no consistent increase or decrease identified in velocities when the profiles were compared in the downstream direction, indicating that the differences were not due to flow non-uniformity. The comparison of the velocity profiles along the flume demonstrated that the flow was uniform within the working section. The minor differences could be attributed to differences in turbulence experienced locally for flows with higher roughness.

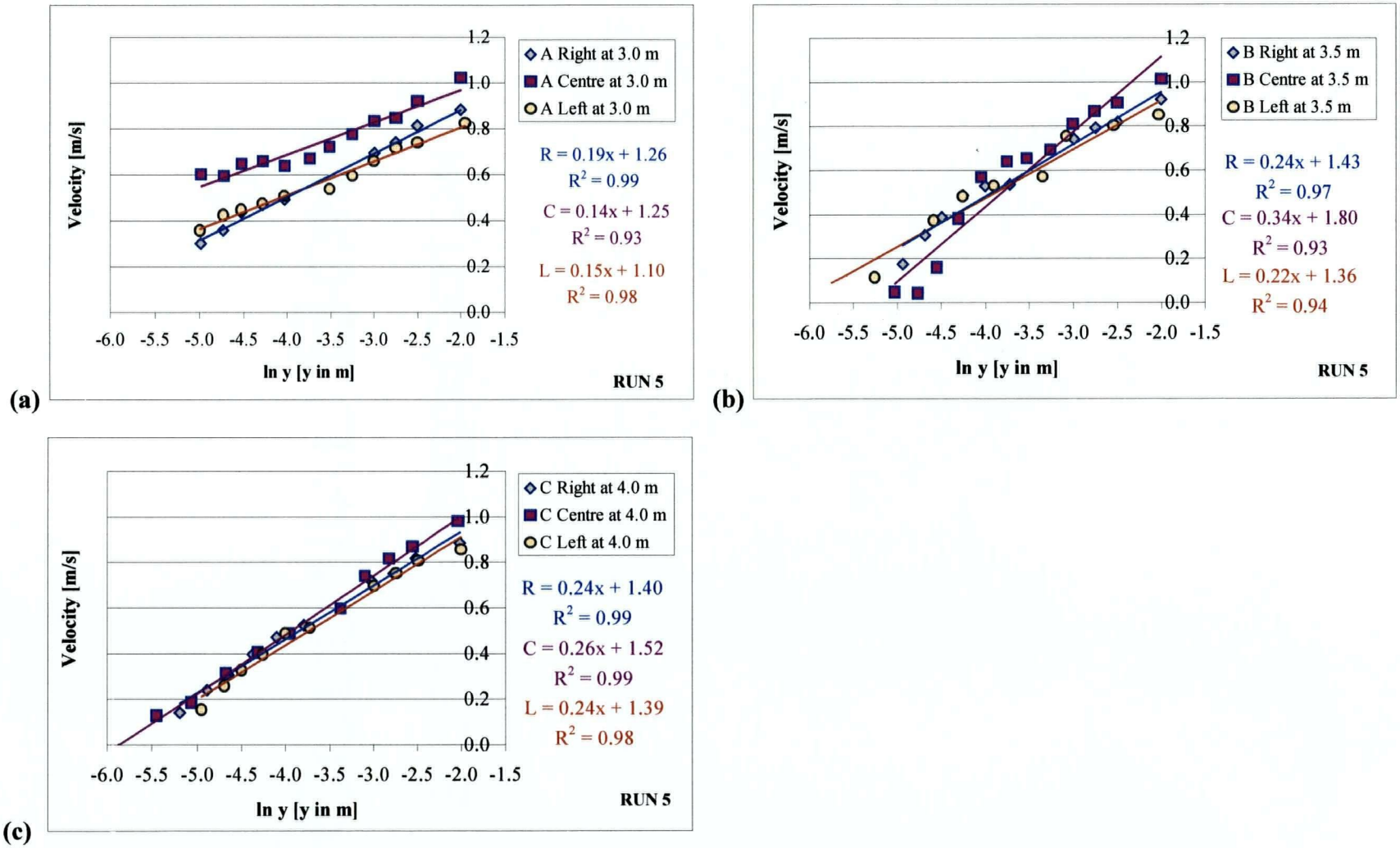

Figure 4.11. *Velocity profiles compared* ***across*** *the flume for Run 5: (a) cross section A; (b) cross section B; (c) cross section C.*

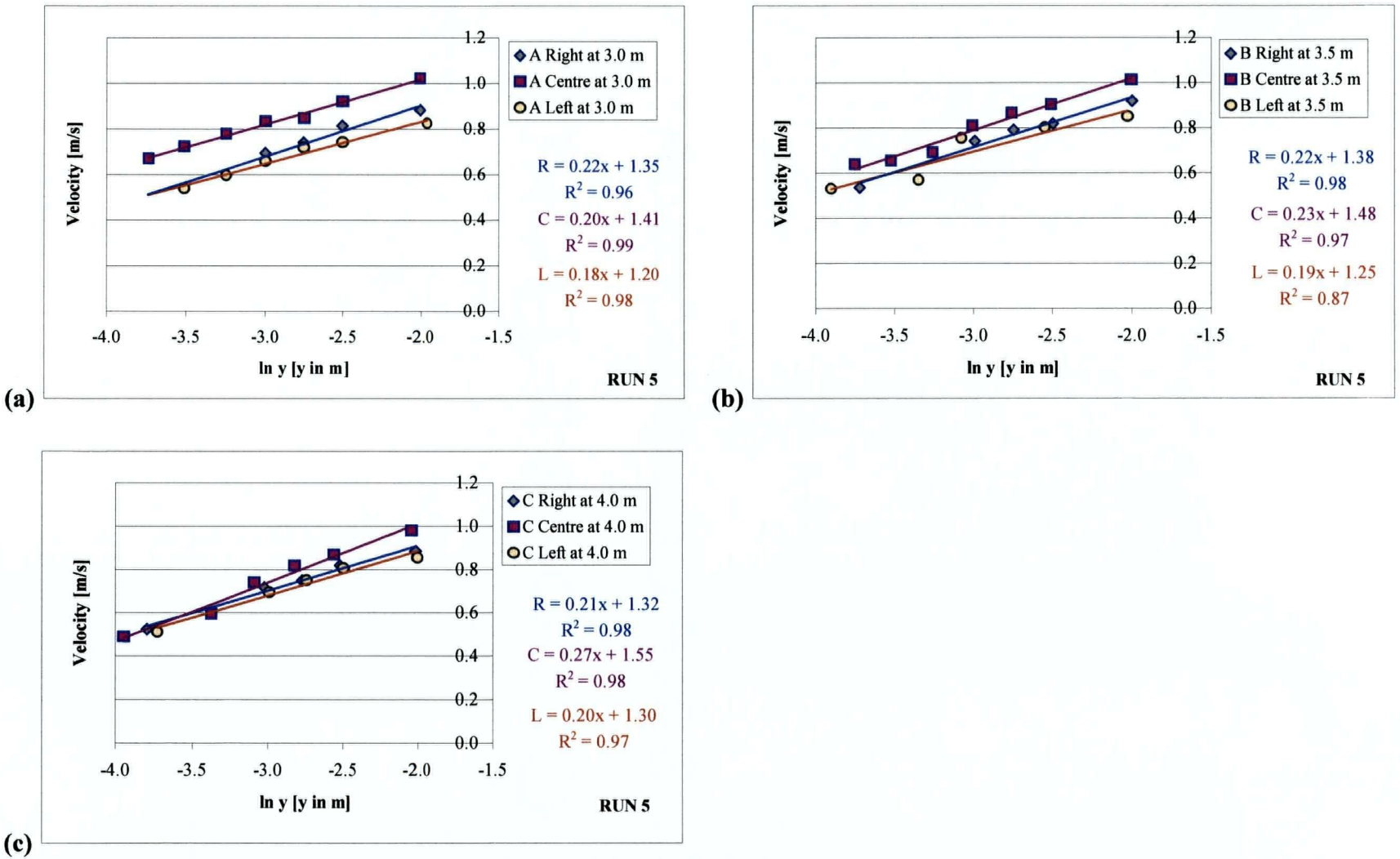

Figure 4.12. *Velocity profiles compared* ***across*** *the flume for Run 5 without data for bottom 2 cm: (a) cross section A; (b) cross section B; (c) cross section C.*

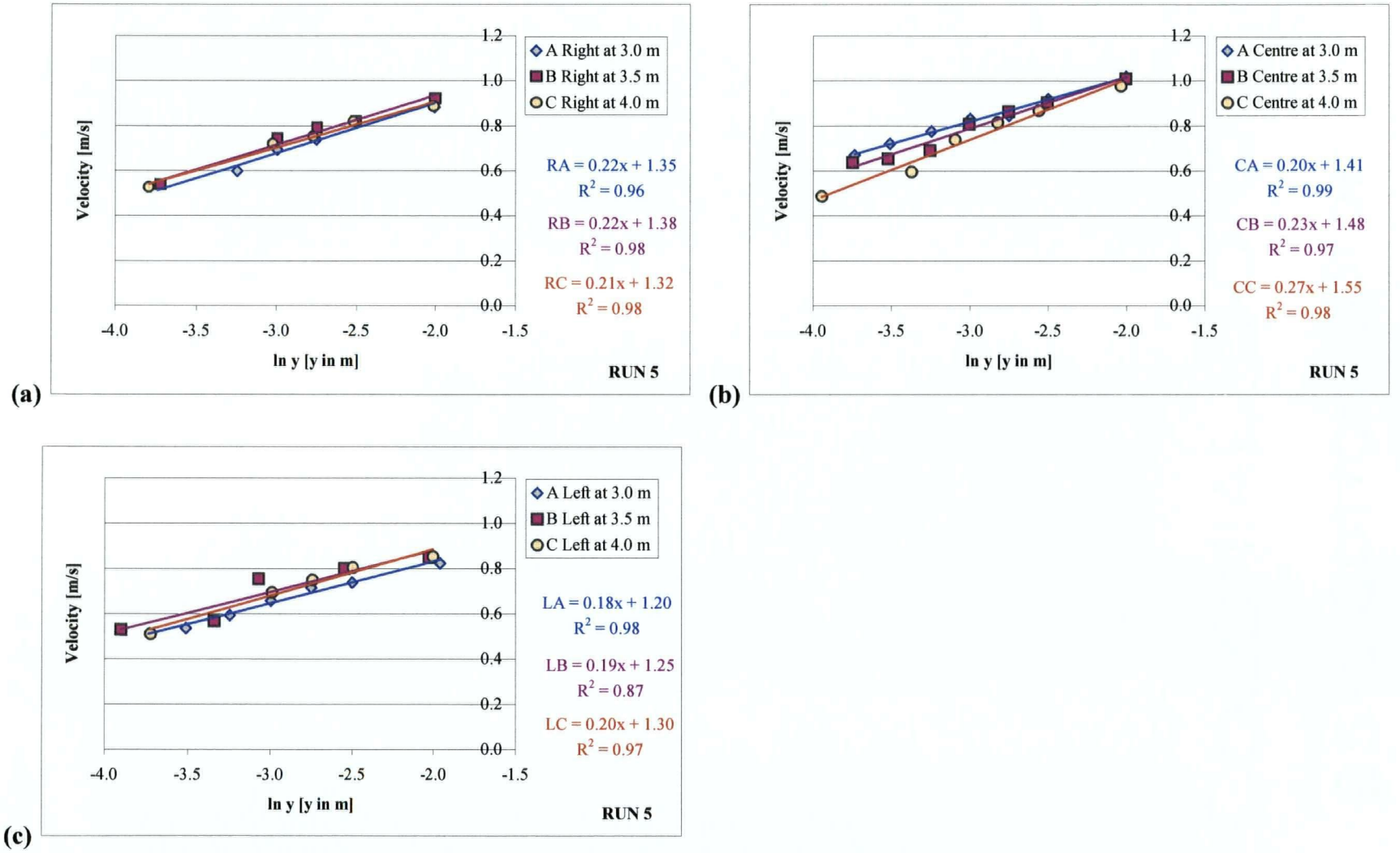

Figure 4.13. *Velocity profiles compared* ***along*** *the flume for Run 5 without data for bottom 2 cm: (a) Right profiles; (b) Centreline profiles; (c) Left profiles.*

4.4. Reynolds Stresses from ADV Measurements

Turbulence measurements obtained with the ADV were used to derive the Reynolds stress, $-\rho\overline{u'w'}$, where ρ is the water density equal to 1000 kg/m^3, and u' and w' are the longitudinal and the vertical velocity fluctuations. When the Reynolds stress is plotted against the depth, the shear stress profile is obtained, and the shear velocity at the bed can be calculated. Theoretically, the shear stress is equal to zero at the water surface and increases linearly with depth, reaching a maximum value at the bed. In reality, the shear stress at the surface can be negative because of the wavy surface (Martin, 1996), which is the case in rough turbulent flows, noticing that it is almost impossible to do reliable measurements in the surface zone if it is not flat. The shear stress can also decrease substantially close to the bed if there are larger protruding grains, dunes or other roughness elements present on the bed, or if there are moving particles interacting with the flow (Biron et al, 1998; Voulgaris and Trowbridge, 1998; Nikora and Goring, 2000; Afzalimehr and Anctil, 2001, Martin et al., 2002).

For the experiments in this research, Reynolds stresses were observed to linearly increase from the water surface towards the bed, and then to decrease at elevations of approximately 2 cm above the bed, even though there were variations between the runs and between the different profiles in each run. These elevations generally coincided with elevations where the velocity profiles changed slope (see Section 4.3.3. for details). Therefore, to estimate the total shear stress at the bed (and thus the shear velocity), a least squares linear regression line was fitted to that part of Reynolds stress profile where a linear distribution was observed, which was then interpolated to the bed (Fig. 4.14.). For example, for the centreline profile of cross-section A in Run 4, the linear regression line was fitted to the data measured at 2 cm

and above (shaded diamonds in Fig. 4.14.), which was extended to the bed to obtain the maximum shear stress there, equal to $\tau_0 = 5.6$ N/m^2 in this case. The lowermost three points were omitted when fitting the regression line (open diamonds in Fig. 4.14.), because the shear stress at these points was decreasing, indicating that the higher protruding grains on the surrounding bed were picking up the difference in shear.

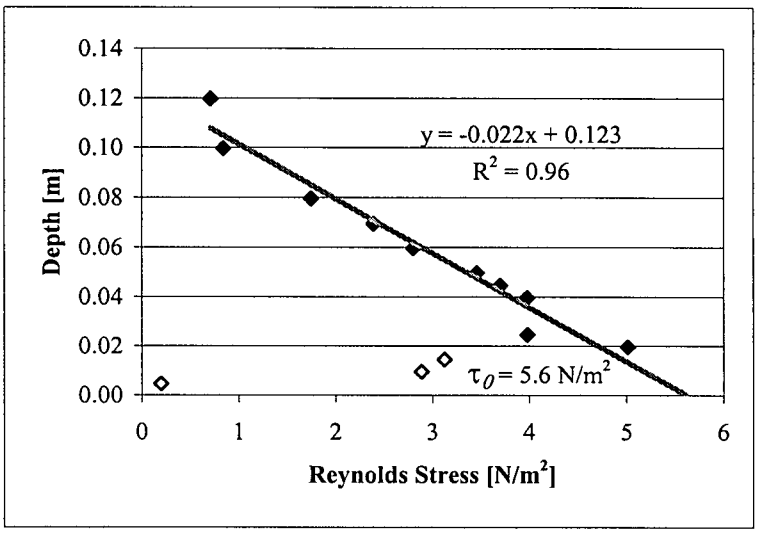

Figure 4.14. *Determination of the total shear stress at the bed from Reynolds stresses for Run 4, cross-section A, centreline profile.*

Several issues needed to be considered when analysing Reynolds stresses:

- Measurements where boundary interference was experienced,
- Inclusion of data edited with the 40% correlation filter; and
- Inclusion of the zero shear stress value at the water surface.

4.4.1. Boundary interference

Data where boundary interference was experienced were not used in the analysis, because the correlations were usually very low for those measurements. In these regions, the return signal from the bed interferes with the return signal from the sample volume, creating a "velocity hole" (Lane et al., 1998), thus it was considered that the data were not reliable. These regions could be identified because the ADV tries to change the velocity range that was set by the operator before taking measurements.

4.4.2. Inclusion of data edited with the 40% correlation filter

The ADV data were edited and bad data removed using correlation filters set at 40% and 70%, as discussed in detail in Section 4.3.2. Data filtered with 40% correlation would presumably include more noise. Since the velocity data for all experiments were edited using the 40% and 70% correlation filters, the same principles were also applied when analysing the Reynolds stresses. In Figure 4.15.a, the Reynolds stress profiles vs. depth are plotted for Run 5, and the values derived after applying the 40% (squares) and the 70% (diamonds) correlation filters are illustrated. The trendlines in Figure 4.15.a are fitted to the linear part of the profiles (i.e. the top four points are used in determining each trendline), and the corresponding values of the interpolated bed shear stresses are given for the two correlation criteria. Since some of the Reynolds stress values in the near bed region differed substantially for the two correlation filters, the same data were plotted in Figure 4.15.b in terms of the percent of data retained vs. depth. It is evident in this figure that for some of the points, less than 20% of data was retained when the correlation filter was set to 70%, and calculating the Reynolds stresses with such few data affected the final values. However, when comparing the

total bed shear stress, the difference is only 2% (5.46 vs. 5.35 N/m^2) if the derived values are based on 70% or more data retained. Therefore, some further analysis was needed to determine if the Reynolds stress data obtained with the 40% correlation filter should be used when determining the local bed shear stress.

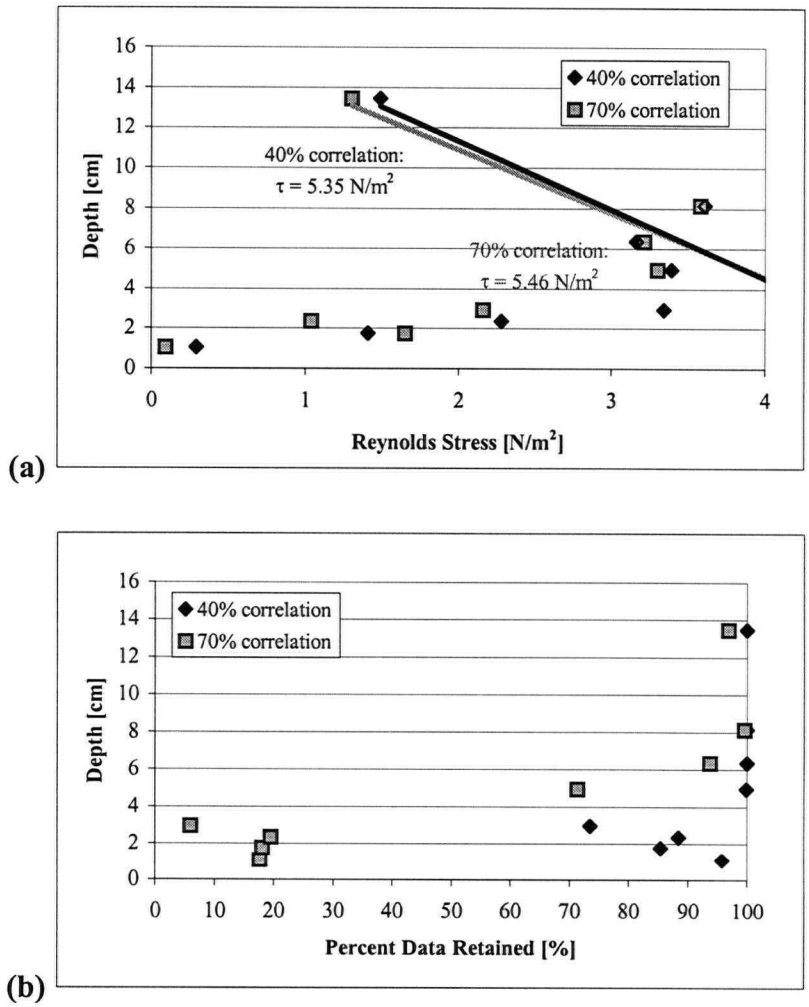

Figure 4.15. *ADV measurements for the centreline profile of cross-section B, Run 5: (a) Reynolds stresses; and (b) Percent of data retained for analysis.*

For the experiments represented in this thesis, and for the ADV measurements undertaken in the region sometimes even up to 5 cm above the bed, the average correlation was often lower then 70%. This meant that insufficient data would be retained after applying the 70% correlation filter (see Section 4.3.2. and Appendix A for additional discussion). Therefore, many of the data points in this region were analysed using the 40% correlation filter, although the points higher up in the flow were analysed using the 70% correlation filter. To examine if the Reynolds stresses derived from such edited data should be used when determining the shear stress on the bed, the shear stresses were compared for 40% and 70% correlation filters (Fig. 4.16.). For many points the inclusion of the 40% data did not change the estimated value of the shear stress on the bed substantially (i.e. $< \pm 10\%$). However, there were profiles for which the value changed by 20% or more, especially for higher shear stress runs, for which the higher variability in the estimated values could be attributed to the increased turbulence near the bed. Also, in Run 5 more measurements were taken closer to the bed than higher above (see Fig. 4.15.a), thus the trendlines were determined on a smaller number of data points and that could introduce some uncertainty.

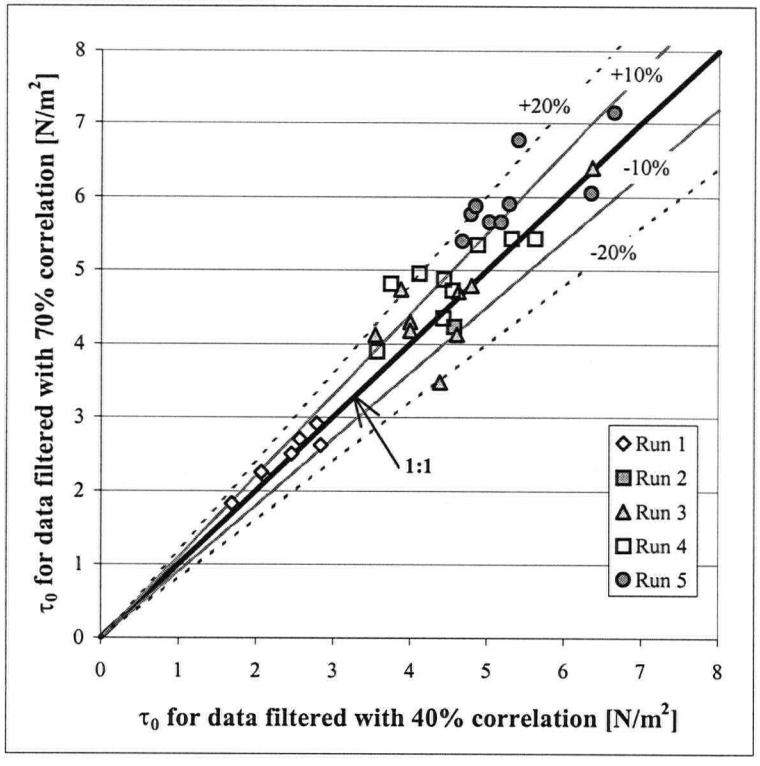

Figure 4.16. *Shear stress estimates at the bed for all runs determined from Reynolds stress profiles derived from data edited with 40% vs. 70% correlation filter.*

Numerical tests were performed to determine the sensitivity of average velocities (Appendix A.2, Fig. A-4 a, c and e) and Reynolds stresses (Appendix A.2, Fig. A-4 b, d and f) for different levels of filtering based on the correlation coefficient. It was shown that the average velocities were fairly consistent irrespective of the correlation filter setting, since averaging cancelled the effects of noise. However, it appears that the Reynolds stresses were much more sensitive to the percentage of data retained, although the expectation was that averaging would also cancel the noise for this parameter. It is possible that some of the variability in Reynolds stress values might diminish with longer data acquisition, and consequently longer averaging periods.

Considering all of the above, it was concluded that, for determining the Reynolds stresses, the values should be based on those measurements for which at least 70% of data are retained for analysis after applying the 70% correlation filter.

4.4.3. Inclusion of the zero shear stress value at water surface

Theoretically the shear stress value should be zero at the water surface if the logarithmic velocity law extends right up to the surface. It was considered whether this zero value should be included as one of the points in the Reynolds stress profile, or alternatively, if the profile should be forced to zero at the surface. The alternative is to ignore the zero stress point at the water surface and rely on the linear fit to the data points (Fig. 4.17.).

In general, the surface region is a very low stress region, with low turbulence and large eddies, and it does not have much influence on the high shear stress region at the bed. Forcing the trendline (dashed black line in Fig. 4.17.) to zero at the water surface appears to distort the rest of the data and it is judged that valuable information from the linear part of the data is lost. The alternative of including the zero point at the water surface as an extra data point (black solid trendline in Fig. 4.17.) fits the data somewhat better, but some of the information is still not captured as well as if only the linear part of the profile is considered (grey solid trendline in Fig. 4.17.).

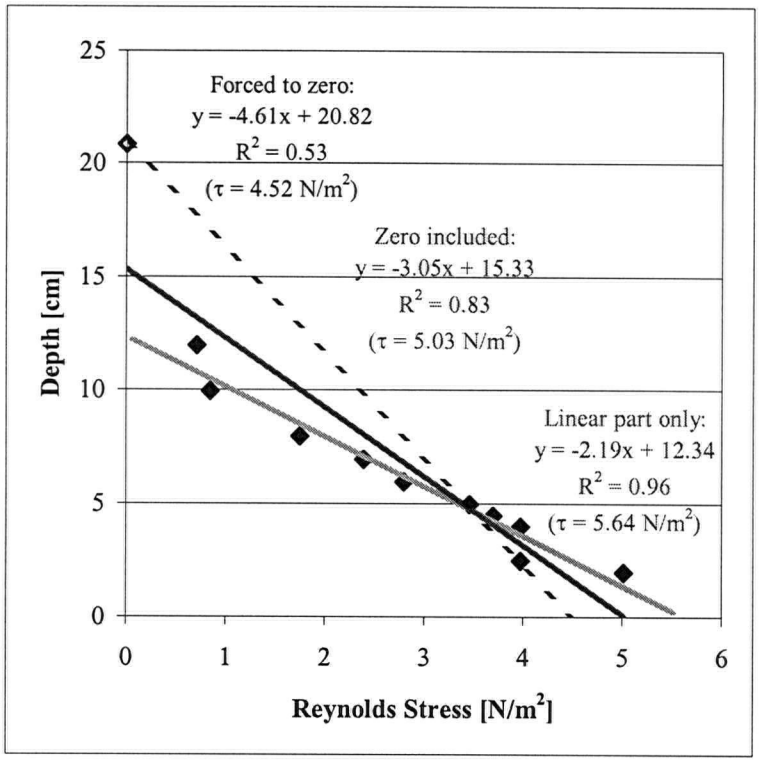

Figure 4.17. *Determination of the bed shear stress based on the Reynolds stress, where the (– –) trendline is forced to zero at water surface; the (—) trendline includes the zero value at water surface; and the (—) trendline considers only the measured data of the linear part of the profile.*

The comparison between the total bed shear stress determined from the Reynolds stress profile calculated with zero stress at the water surface included in the trendline and the stress determined from the linear part of the Reynolds stress profile only, is illustrated for all profiles and all runs in Figure 4.18. In general, the inclusion of the zero value at the water surface decreased the estimate of the total shear stress on the bed.

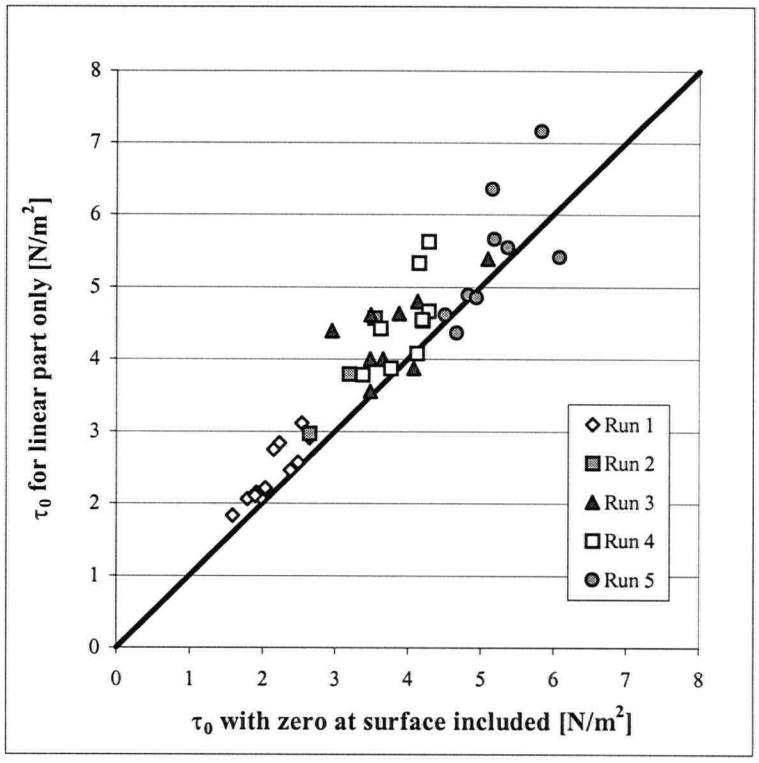

Figure 4.18. *Total bed shear stress values determined with the zero value at the water surface included in the trendline vs. the total bed shear stress values determined from the linear part of the Reynolds stress only.*

In conclusion, the ADV measurements can be used to determine the Reynolds stresses, $-\rho\overline{u'w'}$, at different elevations above the bed. Reynolds stresses often decrease in the bed region, and these points are commonly not taken into account if the total bed shear stress is to be determined. When analysing the measured data for some points near the bed, boundary interference was experienced, and these data were not included in the Reynolds stress profile. Data edited with the 40% correlation filter could be included in the profile to determine the total bed shear stress (Fig. 4.16.) if at least 70% of data are retained for the analysis after filtering. However, because of the high variability and uncertainty identified in the Reynolds

stress values determined for data filtered with different correlation percentages in higher shear stress runs, it was decided that only data edited with the 70% correlation filter for which at least 70% of data are retained, should be used in determining the Reynolds stress values at a point. The zero stress at the water surface should not be included in the Reynolds stress profile, because some of the information throughout the water column would be lost if this was done.

Considering all of the above, the Reynolds stress profiles were plotted for each examined vertical, least squares regression lines were fitted to the linear part of the profile, and then extrapolated to the bed to obtain the local bed shear stresses. These bed shear stresses are turned into bed shear velocities which, in Chapter 5, are compared to shear velocities determined from logarithmic velocity profiles and from the depth-slope method.

4.5. Sediment Sampling and Analysis

There were two types of sediment sampling performed in these experiments:

- *Volumetric* sampling, where the sample is dug out and therefore has three dimensions and thus a volume. This type of testing was performed for the original and the transported material; and
- *Areal* sampling, which is an attempt to sample the bed surface only, and is therefore considered to have two dimensions only. In this case, the sample depth is one grain diameter thick, which is very small compared to the other two sample dimensions. This type of sampling was used to obtain the bed surface grain size distributions.

In this work, to obtain the appropriate grain size distributions both types of samples were analysed by sieving and weighing. In addition, if the two samples need to be compared, a conversion should be applied to the areal sample, which was first introduced by Kellerhals and Bray (1971).

4.5.1. Original material

The sediment used in these experiments was previously used in experiments by Church et al. (1998), in which sediment sizes ranged from 0.18 mm to 32.0 mm. However, sizes less than 1.0 mm were removed for the current experiments, because these smaller sizes could easily be transported and were clogging the downstream screen system. It was considered that the exclusion of these smaller sizes would not change the armouring process and the overall

roughness of the armoured bed because the resistance to flow is created by the largest grains, while the smaller sizes are sheltered and do not carry much shear stress.

After removing the fine material, there were approximately 1100 kg of sediment left, which was well mixed and used in the experiments. It was determined, based on the volume of the maximum grain size (D_{100} = 32.0 mm), that the minimum weight of a sample for sieving should be 55 kg. A total of three samples were taken from various parts of the stack, and then split into smaller samples of about 9 kg each, and sieved. The sieving was performed using the following set of sieves: 1.0, 1.41, 2.0, 2.36, 3.36, 4.75, 6.35, 9.52, 12.5, 18.85, 25.4 and 32.0 mm. All the samples were sieved initially through a set of coarser sieves (4.75 to 32.0 mm) and then through a set of finer sieves (1.0 to 3.36 mm) by shaking in a mechanical shaker for 10 minutes. The accuracy of sieving, as well as the splitting procedure and its accuracy were tested in these experiments, and the results are shown in Appendix C.

The grain size distributions for all three samples are plotted in Figure 4.19, together with the composite curve, which represents the average values for the three samples. The differences between the three curves ranged from 0.2 to 5.46 %, with the average difference of 3.55 %. The composite curve of the original material was used for the various calculations in the thesis. The main characteristics of the grain size distribution for the original material can be found in Table 4.4.

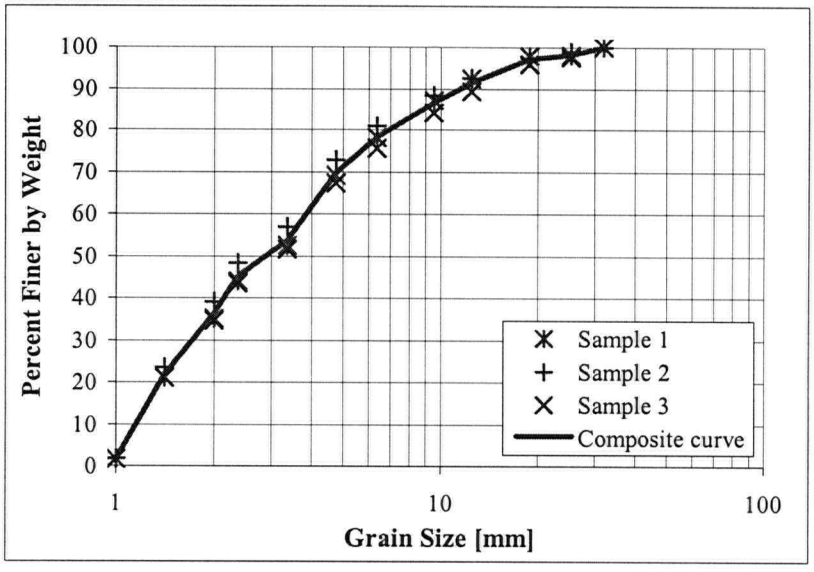

Figure 4.19. *Grain size distributions for three different samples of the original material.*

Besides volumetric sampling of the original material, some areal samples were taken from the prepared bed before the commencement of a run. The sieving and the subsequent analysis tested the validity of the conversion from an areal to a volumetric sample. It was demonstrated (Fig. 4.20.) that the Kellerhals and Bray correction factor (1971) overestimated the amount of finer particles. On the contrary, the Proffitt correction factor (1980) gave a result that compared very well with the original material tested in this study, and therefore the decision was to use Proffitt's conversion exponent of –0.50 to translate the areal samples into volumetric samples. In this procedure, to obtain the corrected or volumetric weights, the retained weights from the areal sample are multiplied by $D_{gi}^{-0.5}$ for each sieve size (D_{gi} is the geometric mean size of the sieve interval). These corrected weights are than summed, and the percentages and the cumulative percentages are calculated.

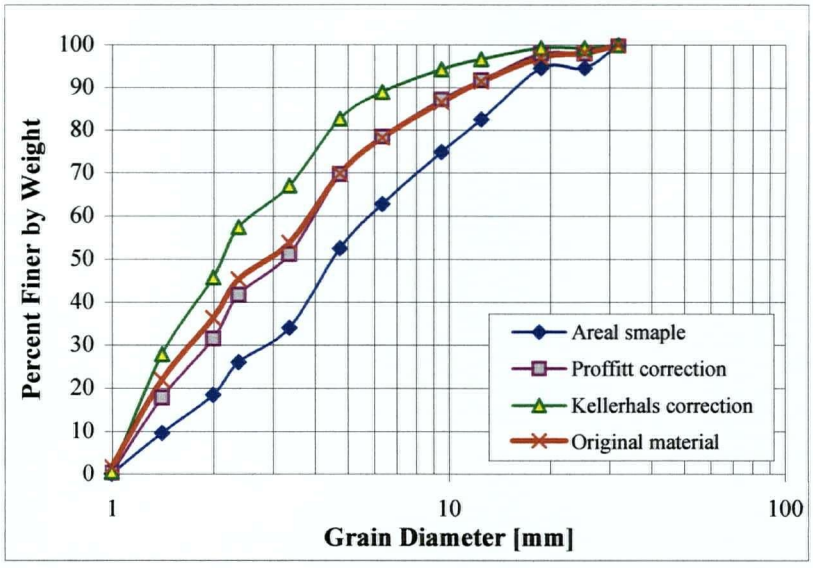

Figure 4.20. *Results of a conversion from an areal to a volumetric sample.*

4.5.2. Bed surface material

The armour layer is usually one grain diameter thick, and therefore an areal sampling procedure is required. The bed surface was sampled using a piston, 15 cm in diameter, coated with a thin layer of potter's clay (Church et al., 1998). To ensure that there was sufficient material for a representative sample, six imprints were taken in each run to obtain a total sample area of 0.1 m^2 (Fripp and Diplas, 1993). These sets of samples were taken on the centreline, and on the left and right quarters across the width of the flume, with two impressions at each position in an alternating fashion. For the clay sampling technique, it was not necessary to dry the bed surface prior to sampling, however the samples were usually taken a few days after the end of the run, when the bed surface was dry. The clay was washed off the sampled material with running water through a mesh with 1 mm openings; the material was then dried, weighed, sieved and analysed.

Because the clay layer is thin (< 5 mm), it was noticed that the fine material accumulated in the lee of the largest and highest protruding blue grains (size ranging from 22.6 to 32 mm) was not picked up, thus leaving some of the piston area uncovered. To avoid this problem, the largest grains contained within the test area were removed by hand before the imprint was taken. A little hole remained on the bed in the place of the removed grain with the elevation now below the surrounding bed surface. Consequently, when the imprint was taken the finer grains in the hole were not picked up (Fig. 4.21.).

Figure 4.21. *Imprint after an areal sample was taken.*

The bed surface samples were taken between 3 and 4 meters downstream from the beginning of the test section. To assure that this was a typical section where the armour layer was fully developed and not influenced by the entrance or the outlet conditions, the bed surface was sampled just upstream and just downstream from the above test section. It was found that the grain size distributions of the three sampled areas were very similar (Appendix C), confirming that the test section was reasonably representative.

Another test was performed to investigate how much the armour layer changed during the run, after the initial transport phase was over. The minor differences in the grain size distributions (Figure 4.24. in Section 4.5.3. and Figure C-5 in Appendix C) were mainly due to the different positions where the samples were taken, and it was concluded that the run duration was sufficient for a full armour layer development.

The increase in shear stress for different runs was accompanied by coarsening of the bed surface, which will be discussed in the following Sections. The grain size distributions for the armour coats are represented in Figure 4.22. and Table 4.4., where the values are already converted to the so-called volumetric sample.

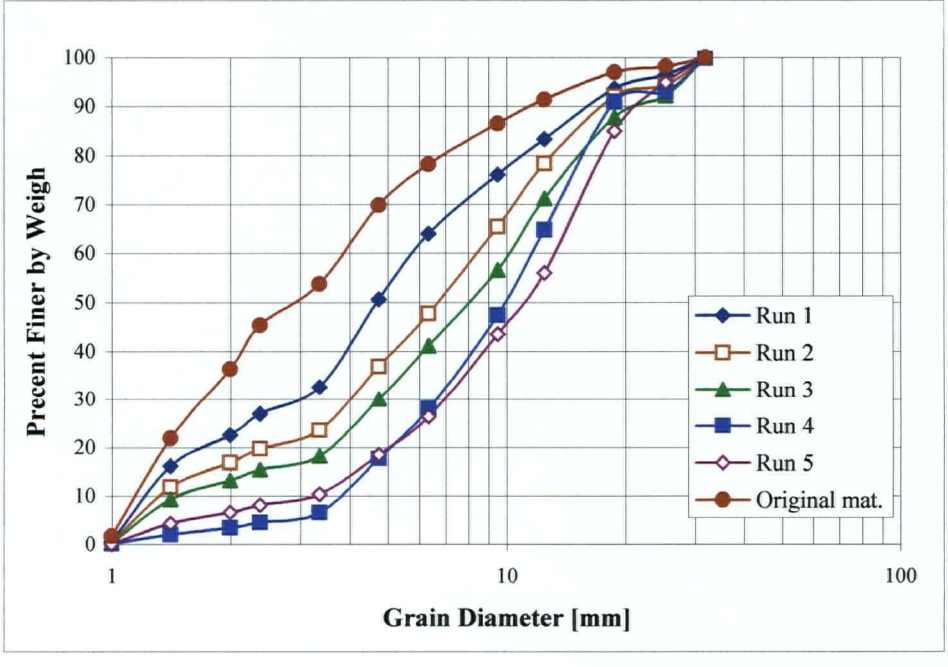

Figure 4.22. *Grain size distributions for armour layers developed in Runs 1 through 5.*

		ORIGIN.	RUN 1	RUN 2	RUN 3	RUN 4	RUN 5
D_i	Dgi	Cumulat. Finer	Cumulat. Finer	Cumulat. Finer	Cumulat. Finer	Cumulat. Finer	Cumulat. Finer
[mm]	[mm]	[%]	[%]	[%]	[%]	[%]	[%]
32.00		100.00	100.00	100.00	100.00	100.00	100.00
25.40	28.51	98.21	96.50	94.43	92.22	93.05	94.93
18.85	21.88	97.05	93.72	92.08	87.88	91.02	85.08
12.50	15.35	91.46	83.42	78.51	71.35	64.87	56.10
9.52	10.91	86.62	76.20	65.55	56.65	47.49	43.58
6.35	7.78	78.31	64.10	47.78	41.20	28.12	26.48
4.75	5.49	69.96	50.69	36.95	30.14	17.81	18.59
3.36	3.99	53.85	32.71	23.66	18.35	6.63	10.44
2.38	2.83	45.44	27.02	19.82	15.49	4.59	8.21
2.00	2.18	36.44	22.60	16.94	13.26	3.47	6.72
1.41	1.68	21.98	16.24	11.87	9.43	2.09	4.42
1.00	1.19	1.76	0.59	0.43	0.31	0.12	0.13
<1		0.00	0.00	0.00	0.00	0.00	0.00
Summary statistics:							
D_{16}	[mm]	1.29	1.40	1.89	2.56	4.53	4.31
D_{50}	[mm]	2.92	4.70	6.75	8.16	9.95	11.05
D_{84}	[mm]	8.55	12.86	15.07	17.36	17.14	18.61
D_{95}	[mm]	16.52	21.87	26.08	27.76	27.25	25.49
D_{100}	[mm]	32.00	32.00	32.00	32.00	32.00	32.00
σ_G		2.57	3.03	2.82	2.61	1.95	2.08
D_G	[mm]	3.32	4.25	5.34	6.66	8.81	8.95

Table 4.4. *Grain size distributions for the armour layers*

In the above table, the geometric standard deviation (σ_G), which describes the size range for close to log-normally distributed sediments, and the geometric mean (D_G) are calculated as:

$$D_G = \sqrt{D_{84} \times D_{16}}, \tag{4-4}$$

$$\sigma_G = \sqrt{D_{84} / D_{16}}, \quad \text{and} \tag{4-5}$$

$$D_{gi} = \sqrt{D_i \times D_{i+1}}. \tag{4-6}$$

The values of D_{gi} were used as input data for the Grain Protrusion Model.

4.5.3. Bed surface appearance

Variation with shear stress - Figure 4.23. illustrates the bed coarsening due to increased shear stress. The initial bed conditions for all five runs were similar to the conditions in Figure 4.23.a. The run numbers are in the order of increased initial shear stress. All photographs are taken from the same height above the bed and represent the same area, which is equal to a rectangle with the width equal to the width of the flume (50 cm) and a length of 17 cm in the direction of flow. The photographs were taken 3.5 m downstream from the beginning of the test section.

In Run 1 only particles up to the size of yellow grains moved (8 to 11.3 mm), degradation was very limited and the other coloured grains were only partially exposed. There were many smaller black gravel particles, as well as sand, visible on the bed surface (Fig. 4.23.b). The shear stress was increased for Run 2, but it was still insufficient to move the largest blue grains (22.6 to 32 mm), and even the red grains (16 to 22.6 mm) moved only occasionally. There was more degradation than in Run 1, hence the coloured particles were more uncovered (Fig. 4.23.c). The space between these grains was mostly covered with smaller black gravel grains, while the amount of sand on the bed surface was reduced compared to Run 1. The shear stress was further increased in Run 3, putting more coloured grains into motion. However, it was observed that only a few of the blue grains moved at the very beginning of the run (i.e. in the first half hour) for quite short distances. After this time the bed roughness increased, causing readjustment in flow depth and energy slope, thus decreasing the shear stress, which became insufficient to move the blue grains. The amount of black gravel grains and sand was further reduced on the surface (Fig. 4.23.d).

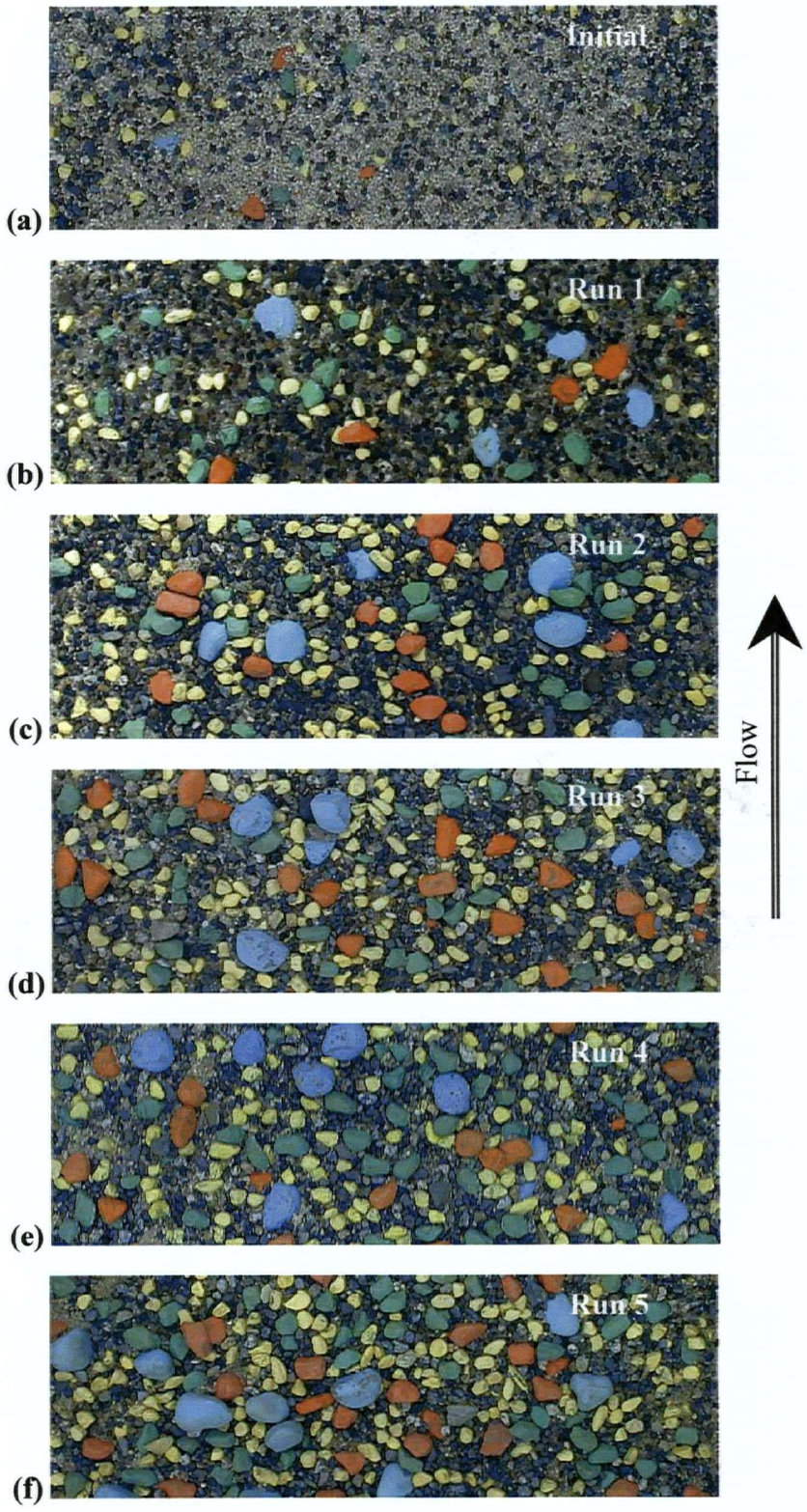

Figure 4.23. *Bed coarsening due to increased shear stress: (a) Initial bed conditions; and (b) through (f) Final bed conditions for Runs 1 to 5.*

In Runs 4 and 5, with further increase in shear stress, the number of coloured particles moved by the flow was larger, and the distances they travelled increased. The number of smaller uncoloured gravel particles and the amount of sand visible on the surface decreased (Fig. 4.23.e and f), while the concentration of larger particles increased. The depth of degradation increased with each run (also see Section 4.2.1).

Variation with time – The bed appearance was examined through time after the initial transport phase was over and the bed surface armoured. Figure 4.24. illustrates the surface of the bed 3 meters downstream from the beginning of the test section in Run 4. This run was stopped 45 hours after the beginning, photographs and surface samples were taken, the experiment was then continued for another 17 hours, and finally stopped at 62 hours. At the end of the run (Fig. 4.24.b), the bed did not look much coarser than midway through the run (Fig. 4.24.a), although there is evidence that the yellow grains and the finer fractions moved noticeably more than the green, red or blue grains. When restarting the run, the flow was increased very slowly, so that the shear stresses did not exceed those that were acting on the grains before the run was stopped. However, even some of the coarser coloured grains moved in these late stages of the run, but it is hard to say if the movement was due to stopping and restarting the experiment, or it was due to the random nature of bed armouring.

None of the blue grains moved between the two stops, so they are not examined further. The green and red grains were examined more closely, and those grains that moved downstream were marked with the same symbols in both photographs. The grains that were not present in the examined section at 45 hours, but moved into the view from upstream, or became

exposed when the run was restarted, were marked with a question mark. One red grain was marked in the first photograph, and three in the second, of which: one new red grain got exposed, one new grain moved into the reach, and one moved within the reach. For green grains, there were nine grains marked in the first and twelve in the second photograph, where some grains moved within or out of the reach, while some new grains moved into the reach. Generally, the red and green grains moved very short distances, and it seems that they moved into more stable positions and stopped against other stable grains of similar sizes.

There were too many yellow grains to be analysed the same way, so they were counted instead. At 45 hours there were 237 yellow grains, while at 62 hours there were 275 yellow grains. This is a 16% increase, while for red and green grains there was only 5% change, indicating that there was a relationship between the grain mobility and the grain size.

There are five blue grains in these photographs (all five on the right hand side) that are clearly not protruding into the flow, but are almost buried and just starting to show. These grains will be discussed further in Chapter 5, when the grain protrusion (H_i) predicted from the numerical model is compared to the protrusion measured by the laser.

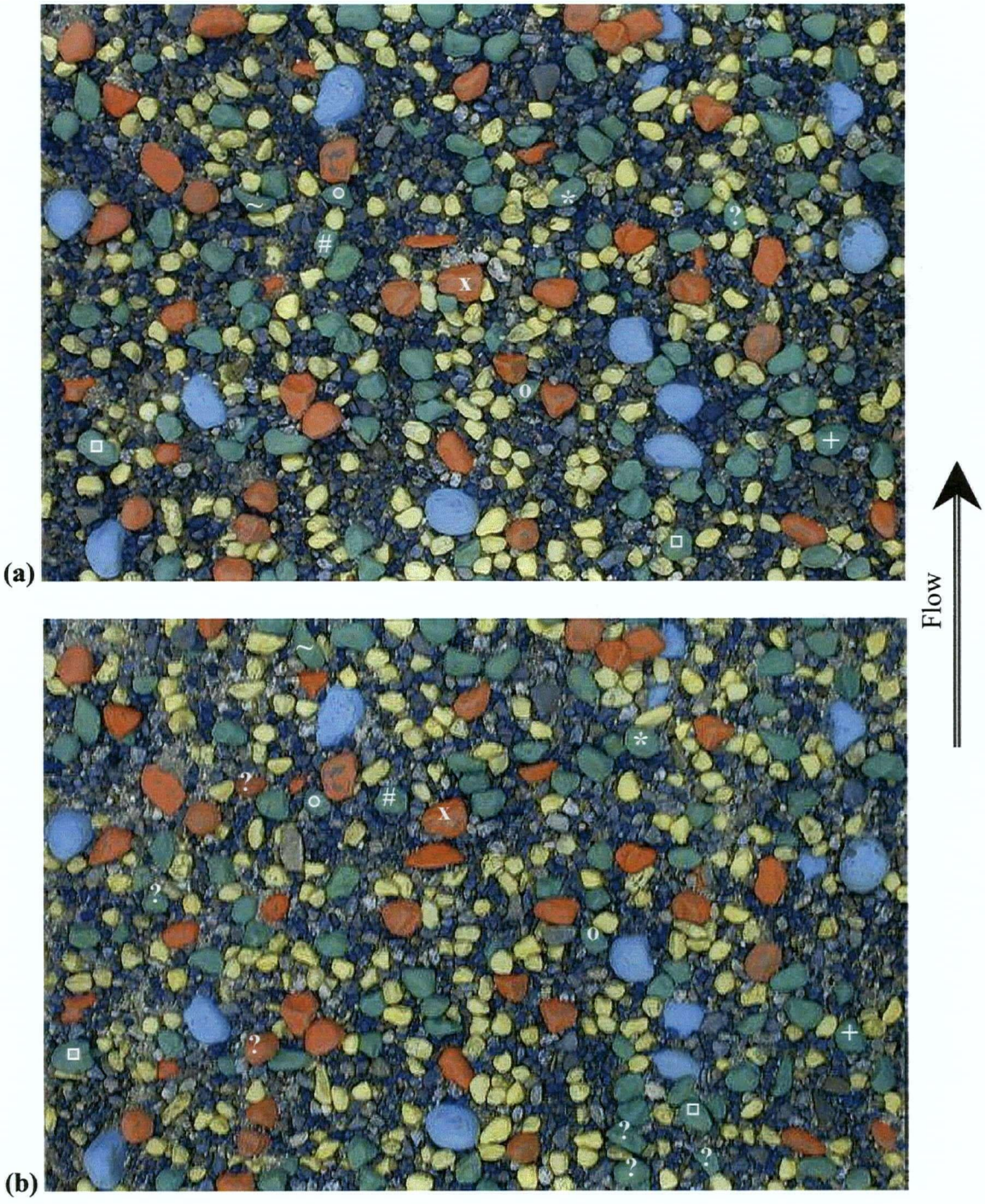

Figure 4.24. *Run 4 - Bed surface comparison: (a) After 45 hours; and (b) After 62 hours. (Same symbols are used in both photographs to mark the grains that moved, while question marks denote grains that are not present in both photographs.)*

4.5.4. Eroded material

The grain size distribution of the eroded, or transported material is not necessarily a direct concern of this study, but the measurements were performed for completeness. The eroded material grain size distributions relate to the final state of the bed, but cannot be used directly to establish that final state of the bed. They are more qualitative than quantitative indices of the processes involved, and were not used in further analysis. The possible correlation between the eroded material and the final state of the bed has not been dealt with in this thesis.

However, the transported material grain size distributions can be used to examine the particle mobility that occurred during a run. If all grains are equally mobile (Parker and Sutherland, 1990), the eroded material should have a distribution similar to that of the bed surface or, in this case, to the original material from which the bed development started. However, in these experiments that condition could not be fully achieved because of the bed armouring process, in which coarser grains became less mobile as the run progressed.

After each experiment, the entire eroded material was collected and dried. The dry sediment was weighed and split into smaller samples for sieving. Table 4.5. illustrates the total amounts of transported and analysed material, together with the original and eroded material properties for all the runs. Figure 4.25. shows the grain size distributions for the original and for the transported materials for all five runs. All grain size distributions for the transported material are finer than the grain size distribution for the original material, indicating partial

transport and uneven mobility for different grain sizes, where coarser sizes are less mobile (Wilcock and McArdell, 1993).

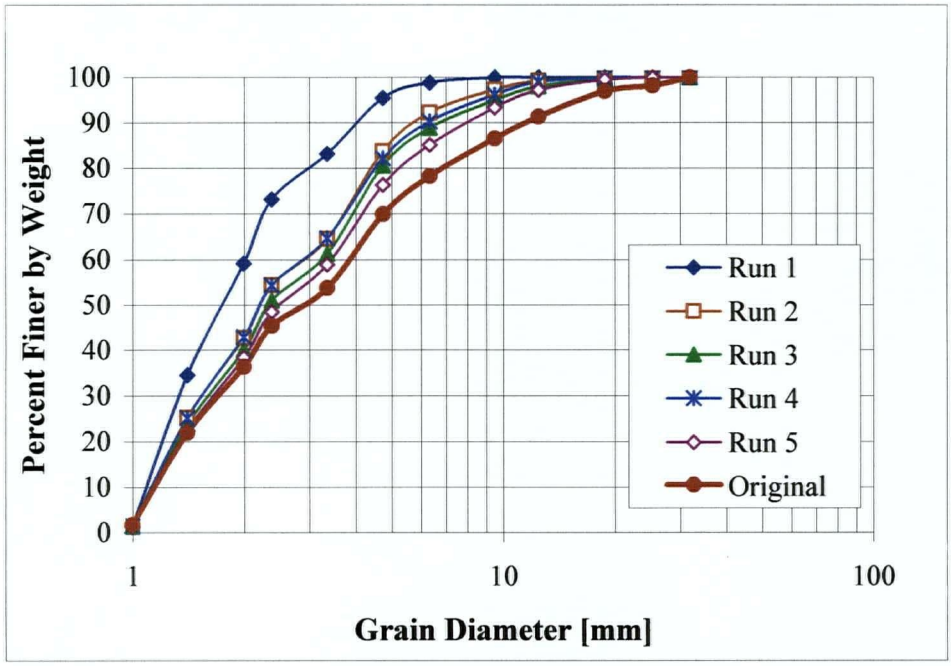

Figure 4.25. *Grain size distributions for the eroded materials.*

Experimental Runs 1 through 5 were conducted in the order of increasing initial shear stress, which resulted in coarsening of the eroded material (Fig. 4.25.). This result was expected since, with the increase in shear stress, more of the larger particles were mobilized and the grain size distributions of the transported material were becoming more similar to the distribution of the parent material, especially in Run 5. In Run 1, sizes bigger than 9.52 mm (i.e. green, red and blue grains) did not get transported; in Run 2, green and red grains started moving; in Run 3 even few of the coarsest blue grains moved, but travelled very short distances and rarely out of the test reach, while in Runs 4 and 5, all sizes were mobilized. However, the grain size distribution of Run 4 appears finer than that of Run 3, and is almost

identical to the distribution of Run 2. A possible explanation is that in Run 4 organised bed structures, or microbedforms, that were observed may have increased the stability of the bed and therefore influenced the sediment transport before it decreased to diminishing levels (see discussion in Chapter 6). More experiments are needed to investigate the formation and the influence of microbedforms on bed armouring, or on sediment transport processes.

		ORIGIN.	RUN 1	RUN 2	RUN 3	RUN 4	RUN 5
D_i	Dgi	Cumulat. Finer	Cumulat. Finer	Cumulat. Finer	Cumulat. Finer	Cumulat. Finer	Cumulat. Finer
[mm]	[mm]	[%]	[%]	[%]	[%]	[%]	[%]
32.00		100.00	100.00	100.00	100.00	100.00	100.00
25.40	28.51	98.21	100.00	100.00	100.00	100.00	100.00
18.85	21.88	97.05	100.00	100.00	99.67	100.00	99.58
12.50	15.35	91.46	100.00	99.31	98.06	99.09	97.28
9.52	10.91	86.62	100.00	97.36	95.08	96.25	93.41
6.35	7.78	78.31	98.89	92.39	88.94	90.41	85.25
4.75	5.49	69.96	95.56	83.86	80.60	82.24	76.37
3.36	3.99	53.85	83.25	64.59	61.34	64.69	58.95
2.38	2.83	45.44	73.22	54.43	51.04	54.39	48.56
2.00	2.18	36.44	59.16	42.87	40.19	42.97	38.47
1.41	1.68	21.98	34.56	25.30	23.78	25.24	22.58
1.00	1.19	1.76	1.32	1.37	1.49	1.56	1.42
<1		0.00	0.00	0.00	0.00	0.00	0.00
Summary statistics:							
Total eroded [kg]:			32.64	100.41	120.29	133.85	224.56
Total analysed [kg]:			3.96	3.42	7.14	8.55	7.25
D_{16}	[mm]	1.29	1.18	1.25	1.27	1.25	1.28
D_{50}	[mm]	2.92	1.78	2.23	2.34	2.23	2.52
D_{84}	[mm]	8.55	3.44	4.78	5.40	5.10	6.13
D_{95}	[mm]	16.52	4.69	8.02	9.48	8.84	10.75
D_{100}	[mm]	32.00	9.52	18.85	25.40	18.85	25.40
σ_G		2.57	1.71	1.95	2.06	2.02	2.19
D_G	[mm]	3.32	2.02	2.44	2.62	2.52	2.80

Table 4.5. *Grain size distributions for the original and eroded materials.*

4.6. Grain Protrusion Measurements

Measurements of the bed surface topography, or grain protrusion measurements were obtained using a DynaVision SPR-04 laser displacement meter (Fig. 4.26.a) and analysed using Surfer®, version 7.0. The purpose of these measurements was to develop three dimensional digital elevation models (DEMs) comprising X, Y and Z coordinates of the bed surface. DEM data can be used to perform comprehensive analyses of surface roughness characteristics, so that the statistical properties of bed elevations and protrusion heights could be calculated. As will be explained in more detail later, these protrusion heights were related to different grain sizes using photographic comparison. A comparison of these measured protrusions (H_i) for different grain sizes with those calculated in the Grain Protrusion Model, will allow us to test the hypothesis that the grains protrude as much as to be on the threshold of motion.

4.6.1. Measurements

The sensor DynaVision SPR-04 is manufactured by LMI Technologies Inc. It is a class IIIa laser with a measuring range of 50 – 250 mm, and resolution of 0.025 mm at rates of up to 1.8 kHz. The laser was mounted on a frame on the top of the flume (Fig. 4.26.b) and programmed to sample a predetermined area of the bed on a 1 millimetre grid. The X, Y, Z data were directly sent to a computer, which also controlled the movement of the instrument. A control frame with precise reference points, which were thin wires stretched across the frame, was mounted above the bed (Fig. 4.26.c). These wires were scanned to monitor the accuracy of the instrument movement in the X and Y directions. The accuracy of Z

measurements was confirmed by repeated scanning of a small reference area, and the average difference in measured elevations for 2200 points was 0.15 mm, which was equivalent to 0.4% of the range of the bed elevations examined (the range was 37.3 mm).

(a)

(b)

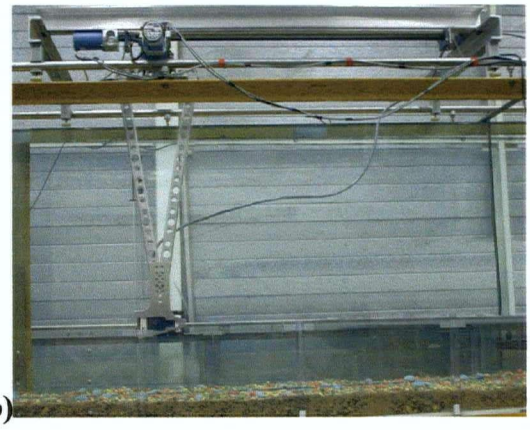

(c)

Figure 4.26. *(a) The DynaVision SPR-04 laser displacement meter (from LMI Technologies Inc. web site); (b) Instrument mounting; and (c) The control frame with the white wires as reference points lowered into the flume.*

The measurements were performed for Runs 4 and 5, at the end of the experiments after the water was drained and the bed was dried. The time needed for the laser to move 1 mm, stop and take a measurement was approximately 0.23 seconds, thus 4.3 points were measured per

second and to scan the whole examined area of 900 x 400 mm in Run 4 took almost 24 hours (the scanned area in Run 5 was 900 x 390 mm). The laser scanning is a relatively slow process if compared to aerial photogrammetry, but the measurements have a higher accuracy and the equipment and data processing are simpler and less expensive. For larger scale experiments or field measurements, aerial photogrammetry seems to be a more practical tool at the present time (Chandler et al., 2000; Lane et al., 2001), however, processing the stereo photographs into DEMs also takes time.

There were no problems experienced when measuring the bed topography of Run 4, and of the total of 360,000 data points, only 845 had erroneous readings (0.23%). The reference wires represented another 1% of the total data set, and these points were removed before obtaining the DEMs. However, for Run 5 up to 30% of the data points had ambiguous values and the reason was attributed to dubious reflections off the bed, which confused the laser. To correct for the problem, a very fine layer of baking powder was spread over the bed, which significantly improved on scanning results. After the coating, only 2.2% of the points had erroneous Z values. An example of a section of a DEM for Run 5 before and after coating with baking powder can be seen in Figure 4.27., where the Nearest Neighbour method was used for gridding for both data sets. The contours are 2 mm apart for both figures, but it is evident that much information was lost (Fig. 4.27.a) before the bed was coated (Fig. 4.27.b).

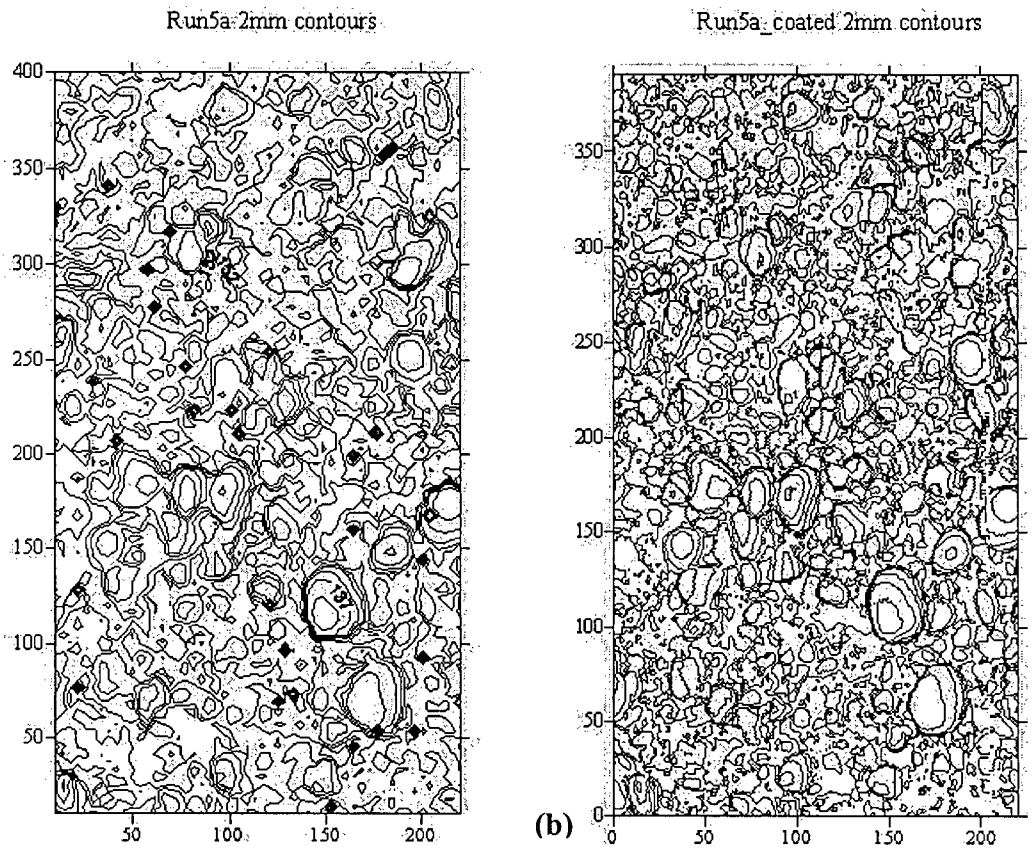

Figure 4.27. *DEMs for Run 5 with a 2 mm contour spacing in Z direction (units in mm): (a) Initial measurements; (b) Measurements after coating with a fine layer of baking powder.*

4.6.2. Data analysis

As stated earlier, all the measured data were analysed and the DEMs were developed using Surfer® with the Nearest Neighbour method for gridding. Once the grid files were calculated, the measured data could be represented as contour plots, which were then super-positioned over coloured photographs of the same area (Fig.4.28.a), or represented as shaded relief maps (Fig.4.28.b), which resemble black and white photographs.

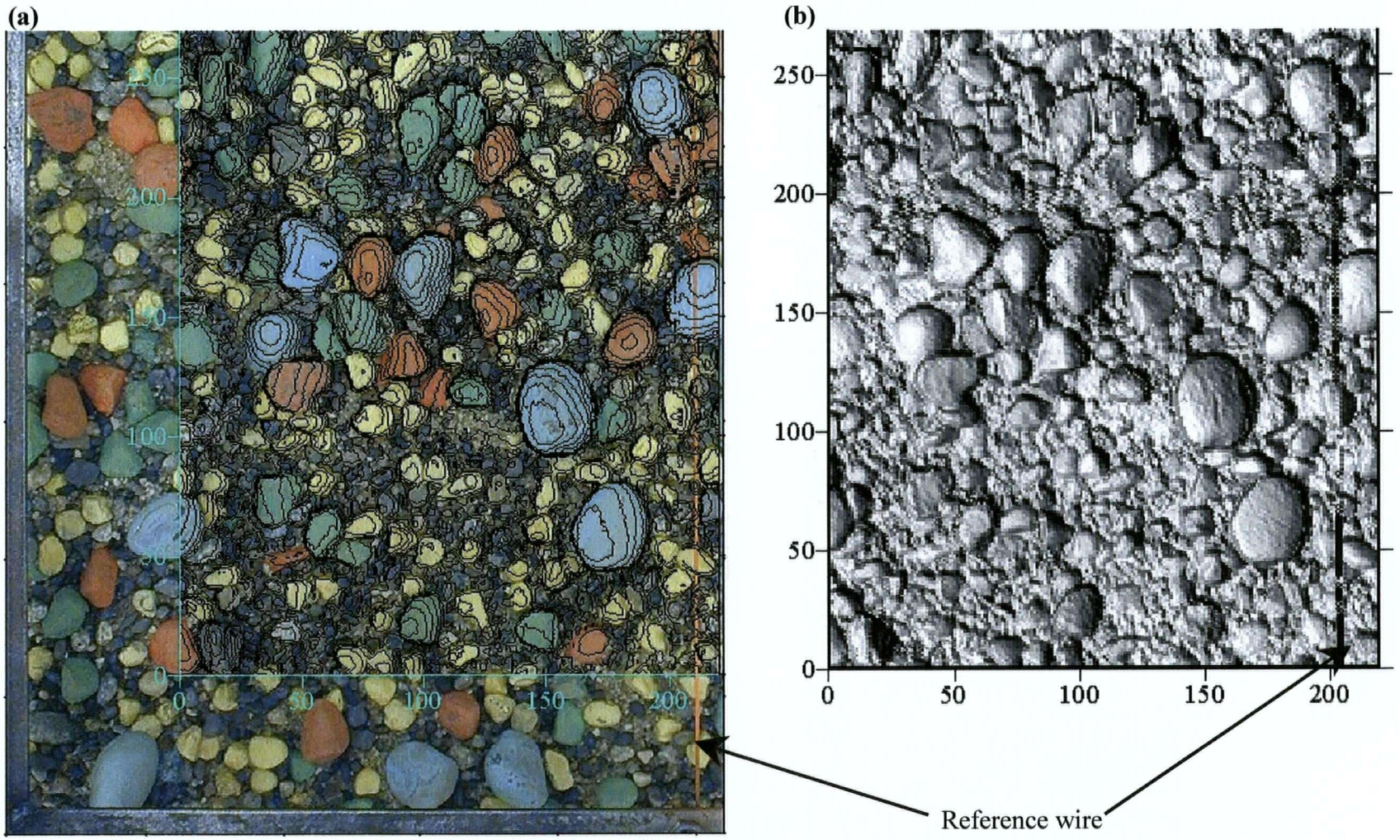

Figure 4.28. *Run 5 (units in mm): (a) A section of a DEM with a 2 mm contour spacing, super-positioned over a photograph of the same area; and (b) A shaded relief map for the same area generated from laser measurements.*

The agreement between the photographs and the overlaying contour plots was very realistic. Some minor discrepancies could be noticed towards the corners of the examined area for some of the photographs, which occurred because the photographs were not rectified to correct for the curvature of the lens. This problem could have been somewhat corrected if the photographs had been taken from a higher camera position, so that the area of interest would fall in the centre of the photograph, where the curvature of the lens has the smallest effect. However, the photographs were not distorted significantly and the method could be used to recognize and relate the contours to appropriate grains.

Slope de-trending - To obtain realistic bed elevation statistics, the raw DEMs had to be de-trended, and the influence of the channel slope had to be removed by reducing the bed levels to a local datum. The instrument was mounted from the top of the flume and moved in a plane parallel to the flume bottom, which was not necessarily parallel to the final water worked gravel bed that formed during the experiment. To calculate and correct for the difference in the two slopes, the raw DEMs were digitised for data points lying on the grid nodes and the elevations of these grid points were determined using the residual function in Surfer®. The bed elevations (Z) on each grid node were plotted against the distance along the flume (X) and the slope was determined as the best fit linear regression line. The grid size was determined such that it was larger than the biggest particles on the bed (D_{100} = 32 mm), but smaller than the smallest bed forms. According to Church et al. (1998), the characteristic dimensions of stone cells in Harris Creek and in their experiments (in which the same bed material was used as in these experiments), were approximately $10D_{84}$ (longitudinally) x $6.5D_{84}$ (laterally). However, particle clusters could have much smaller

dimensions than stone cells, and could be of similar sizes as the largest grains on the bed. Thus, a grid size of $2D_{84}$ seemed reasonable, which for Run 4 formed a grid size of 34 mm (D_{84} = 17.1 mm) and for Run 5 a grid size of 37 mm (D_{84} = 18.6 mm) (Fig. 4.29. and 4.30., respectively). The result of slope de-trending was a planar DEM, which was distorted only by grain-sized roughness features.

Based on the above analysis, it was determined that raw bed elevations had to be corrected for a slope of 0.003 in Run 4, and 0.012 in Run 5. The effect of this slope correction can be identified in the raw and slope corrected DEMs in Figures 4.31. and 4.32., for Runs 4 and 5 respectively. The flow was from right to left in these figures, and since the final degraded beds developed to a less steep slope than initially imposed (the initial bed slope was parallel to the flume bottom), the upstream or right side in Figures 4.31.a and 4.32.a are further away from the laser and thus lighter. However, in Figures 4.31.b and 4.32.b, after the slope correction was applied, there is no such difference in the colours for the right and left-hand sides of the DEMs.

The bed elevations in Figures 4.31. and 4.32. are represented with a grey scale, where the numbers show the distance from the laser to the bed. The grains that protrude higher are closer to the instrument and are shown in darker shades. It appears that the bed degraded somewhat more around the centreline of the flume, as opposed to the regions closer to the flume walls for both runs. This was not unexpected, since the velocities were higher in the centre of the flume.

Bed elevation statistics – After de-trending the DEMs for slope effects, the bed elevations on grid nodes were sampled to obtain the mean bed levels, standard deviations (σ_z) and other statistical parameters for Runs 4 and 5. Then, the elevation statistics for different grain sizes were obtained by identifying grain sizes from the photographs, and these were compared to the mean bed levels to provide grain protrusion results (detailed analysis in Chapter 5).

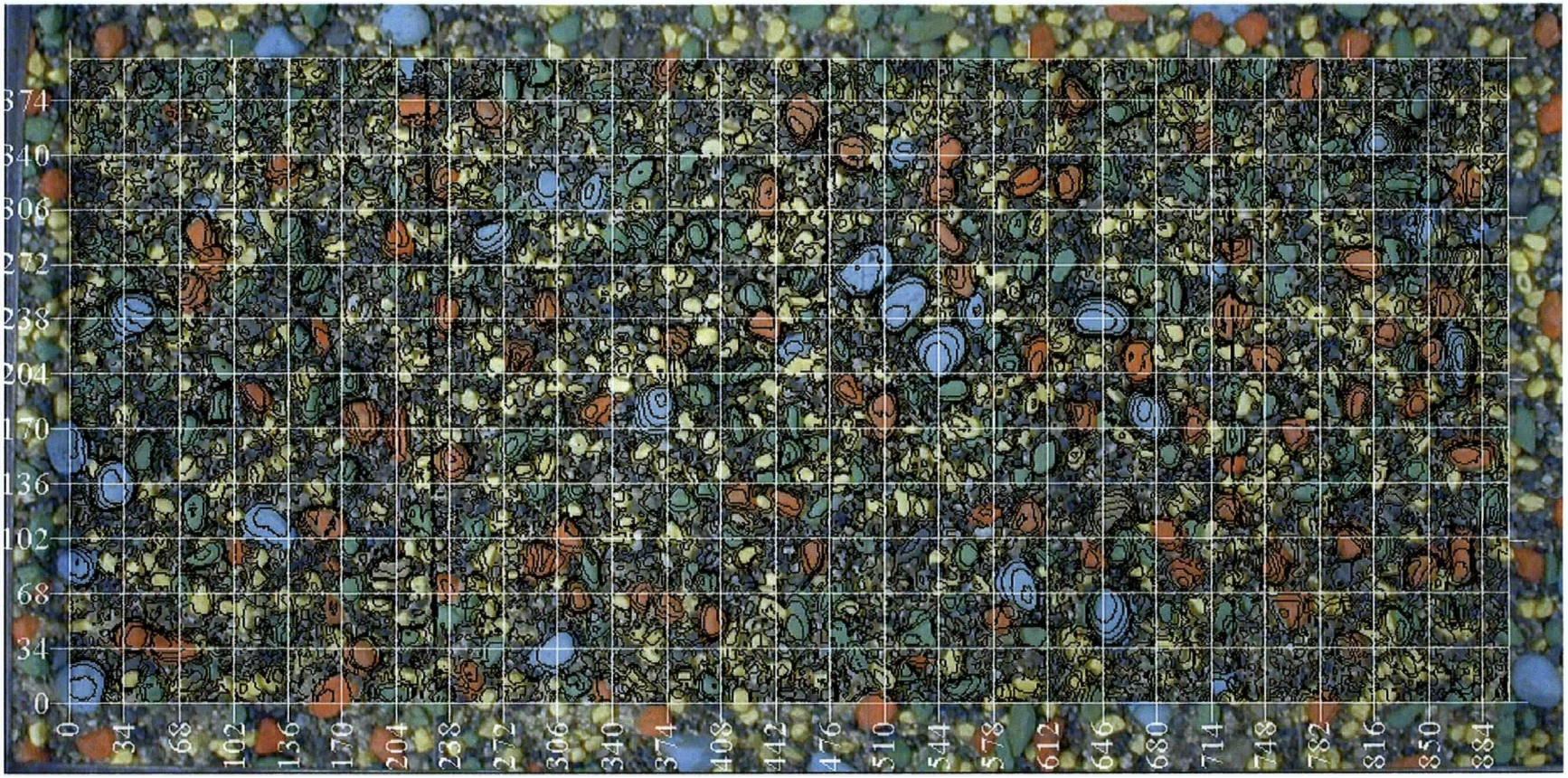

Figure 4.29. *DEM for Run4 super-positioned on the photograph of the same area; the grid size is* $2D_{84}$ *= 34 mm (grid units in mm).*

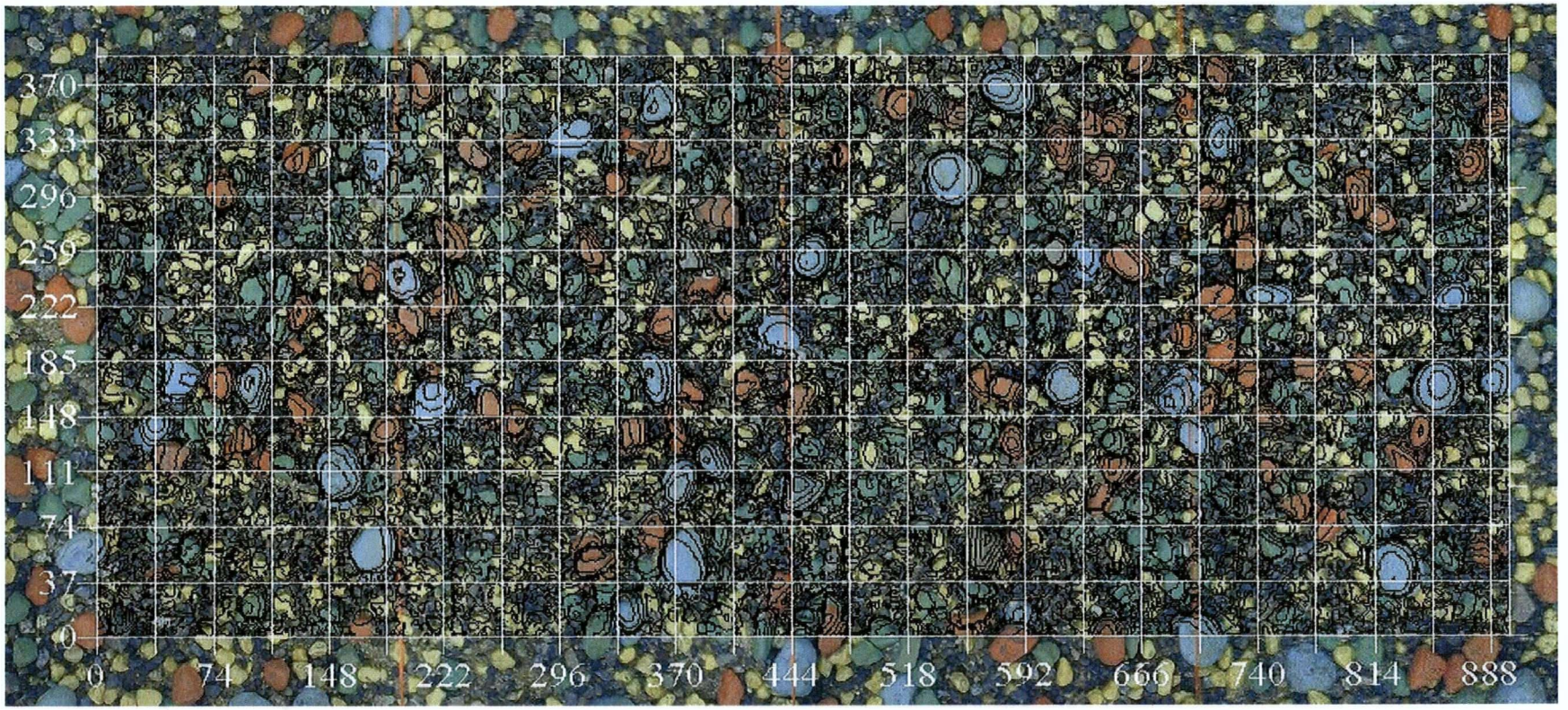

Figure 4.30. *DEM for Run 5 super-positioned on the photograph of the same area; the grid size is* $2D_{84}$ *= 37 mm (grid units in mm).*

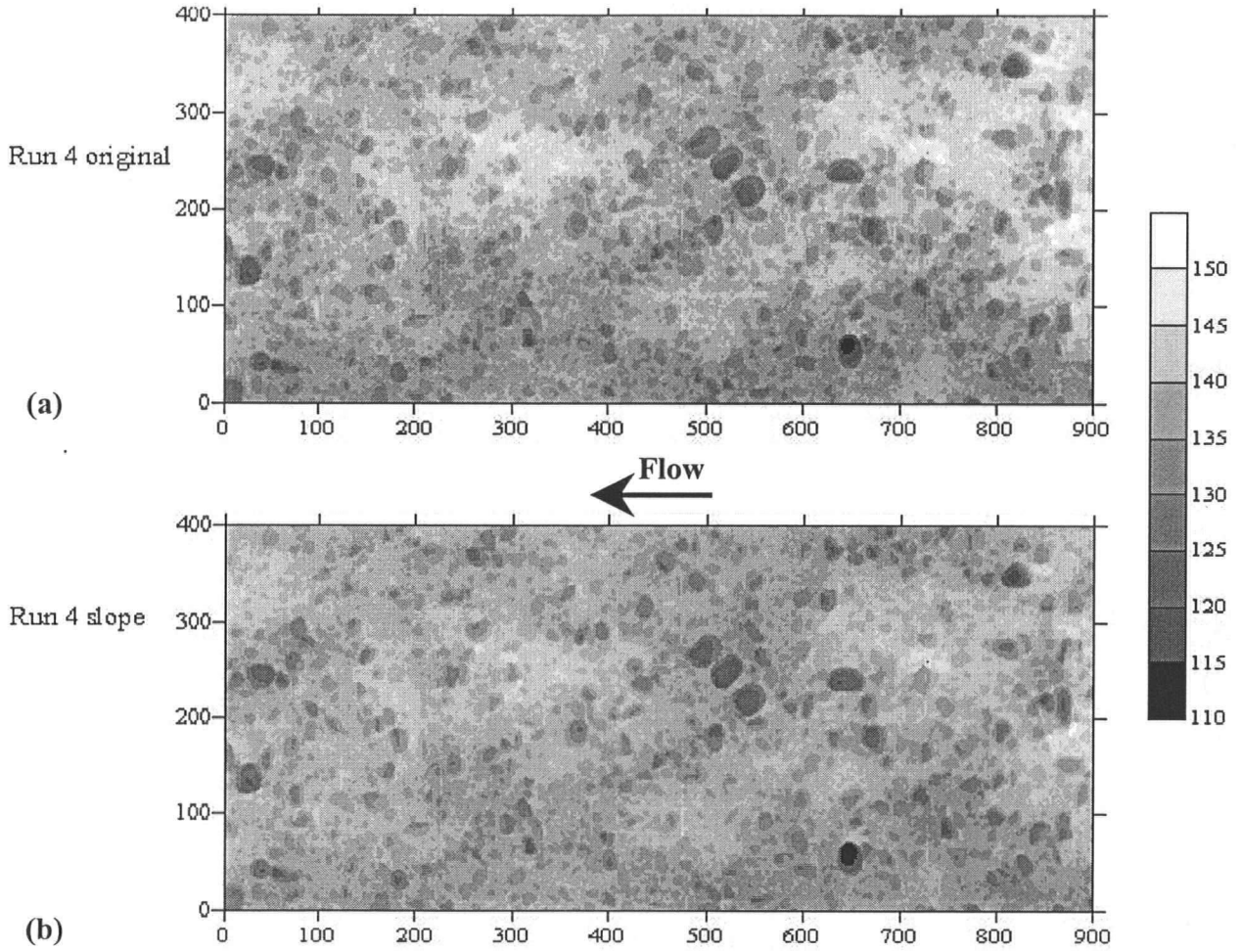

Figure 4.31. *Run 4 (units in mm): (a) A contour map of the laser scanned area before slope correction; (b) A contour map of the laser scanned area corrected for a slope of 0.003, the mean bed level is at 135 mm.*

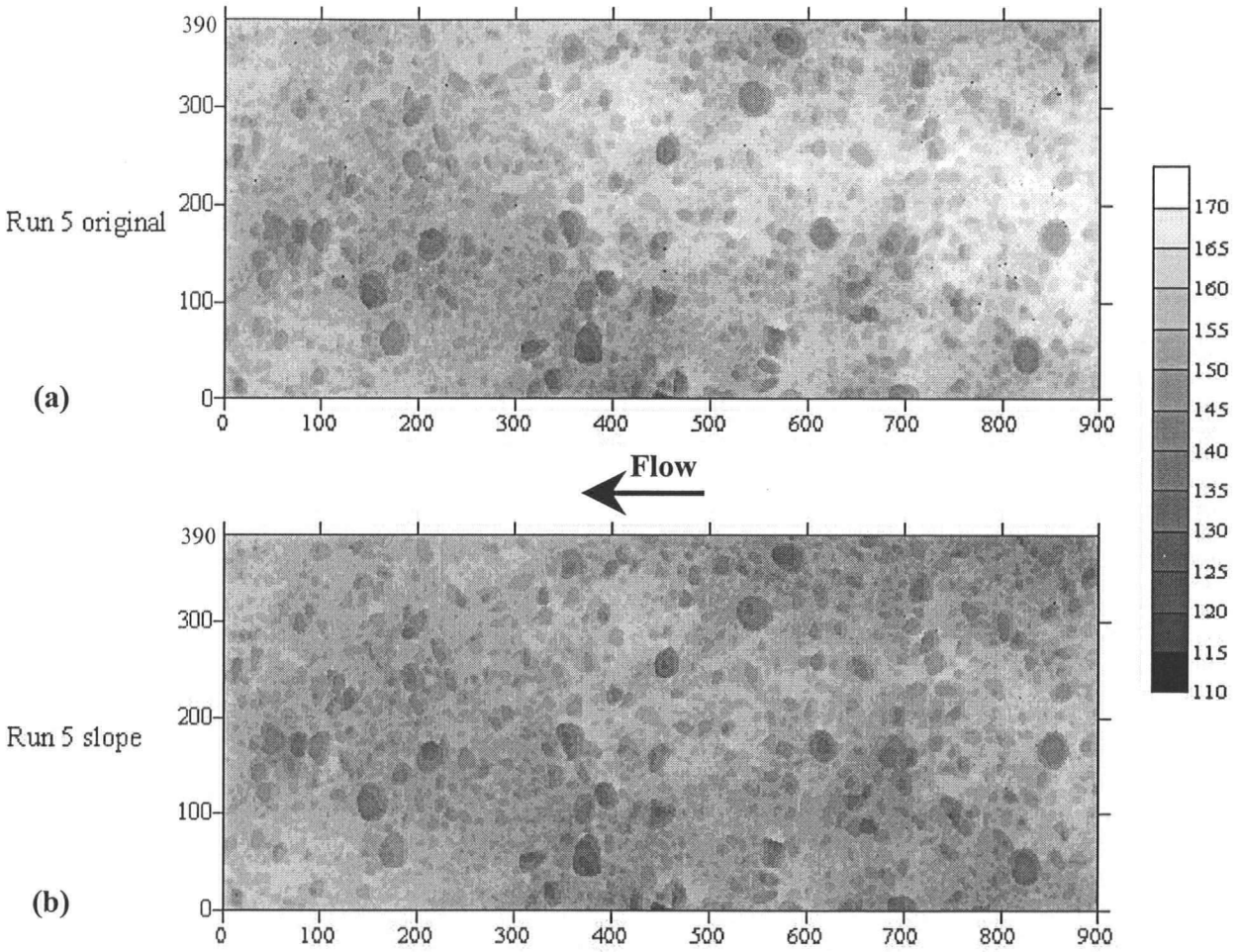

Figure 4.32. *Run 5 (units in mm): (a) A contour map of the laser scanned area before slope correction; (b) A contour map of the laser scanned area corrected for a slope of 0.012, the mean bed level is at 149.5mm.*

4.7. Experimental Conclusions

Observations and calculations in this study confirm findings from previous similar studies. Intensive sediment transport occurred in the beginning of each experiment. The sediment transport decreased during each run to vanishing levels, with coarsest grains practically not moving at all after several hours into the run. The sand and smaller gravel grains contained on the bed surface never completely stopped moving and rearranging. The bed adjusted to flow conditions through reduction in bed slope, followed by degradation and surface coarsening. The armour layer was coarser for the experimental runs with initially higher imposed shear stresses, so that the formation of the armour layer was accompanied with increased bed roughness, which in turn caused increase in flow depths and decrease in flow velocities. The rate and amount of transported material and, consequently degradation, depended on the imposed shear stress.

All measured velocity profiles were logarithmic, or close to logarithmic, confirming the validity of the assumption for related calculations in the numerical model. The Reynolds stresses measured with the ADV could be used to predict shear stress profiles and estimate the local bed shear stresses. However, in highly turbulent flows over rough boundaries, the ADV data are not necessarily well correlated, but the average values are not highly affected. It was demonstrated that for converting the areal sediment samples into volumetric samples, Proffitt's conversion coefficient of –0.5 was appropriate for the given sediment mixture. The laser measurements were de-trended for slope effects and the data were used to develop digital elevation models, which enabled protrusion calculations for different grain sizes.

CHAPTER 5

RESULTS

In this chapter, the experimental results are discussed, and then compared with results from other studies. The experimental results are followed by the Grain Protrusion Model results, where the predicted depths (Y), mean velocities (U), roughness parameters (k_s) and protrusion heights (H) are compared with measured values.

5.1. Experimental results

This Section will focus on parameters calculated from measured values, and on comparison of those parameters obtained by different methods. Firstly there will be an examination of the shear velocity and roughness coefficient calculations and comparisons, followed by an examination of how the different hydraulic parameters change through time during the experiment. Then, the laser data will be examined statistically and the grain protrusions will be calculated.

*5.1.1. Shear velocities, u**

One of the most important parameters used in hydraulic calculations is the shear stress, and consequently the shear velocity. The shear velocity, u^*, was obtained using three different methods:

1. The depth-slope method:

$$u^* = \sqrt{gYS_f} \qquad (5\text{-}1)$$

2. The logarithmic velocity profile:

$$u_y = 5.75u^* \log\left(\frac{30y}{k_s}\right) \qquad (5\text{-}2)$$

where u^* can be calculated from the slope of the line fitted through the velocity data plotted on a semi-logarithmic graph (see Section 4.3.3).

3. The Reynolds stress profile:

$$\tau = -\rho\overline{u'w'}, \qquad (5\text{-}3)$$

from which the total bed shear stress (τ_0) and the shear velocity can be estimated (see Section 4.4.), using:

$$u^* = \sqrt{\frac{\tau_0}{\rho}} \qquad (5\text{-}4)$$

The above three estimates of u^* do not necessarily measure the same quantity. The depth-slope method (equation 5-1) is an integral measure over an arbitrarily extensive area of the bed, and may include side-wall effects, which should be corrected for. The log law reflects local conditions (equation 5-2), where the extension of the local surrounding depends on what fraction of the profile is used, particularly when the profile is segmented. It was expected that by taking the upper segments of several velocity profiles measured across and along the flume, a reasonable estimate of the average shear stress in the test section could be obtained. The Reynolds stress (equation 5-3) gives the local value of the turbulent shear stress at a point. These aspects of the shear stress estimation are discussed in more detail in the relevant sections of the thesis. In a flume study with relatively uniform bed topography, all three estimates of u^* converge to the same result. It will be shown in this chapter that all three

methods produced a range of values, but in general the average shear velocities obtained by the three methods compared reasonably well.

Shear velocities from the depth-slope method - This is the most general method commonly used by practitioners, because the depth and the slope are values which are typically measured in the field or in the lab. Comparing bed slope with water surface slope determines whether the flow is uniform or non-uniform. For all the runs, the flow was reasonably uniform, or mildly non-uniform and, because of that, the surface slope or the bed slope were not used to determine the shear stress. However, even in non-uniform flows, the friction slope is the correct measure of the average bed shear stress for the reach, and this slope was used to obtain the reach average shear stresses and shear velocities. The friction slope is not an easy parameter to obtain, because it is very sensitive to accurate measurements of water surface and bed slopes. We are generally dealing with relatively small slopes and an inclusion or exclusion of just one point can change the slope estimates significantly. Placing the point gauge or the staff gauge on a large roughness element on the bed, or placing them beside it, could make a considerable difference when the linear regression lines are fitted through the measured points, particularly if there are not very many points. This also affects the local depth and local velocity estimates, which are used to calculate the friction slopes. It was expected that this would not be a major issue under controlled laboratory conditions, where the flume was equipped with precise measuring instrumentation. However, a range of slope values was obtained for each experiment, depending on what segment of the test section was taken into account when determining the slopes. A comprehensive study on how

to determine the segment that best represented the flow conditions for each run was given in Section 4.2.1. (Bed, water surface and friction slopes), and in Figure 4.5.

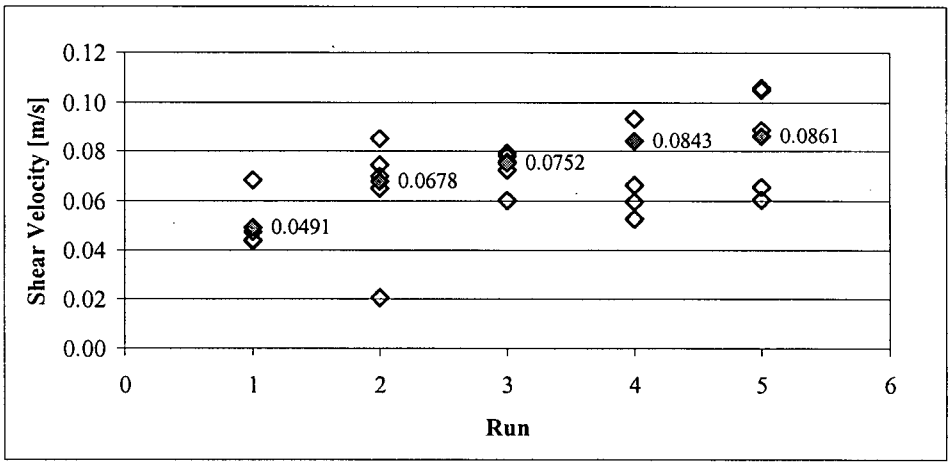

Figure 5.1. *Shear velocity values obtained for all five runs using the depth-slope method; the shaded diamonds represent the values accepted for further calculations.*

Figure 5.1. and Table 5.1. illustrate the range of shear velocity values obtained for friction slopes and average depths determined for different segments of the test section (no sidewall correction applied). The shaded diamonds in the figure represent the values that are considered to be the most representative of the flow conditions and are primarily determined based on friction slope considerations (see discussion in Section 4.2.1). These values are accepted for future calculations and comparisons with shear velocities determined using the other two methods. The open diamonds were obtained using different friction slopes calculated for each run, and show the range of shear velocity values for each run.

In the above analysis, the estimates of the representative shear velocity are based on visual inspection of data. However, if a statistical approach is taken, and the average shear velocities and the standard deviations are calculated for the data excluding the extremes, the visual estimates vary by less than a standard deviation and are considered reasonable.

Run	Flume Section [m]	Depth [m]	Slope	Shear Velocity [m/s]
1	0 - 5	0.165	0.0012	0.0441
	1.5 – 4.5	0.164	0.0015	0.0491
	2 – 4	0.163	0.0012	0.0438
	2.5 – 4.5	**0.164**	**0.0015**	**0.0491**
	3 – 4.5	0.163	0.0014	0.0473
	3 - 5	0.164	0.0029	0.0683
2	0 - 5	0.212	0.0002	0.0204
	1.5 – 4.5	0.209	0.0027	0.0744
	2 – 4	0.207	0.0024	0.0698
	2.5 – 4.5	**0.204**	**0.0023**	**0.0678**
	3 – 4.5	0.205	0.0021	0.0650
	3 - 5	0.205	0.0036	0.0851
3	0 - 5	0.205	0.0018	0.0602
	1.5 – 4.5	0.200	0.0032	0.0792
	2 – 4	0.199	0.0031	0.0780
	2.5 – 4.5	**0.198**	**0.0029**	**0.0752**
	3 – 4.5	0.198	0.0027	0.0724
	3 - 5	0.200	0.0029	0.0756
4	0 - 5	0.202	0.0014	0.0527
	1.5 – 4.5	0.201	0.0018	0.0596
	2 – 4	0.203	0.0022	0.0662
	2.5 – 4.5	**0.201**	**0.0036**	**0.0843**
	3 – 4.5	0.202	0.0036	0.0843
	3 - 5	0.201	0.0044	0.0934
5	0 - 5	0.211	0.0038	0.0887
	1.5 – 4.5	0.219	0.0017	0.0604
	2 – 4	0.219	0.0020	0.0655
	2.5 – 4.5	**0.216**	**0.0035**	**0.0861**
	3 – 4.5	0.213	0.0053	0.1052
	3 - 5	0.212	0.0054	0.1060

Table 5.1. *Measured depths and friction slopes, and calculated shear velocities for all five runs for various segments of the test section.*

Shear velocities from velocity profiles – The velocity profiles were plotted for data measured 2 cm and higher above the bed. Least square regression lines were fitted to these velocity profiles and the shear velocities were calculated from the slopes of these lines (see details in Section 4.3.3.). Full equations for the regression lines, together with the slopes from which the shear velocities were calculated, are included in Figure 4.12. in Section 4.3.3. and Figures B-5 through B-9 in Appendix B.

Table 5.2. contains the shear velocities calculated for all velocity profiles measured in the five experiments (for cross section positions, please refer to Fig. 4.10. in Section 4.3.1). The average values calculated from all profiles, as well as the averages based on the centreline profiles only, are given at the bottom of the table. The standard deviations are calculated for all profiles measured in each run, and range between about 5% for Run 3 to 12.5% for Run 5, relative to the reach average shear velocity.

The graphical representation of the results from Table 5.2. is given in Figure 5.2., where the diamonds represent reach averages, and the error bars cover the range of values obtained in each run. It is evident from Figure 5.2. and from Table 5.2. that there is variability in shear stress values, and that it is desirable to take measurements at several locations if a reasonable average value is to be obtained. Measuring one velocity profile on the flume centreline will not necessarily provide a value for shear velocity that is an accurate representation of the average for the reach. It was shown in Section 4.3.3. when the velocity profiles were compared across the flume, that the slopes of the velocity profiles were similar and that the

walls did not impose a considerable effect on the shear velocities. Therefore, the shear velocities measured closer to the wall were included in further analysis.

Cross-section	Position	Run 1 u* [m/s]	Run 2 u* [m/s]	Run 3 u* [m/s]	Run 4 u* [m/s]	Run 5 u* [m/s]
O	Right	0.0541				
	Centre	0.0601				
	Left	0.0561				
A	Right	0.0647		0.0860	0.0880	0.0898
	Centre	0.0654	0.0814	0.0773	0.0995	0.0791
	Left	0.0545		0.0796	0.0889	0.0737
B	Right	0.0640		0.0912	0.0794	0.0885
	Centre	0.0710	0.0860	0.0794	0.0844	0.0922
	Left	0.0637		0.0808	0.0930	0.0740
C	Right	0.0525		0.0765	0.0976	0.0822
	Centre	0.0714	0.0576	0.0870	0.0639	0.1080
	Left	0.0565		0.0864	0.0919	0.0818
Reach Average:		**0.0612**	**0.0750**	**0.0827**	**0.0874**	**0.0855**
Average Centre:		0.0670	0.0750	0.0813	0.0826	0.0931
Standard Deviation		0.0065	0.0152	0.0051	0.0108	0.0107

Table 5.2. *Shear velocities obtained from velocity profiles for all five runs.*

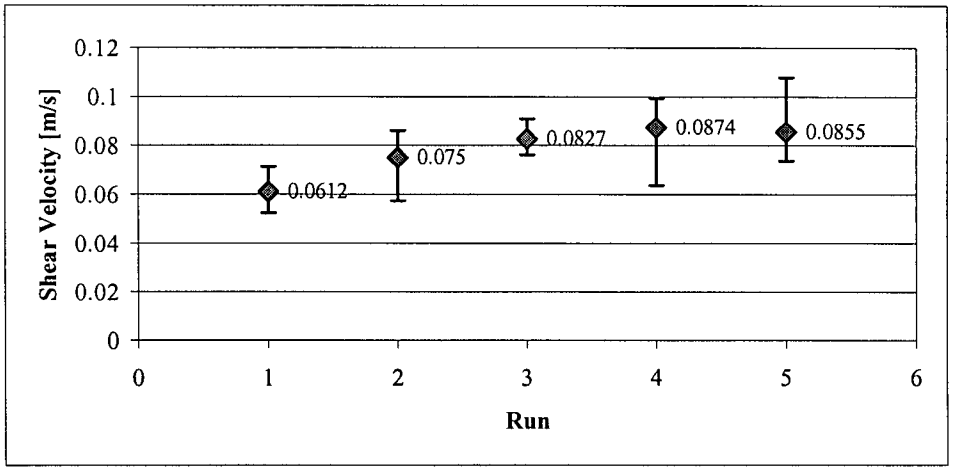

Figure 5.2. *Average shear velocities calculated from the velocity profiles (error bars represent the range of measured values).*

Shear velocities from Reynolds stresses – The ADV measurements were also used to calculate the Reynolds stress at each point where a velocity measurement was taken. The Reynolds stresses were then plotted against depth to obtain a shear stress profile, and the regression line fitted to the linear part of the profile was extended to the bed to obtain the local bed shear stress, τ_0 (details given in Section 4.4.). The shear velocities were then calculated using equation 5-4, and the values for all profiles and all runs are given in Table 5.3. Again, the average values are calculated for all profiles in each run, and for centreline profiles only. The standard deviations are somewhat smaller than for the shear velocities obtained from velocity profiles and range between 4.5 and 9.1% of the mean values. The results from Table 5.3. are graphically represented in Figure 5.3., where the reach average shear velocities and their matching error bars are presented.

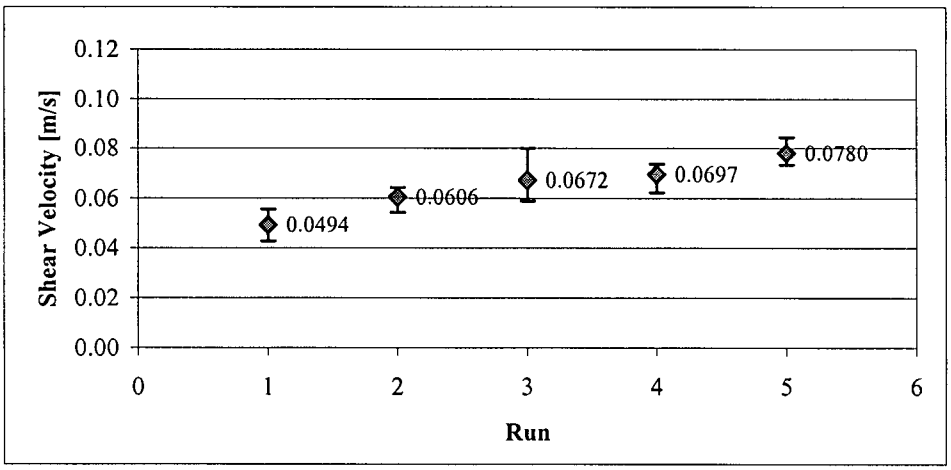

Figure 5.3. *Average shear velocities calculated from Reynolds stress profiles (error bars represent the range of measured values).*

Cross-section	Position	Run 1 u* [m/s]	Run 2 u* [m/s]	Run 3 u* [m/s]	Run 4 u* [m/s]	Run 5 u* [m/s]
O	Right	0.0428				
	Centre	0.0539				
	Left	0.0470				
A	Right	0.0474		0.0692	0.0694	0.0846
	Centre	0.0500	0.0646	0.0643	0.0738	0.0823
	Left	0.0464		0.0686	0.0731	0.0769
B	Right	0.0512		0.0800	0.0704	0.0752
	Centre	0.0557	0.0626	0.0656	0.0660	0.0791
	Left	0.0524		0.0642	0.0738	0.0760
C	Right	0.0454		0.0688	0.0688	0.0735
	Centre	0.0520	0.0545	0.0590	0.0624	0.0778
	Left	0.0482		0.0647	0.0699	0.0767
Reach Average:		**0.0494**	**0.0606**	**0.0672**	**0.0697**	**0.0780**
Average Centre:		0.0529	0.0606	0.0629	0.0674	0.0797
Standard Deviation:		0.0038	0.0054	0.0058	0.0038	0.0035

Table 5.3. *Shear velocities obtained from Reynolds stresses for all five runs.*

Shear velocity comparisons – To test the agreement between shear velocities obtained using the three different methods, they are plotted against each other in Figure 5.4. For the depth-slope method, the shear velocities were plotted two ways: the shaded diamonds illustrate shear velocities calculated from raw measurements; while the stars illustrate the same data but corrected for sidewall effects using the method of Vanoni and Brooks (1957). It seems that the shear velocities determined from Reynolds stresses agree slightly better with the shear velocities from the depth-slope method if the sidewall correction is applied. However, comparing the shear velocity values from the velocity profiles with those from the depth-slope method, shows that the agreement is slightly better if the sidewall correction was not applied. Interestingly, the agreement is somewhat worse when both u^* values are derived

from ADV measurements, namely from the slope of the velocity profiles and from the Reynolds stresses.

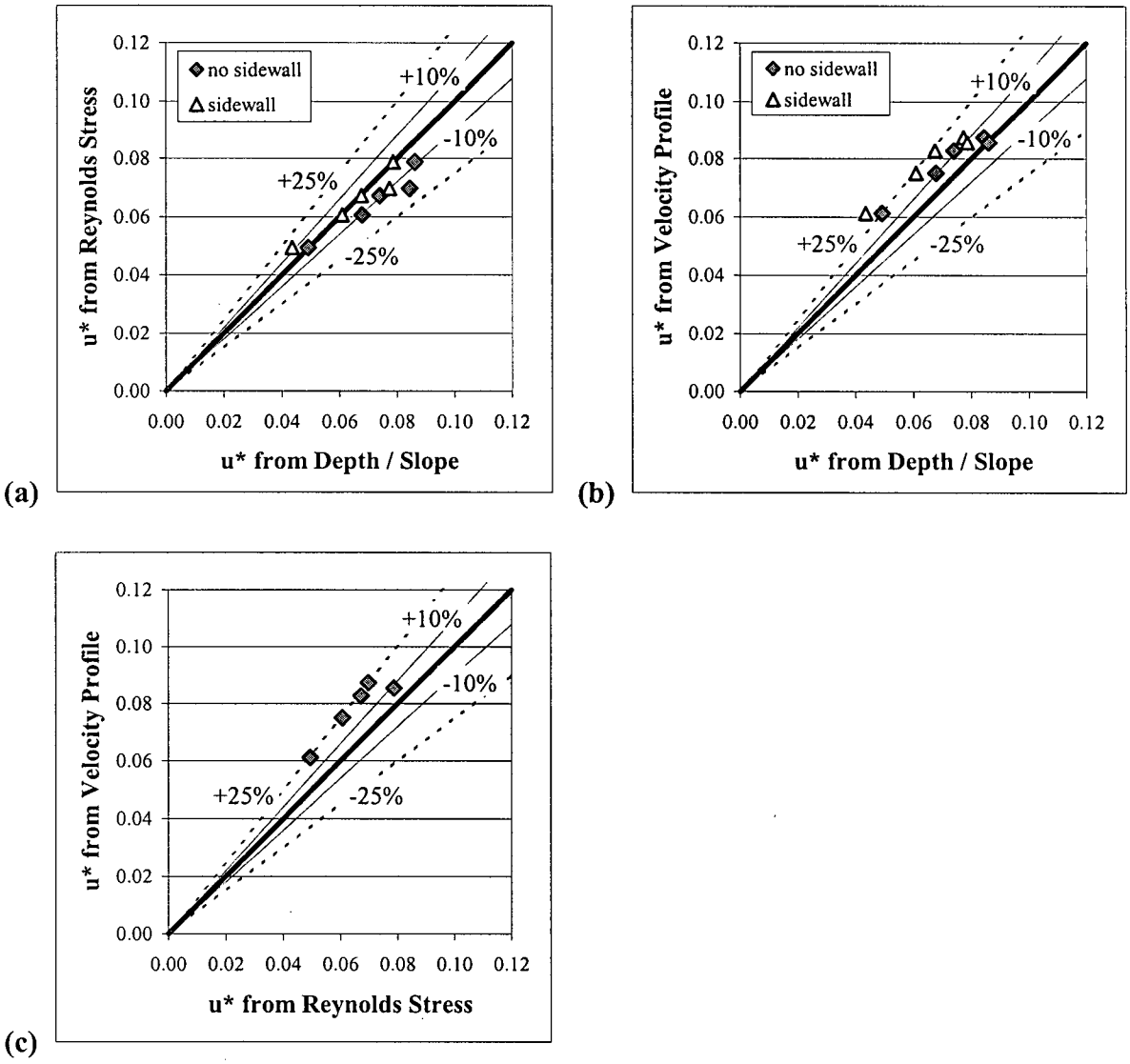

Figure 5.4. *Comparison of shear velocities [units in m/s] determined by using different methods: (a) Depth-slope and Reynolds stress; (b) Depth-slope and velocity profile; and (c) Reynolds stress and velocity profile.*

In general, all three values of u^* are in a reasonable agreement, proving that any of the three methods can provide acceptable estimates of shear velocities or shear stresses, if they were calculated properly. The agreement in u^* values from the Reynolds stress and from the depth-slope method is slightly better than that from the velocity profiles, which is similar to observations of Afzalimehr and Anctil (2001). The differences are not very significant and most of the values fall within ±10% (Fig. 5.4.a and b). However, the velocity profile is easier to measure than the Reynolds stress, especially in the field where measurements are commonly done with current meters. These instruments do not provide information on velocity fluctuations, which are needed to estimate the Reynolds stresses. Interestingly, the differences in u^* values are most evident when the two estimates from ADV measurements are compared (Fig. 5.4.c), and are of the order of 25%.

5.1.2. Roughness parameter, k_s

Values of the roughness coefficient (k_s) obtained from the depth, slope and mean velocity measurements (calculated using equation 3-17) will be compared against the values obtained from velocity profiles. The depths and slopes are the average values for the 2.5 – 4.5 m segment of the test section, while the mean velocities are obtained from continuity using the discharge measurements (values given in Table 4.1.). The roughness parameter from velocity profiles is obtained from the intercept of the regression line fitted to the data measured at 2 cm and higher above the bed (see details in Section 4.3.3.). Table 5.4. is the summary of roughness coefficients obtained from the two different methods.

Values obtained from velocity profiles:						
Cross-section	**Position**	**Run 1 k_s [m]**	**Run 2 k_s [m]**	**Run 3 k_s [m]**	**Run 4 k_s [m]**	**Run 5 k_s [m]**
O	Right	0.0123				
	Centre	0.0153				
	Left	0.0143				
A	Right	0.0282		0.0557	0.0566	0.072
	Centre	0.0216	0.0330	0.0238	0.0661	0.0235
	Left	0.0139		0.0473	0.0689	0.0443
B	Right	0.0287		0.0631	0.0300	0.0583
	Centre	0.0361	0.0452	0.0284	0.0286	0.0481
	Left	0.0283		0.0418	0.0692	0.0343
C	Right	0.0099		0.0356	0.0822	0.0484
	Centre	0.0314	0.0056	0.0385	0.0078	0.0957
	Left	0.0152		0.0615	0.0704	0.0533
Reach Average:		0.0213	0.0280	0.0440	0.0533	0.0531
Average Centre:		0.0261	0.0280	0.0302	0.0342	0.0558
Standard Deviation		0.0088	0.0203	0.0140	0.0251	0.0211
Values obtained from depths, slopes and mean velocities:						
Not corrected for s/w:		0.0125	0.0311	0.0456	0.0483	0.0489
Corrected for s/w:		0.0066	0.0192	0.0316	0.0347	0.0337

Table 5.4. *Values of the roughness coefficient, k_s, calculated from velocity profiles, and from depths, slopes, and mean velocities for all five experiments.*

The roughness coefficient is often higher for the profiles closer to the sidewalls than for those on the centreline, indicating increased resistance because of the wall effect. However, it is hard to distinguish which part comes from the bed and which from the wall. For comparison, the bottom two rows of the Table 5.4. represent the values calculated from depths, slopes and mean velocities, before and after applying the sidewall correction. The variability between

the calculated roughness values is considerable, indicating how sensitive this coefficient is to the variations in values from which it is calculated, (partly because k_s appears as a logarithmic term). Regardless of the above, there is a definite increasing trend in k_s values from lower to higher shear stress runs, but the value levels off at the high end.

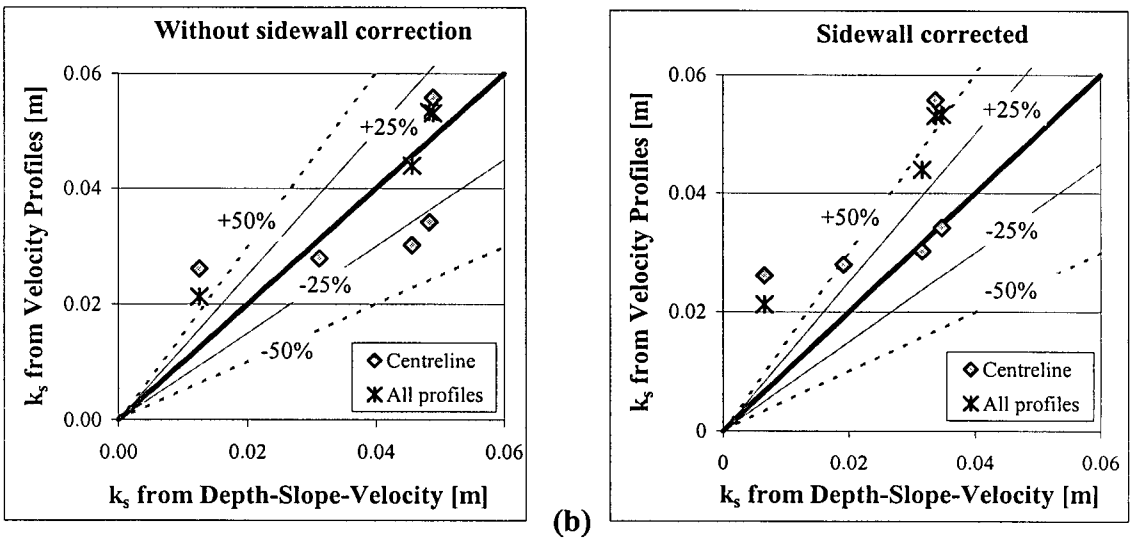

Figure 5.5. *Roughness coefficient comparison for values calculated form depth, slope and mean velocities vs. values calculated from velocity profiles for the centreline only or for all profiles for Runs 1 – 5: (a) without sidewall correction; and (b) with sidewall correction.*

The relationships between these calculated values are best represented in Figure 5.5. Figure 5.5.a illustrates the k_s values calculated before the sidewall correction was applied, and these values are compared to the values obtained from the centreline velocity profiles only (diamonds), or to the values that represent the average values from all velocity profiles measured in each run (stars). Figure 5.5.b compares the k_s values calculated after the sidewall correction was applied to the shear velocities. As expected, the values without

sidewall correction agree better with the values obtained as averages from all velocity profiles (within ±25%), since for these averages the sidewall effects are included in the velocity profiles that were measured closer to the walls (Fig. 5.5.a). On the contrary, the k_s values calculated after the sidewall correction was applied agree somewhat better with the values obtained from the centreline velocity profiles only, because the sidewall effects were most probably not as strong there.

To compare the calculated values of the roughness parameter (k_s) from the Grain Protrusion Model, the sidewall corrected shear velocities derived from the depth-slope method ($u_*' = \sqrt{gYS_f'}$) will be used to calculate the "observed" k_s values using equation 3-17. This shear velocity was chosen to be consistent with the other two studies used to test the model, and because the locally derived k_s values from velocity profiles are quite variable, while the depth-slope method provides more of an average estimate.

5.1.3. Hydraulic conditions – variation with time

To examine the behaviour of the system during the experiments, several hydraulic parameters were plotted against time in Figure 5.6. for the lowest and the highest shear stress runs, i.e. Run 1 and Run 5, respectively. These are the depth, friction slope, shear velocity and the Darcy-Weisbach friction factor ($\sqrt{f/8} = u^*/U$). There were no considerable changes in Run 1 for the whole duration of the experiment, and all the parameters were relatively constant with a slight reduction in slope. The only anomaly is a significant slope change 30 minutes into the run, indicating passing dunes during the high initial transport rate

phase. Runs 2 through 4 behaved similarly to Run 1, but the fluctuations in hydraulic parameters during the initial high transport rate phase were somewhat more pronounced.

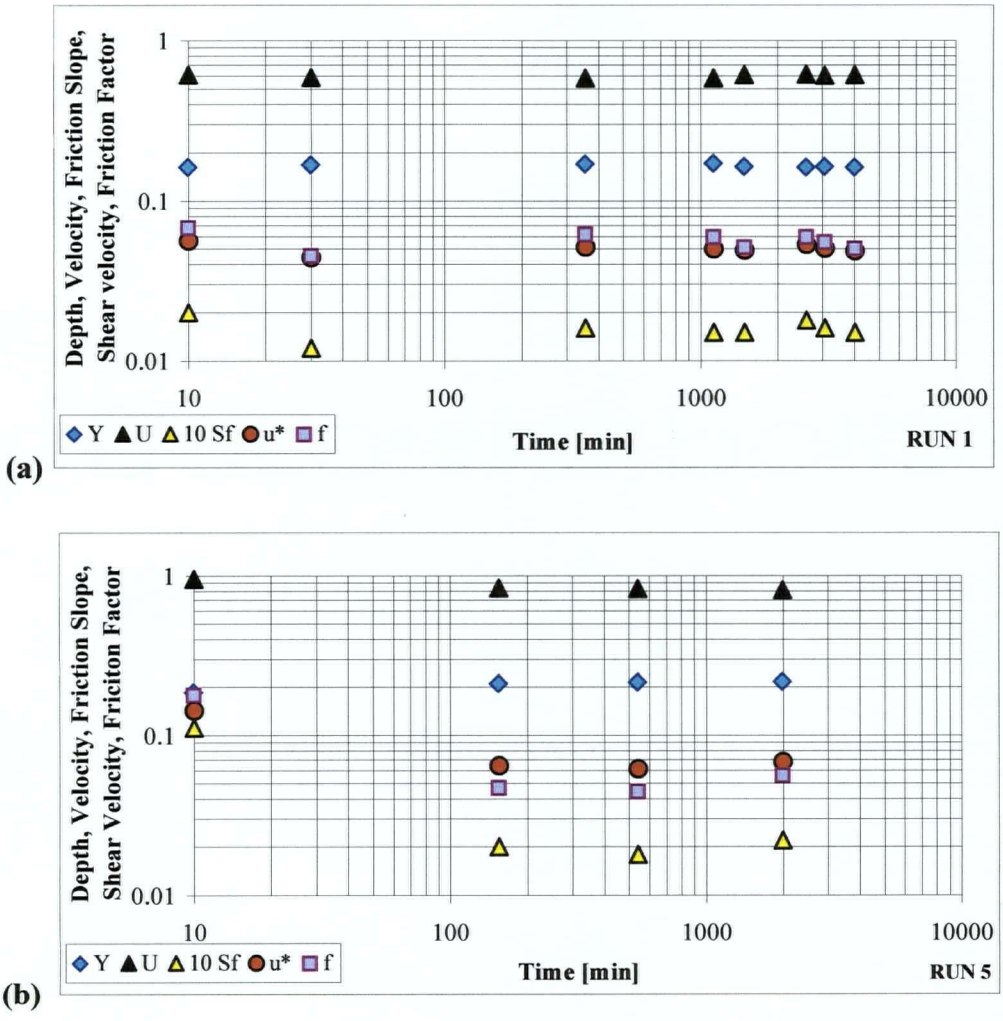

Figure 5.6. *Variation in depth (Y in m), mean velocity (U in m/s), friction slope (S_f), shear velocity (u^* in m/s) and Darcy-Weisbach friction factor (f) with time: (a) Run 1; and (b) Run 5.*

In Run 5, most of the changes occurred in the initial phase of the run, i.e. in the first 100 minutes (Fig. 5.6.b). The reduction in friction slope was followed by an increase in depth

and decrease in mean velocity, which caused fluctuations in shear velocities. However, when the high initial transport rate was over, the shear velocity (and hence the shear stress) stabilised, and this was considered to be the dominant shear stress for the run. The initial reduction in the friction factor and the shear velocity were dominated by the significant reduction in friction slope at the beginning of Run 5. After this initial reduction, the bed surface coarsening caused the transport rate to drop and, as a result of grain roughness, the friction factor started to increase. The hydraulic roughness of the bed continued increasing slightly through the rest of the run, causing a small increase in depth, which was also reflected in a minor increase in shear velocities and a decrease in mean flow velocities.

5.1.4. Grain protrusion calculations

The measurements from the laser displacement meter were statistically analysed to derive the mean protrusions for different grain sizes. After de-trending the DEMs for slope effects, the bed elevations on grid nodes (see Section 4.6.2. and Fig. 4.35. and 4.36.) were sampled to obtain the mean bed level, the standard deviation (σ_z) and other statistical parameters (Tables 5.5. and 5.6.). The Kolmogorov-Smirnov test was performed to compare sample distributions to a normal distribution, and it was found for both analysed runs (Runs 4 and 5) that the elevation distributions were not significantly different than the normal, or Gaussian distribution at the 90% significance level or higher (see critical K-S values for α=0.1 and 0.05 given in Tables 5.5. and 5.6). The frequency distribution plots (Fig. 5.7.) confirmed that bed elevations deviated somewhat from the normal law, and were moderately skewed. The theoretical normal distributions in Figure 5.7. were derived using the mean and the standard deviation from the measured bed elevations. The mean bed elevation is about 3 to 4 standard

deviations below the high points of the bed for both runs. These findings are similar to the results from some other studies (Nikora et al., 1998; Smart and Walsh, 2002).

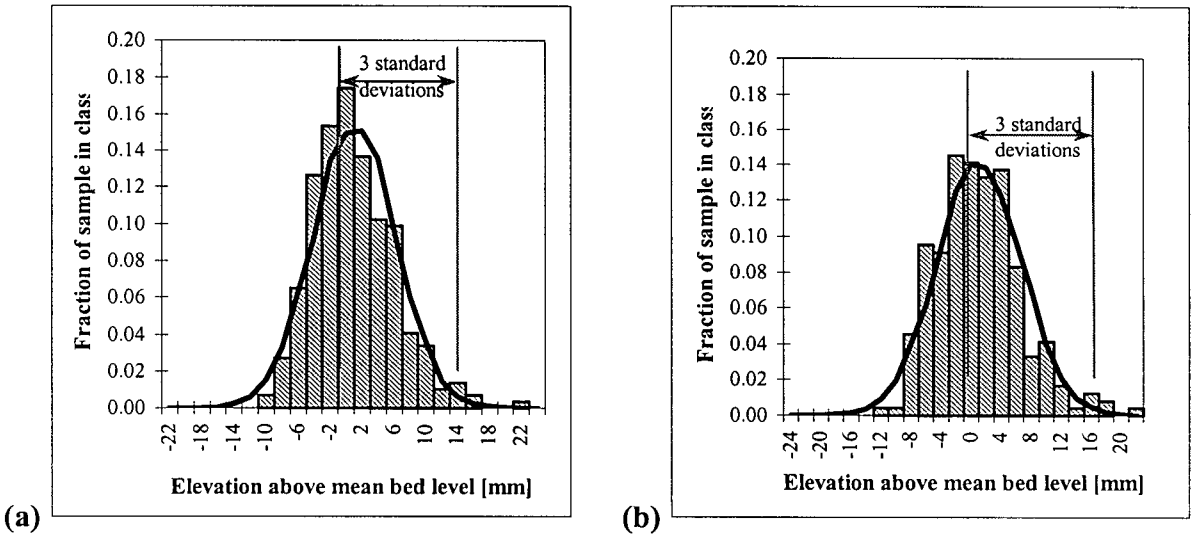

Figure 5.7. *Frequency distributions of bed surface elevations:*

(a) Run 4, σ_z = 5.1 mm; and (b) Run 5, σ_z = 5.6 mm

The next step in the analysis was to determine the statistical properties for various grain sizes. The contour plot super-positioned over a coloured photograph was used to identify different grain sizes, which were coloured in different colours (Fig. 4.35. and 4.36.). Then, each colour was examined separately by digitising the highest point on every grain within the image and determining the elevation from the DEM. Four different mean elevations were obtained for the coarsest four grain fractions (blue, red, green and yellow), and these were compared to the mean bed elevation of the whole area to obtain the average grain protrusions. In addition, the non-coloured grains representing the fractions between 1 and 8 mm were also digitised to provide the information about the background bed elevation. This determination of grain protrusion assumes that the mean bed elevation corresponds to the

zero bed level where the logarithmic velocity profile approaches zero. Tables 5.5. and 5.6. contain the information about the statistical properties for different grain size elevations for Runs 4 and 5, respectively, where the mean, maximum and minimum are the appropriate distances from the laser. The Kolmogorov-Smirnov tests for different grain sizes showed that the distributions for elevations of various grains are also similar to Gaussian for the 90% significance level or higher. (Compare the K-S test values against the critical K-S values for α=0.1 and 0.05 given in the bottom two rows of Tables 5.5. and 5.6. If the test values are less than the critical value, the distribution is not significantly different than normal).

Figure 5.8. represents graphically the mean values for the whole bed and for the different grain-size elevations in terms of the measured distance from the laser for the two runs. The error bars illustrate the range of measured values (i.e. the maximums and the minimums), and the horizontal line is the mean bed elevation. The background bed elevations are just below the mean bed level, which could be interpreted as an effect due to sheltering, such that these finer grain sizes can remain on the bed surface and they do not get transported downstream. The coloured grains protrude increasingly higher into the flow, as the grain size increases, because larger grains can withstand higher forces imposed by the flow.

The grain-size protrusions obtained from the laser measurements will be compared with protrusion calculations from the Grain Protrusion Model in Section 5.2.4.

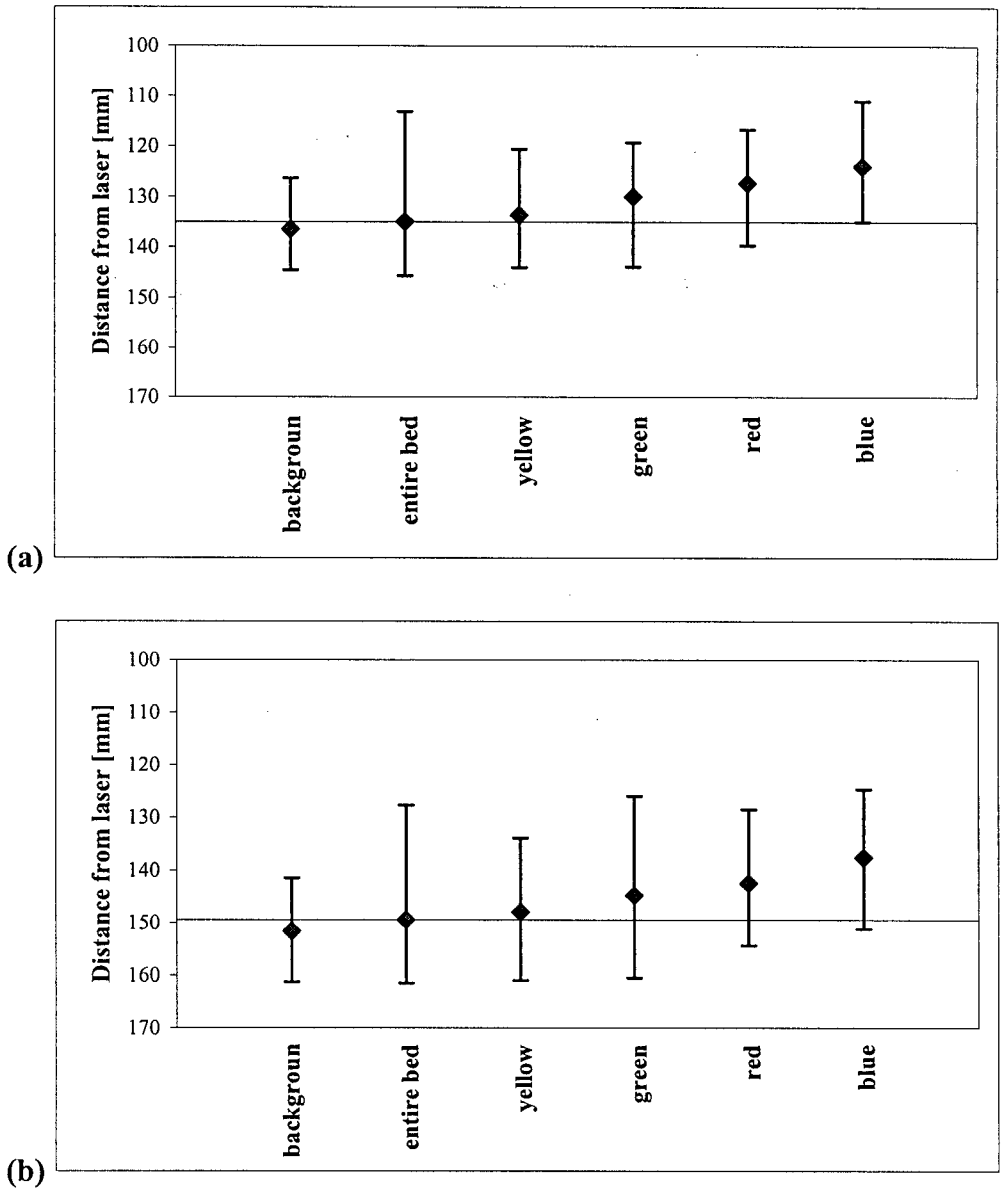

Figure 5.8. *Mean bed elevation and mean elevations for different grain sizes (the error bars represent the measured maximums and minimums): (a) Run 4, mean bed is at 135 mm; and (b) Run 5, mean bed is at 149.5 mm.*

Units in [mm]	whole bed	back-ground	yellow	green	red	blue
Grain size	1 - 32	1 - 8	8 – 11.3	11.3 - 16	16 – 22.6	22.6 - 32
Number of values	293	105	501	177	86	22
Minimum	113.1	126.3	120.6	119.2	116.7	110.9
Maximum	145.7	144.5	144.1	143.9	139.7	135.0
Range	32.5	18.2	23.5	24.7	23.0	24.1
Mean	**135.0**	**136.4**	**133.6**	**130.1**	**127.4**	**124.4**
Median	135.5	136.9	134.2	129.8	127.6	122.6
Standard deviation	5.09	3.96	4.33	4.52	4.97	5.96
Standard error	0.30	0.39	0.19	0.34	0.54	1.27
Skew	-0.67	-0.30	-0.27	0.17	0.05	-0.03
Kurtosis	0.86	-0.21	-0.24	0.19	-0.34	-0.28
Kolmogorov-Smirnov test	0.06	0.06	0.06	0.05	0.05	0.17
Critical K-S, α=0.10	0.07	0.12	0.05	0.09	0.13	0.25
Critical K-S, α=0.05	0.08	0.13	0.06	0.10	0.15	0.28

Table 5.5. *Statistical properties for the whole bed and for different grain size elevations in Run 4.*

Units in [mm]	whole bed	back-ground	yellow	green	red	blue
Grain size	1 - 32	1 - 8	8 – 11.3	11.3 - 16	16 – 22.6	22.6 - 32
Number of values	240	96	469	202	88	33
Minimum	127.7	141.4	133.9	126.0	128.5	124.7
Maximum	161.5	161.2	160.9	160.4	154.3	151.2
Range	33.8	19.8	27.0	34.5	25.8	26.5
Mean	**149.5**	**151.6**	**148.0**	**144.8**	**142.5**	**137.5**
Median	150.1	151.3	148.1	144.8	142.7	135.7
Standard deviation	5.62	4.80	4.65	5.14	5.82	7.92
Standard error	0.49	0.36	0.21	0.36	0.62	1.38
Skew	-0.70	-0.13	-0.14	-0.30	-0.09	0.33
Kurtosis	0.97	-0.81	-0.16	0.79	-0.13	-1.06
Kolmogorov-Smirnov test	0.05	0.08	0.04	0.05	0.05	0.12
Critical K-S, α=0.10	0.08	0.12	0.056	0.09	0.13	0.21
Critical K-S, α=0.05	0.09	0.14	0.062	0.10	0.14	0.23

Table 5.6. *Statistical properties for the whole bed and for different grain size elevations in Run 5.*

To test if the mean elevations for different grain sizes are significantly different, the analysis of variance or the ANOVA test was performed. The test showed that at a significance level of 99%, there was significant difference between the means for both runs. Subsequent analysis was needed to determine for which of the means the difference was significant and a multiple comparison procedure called the Tukey test was performed. In this test, for all the pairs of data sets that are compared, the difference of their means is divided by the standard error, and this value is compared to the critical value. The critical values are tabulated in statistical textbooks, and depend on the required significance level, the total number of means being tested, and on the error of degrees of freedom for the analysis of variance. If the value from the Tukey test is equal or greater than the critical value, that indicates that the means for the tested pair are significantly different, and that the values of the means are not due to few outliers. For a 99% significance level, the test showed that the comparison of each pair of means was significantly different. This can be interpreted such that the mean protrusion of blue grains, for example, is truly different than the mean protrusion of red grains. The tests indicate that the observed difference in the means is not due to few highly protruding grains which are very different from the other grains in a size fraction, but that the means are true representatives of the protrusion for that size.

To inspect the difference in the means graphically, the mean protrusions are plotted with error bars that represent ± one standard error in Figures 5.9.a and 5.9.b for Runs 4 and 5, respectively, where the standard error estimates the uncertainty in determining the means. It is evident in the two figures, that the means were estimated with very little uncertainty for all

grain sizes. The standard errors are somewhat increasing with a decreasing number of values or, the number of grains digitised in a size fraction, for which the mean was estimated.

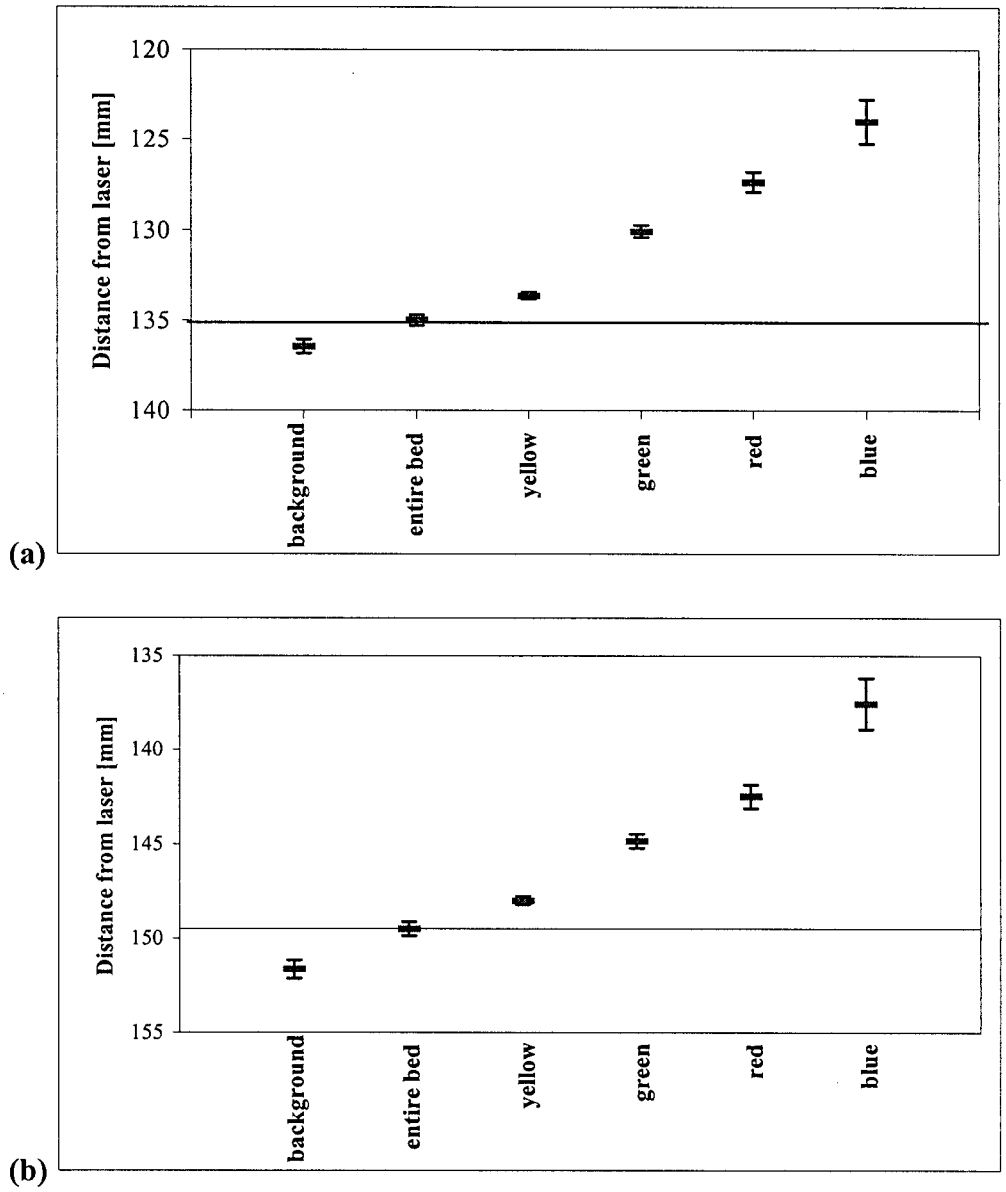

Figure 5.9. *Mean grain protrusions with error bars of ± one standard error: (a) Run 4, mean bed is at 135 mm; and (b) Run 5, mean bed is at 149.5 mm.*

5.2. Numerical Model Results

The experimental results from this study and from the studies of Proffitt (1980) and Saad (1986) were used to test the calculations from the Grain Protrusion Model. The model predictions for the roughness coefficient (k_s), mean velocity (U) and depth of flow (Y) were compared to the measured values in these three studies. In addition, the protrusion measurements from this study will be compared to protrusions predicted in the numerical model.

5.2.1. Selection of experimental data for testing

Several studies including experiments on gravel bed armouring were considered for testing the Grain Protrusion Model (Proffitt, 1980; Chin, 1985; Saad 1986; Gomez, 1993; and Church et al., 1998). All these experiments were conducted in a laboratory flume under zero sediment feed conditions. Poorly sorted sediment was placed on the bed, and allowed to coarsen through degradation until a stable armour layer had developed in which sediment transport declined to vanishing levels. In general, the coarsening was accompanied by a slight to a moderate reduction in bed slope. However, because of insufficient data, or data where some of the results were uncertain, several studies had to be rejected.

The experimental results of ***Chin*** (1985 and 1994) could not be used, because the values of slopes, velocities, or discharges were not reported. Only the values of depths, shear velocities and bed surface composition were accounted for in this work, which was insufficient for purposes of testing the validity of the proposed numerical model because,

without the measured velocity data, the "observed" roughness could not be obtained and the model predictions for k_s and U verified. In addition to insufficient data, the shear stress was kept constant throughout the runs by constantly readjusting the sediment table to match the degradation. The purpose of Chin's studies was to find the "critical" shear stress for a given sediment mixture and, for each set of runs, the shear stress was increased until no armour could form. Keeping the shear stress constant throughout the entire duration was important, because the experimental conditions were better controlled and less variability was present due to self adjustment of hydraulic parameters. While forcing the shear stress to stay constant seems to be a reasonable thing to do, it was found in our experiments that if this was done, the bed armoured differently than if it armoured through an interactive readjustment of slope, depth, and velocity. As a consequence, there was no reduction in shear stress through time, the final degradation was higher, and the bed surface probably somewhat coarser. A similar effect occurs if the tail-gate is readjusted through the run.

The study of ***Gomez*** (1993 and 1994) contained all the necessary data, with depths, flow rates and velocities similar to the same parameters in our study. The bed material ranged from 1 to 64 mm and the experiments with rounded sediment were considered for our analysis. However, the reported initial slopes of 7%, 10%, 14%, 17% and 20% appeared quite high and were actually supposed to be 0.7, 1.0, 1.4, 1.7 and 2.0% (personal communication with B. Gomez, 2000). Furthermore, the final energy slopes and shear velocities seemed very high, with u^* ranging from 0.094 to 0.243 m/s (compared to approximately 0.04 to 0.079 m/s in our experiments). At the same time, the variation in D_{50} was surprisingly low, between 12.1 and 17.9 mm, while for a much smaller range of imposed

shear stresses in our experiments, D_{50} changed from 4.7 to 11 mm (more than doubled). After obtaining the original set of bed and water surface elevation measurements from the author, the appropriate slopes were recalculated and it appeared that the problem occurred when the elevation measurements were converted to a horizontal datum. The bed and energy slope reduction was considerable for all runs (Fig. 5.10.), which was contrary to the reported values. The degradations ranged between about 4 cm for the lowest and 11.5 cm for the highest shear stress runs, while the initial depth of sediment was only 12 cm, which meant that there were sections where the depth of sediment was less than one grain diameter thick for the coarsest grain sizes. It was uncertain if the roughness was due to grain protrusion only, or if substantial bed forms developed to stabilise the bed, thus, the results from this study were not used in testing the Grain Protrusion Model.

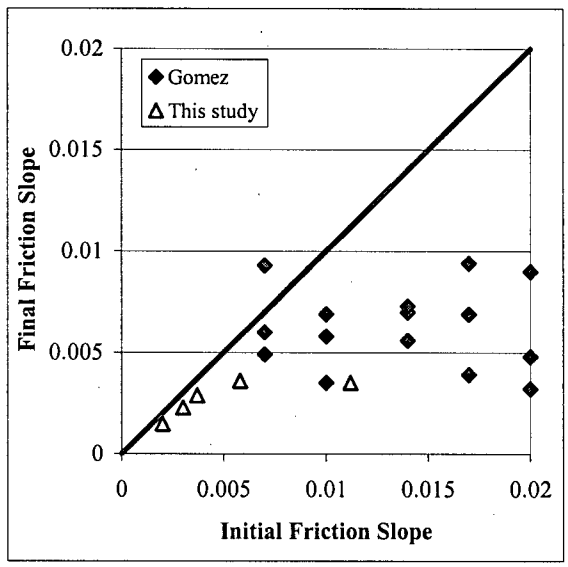

Figure 5.10. *Initial vs. final friction slopes for the experiments of Gomez (1993), and for this study.*

It is interesting to recognise in Figure 5.10. how the final friction slopes level off despite the increase in the initially imposed slopes for both studies. This levelling off was lower for our study at $S_f \approx 0.035$, than for Gomez at $S_f \approx 0.07$, on average. The possible explanation is in reaching the limiting, or "critical" shear stress for the given sediment mixture, which was in part governed by slope reduction. The original sediment mixture of Gomez was coarser than in our study, thus the limiting slope was higher. However, it seems that the system is less able to stabilise as the slopes are pushed further over the limit, so that there is a higher variability in final slope estimates for the repeated tests of the highest two initial slopes for Gomez.

Church et al. (1998) performed experiments on gravel bed armouring, and while the observations from the study were confirmed in our experiments as well, there appeared to be some disagreement with several of the reported measurements. For example, the reported discharges were calculated from velocity measurements (personal communication with M. Hassan, 2000), but when the velocities were back-calculated from these reported discharges and depths, they appeared quite high (ranged between 0.8 and 1.4 m/s) compared to our velocities (0.6 to 0.84 m/s). The velocity measurements are very important when testing the model, because the "observed" k_s values are calculated from them. The conclusion that the velocities seemed higher than expected was supported by direct comparisons of some of the other results from both studies, which was possible, because the same bed material was used. The reported hydraulic radius ranged between 0.035 and 0.066m for the runs considered for testing (compared to 0.13 – 0.18 m in our study), while the slopes were between 0.0066 and 0.0105 (0.0015 and 0.0036 were the final slopes in our study). The reported depths of

degradation were between 2 and 13 mm, which seemed quite low for the given velocities and slopes, and when compared to our experiments in which the depths of degradation ranged between 7 and 34 mm. All sizes were reported to be moving despite low degradations (the coarsest grain size was 32 mm), while for our first two runs the coarsest fractions did not move. Because of all of the uncertainties, these experiments were not used to test the numerical model.

The work of ***Proffitt*** (1980) seemed to contain all the necessary data for the input to the numerical model, as well as other measured data that were also needed for verification of the model predictions. Run 1-6 was the only experiment not used in our analysis, because it lasted only for 2 hours and the final reported armoured bed was finer than the parent material. It was considered that this run had a very low imposed shear stress and was not a true representation of the bed armouring processes. In his experiments, Proffitt tested four different sediment mixtures.

In the experiments of ***Saad*** (1986), six different sediment mixtures were tested and bed armouring was examined. This study was also used to test the numerical model, despite some discrepancies in how the data analysis was conducted. Saad readjusted the tail-gate to keep the water surface slope constant, and he calculated this slope as an average of all the water surface elevations throughout the entire run, even though there were some runs in which the initial water surface slope was obviously different than the final slope. The bed slopes were measured only initially and at the end of each run, while the friction slopes were obtained by combining the final bed slopes and the average of the water surface slopes

throughout the run, by using the equation $S_f = S_w - \frac{U^2}{2g}(S_w - S_b)$. Although there were some questions about the data and the slope determination, it was decided to test these data against the Grain Protrusion Model. All of the slopes were relatively low (between 0.00145 and 0.0066), and it was reasoned that, even if the final, instead of the average, water surface slope was used to estimate the friction slopes, the difference in friction slopes would not be significant.

5.2.2. Comparison with previous studies

Before testing the numerical model, the experimental results of Proffitt (1980), Saad (1986) and this study will be compared. Proffitt tested four, while Saad tested six different sediment mixtures in their experiments. Figure 5.11. was plotted to illustrate the difference in the behaviour of the mean grain size for the armour material (D_{50arm}), and the hydraulic roughness coefficient (k_s) with an increase in shear stress (u^*). The relationship between D_{50arm} and u^* is close to linear, indicating that the bed surface coarsens with more fine material being transported due to the increased shear stress. However, there must be some limitation to this size increase constrained by the coarsest available grain size on the bed. In addition, for different values of u^*, the values of D_{50arm} were calculated by assuming τ^*_{50arm} = 0.03, or τ^*_{50arm} = 0.06, which represent the commonly assumed range of non-dimensional shear stresses for incipient motion (solid lines in Fig. 5.11.a). All but two data points fall within this range.

If the ratio of k_s / D_{50arm}, is plotted against u^* (Fig 5.11.b), much scatter is evident, indicating that the hydraulic roughness coefficient, k_s, is not due to surface coarsening only (and

consequently increase in D_{50arm} only). It could also incorporate form roughness possibly originating from organised bed structures. Therefore, even in these relatively simple and straightforward laboratory conditions, the roughness coefficient did not always have a linear relationship with particle size. Some investigators consider that the particle size is not a precise indicator of surface roughness, and not useful for predicting flow resistance in alluvial channels (Gessler, 1990; Smart, 1999; Millar,1999). For fully developed rough turbulent flow, the hydraulic roughness depends on the bed surface topography, and this may or may not reflect the particle size distribution.

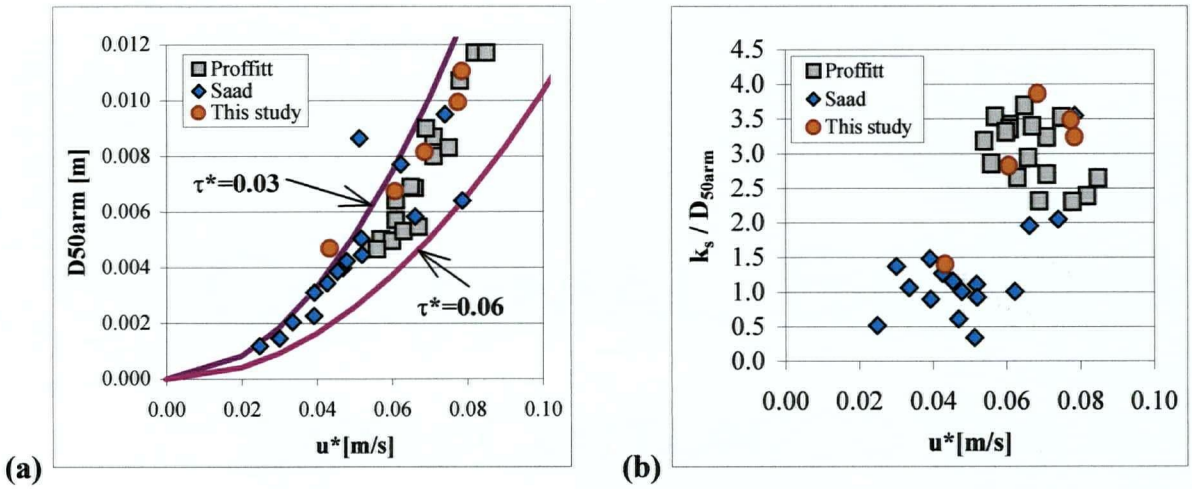

Figure 5.11. *Increase in (a) median grain size, and (b) roughness coefficient, with increasing shear velocity for experiments of Proffitt, Saad and current study.*

The bed coarsening, represented by D_{50arm}, is plotted against the Shields' number for the initial mixture ($\tau_0 / g(\rho_s - \rho)D_{50orig}$) in Figure 5.12.a. Here, all the different sediment mixtures that were tested in the experiments of Saad, Proffitt and this study were represented as separate data series, and it appears that for all sediments there is an increase in the armour

coarseness with increasing shear. To collapse the data, D_{50arm} was non-dimensionalised by D_{50orig} for each sediment mixture and plotted in Figure 5.12.b, which represents the relative bed coarsening as a function of the Shields parameter based on the original sediment size. A definite increasing trend in bed coarsening with increasing dimensionless shear stresses is evident, and the scatter could be attributed to different gradings of the tested sediments. Proffitt (1980) showed that mixtures with wider gradings for the original sediment produced larger values of D_{50arm} / D_{50orig} for a given value of dimensionless shear stress, but it seemed that these different gradings had little effect on the relative increase in the D_{50arm} size.

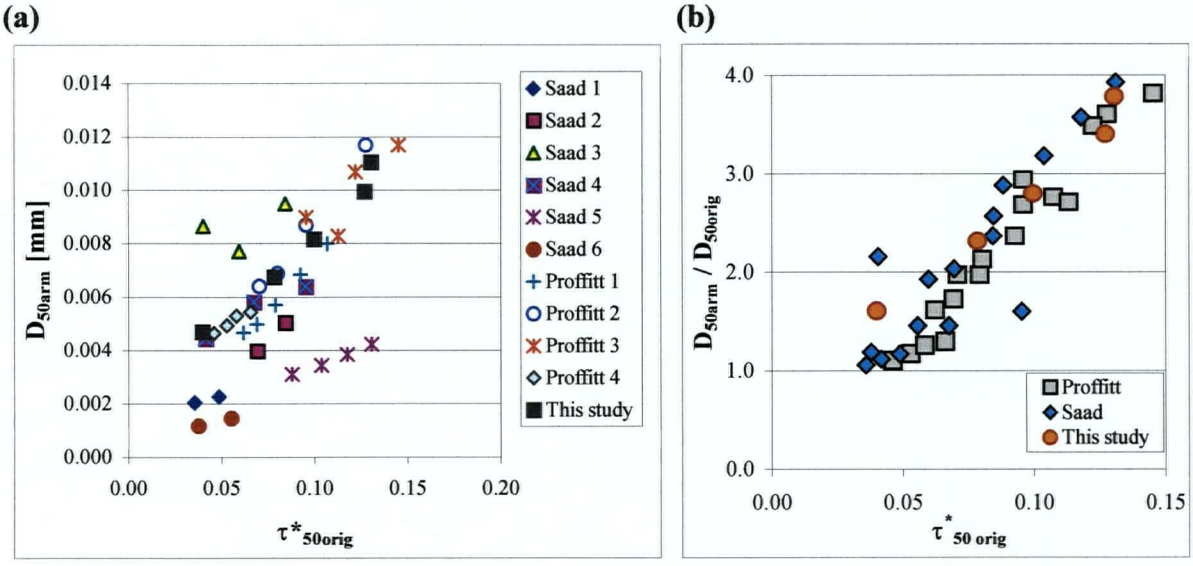

Figure 5.12. *Increase in bed coarsening with increasing bed shear stress: (a) The mean armour grain size, D_{50arm}; and (b) The relative coarsening, D_{50arm} / D_{50orig}.*

Figure 5.13. illustrates the relationship of the Shields' number for the armour layer and the relative depth R_{bed} / k_s, where R_{bed} is the hydraulic radius corrected for sidewall effects. In general, the dimensionless shear stress values are in the range between 0.03 and 0.06, with the exception of a couple of outliers (similar to results in Fig. 5.11.a). These values fall

within the range of commonly assumed values for the critical Shields' stress for gravel-bed rivers (Buffington and Montgomery, 1997; Wilcock et al., 1996, and others). The outliers are Run 5 of Saad and Run 1 from this study, which were both very low shear stress runs with low transport rates in which not all grain sizes moved, thus the Shields' number for these runs was below the critical value for the sediment mixture. However, the non-dimensional shear stress has a somewhat increasing trend for rougher beds, for which the relative depth R_{bed} / k_s was lower, as shown by the left hand side of Figure 5.13. This result is an indication that armoured beds can withstand higher shear stresses possibly due to protrusion of larger particles, and perhaps bed rearrangement into clusters and stone cells (Sutherland, 1987; Church et al., 1998).

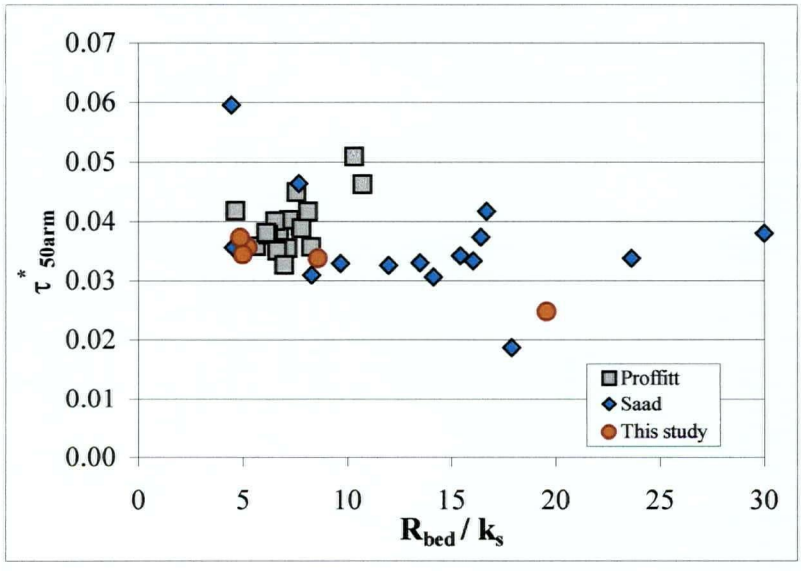

Figure 5.13. *Variation in Shields' number for the armour layer for different relative depths.*

5.2.3. Grain Protrusion Model predictions for k_s, U and Y

The model calculates the flow parameters based on the hypothesis that all grains on the bed surface are just on the threshold of motion (see Chapter 3). The input parameters are the friction slope (corrected for sidewall effects for flume studies), flow rate and bed surface grain size distribution, and the iterations towards a solution start with assuming initial values for the depth and the hydraulic roughness coefficient, k_s. The different grain size protrusions are calculated by equating the applied shear stresses on the grains to the critical shear stresses for those grains. If the total sum of grain shear stresses does not match the total shear stress applied by the flow ($\tau_o = \rho g Y S_f$), the value of the roughness coefficient is updated until the whole system is in balance. The mean velocities are then calculated and if continuity is satisfied, a stable solution for the input hydraulic parameters is found, otherwise the model updates the depth and a new iteration starts. Example spreadsheets from the model can be found in Appendix D.

The stability of each grain size fraction is assessed in the numerical model by comparing the imposed shear stress on a particular grain size to the critical shear stress for that grain size, and the protrusion of the grain is adjusted until the grain is just stable. However, there were few experiments with very low imposed shear stresses, and for these cases the critical shear stress for the coarsest grains could not be reached in the numerical model. This meant that the grains were below the threshold of motion, and that they most likely did not move during the experiment, but were exposed slightly only as a consequence of degradation. In these cases, the model indicated that the grains were "over-stable", and the protrusions had to be calculated and entered manually. It was assumed that some of these non-mobile grains did not protrude

and some protruded for the full depth of degradation, thus the average protrusion of these grains was assumed to be equal to one half of the degradation depth (see sample spreadsheet in Appendix D). For example, if the degradation was equal to 3 mm, and the coarsest grain size was 30 mm, this grain did not move, but only got exposed between zero and 3 mm, thus the average relative protrusion (H_i/D_i) was equal to (3 / 30) / 2 = 0.05.

The Grain Protrusion Model results are illustrated in Figures 5.14. through 5.16. The "observed" k_s values were calculated from measured depths, slopes and mean velocities obtained from continuity for all three studies. The discrepancy between the observed and predicted roughness may seem high (Fig. 5.14.), but in general it is within ±30%. More so, if these predictions are compared to predictions from an empirical model of a type $6.8D_{50}$ (see example in Chapter 2, Fig. 2.2.), the Grain Protrusion Model performs quite well. It seems that the model somewhat over predicts the hydraulic roughness for lower shear stress runs (e.g. runs of Saad and Run1 from this study). In addition, there is some uncertainty involved in the "observed" roughness values, which could add to the disagreement between the model and the measured values. Specifically, k_s cannot be measured directly, but is derived from other measured values and it is only as good as the accuracy of these other measurements (see Fig. 5.5.). It is particularly sensitive to small variations in measured values, because the term k_s appears as a logarithm, which magnifies the effects of variation.

In comparison, close agreement is achieved between observed and calculated values for mean velocities and depths (Fig. 5.15. and 5.16.), which are within ±10% of the measured values. It appears that this model can be used to predict the roughness coefficient, mean

velocity and depth for flows over gravel beds for which the relative roughness (k_s / R_{bed}) is low to intermediate, ranging from about 0.03 to about 0.2 in the tested data sets of Proffitt, Saad and the present study (the corresponding relative depths were R_{bed} / $k_s \approx$ 4.5 to 30). The realistic predictions from the model indicate that the basic assumptions underlying the model are physically sound and acceptable for these conditions. For flows with large relative roughness, i.e. above 0.2, it is probable that the logarithmic velocity profile breaks down, cross-flows and secondary currents become significant, and physical processes associated with flow resistance would therefore need to be modified.

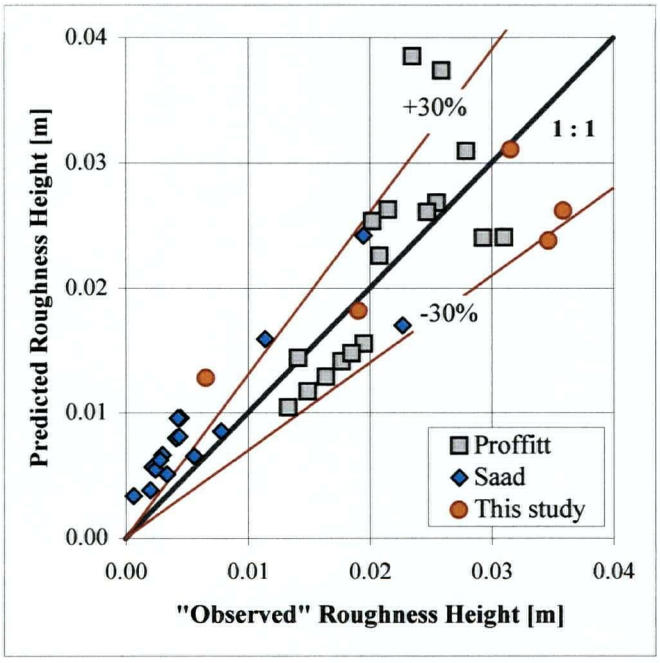

Figure 5.14. *Roughness coefficient comparison with predictions from the numerical model.*

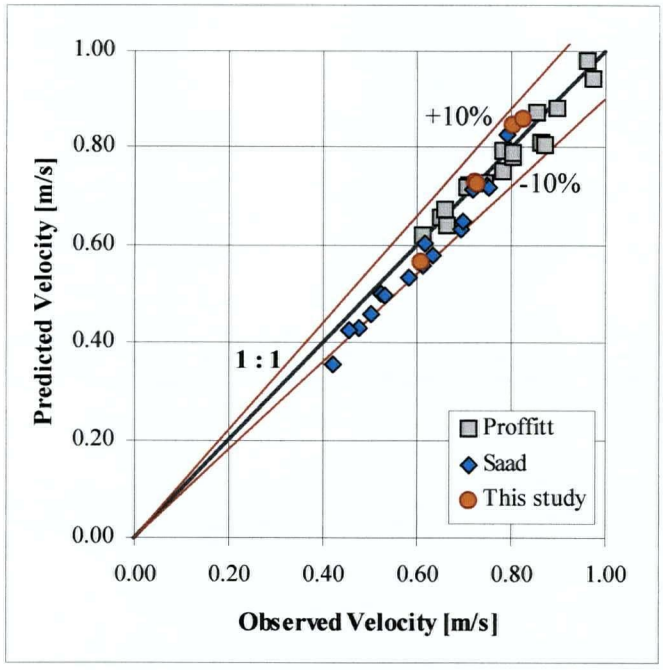

Figure 5.15. *Mean velocity comparison with predictions from the numerical model.*

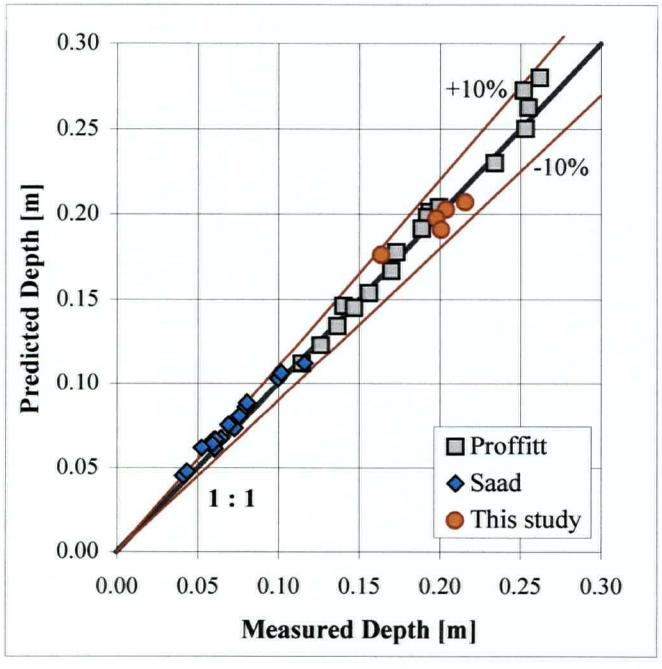

Figure 5.16. *Flow depth comparison with predictions from the numerical model.*

5.2.4. Grain Protrusion Model predictions for H

The predictions of grain protrusion could only be tested for Runs 4 and 5 from this study, for which the laser measurements were carried out and the DEMs were developed. These protrusions were calculated as a difference between the mean bed elevation for the whole bed and the mean elevation for a particular grain size (see Tables 5.5, 5.6. and 5.7.). The grain protrusions from the numerical model were compared to those measured with the laser for the four coarsest fractions (Table 5.7. and Figure 5.17.).

Good agreement for both runs was obvious, with the best protrusion predictions for the two coarsest fractions of Run 5. The predicted protrusions were within 20% of the measured ones, except for the smallest yellow grains, for which the model over predicted the protrusion heights. The good agreement between the measured and modelled protrusion indicates that the selection of the measured mean bed elevation as a reference level, from which to calculate the protrusion, coincides with the zero bed level calculated in the model. This confirms the findings of Nikora et al. (1998) and Smart (2001 and 2002a), who suggested that the virtual bed where the log velocity becomes equal to zero is equivalent to the mean grain-elevation level (i.e. mean bed level).

	Grain size [mm]	**Run 4 laser H_i [mm]**	**Run 4 model H_i [mm]**	**Run 5 laser H_i [mm]**	**Run 5 model H_i [mm]**
blue	22.6 - 32	10.61	12.18	11.95	11.8
red	16 - 22.6	7.61	6.86	7.02	6.72
green	11.3 - 16	4.92	4.07	4.67	3.99
yellow	8 - 11.3	1.35	2.43	1.50	2.39

Table 5.7. *The protrusions measured with the laser and the protrusions predicted in the Grain Protrusion Model for Run 4 and Run 5.*

However, for the blue grains in Run 4, there are two possible results, seen as the green star and the top green triangle in Figure 5.17. The protrusion of the blue grains was initially obtained by digitising all of the blue grains in Run 4 (the green star). This result included about 8 blue grains that were almost buried and had not yet been uncovered (also see Fig. 4.30 and the accompanying discussion). For these grains the elevation of the top of the grain was below the mean bed level (some were more than 10 mm lower), so that these grains did not carry any of the shear, or create resistance to the flow, nor could move to find stable positions on the bed. Consequently, they did not compare well with the protrusion prediction from the numerical model, as shown with the star in Figure 5.17. Considering that almost one third of the total number of blue grains were buried in this run (8 out of 30 blue grains visible in the photograph – Fig. 4.36.), the mean bed elevation and the protrusion were quite affected by these grains. However, if these buried grains were excluded from the analysis, a much better agreement with the numerical model was obtained (top triangle in Fig. 5.17.).

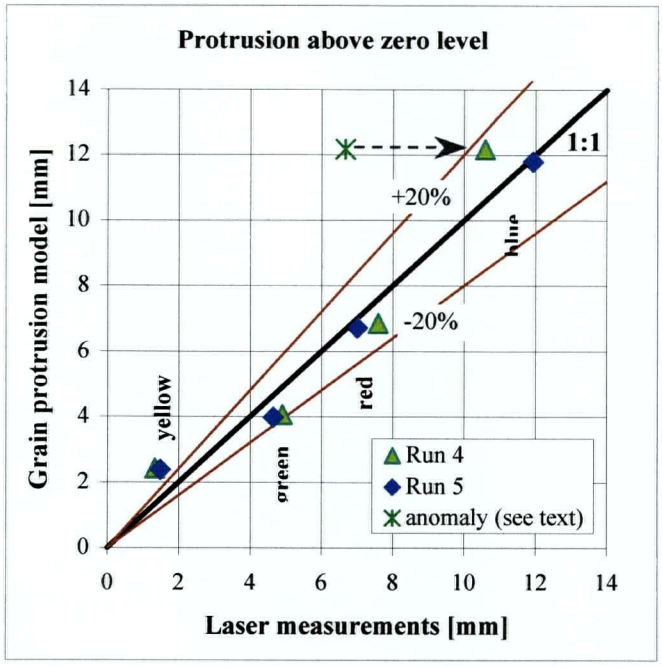

Figure 5.17. *Comparison between the protrusion measurements obtained with the laser and the predicted protrusions in the Grain Protrusion Model for Run 4 and Run 5.*

CHAPTER 6.

DISCUSSION AND CONCLUSIONS

The goal of this research was to investigate the hydraulic roughness for static armoured water-worked gravel beds. Static armoured beds develop in clear water flows with no sediment input, contrary to mobile armoured beds for which the armour layer refreshes in exchange with the sediment passing through the system. It can be said that the armour is stable for flows that are lower than the constructing flow, which means that the constructing flow is ultimately the critical flow (and critical shear) for the given armour.

The approach in the study was theoretical and experimental. An attempt was made to model the bed forming processes and deal with the way in which sediment would adapt to the shear stress. The theoretical approach resulted in a numerical model, in which the hydraulic roughness, k_s, and bed stability were related to the relative grain protrusion, H/D. The model was then tested against existing data. However, some data were found to be unreliable, while some other studies had insufficient information and data, which created a need for a new experimental investigation. The experimental work has resulted in a better understanding of the processes involved in gravel bed armouring. Some of the assumptions underlying the numerical model were examined, additional data were obtained, and a detailed study on individual grain protrusion was conducted.

The basic hypothesis in this work is that the bed organises so that the surface particles are all at the threshold of motion, at least statistically, which is considered to be a limiting case of

equal mobility (Parker and Sutherland, 1990). Alternatively, if the flow conditions are such that all grain sizes are in motion, then a stable armour layer can develop only after a slope reduction takes place and the forces decrease to levels that allow the most resistant particles to become stable.

6.1. Analytical Considerations

The numerical model operates under the assumption of no upstream sediment supply, so that the bed degrades to an armoured state. In this process, it is assumed that the sediment protrusion of different sized grains adjusts in such way that each grain on the bed surface reaches the threshold of motion. Sheltering behind larger particles is not considered, but sheltering by being buried by surrounding particles is modelled by protrusion.

When developing the Grain Protrusion Model, several assumptions were made, because the procedure had to be logical and had to be expressed mathematically to make the computation possible. The numerical model is based on an assumption of a limiting case of equal mobility, where the grains on the bed surface are at the threshold of motion. Many factors such as particle weight, size and shape, together with packing, imbrication and sheltering effects, would influence the particle's mobility. However, it was felt that in a simplified model to simulate particle mobility, a particle's relative protrusion (H/D) could represent a reasonable modelling parameter, because it is possible to account for differences in applied forces on various grains if the grain exposure is known. It was assumed that the lift force is implicitly accounted for in the critical shear stress relationship, and an equation was

developed to predict the modified drag coefficient relative to the particle protrusion. Likewise, the critical shear stress calculations were related to grain protrusion, which was possible from Fenton and Abbott's (1977) and Chin's (1985) experimental work. In all this, it was important to establish the virtual bed from which the protrusion is measured, and an assumption was made that the zero bed level is equivalent to the elevation where the logarithmic velocity profile extrapolates to zero.

The last assumption automatically puts a limitation for the model's applicability to flows with intermediate to high relative depths (or intermediate to low relative roughness), in that the virtual bed position calculation would be incorrect for flows for which the logarithmic velocity law breaks down, which happens for low relative depth. The alternative would possibly be to incorporate into the model a velocity law that applies in such flows, but modifications for other assumptions in the model would probably also have to be made.

It was anticipated that a larger part of the shear stress would be carried by a few of the most exposed, largest grains present on the bed surface. The grain protrusion measurements obtained from DEMs confirmed that the largest grains were exposed the most, providing that they moved during the experiment. The numerical model also predicted this correctly, and estimated the protrusions of the coarsest grains to be the highest, such that the coarsest few fractions received 70%, or more of the applied forces.

The input parameters to the model are the friction slope, the flow rate and the bed surface grain size distribution. All these parameters, when measured in the field, can be uncertain to

some extent, and some of these uncertainties are discussed below. For example, it was shown that, even in laboratory conditions, accurate slope measurements were not easy to obtain, because the slopes we deal with are very low, and their estimates are sensitive to the number of points used and to the position where the staff gauge is placed (on the top of a large grain vs. a depression between the grains, which affects the depth, bed slope and friction slope estimates). Flow rate measurements are often obtained from transects, where the cross-sectional area and the velocities are measured and converted to flow rates; or predicted from staff gauges and stage-discharge curves; or some other means. All these methods provide an estimate, rather than an accurate measure of the discharge. In the field, grain size distributions are often obtained from exposed bars, which usually have somewhat finer grain size distributions than mid-channel regions, because the tops of bars are usually formed during the receding limb of a flood curve when finer material is deposited. Also, the velocities in the mid-channel are usually higher, imposing higher forces on grains. In addition, the method used to sample the surface is not always reported, and there is a difference in distributions if the data were obtained by Wolman (1954) count, or by areal sampling, or if a part of the substrate was included in the sample. All of the above uncertainties are only part of the causes that influence the accuracy of input parameters.

Needless to say, predictions from any numerical model are only as good as the input parameters. When dealing with natural phenomena, the variability in the basic parameters is considerable, but this should not discourage us from trying to model these occurrences. Every step towards a better understanding of the physical processes involved is a step

forward in producing better models that would make better predictions of future, or estimates of past events.

The Grain Protrusion Model works very well for the conditions tested, and the predicted hydraulic roughness, mean velocities and depths were reasonable estimates of measured values. There are no calibration coefficients in the model, although the surface grain size distribution is required as input. These good results are at least a very good first step in justifying the assumptions made. The agreement with the numerical model is very encouraging and indicates that the assumptions made might be extended to other situations, such as when there is a specified sediment supply.

6.1.1. Protrusion prediction

The measurements obtained with the laser displacement meter set the stage for the study of grain protrusion, with the possibility of fitting the measurements to the exact grain size by using the colour-coded sediment mixture. The grain protrusion measurements made it possible to further examine the validity of the numerical model and to test some of the assumptions on which it was based. The case of bed armouring, where the grain protrusion was the dominant feature in creating the hydraulic roughness, was modelled successfully using the Grain Protrusion Model. When other bed features became notable and the roughness was not due to grain protrusion only, but also to organised bed structures, the hydraulic roughness was somewhat under-predicted (Runs 4 and 5).

It was observed that the numerical model predicted higher relative protrusions for lower shear stress runs. For example, H_i/D_i were higher for Run 3 than for Run 4, and both previous runs had higher protrusion predictions than for Run 5, which seemed somewhat contradictory. Intuition suggests that higher grain protrusions are needed to counterbalance higher shear stresses. The possible explanation is that if the exposure is too high, the grains cannot withstand higher shear stresses, and therefore they do not adjust their position by further increasing the protrusion, but carry the extra shear stress by having higher concentrations of larger particles on the bed surface. If this higher concentration of larger particles organises into bed structures, then the grains are even more resistant to shear. Otherwise, if the individual grain protrusions increase further, the grains would become less stable, which in turn would jeopardise the overall stability of the bed.

Gomez (1994) defined the representative roughness height as the height for which 95% of the effective roughness is lower, which translates into the effective height of the highest 5% of protruding grains. He observed that the representative roughness height might tend to increase initially, but then decrease with further increasing flows. Gomez speculated that this happens "because roughness height is constrained by the size of the coarsest particles present on the bed", and further that "It is also regulated by particle protrusion and increasing roughness concentration, which eventually acts to smooth the bed".

Such a trend was observed in the average protrusion height predictions for the coarsest grains in the Grain Protrusion Model. The predicted protrusions (H_i) for blue, red and green grains are compared for Runs 3, 4 and 5 in Table 6.1. The smaller yellow grains were not

considered here, because the differences in calculated protrusions for the three runs became insignificant. The geometric mean size (D_{gi}), and the percentage of grains by weight (F_i) that were sampled for the bed surfaces in these experiments are also given for the three runs. It seems that the predicted protrusion heights from the numerical model decreased with increasing concentration of grains (F_i) on the bed surface for each grain size, which is similar to Gomez' (1994) observations. The only exception is the prediction for the blue grains in Run 3, for which seems as if the fraction of these grains was higher than expected. A possible explanation is that the experimental F_i for this run could have been somewhat incorrect, because during the bed surface sampling with potter's clay, some blue grain, or grains that were buried under a thin layer of fine sediment, or just starting to become exposed, could have been picked-up, thus increasing the F_i.

	Blue grains D_{gi}=26.9 mm		Red grains D_{gi}=19.0 mm		Green grains D_{gi}=13.4 mm	
Run	**F_i [%]**	**H_i [mm]**	**F_i [%]**	**H_i [mm]**	**F_i [%]**	**H_i [mm]**
3	9	16.0	9	7.8	16	4.5
4	7	12.2	13	6.9	20	4.1
5	9	11.8	19	6.7	20	4.0

Table 6.1. *Comparison of protrusion heights calculated in the model.*

The protrusion heights were measured with the laser for Runs 4 and 5, and it is interesting to note that slightly higher protrusions (see Fig. 5.17.) were measured for green and red grains in Run 4 than in Run 5, which is similar to the numerical model predictions. Probably, the good agreement between the model predictions and the measured protrusions for red and green grains in both runs occurred because the majority of these grains present on the surface moved during the run, and adjusted their positions in order to stabilise. This was not the case

for the blue grains in Run 4, because the model calculates the protrusions for the grains that are on the threshold of motion, while the measured protrusions included all the blue grains, some of which were almost fully buried, or only slightly exposed (see the related discussion in Section 5.2.4). In contrast, for Run 5, most of the blue grains also moved during the run until stable positions were found, and that is why the agreement between the model and the measurements is so good. It would be useful to know what were the actual grain protrusions in Run 3 to further evaluate the numerical model but, unfortunately, these were not measured because of the equipment unavailability.

The good agreement between the measured protrusions and those calculated in the model supports the basic assumption of equal mobility, which was used to calculate the protrusions for different grain sizes such that they are at the threshold of motion. Implicitly, these results also confirm the critical shear stress definition, and the overall validity of the model.

6.2. Experimental Considerations

Conditions equivalent to situations just downstream of a dam, a lake outlet or another feature that captures the sediment from passing downstream, were modelled in the experiments. These conditions were achieved by having a flow without a sediment supply, where the response of the system was bed armouring through degradation and slope adjustment.

The experiments proved to be much more difficult than anticipated because the system did not respond to the preset conditions as expected when the imposed conditions were pushed

too far. For example, for imposed slopes and initial shear stresses, the simple and expected outcome would be for the bed to coarsen through degradation, and for the slope not to change much. However, when the initial conditions were set too high, the system found another way to respond to the imposed shear stresses, namely, for the shear stress to decrease. It is considered that such high pre-set conditions could be equivalent to very high discharges, which occur in natural systems with the passage of floods through a lake-river system, or in a man-made system with flushing flows released from a dam. Under such circumstances, the upstream sections of a river would feed the downstream sections, and the response of the system would be degradation, but also a considerable bed and friction slope reduction.

In these experiments, the initial shear velocities (and shear stresses) were gradually increased for each successive run until some kind of "limiting" or "critical" conditions were reached at about $u^* = 0.08$ m/s for the given sediment mixture (Fig. 6.1. in which the shear velocities were corrected for sidewall effects). This increase in shear velocities was achieved by pre-setting the slope and increasing the discharge in such way to obtain similar depths at the beginning of each experiment. It seems that the slope and depth adjustments during the first three runs were minor and, consequently, the initial and the final shear velocities were approximately equal (i.e. $u^*_{init} \approx u^*_{final}$). For the last two runs, however, it seems that the "critical" imposed slope was exceeded, thus the slope reduction was considerable, followed by depth and velocity adjustments, such that $u^*_{init} > u^*_{final}$. This was a necessary adjustment before the coarsest available grain sizes were able to stabilise. It seems that different mixtures have different critical conditions, and that mixtures with larger D_{100} could stabilise

at higher slopes, which is possible because larger grains can resist higher forces (see the comparison of final slopes for Gomez' data and data from this study in Chapter 5).

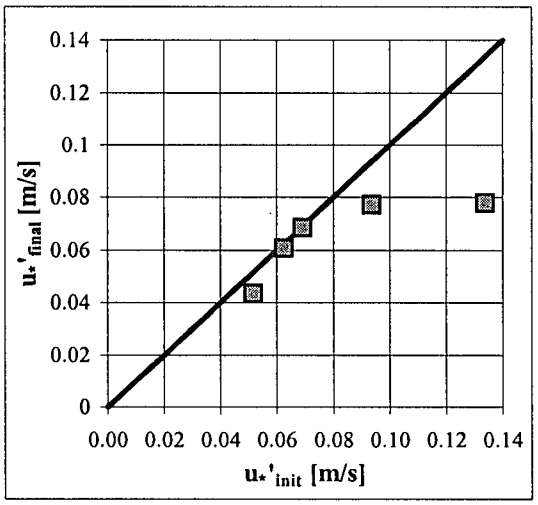

Figure 6.1. *Initial vs. final shear velocities for Runs 1 through 5 (values corrected for sidewall effects).*

6.2.1. Bed formation processes

Two possible mechanisms for bed armouring were observed in the experiments, and these mechanisms could be considered to be the response of the system to the initial conditions. In both cases, the initial transport phase is associated with formation of dune-like features, or transverse gravel bars, that are moving downstream through the channel. The first case occurs when not all grain sizes are set in motion, and in this case the armouring is mostly through degradation and a mild slope reduction, because most of the transported material passes through the whole system. The second case occurs when more extreme conditions are imposed, considerable sediment transport takes place, and all grain sizes are set in motion. Here, the upstream sections start feeding the downstream sections and, initially, aggradation

could occur in the downstream sections, resulting in considerable bed and friction slope reduction. In the upstream sections, the armouring is through degradation only, while in the downstream sections the coarser material being transported becomes able to resist the flow and starts armouring the bed. From this point, the bed armouring proceeds, as in the first case, through degradation due to selective transport of the finer material exposed on the bed.

The shear stress acting directly on the grains is available for sediment transport, and for rearrangement and organisation of sediment into bedforms and other channel bed features. After the bed is rearranged, there is a reduction in the shear stress near the bed, which is not sufficient for significant sediment transport, and makes it possible for smaller sizes to remain on the surface. This is due to the sheltering effects made by the larger, more exposed grains, and/or to bed structures. The reduction in near-bed shear stress was confirmed experimentally with Reynolds stress measurements (Fig. 4.14. and 4.15.), while the bed surface samples confirmed the presence of even the smallest grain sizes for all runs (Fig. 4.23. and 4.24.).

6.2.2. Slopes

It is difficult to determine an accurate measure of slopes in the laboratory or in the field, because the bed and water surface slopes are low, and inclusion or exclusion of just one point can change the resulting estimates of friction slopes, which are used to calculate the bed shear stresses. To avoid this problem, it would be advantageous to have longer test sections and more measurements along the channel so that there are more points on which to base the regression line. The slope determination would be somewhat easier if the flow was uniform

and the bed, water surface and friction slopes were truly parallel. However, uniform flows are difficult to achieve, especially if the slopes and depths are adjusting freely to the imposed conditions. Nevertheless, even for non-uniform flows, the friction slope is the correct slope for determining the bed shear stress, which represents the average shear stress for the reach.

6.2.3. Velocities

The numerical model assumption that the velocity profiles are logarithmic was tested by measuring several velocity profiles across and along the flume with an ADV. Certain problems were experienced when processing the ADV data because the correlations were not what were expected, or recommended (i.e. 70% or higher), and this was a consequence of turbulent flows over rough boundaries. Despite low correlations in the near-bed region, it was demonstrated that the measurements could be used for determining the average values for velocities or Reynolds stresses at a point. This was further confirmed by the good agreement in shear velocities obtained using the three different methods, namely from the depth-slope method, from the velocity profile, or from the linear part of the Reynolds stress profile.

The ADV velocity measurements demonstrated that the velocities corresponded to local depths, with velocities decreasing when the depth was increasing. Examination of velocity profiles across the flume confirmed the existence of sidewall effects, however these typically did not influence the shear velocities, but only the hydraulic roughness coefficients, k_s. Examination of velocity profiles along the flume showed reasonably uniform conditions in a downstream direction, and fully developed boundary layers. Some of the velocity profiles in higher shear stress runs were segmented, indicating the existence of grain and form roughness.

The lower segment was considered to refer to the grain roughness and was considered to be representative of local conditions, while the upper segment was considered to represent the overall roughness in the channel, and this segment was used to determine the shear velocities.

6.2.4. Protrusions

Bed surface elevations were measured with a laser displacement meter. From these data DEMs were developed from which contour plots were drawn. These contour plots were super-positioned over coloured photographs, which made possible the calculation of protrusions for different grain sizes. Statistical analysis of the DEMs showed that the final bed surface elevations were similar to natural beds examined by Nikora et al. (1998), and Smart and Walsh (2002b). In the analysis, it was assumed that the mean bed elevation is equivalent to the zero velocity datum from which the protrusions in the numerical model were calculated. The good agreement between measured and predicted protrusions appears to confirm that this assumption was correct. The protrusions were discussed in more detail in Section 6.1.1.

6.2.5. Microbedform development

For bed structures to start developing, larger stable grains are needed, which serve as anchors or key-stones. Other moving grains of similar size roll into contact with these static grains, and stop. With this, a cluster development starts, more grains are stopped and the structure grows into particle lines, which could be further linked into reticulate structures (Church et al., 1998). In these experiments, the observation of bed features was possible and relatively easy, because of the combination of having coloured sediment particles that showed well in

coloured photographs, and having the laser measurements which provided information on particle elevation.

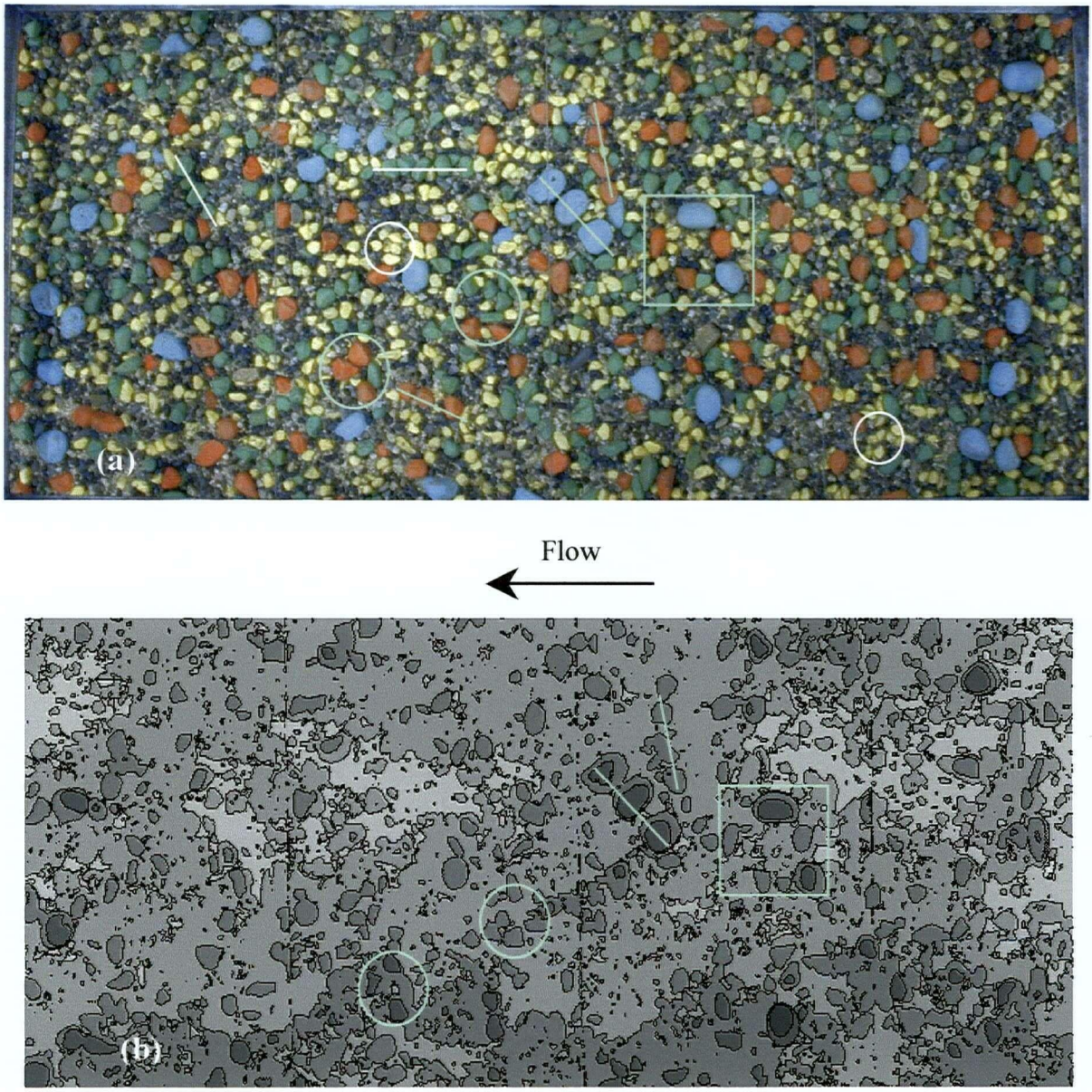

Figure 6.2. *Microbedforms in Run 4: (a) A photograph of a bed surface; and (b) A coarse DEM for the same bed, with contours 8 mm apart.*

Some of the bed features are shown in Figure 6.2, where Figure 6.2.a is the photograph of the final bed surface condition in Run 4, and Figure 6.2.b is the rough digital elevation model with contours 8 millimetres apart. The larger features show well on both representations of the bed. However, there are some smaller particle lines or clusters that can be observed in a photograph, but cannot be recognised in the DEM, because they actually do not protrude very high into the flow. These smaller features are made from smaller particle sizes, such as the particle lines made of green grains (marked with white lines in Fig. 6.2.a), or clusters made of yellow grains (marked with white circles in Fig. 6.2.a). The larger features are clusters made of mixed red and green particles, or lines made of blue or red particles, or stone cells made of various sizes, and are marked with turquoise symbols in both figures.

6.3. Discussion on Bed Armouring Processes

It was obvious from these experiments that there were two different mechanisms of bed armouring. The first mechanism occurred through selective erosion, which was accompanied with degradation and slight friction slope adjustment in Runs 1, 2 and 3 (Fig. 6.3.a). This was enhanced with bed roughening and increased hydraulic roughness (Fig. 6.3.b). For the first three runs, there was almost no difference between the initial and final shear stresses (Fig. 6.1.), and for Runs 2 and 3, the depth increased and the mean velocity decreased (see Table 4.1. in Chapter 4). For Run 1, there was almost no change in the depth and mean velocity, but only a slight change in slope, which caused the final k_s' to somewhat decrease ("prime" denotes that the value is calculated using the sidewall corrected shear velocity).

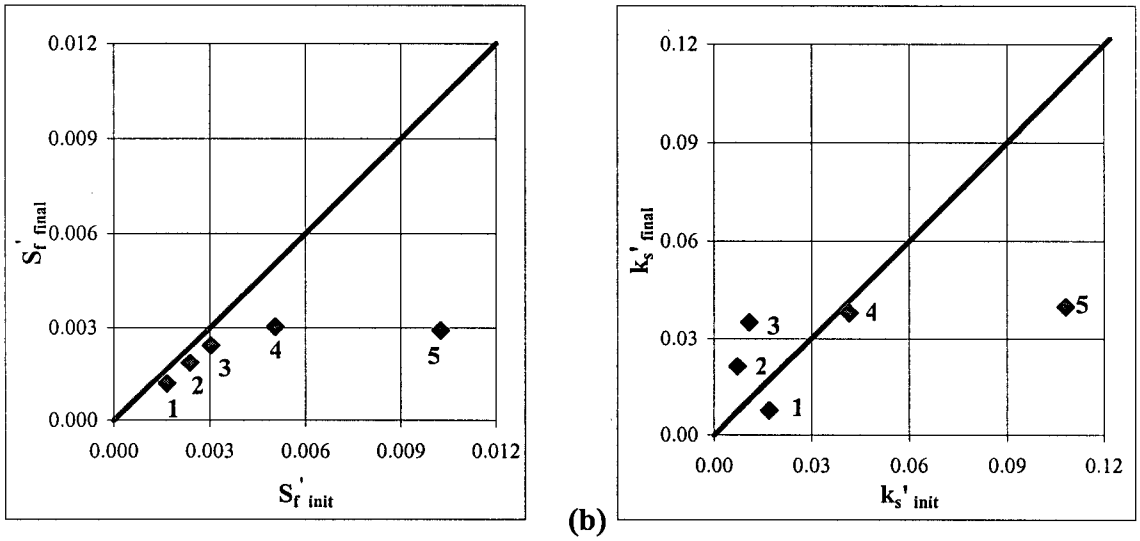

Figure 6.3. *Initial vs. final conditions for Runs 1 through 5 (numbered in figures): (a) Friction slope; and (b) Hydraulic roughness (both shown with sidewall correction).*

The second mechanism occurred in Run 4 and even more evidently in Run 5, for which the initial conditions were pushed beyond the point when the system could adjust in a relatively simple and expected way described above. It is shown in Figure 6.3.a, that the reduction in friction slope was substantial, and there was also a considerable reduction in the hydraulic roughness coefficient with respect to the initial conditions (Fig. 6.3.b). The bed armouring mechanism for these runs was first through degradation during the slope reduction process, followed by selective erosion during the bed coarsening process.

If Runs 3, 4 and 5 are compared, it appears that the bed roughened through bed surface coarsening, so that $D_{50arm,3} < D_{50arm,4} < D_{50arm,5}$, and the concentration of larger grains on the bed surface increased for each successive run with increasing initial shear stress (Table 4.4.). However, it appears that the hydraulic roughness and, consequently, the resistance to flow increased only slightly for each consecutive run, indicating that the bed became hydraulically

"smoother". This is further supported by grain protrusion measurements, for which it was shown that the protrusion of coloured grains was almost the same for Runs 4 and 5, or even somewhat less for the red and green grains in Run 5 (see Fig. 5.17. in Chapter 5). This is counter-intuitive because the initial shear stress was increased from Run 4 to Run 5 by 44%. Furthermore, there was evidence of microbedform development in these runs (Fig. 6.2.). Microbedforms have previously been thought to produce an increase in the hydraulic roughness coefficient (Gomez, 1993; Church et al., 1998). However, these experiments contradict that finding (Fig. 6.3.b).

In addition, there is evidence that, in the presence of microbedforms or other bed structures, the Shields' parameter can increase beyond 0.06 (Church et al., 1998), which indicates that these beds are stronger and more stable. A similar observation was obtained in this study, where τ^*_{50arm} was higher for beds where some structures were observed. However, it was shown in these present experiments that the increase in bed strength was not followed by the expected increase in the hydraulic roughness coefficient. The Grain Protrusion Model and the experimental results together suggest that an increase in bed shear stress results in development of stronger armour layers, either through reduced protrusion, or possibly through the development of pebble clusters and other microbedforms. However, in contrast to Gomez (1993) and Church et al. (1998), our results indicate that once a "critical" u^* is passed, a friction slope reduction occurs, and the bed actually becomes hydraulically smoother. In this upper regime, the bed adjusts by reducing the imposed shear stress and by increasing the strength of the bed by modified grain protrusion and possibly microbedform development.

Hypothetically, particles clumping together into groups form structures that allow them to stabilise, but those grouped particles may actually offer less resistance to the flow, so they may be "smoother" and attract less stress (personal communication with M. Quick, 2002). In the extreme and idealised case, they would form a uniform-sized armoured bed with low individual protrusion, which results in a smoother surface, less shear stress, and lower S_f. However, in such a case microbedforms would not be distinguished any more. Visual inspection of photographs for Runs 4 and 5, suggests that organised bed structures like stone lines and stone cells were somewhat better developed in Run 4, than in Run 5. In Run 5, there was more coarsening and maybe more clustering evident, but hardly any of the more complex bed forms. The τ^*_{50arm} was slightly higher for Run 4 than for Run 5, which may contribute to the evidence that structured beds are stronger and more resistant to erosion. However, this could also mean that there could be some limiting shear, above which microbedforms do not develop any more, but the bed stabilises solely through the increase in concentration of larger grains on the surface. This kind of bed coarsening could result in a further decrease in resistance to flow, or hydraulic "smoothing".

Obviously, the two experiments that suggest hydraulic "smoothing" of the bed are not enough to draw any strong conclusions. The above discussion raises more questions than answers, and is an indication that more tests should be done, where the focus would be on bed adjustment and appearance, as well as on protrusion measurements for the conditions of higher imposed shear stresses (e.g. equivalent to the shear stress range between Runs 3 and 5 in these experiments).

6.4. Recommendations and Possible Future Developments

Several recommendations can be made for future experimental work. Longer flumes may help in establishing uniform flows, while wider flumes can decrease the sidewall effects. To obtain slope estimates that are less sensitive to a value of individual points, the aim should be to have longer test sections and more measurements. Better ADVs or LDVs (laser Doppler velocimeter) could improve the quality of velocity measurements in turbulent flows, and data acquisition should be as long as possible to obtain stable averages for average velocities and Reynolds stresses. The methods used for sediment testing should be well documented, so that later comparisons with other studies are possible and unambiguous.

It has been demonstrated that the Grain Protrusion Model has a potential for predicting correctly the grain protrusion, the hydraulic roughness, and the flow velocities for the tested conditions. The model should now be tested using some field data to confirm its practical applicability. Potentially, the roughness calculated in this model could be used in practice to estimate the grain roughness and then, by adding the form roughness, to estimate the total resistance in a channel. There may be a possibility of extending the model to a mobile armour bed by adding a sediment transport equation to the model. For all these potential developments or tests with field data, the input parameters should be carefully considered and defined appropriately.

6.5. Conclusions

From this study, several relevant conclusions can be drawn for future research. Some of these are related to the experimental work, some to the numerical modelling work, and some to the combination of the two.

An attempt was made to numerically model the roughness coefficient for a flow over a stable armoured gravel-bed. This is a relatively simple case without sediment transport, and with not too many variables. It was considered important to determine the physical behaviour of the model for this simple case before attempting to model a more complex system (e.g. a mobile armour bed). The experimental work confirmed that the processes predicted in the model appear to be correct and physically sound.

Some of the assumptions made when developing the numerical model were tested in the experimental work. The assumption that the velocity profile has a logarithmic distribution was confirmed experimentally for the range of tested flows and for conditions of low to intermediate relative roughness. The assumption on equal mobility, which implies that all grains on the surface adjust their positions through particle protrusions in such way that they are just at the threshold of motion, was also confirmed in the experiments, in that the predicted and measured protrusions were in a good agreement. This also supported the assumption that the mean bed elevation from which the protrusions were measured in the experiments was equivalent to the zero bed level, which is the elevation where the logarithmic velocity profile becomes equal to zero.

The Grain Protrusion Model was tested using published flume data and data from these experiments. The grain protrusion heights (H_i), hydraulic roughness (k_s), mean velocities (U) and flow depths (Y) were predicted quite successfully for the range of examined conditions, apparently justifying the model and the assumptions made.

The dimensionless Shields' stress for armoured beds obtained in these experiments was found to have the usually accepted values, ranging between 0.03 and 0.06, with the tendency to be higher for the beds with higher relative roughness and for the beds with some microbedform development, which add to the bed stability.

It was found in the experimental work that an accurate measure of slopes is difficult to obtain. Good friction slope estimates are necessary for accurate bed shear stress calculations, which are most commonly obtained from balancing the forces ($\rho g Y S_f$). Reynolds stress measurements obtained by the ADV confirmed the expected shear stress distributions with a reduction in the near-bed region for some of the examined flows over rougher boundaries. The comparison of shear velocities obtained from the depth-slope method, from velocity profiles and from Reynolds stresses, showed reasonable agreement, confirming the validity of the methods used to determine these values.

Therefore, as an overall conclusion, the experimental results give good support to the assumptions made in the Grain Protrusion Model, especially the measurements of grain protrusion which show remarkable agreement with theory.

7. REFERENCES

Afzalimehr, H. and F. Anctil, (2001). Vitesse de frottement associée à un écoulement non uniforme et une rugosité relative intermédiaire, (Friction velocity associated to a non-uniform flow and an intermediate scale roughness), *J. Hydraul. Res., 39,* 181-186.

Andrews, E. D., and G. Parker, (1987). Formation of a coarse surface layer as the response to gravel mobility, in *Sediment transport in Gravel-bed Rivers*, edited by C. R. Thorne, J. C. Bathurst and R. D. Hey, *John Willey & Sons Ltd.*, Chichester, pp. 269-325.

Arya, S. P. S. (1975). A drag partition theory for determining the large –scale roughness parameter and wind stress on the arctic pack ice, *J. Geophys. Res., 24,* 3447-3454.

Bagnold, R. A. (1941). *The Physics of Blown Sand and Desert Dunes*, Methuen, London, pp.265

Bray, D. I. (1980). Evaluation of effective boundary roughness for gravel-bed rivers, *Can. J. Civ. Eng., 7,* 392-397.

Bray, D. I. (1985). Flow resistance in gravel-bed rivers, in *Gravel-Bed Rivers,* edited by R. D. Hey, J. C. Bathurst, and C. R. Thorne, *John Wiley,* New York, pp. 109-132.

Biron, P. M., Lane, S. N., Roy, A. G., Bradbrook, K. F., and Richards. K. S. (1998). Sensitivity of bed shear stress estimated from vertical velocity profiles: The problem of sampling resolution, *Earth Surface Processes and Lanforms, 23,* 133-139.

Buffington, J. M., W. E. Dietrich, and J. W. Kirchner (1992). Friction angle measurements on a naturally formed gravel stream bed: Implications for critical boundary shear stress, *Water Resour. Res., 28 (2),* 411-425.

Buffington, J. M., and D. R. Montgomery (1997). A systematic analysis of eight decades of incipient motion studies, with special reference to gravel-bedded rivers, *Water Resour. Res.*, *33*, 1993-2029.

Carling, P. A., Kelsey, and M. S. Glaister, (1992). Effect of bed roughness, particle shape and orientation on initial motion criteria, in *Dynamics of Gravel-Bed Rivers,* edited by P. Billi et al., *John Wiley*, New York, pp. 23-38.

Chandler, J., S. N. Lane, and P. Ashmore, (2000). Measuring river bed and flume morphology and parameterising bed roughness with a Kodak DC460 digital camera, *Int. Arch. Photogramm. and Remote Sensing, XXXIII (B7),* 250-257.

Cheng, E. D. H., and C. G. Clyde (1972). Instantaneous hydrodynamic lift and drag forces on large roughness elements in turbulent open channel flow, in H. W. Shen (Ed.), *Sedimentation: Symposium to Honor Professor H. A. Einstein*, Colorado State Univ., Fort Colins, CO., USA, 3-1 to 3-20.

Chepil, W. S. (1959). The use of evenly spaced hemispheres to evaluate aerodynamic forces on a soil surface, *Transactions, Am. Geophysical Union*, *39*, 397-404.

Chin, C. O. (1985). Stream bed armouring, *Report no. 403*, School of Engineering, Univ. of Auckland, Auckland, New Zealand.

Chin, C. O., B. W. Melville, and A. J. Raudkivi (1994). Streambed armoring, *J. Hydraul. Res.*, *120*, 899-918.

Church, M. (1978). Palaeohydrological reconstructions from a Holocene valley fill, in *Fluvial Sedimentology*, edited by A. D. Miall, *Mem. Can. Soc. Pet. Geol., 5*, 743-772.

Church, M., M. A. Hassan, and J. F. Wolcott (1998). Stabilizing self-organized structures in gravel-bed stream channels: Field and experimental observations, *Water Resour. Res.*, *34*, 3169-3179.

Coleman, N. L. (1967). A theoretical and experimental study of drag and lift forces acting on a sphere resting on a hypothetical stream bed, *Proc., 12th Congress,* IAHR, Vol. 3, Sept. 1967.

Dietrich, W. E., J. W. Kirchner, H. Ikeda, and F. Iseya (1989). Sediment supply and the development of the coarse surface layer in gravel-bedded rivers, *Nature*, *340*, 215-217.

Einstein, H. A., and El-Sayed A. El-Samni (1949). Hydrodynamic forces on a rough wall, *Rev. Mod. Phys.*, *21*, 520-524.

Fenton, J. D., and J. E. Abbott (1977). Initial movement of grains on a streambed: The effect of relative protrusion, *Proc. R. Soc. London A*, *352*, 523-537.

Firpp, J. B., and P. Diplas, (1993). Surface sampling in gravel streams, *J. Hydraul. Eng., 119*, 473-490.

Gartshore, I. S., and K. A. de Croos (1979). Equilibrium boundary layers over very rough boundary, *AGARD Conference Proceedings No.271, Fluid Dynamics Panel Symposium; Turbulent Boundary layers – Experiments, Theory and Modelling,* Hague, Netherlands, pp.7-1 to 7-11.

Gessler, J. (1965). Der Geschiebetriebbeginn bei Mischungen untersucht an natürlichen Abpflästerungsercheinungen in Kanälen, *Mitteilug No. 69,* Versuchsanstalt für Wasserbau und Erdbau, Zürich, Switzerland.

Gessler, J. (1971). Beginning and ceasing of sediment motion, in *River Mechanics*, edited by H. W. Shen, Fort Collins, Colorado, 00. 7:1-7:22.

Gessler, J. (1990). Friction factor of armored river beds, *J. Hydraul. Eng.*, ASCE, 116 (4), 531-543.

Gomez. B. (1993). Roughness of stable, armoured gravel beds, *Water Resour. Res.*, *29*, 3631-3642.

Gomez. B. (1994). Effects of particle shape and mobility on stable armor development, *Water Resour. Res.*, *30*, 2229-2239.

Henderson, F. M., (1966). Open Channel Flow. *Macmillan Publishing Co., Inc.,* New York.

Hey, R. D., and Thorne, C. R. (1986). Stable channels with mobile gravel beds, *J. Hydraul. Eng.*, ASCE, 112, 671-689.

Hey, R. D. (1979). Flow resistance in gravel-bed rivers, *J. Hydraul. Div.*, ASCE, *105*, 356-379.

Jarrett, R. D. (1989). Hydraulic research in mountain rivers, *Proceedings of the International Conference On Channel Flow and Catchment Runoff: Centennial of Manning's Formula and Kuichling's Rational Formula*, ASCE, Univ. of Virginia, 599-608.

Johnston, C. E., E. D. Andrews, and J. Pitlick, (1998). In situ determination of particle friction angles of fluvial gravels, *Water Resour. Res., 34*, 2017-2030.

Kamphuis, J. W. (1974). Determination of sand roughness for fixed beds, *J. Hydraul. Res.*, *12*, 193-203.

Kellerhals, R., and D. I. Bray, (1971). Sampling procedure for coarse fluvial sediments, *J. Hydraulics Division, Proceedings of ASCE, 97 (8)*, 1165-1180.

Keulegan, G. H. (1938). Law of turbulent flow in open channels, *J. Res. of Nat. Bureau of Standards,* 21(6), 707-741.

Kirchner, J. W., W. E. Dietrich, F. Iseya, and H. Ikeda (1990). The variability of critical shear stress, friction angle, and grain protrusion in water-worked sediments, *Sedimentology, 37*, 647-672.

Kironoto, B. A., and W. H. Graf (1994). Turbulence characteristics in rough uniform open-channel flow, *Proc. Inst. Civ. Engrs Wat., Marit. & Energy, 106*, 333-344.

Komar, P. D., and Z. Li, (1988). Applications of grain-pivoting and sliding analysis to selective entrainment of gravel and to flow competence evaluations, *Sedimentology, 35*, 681-695.

Lamberti, A., and E. Paris, (1992). Analysis of armouring processes through laboratory experiments, in *Dynamics of Gravel-Bed Rivers*, edited by P. Billi et al., John Wiley, New York, pp. 227-250.

Lane, S. N., Biron, P. M., Bradbrook, K. F., Butler, J. B., Chandler, J. H., Crowel, M. D., McLelland, S. J., Richards, K. S., and Roy, A. G. (1998). Three-Dimensional Measurement of River Channel Flow Processes Using Acoustic Doppler Velocimetry, *Earth Surface Processes and Landforms, 23,* 1247-1267.

Lane, S. N., Chandler, J.H., and K. Porfiri (2001). Monitoring river channel and flume surfaces with digital photogrammetry, *J. Hydraul. Eng., 127 (10),* 871-877.

Lhermitte, R. and U. Lemmin (1994). Open-channel flow and turbulence measurement by high-resolution Doppler sonar, *J.Atmos. Oceanic Technol., 11,*1295-1308.

Lohrman, A., Cabrera, R. and Kraus, N.C. (1994). Acoustic Doppler velocimeter (ADV) for laboratory use, *Proc., on Fundamentals and Advancements in Hydr. Meas. and Exp.,* C. A. Pugh, ed., ASCE, New York, 351-356.

Martin, V. (1996). Velocity Structure in Gravel Rivers. M.A.Sc. Thesis, UBC, 165 p.

Martin, V., Millar, R.G. and Quick, M.C. (2000). Hydraulic Roughness and Stability of Self-Formed Stable Gravel Beds: The Role of Grain Protrusion, *Gravel-Bed Rivers 2000*, Poster presentation, also published on a CD-ROM, Christchurch, New Zealand.

Martin, V., Millar, R.G. and Quick, M.C. (2001). Hydraulic Roughness of Stable Self-Formed Gravel Beds: The Role of Grain Protrusion. *Proceedings of the 29th CSCE Annual Conference, 15th Hydrotechnical Conference* (CD-ROM), Victoria, B.C.

Martin, V., Fisher, T.S.R. Millar, R.G., Quick, M.C. (2002). ADV Data Analysis for Turbulent Flows: Low Correlation Problem. *Proceedings of the 2002 EWRI/ASCE/IAHR joint Int. Conf. on Hydraulic Meas. and Experimental Methods* (CD-ROM), Estes Park, Colorado.

Meyer-Peter, E., and R. Müller (1948). Formulas for bedload transport, *Meet. Int. Assoc. Hydraul. Structures Res., 2nd* (Appendix 2), 39-64.

Millar, R. G. (1999). Grain and form resistance in gravel-bed rivers, *J. Hydraul. Res., 37*, 303-311.

Miller, M. C., I. N. McCave, and P.D. Komar, (1977). Threshold of sediment motion under unidirectional currents, *Sedimentology, 24*, 507-527.

Miller, R. T. and R. J. Byrne (1966). The angle of repose for a single grain on a fixed rough bed, *Sedimentology, 6,* 303-314.

Neill, C. R. (1968). Note on initial movement of coarse uniform bed-material, *J. Hydraul. Res.*, 6, 173-176.

Nikora, V. I., Goring, D. G., and Biggs, B. J. F. (1998). On gravel-bed roughness characterization, *Water Resour. Res., 34*, 517-527.

Nikora, V. I. and Goring, D. G. (2000). Flow turbulence over fixed and weakly mobile gravel beds, *J. Hydraul. Eng., 126 (9),* 679-690.

Nikuradse, J. (1933). Strömungsgesetze in rauhen Rohren, *Forschg. Arb. Ing. Wes., 361*, 22, 1933. (English translation, Laws of flow in rough pipes, *Tech. Memo. 1292*, Natl. Adv. Comm. For Aeron., Washington, D. C., 1950.)

Paintal, A. S. (1971). Concept of critical shear stress in loose boundary open channels, *J. Hydraul. Res., 9*, 91-113.

Parker, G., and P. C. Klingeman (1982). On why gravel bed streams are paved, *Water Resour. Res., 18*, 1409-1423.

Parker, G., P. C. Klingeman, and D. G. McLean (1982). Bedload and size distribution in paved gravel-bed streams, *J. Hydraul. Div. Am. Soc. Civ. Eng., 108*, 544-571.

Parker, G. (1990). Surface-based bedload transport relation for gravel rivers, *J. Hydraul. Res., 28*, 417-436.

Parker, G., and A. J. Sutherland (1990). Fluvial armor, *J. Hydraul. Res., 28*, 529-544.

Prandtl, L. (1935). The Mechanics of Viscous Fluids in *Aerodynamics Theory* edited by W. F. Durand, 111, 142.

Proffitt, G. T. (1980). Selective transport and armoring of non-uniform alluvial sediments, *Res. Report 80/22*, Dept. of Civ. Eng., Univ. of Canterbury, Christchurch, New Zealand.

Reid, I., Frostick, L. E., and J. T. Layman (1985). The incidence and nature of bedload transport during flood flows in coarse-grained alluvial channels, *Earth Surf. Processes and Landforms, 10,* 33-44.

Robert, A. (1990). Boundary roughness in coarse-grained channels, *Prog. Phys. Geogr., 14* (1), 42-70.

Saad, M. B. (1986). The armouring of alluvial channel beds and the evaluation of the hydraulic characteristics of the armour coat, Ph. D. thesis, Faculty of Engineering and Applied Science, University of Southampton, U. K.

Schlichting, H. (1968). *Boundary Layer Theory*, 6th ed. New York; McGraw-Hill.

Shields, A. (1936). Anwendung der Äenlichkeits-Mechanik und der Turbulenzforschung auf die Geschiebebewegung, *Mitteilungen der Preussische Versuchsanstalt für Wasserbau und Schiffbau.*, Berlin, Heft 26. Translation by W. P. Ott and J. C. van Uchelen, Soil Conservation Service, California Institute of Technology, Pasadena.

Simons, D. B. and Senturk, F. (1992). Sediment Transport Technology, *Water Resources Publications*, Fort Colins.

Smart, G. M. (1999). Turbulent velocity profiles and boundary shear in gravel bed rivers, *J. Hydraul. Eng.*, *125*, 106-116.

Smart, G. M. (2001). A new roughness estimation technique for granular-bed flow resistance, *Proc. XXIX IAHR Hydraul. Eng. Congress*, Beijing.

Smart, G. M., Duncan, M. J., and Walsh J. (2002a). Relatively Rough Flow Resistance Equations, *J. Hydraul. Eng.*, ASCE, *128* (6), 568-578.

Smart, G. M. and Walsh J. (2002b). Direct measurement of Alluvial Channel Roughness, *Proc. on CD-Rom Hydr. Meas. And Exp. Methods; EWRI, ASCE and IAHR,* Estes Park, Colorado.

SonTek (1997). ADV Operation manual, software version 4.0, 109 pp. [Available from SonTek, 6837 Nancy Ridge Drive, Suite A, San Diego, CA 92121.]

SonTek Technical Notes (1997). Pulse coherent Doppler processing and the ADV correlation coefficient, 5 pp. [Available from SonTek, 6837 Nancy Ridge Drive, Suite A, San Diego, CA 92121.]

Sutherland, A. J. (1987). Static armour layers by selective erosion, in *Sediment transport in Gravel-bed Rivers*, edited by C. R. Thorne, J. C. Bathurst and R. D. Hey, *John Willey & Sons Ltd.*, Chichester, pp. 243-267.

Vanoni, V. A., and N. H. Brooks (1957). Laboratory studies of the roughness and suspended load of alluvial streams, *Sediment. Lab. Rep. E68*, 121 pp., Calif. Inst. of Technol., Pasadena.

Van Rijn, L. C. (1982). Equivalent roughness of alluvial bed. *J. Hydraul. Eng.*, ASCE, *128 (10)*, 1215-1218.

Voulgaris, G. and Trowbridge, J. H. (1998). Evaluation of the Acoustic Doppler Velocimeter (ADV) for turbulence measurements, *J. of Atmospheric and Oceanic Technology, 15,* 272-289.

Wahl, T. L. (2000a). WinADV Version 1.845: A Windows-based viewing and post-processing utility for ADV files; User's manuals and on-line help provided with the software (http://www.usbr.gov/wrr1/twahl/winadv/).

Wahl, T. L. (2000b). Analyzing ADV data using WinADV, *Proc. Joint Conference on Water Res. Eng. and Water Res. Planning and Management, Minneapolis, Minnesota.*

White, C. M. (1940). The equilibrium of grains on the bed of a stream, *Proc. R. Soc. London, Ser. A*, 174, 332-338.

White F. M. (1986). *Fluid Mechanics*, Second edition, McGraw-Hill, New York, 732 p.

Wiberg, P. L., and J. D. Smith (1987). Calculations of the critical shear stress for motion of uniform and heterogeneous sediments, *Water Resour. Res.*, *23*, 1471-1480.

Wiberg, P. L., and J. D. Smith, (1991). Velocity distribution and bed roughness in high-gradient streams, *Water Resour. Res.*, *27*, 825-838.

Wilcock, P. R., and Southard, J. B. (1988). Experimental study of incipient motion in mixed-size sediment, *Water Resour. Res.*, *24*, 1137-1151.

Wilcock, P. R., (1992). Flow competence: A criticism of a classic concept, *Eart Surf. Processes Landforms, 17*, 289-298.

Wilcock, P. R., and McArdell, B. W. (1993). Surface-based fractional transport rates: Mobilization thresholds and partial transport of sand-gravel sediment, *Water Resour. Res.*, *29*, 1297-1312.

Wilcock, P. R., A. F. Barta, C. C. Shea, G. M. Kondolf, W. V. G. Matthews, and J. Pitlick, (1996). Observations of flow and sediment entrainment on a large gravel-bed river, *Water Resour. Res.*, *32*, 2897-2909.

Wolman, M.G. (1954). A method of sampling coarse river bed material, *American Geophysical Union Transactions 35*, 951-956.

APPENDIX A: VELOCITY MEASUREMENTS

A.1. Correlation parameter for flows over smooth vs. rough boundaries

Experiments - To test the assumption that the correlation parameter for ADV measurements decreases with increased turbulence, an additional experiment was carried out in a smaller recirculating flume (width = 0.15 m, length = 6.0 m). Four velocity profiles for four different set-ups were measured on the centreline of the flume. The first profile was measured in a flow over a smooth bed (Figure A-1a), 4.0 meters downstream from the flume inlet. Low turbulence intensities and thus high correlations were expected in this case. The second profile was taken in a somewhat more turbulent environment for a flow over a smooth bed. The velocities were measured just downstream from the inlet screen at the flume entrance (Figure A-1b). For the third and the fourth profile, large roughness elements were placed on the flume bed. The third profile was taken over a rough boundary (Figure A-1c), while the fourth profile was taken in the wake of a large rock somewhat upstream of Profile 3 (Figure A-1d). The correlation results for these four profiles were compared with correlation results for one of the profiles taken in the original set of experiments for Run 5 (Figure A-1e).

To examine how the ADV velocity range setting affects the correlation, at most of the measured points this setting was varied between 100 cm/s and 250 cm/s.

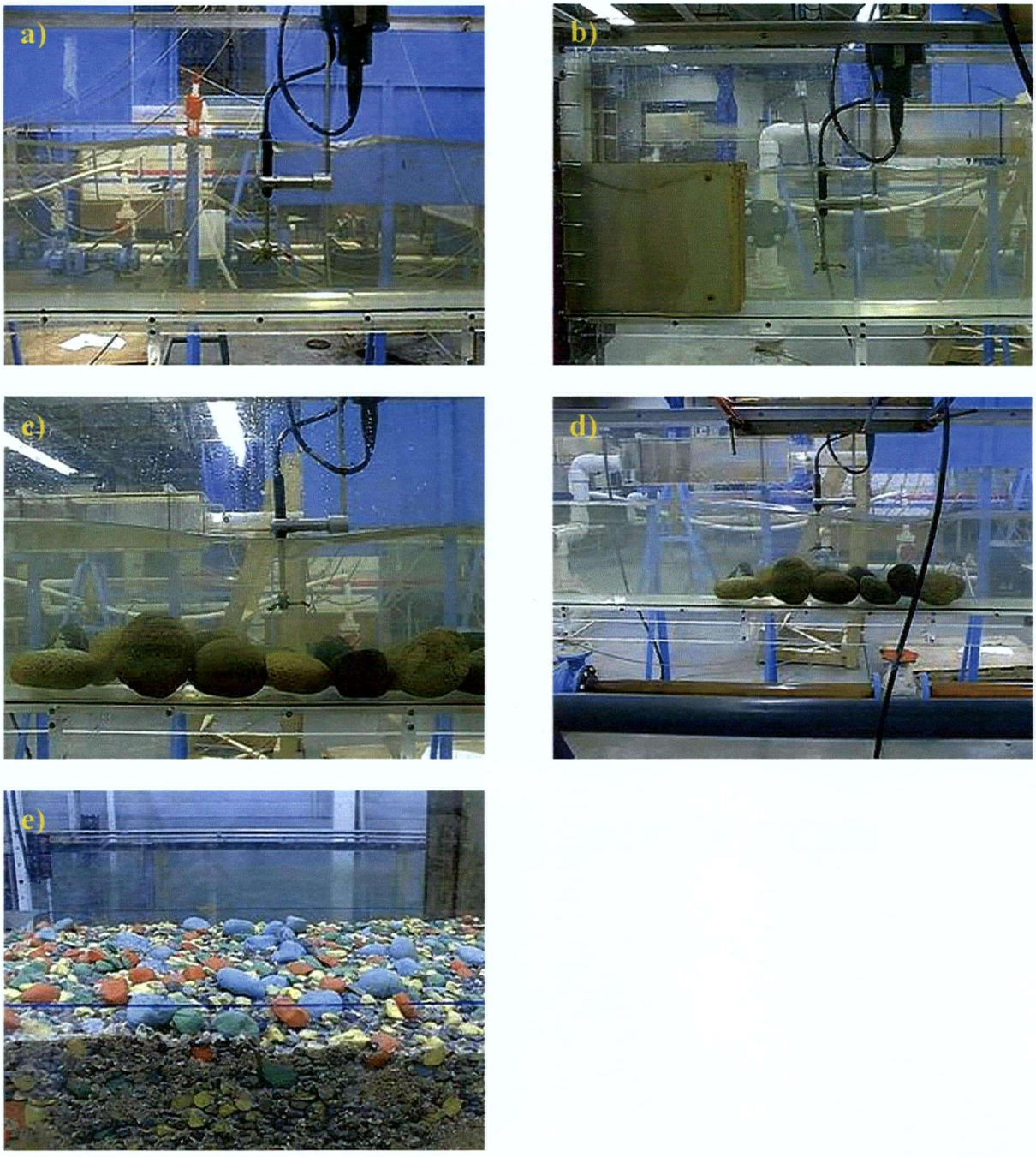

Figure A-1. *Testing the correlation parameter for ADV measurements in: (a) flow over a smooth boundary; (b) flow over a smooth boundary behind a screen; (c) flow over a rough boundary; (d) flow over a rough boundary in the wake of a large element; and (e) original experimental set-up, Run 5.*

Results - The results of the above measurements were analysed in terms of average correlation vs. distance from the boundary for each point where the measurements were taken. These results are illustrated in Figure A-2a for measurements where the ADV velocity range was set to 100 cm/s, and in Figure A-2b for measurements where the velocity range was set to 250 cm/s.

Figure A-2a clearly demonstrates how the average correlation decreased with measurements taken in increasingly turbulent conditions. Profile 1 was taken over a smooth boundary and the corresponding average correlations were 90% or higher for all distances away from the boundary. Profile 2 was taken under similar boundary conditions, but just downstream of the inlet screen. The increase in turbulence caused by the screen resulted in decrease in average correlation by about 20 % (ranging from 69 % to 74 %), and it was relatively insensitive to the distance from the boundary. Profile 3 was measured above a rough boundary and this change was expected to be followed by a further increase in turbulence. The average correlation decreased to about 47 % to 66 % depending on the distance from the boundary. The last profile (Profile 4) was measured immediately downstream of an obstacle, in the wake of a large rock. The average correlation in this case was only about 35 %.

For comparison, one profile of Run 5 from the primary set of experiments for this study was plotted on the same graph showing that the average correlations ranged from about 40 % to about 68 % (Fig. A-2a). The lowest correlations for Run 5 were experienced at the elevation of about 3 to 4 cm above the bed, and it is anticipated that the boundary interference was the primary reason for this decrease in correlations. (Note: different types of roughness will

cause the boundary interference to occur at different elevations.) Overall, for all runs for flows over a rough boundary, the average correlation was below 70%, while for flows over a smooth boundary, the average correlation was 70% and above.

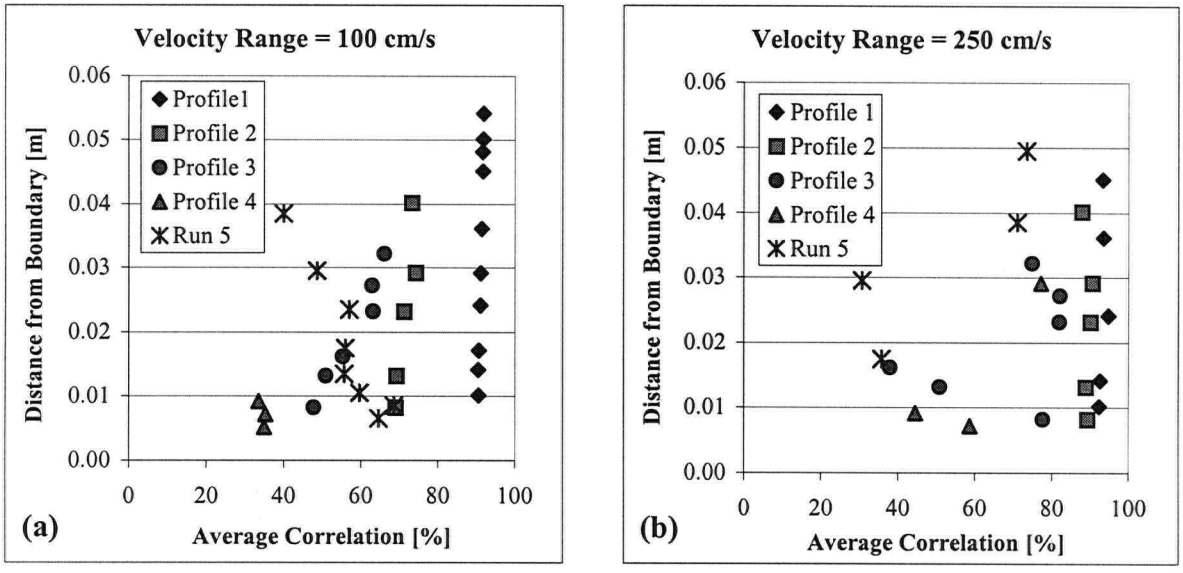

Figure A-2. *Correlation parameter for ADV measurements in flows over smooth and rough boundaries for: (a) ADV velocity range set to 100 cm/s; and (b) ADV velocity range set to 250 cm/s.*

Figure A-2b shows the variation in average correlation with the distance from the boundary for all five set-ups for measurements for which the velocity range was set to 250 cm/s. For flows over a smooth boundary (Profiles 1 and 2), the average correlation increased for all points if compared to corresponding values of Figure A-2a. This is more evident for Profile 2, where the correlation increased from about 70% in Figure A-2a to about 90% in Figure A-2b. This result is consistent with guidelines from SonTek (1997), in that the correlation increases with setting a higher velocity range, even though they do not recommend it because

of higher levels in instrument noise ("Instrument noise in velocity data is proportional to the velocity range setting; higher velocity ranges have higher noise levels.", quote from SonTek Operational Manual (1997)). In the case of flows over rough boundaries, the signal became more chaotic and for distances ≤ 0.03 m from the boundary, the average correlation could even decrease, which could be associated with boundary interference. For some of the measurements the correlation increased by more than 60% (the lowest points of Profile 3 and 4), but in general the increase was of the order of 30 % for the points measured higher than 0.03 m away from the boundary.

Overall, for the ADV velocity setting of 250 cm/s, the average correlations were higher than 70% for measurements taken at 0.03 m or higher above the boundary, but below that depth it seemed that the velocity setting of 100 cm/s gave more consistent results even though the correlations were lower.

A.2. Average Velocities and Reynolds Stresses

When the measurements for the two velocity range settings are plotted in terms of velocities vs. distance from the boundary, these measurements sometimes differ from each other. For example, in Figure A-3 the measurements for Profile 3 were analysed using WinADV (Wahl, 2000), where the correlation filter was set to remove all the data with correlations lower than 70%. Velocity data are plotted in Figure A-3a, while in Figure A-3b the percentage of data retained for further analysis vs. distance from boundary is analysed.

The velocity data differ between 5 and 15% for the two velocity settings for the analysed profile, and the question of which data should be used in further analysis has to be addressed. The graph illustrating the percentage of data retained for further analysis after applying the correlation filter of 70% (Figure A-3b) shows that there are often fewer than 60% of acceptable velocity data left. Lane et al. (1998) argue that significant changes in estimated average velocities occur if less than 80% of velocity values are retained after removing data points with low correlations, where low correlation is considered to be below 70%. Considering that much of our data measured in turbulent flows had correlations lower than 70 %, and consequently the percentage of retained values was much lower than 80%, it was necessary to relax the correlation criterion in order to optimise the measurements.

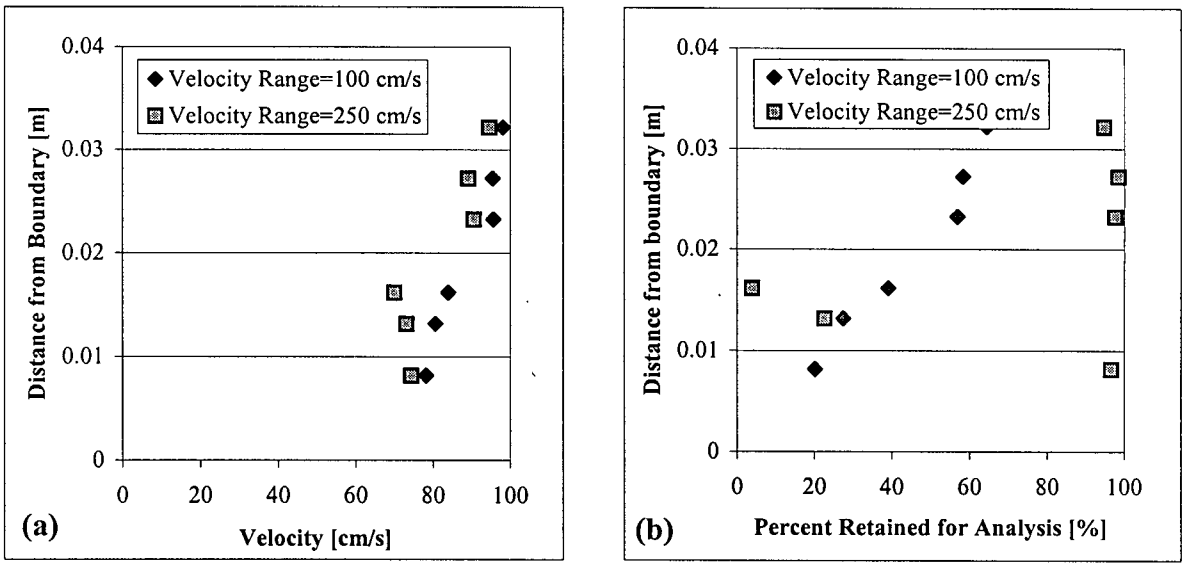

Figure A-3. *ADV Measurements for Profile 3 - flow over a rough boundary: (a) Velocity data; (b) Percent of data retained for analysis after applying the correlation filter.*

Sensitivity analysis - numerical tests were performed to determine the sensitivity of average velocities (Fig. A-4 a, c and e) and Reynolds stresses (Fig. A-4 b, d and f) for different levels of filtering based on the correlation coefficient. In addition, the spike detection filter was tested using the acceleration threshold of 1.5 g's (Nikora and Goring, 1999; Wahl, 2000) and compared to the values derived from the correlation filter.

Data illustrated in Figure A-4 were measured at different elevations (y) in Run 5, which had the highest shear stress and the highest roughness of the armoured bed, with D_{50} = 11.1 mm and D_{84} = 18.6 mm. The velocity data appear to be less sensitive than the Reynolds stress to the correlation filter. Furthermore, the velocity values calculated using the spike detection filter (open symbols) were consistent with velocities derived using the correlation filter (shaded symbols). However, the percentage of data retained (stars) decreased fairly rapidly with the increase in the correlation filter value in the near-bed region, indicating more complex turbulence structures. It appears that Reynolds stresses were much more sensitive to the percentage of data retained and that Reynolds stresses calculated after applying the spiking filter were often quite different.

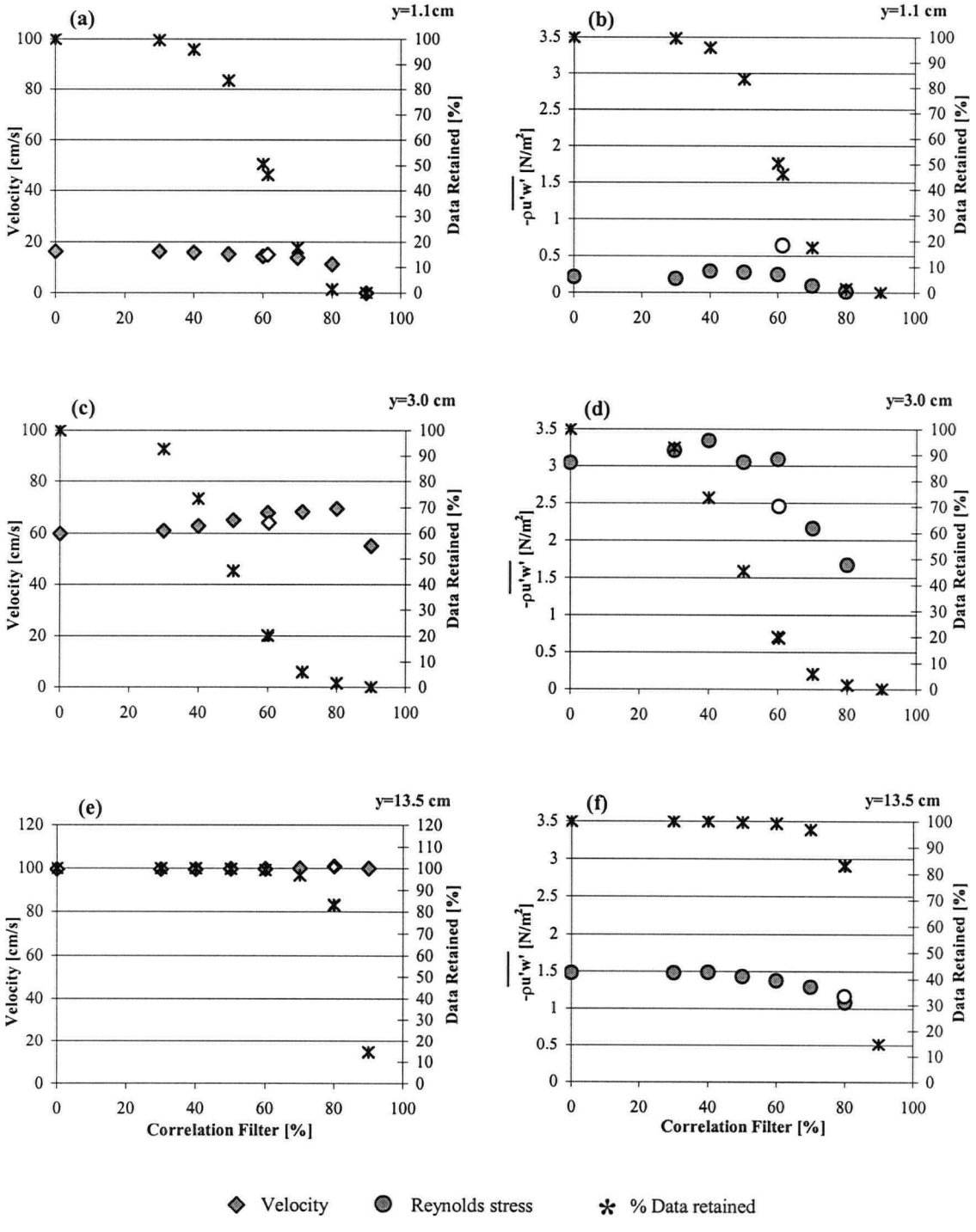

Figure A-4. *Filtering based on the correlation coefficient (shaded symbols), or on the spike detection filter with the acceleration threshold of 1.5 g's (open symbols): (a), (c) and (e) are the average velocities at a point; (b), (d) and (f) are Reynolds stresses.*

For determining the Reynolds stresses, data edited with the 40% correlation filter could be included in the profile to determine the total bed shear stress if at least 70% of data are retained for the analysis after filtering. However, this must be done with some caution because of the high variability and uncertainty identified in the Reynolds stress values determined for different correlation percentages (Fig. A-4b and d). It is possible that some of the variability in Reynolds stress values might diminish with longer data acquisition and consequently, longer averaging periods. Based on the above discussion, only data edited with the 70% correlation filter for which at least 70% of data were retained, were used in determining the Reynolds stress values in our experiments. For the points in the near-bed region where average correlations lower than 70% were commonly experienced, the Reynolds stresses decreased due to the larger roughness elements present on the bed. These were also the data points edited with the 40% correlation filter and were not considered when determining the total bed shear stress. The spike detection filter generally did not seem to produce reasonable values for Reynolds stresses.

Including more data, even if the correlations are less than 70%, is preferable to using averages based on very small number of data points. Comparison of the results using the 70% and 40% correlation filters indicated that the 40% data gave reasonable results for velocities (Fig. A-5a, triangles). Average velocities calculated using the 70% correlation filter were often based on a fairly small number of data points (Fig. A-5b, triangles), and were probably not true representatives of the mean.

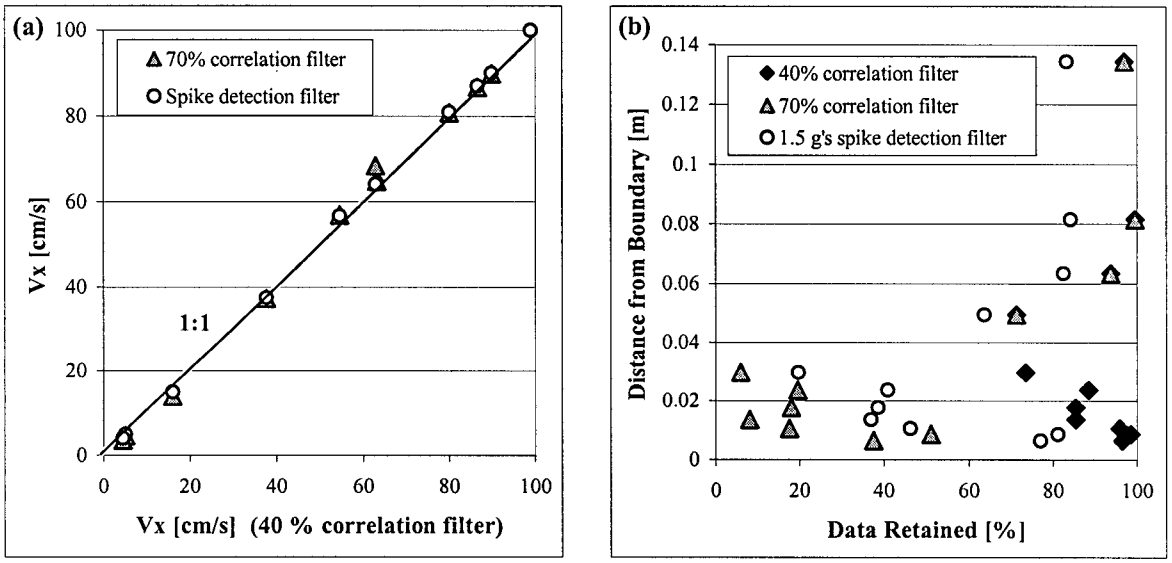

Figure A-5. *(a) Velocity values obtained using the 40% correlation filter vs. the 70% correlation filter, or the spike detection filter with acceleration threshold set to 1.5 g's; (b) Percentage of data retained for different filtering methods vs. distance from the boundary.*

The 40% correlation filter was found preferable to the spike detection filter, because even though both methods estimated similar velocity values (Fig. A-5a, circles), in the case of the spike detection filter with acceleration threshold of 1.5 g's, there were often less than 50% data left in the bottom 5 cm of flow (Fig. A-5b, circles). To retain more data when using the spiking filter, the acceleration threshold was varied between 1 and 3 g's. The results were inconsistent, with some apparently realistic points being rejected as spikes, while some obvious spikes were allowed through.

Conclusions - Based on the above discussion, it is recommended to set the ADV velocity range to 100 cm/s when taking measurements in flows over rough boundaries for distances up to 3 cm above the boundary. For distances higher than 3 cm, the ADV velocity setting of 250 cm/s consistently gave better results. When analysing the measured data, it is common

to apply a filter for editing the data based on the ADV correlation parameter. Additional experiments demonstrated that in turbulent flows over rough boundaries, the average correlation is often lower than 70%, especially close to the boundary. However, the average velocity values are reasonable estimates even with lower average correlations. Therefore, when analysing the velocity data, the correlation filter can be set to as low as 30%. The percentage of data retained after applying the correlation filter does not indicate if the average velocity value is consistent. However, including more data, even if the correlations are less than 70%, is probably preferable to using averages based on very small percentages of the total data.

The velocity measurements in our experiments were analysed with the correlation filter set to 70% and the average velocities were kept for points for which there were at least 70% data retained. For points with less than 70% data retained, the analysis was repeated with the filter set to 40% correlation, and again the average velocities were kept if there were more than 70% data retained. This made it possible to have velocity values closer to the bed, which is important when determining shear velocities from velocity profiles.

The Reynolds stress estimates are much more sensitive to the value of the correlation filter, and these data should be examined with more attention. It is important to have sufficient time for data acquisition, so that averaging cancels the effect of noise. In general, if the percentage of data retained was consistently high for different levels of filtering based on correlation, the value of the Reynolds stress was quite stable.

APPENDIX B: VELOCITY PROFILES

Profiles compared across the flume - Figures B-1 through B-4 represent the velocity profiles compared across the flume for Runs 1 through 4, respectively. In these figures all the measured velocity data were plotted against ln(y) to estimate the shear velocities and the hydraulic roughness coefficient. However, it was concluded in Chapter 4.3.3. that the velocity data measured within 2 cm above the bed should be excluded from the analysis. Figures B-1 through B-4 are re-plotted without this bottom velocity data, and can be found in Figures B-5 through B-8. (Note: the scale of the x-axis is not the same in all the figures, which was changed because of better representation.)

Profiles compared along the flume – Figures B-9 through B-12 represent the measured velocity profiles in Runs 1 through 4, but now compared along the flume and with the data from the bottom 2 cm excluded, as explained in Chapter 4.3.3. Velocity profiles for Run 5 are given in Chapter 4.3.3.

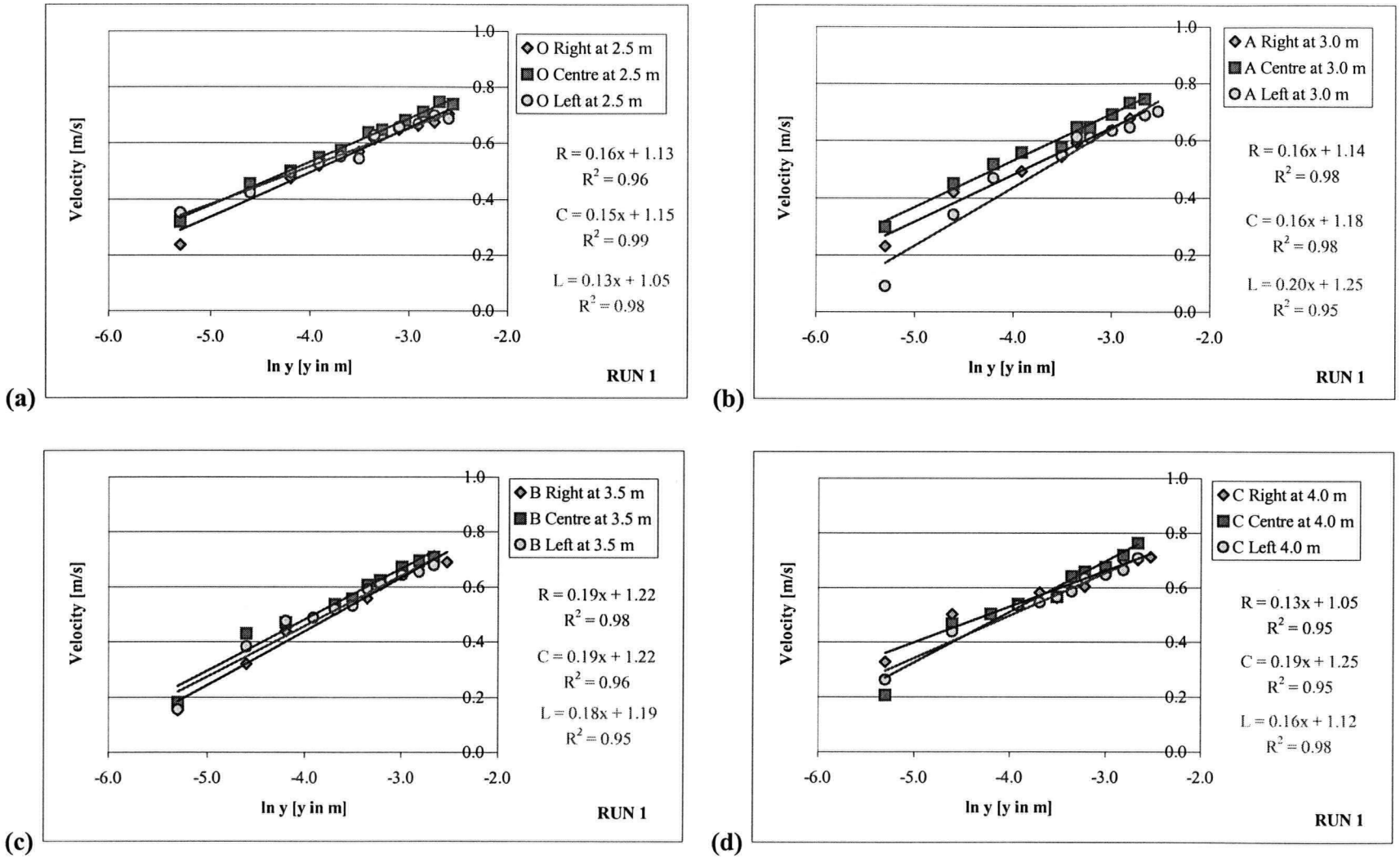

Figure B-1. *Velocity profiles* ***across*** *the flume for Run 1: (a) cross section O; (b) cross section A; (c) cross section B; and (d) cross section C.*

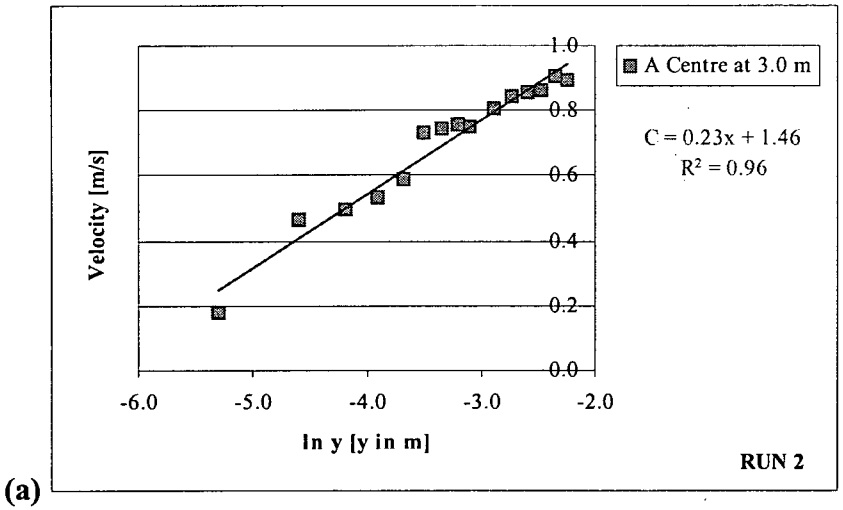

(a)

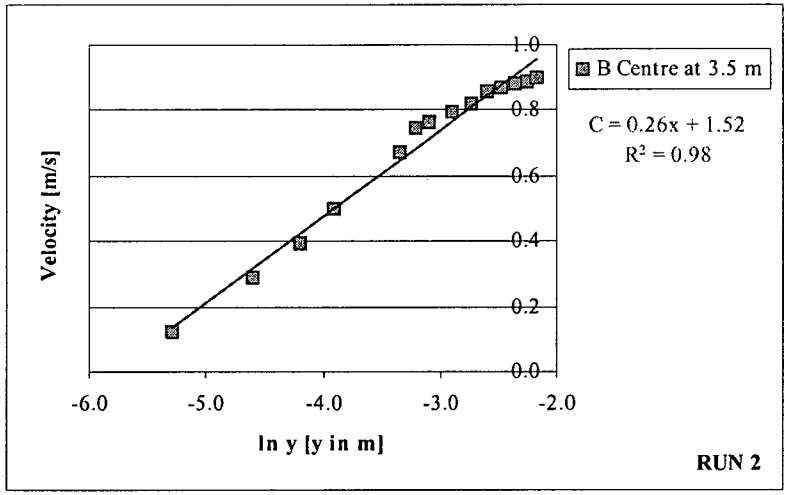

(b)

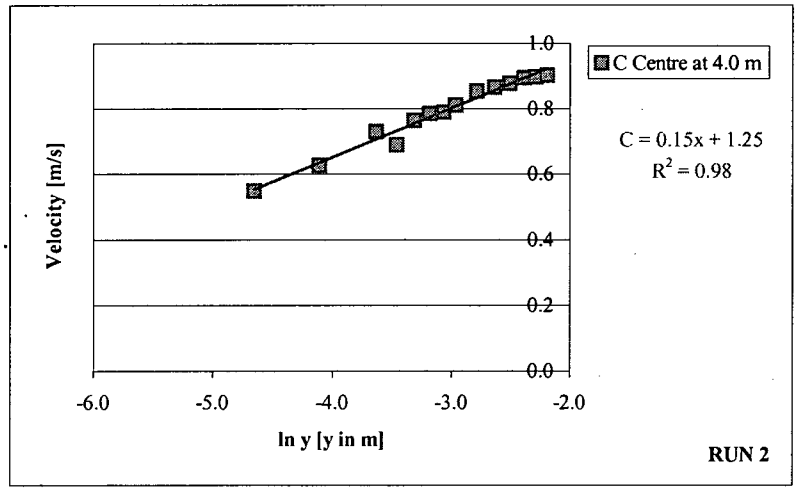

(c)

Figure B-2. *Velocity profiles* ***across*** *the flume for Run 2: (a) cross section A; (b) cross section B; (c) cross section C.*

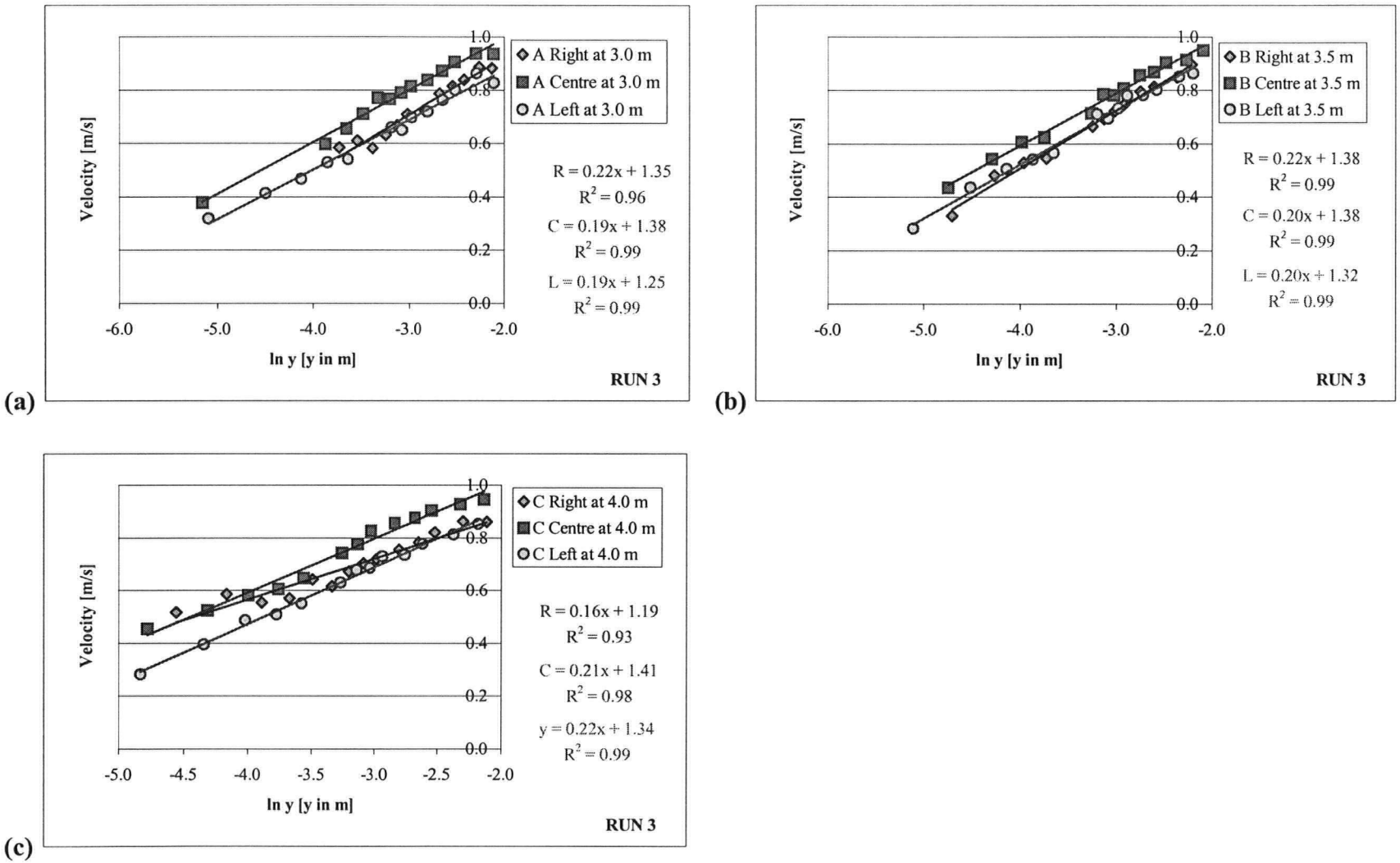

Figure B-3. *Velocity profiles* ***across*** *the flume for Run 3: (a) cross section A; (b) cross section B; (c) cross section C.*

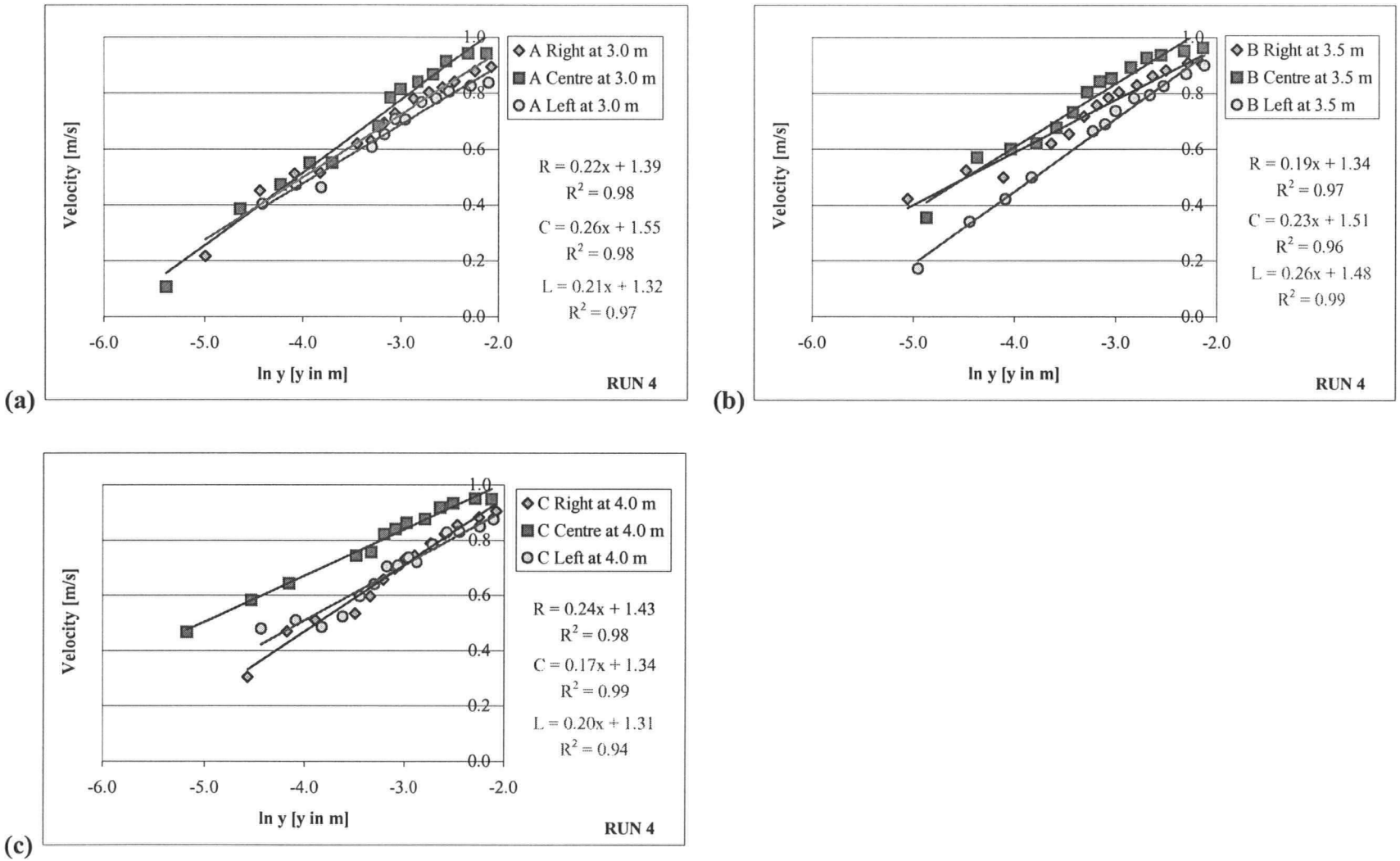

Figure B-4. *Velocity profiles* ***across*** *the flume for Run 4: (a) cross section A; (b) cross section B; (c) cross section C.*

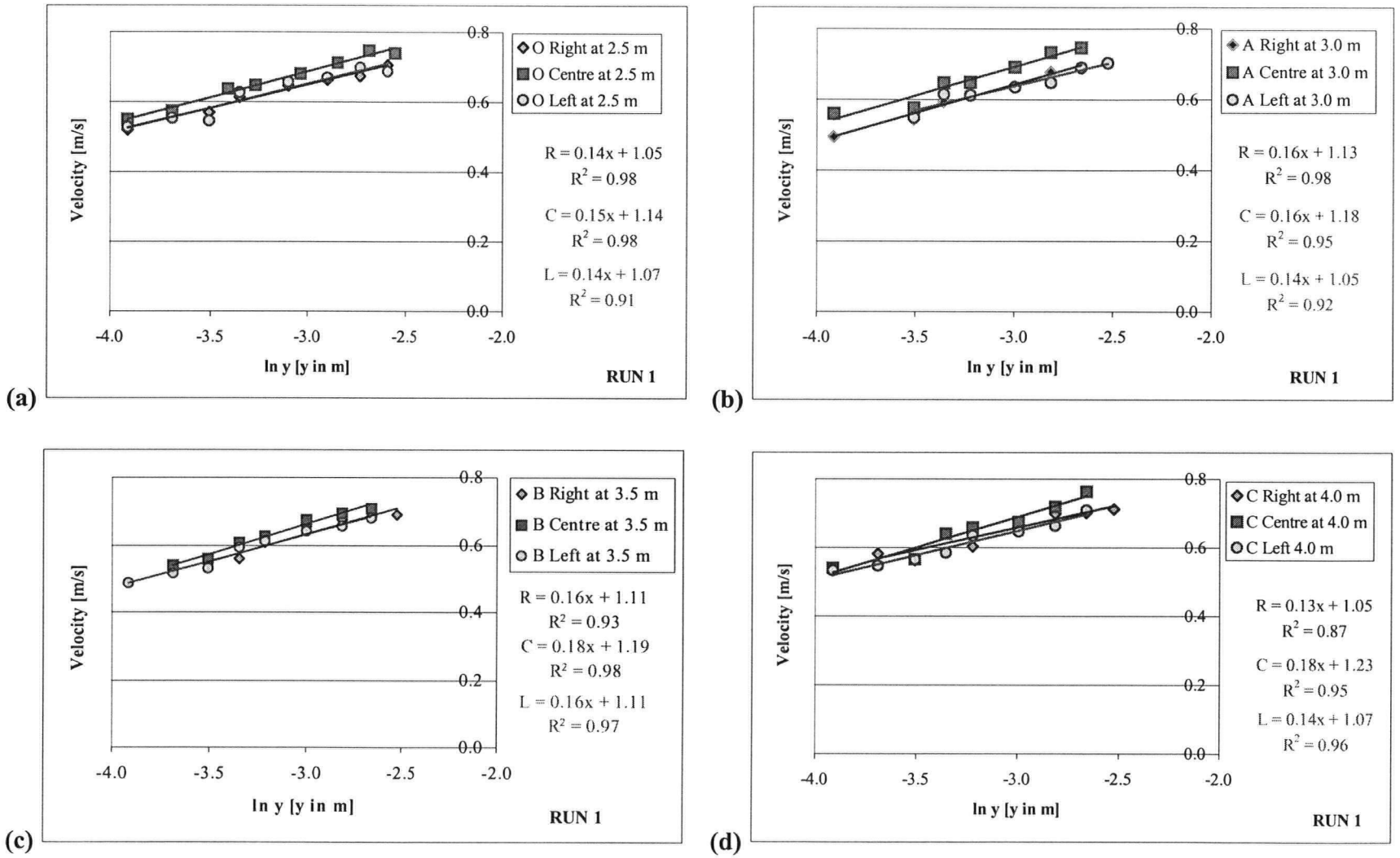

Figure B-5. *Velocity profiles* ***across*** *the flume for Run 1 without data for bottom 2 cm: (a) cross section O; (b) cross section A; (c) cross section B; and (d) cross section C.*

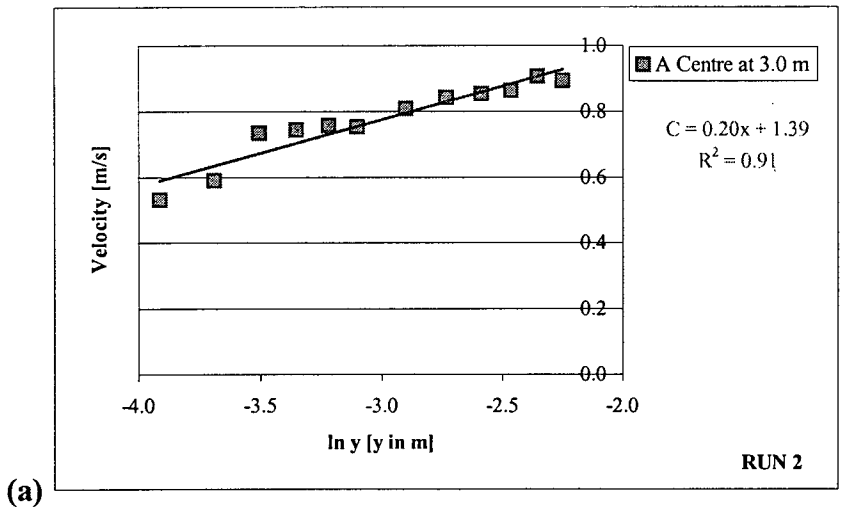

(a)

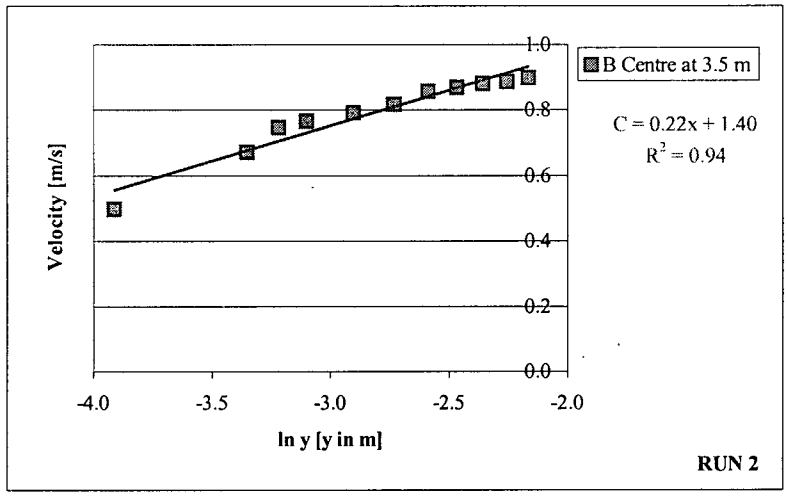

(b)

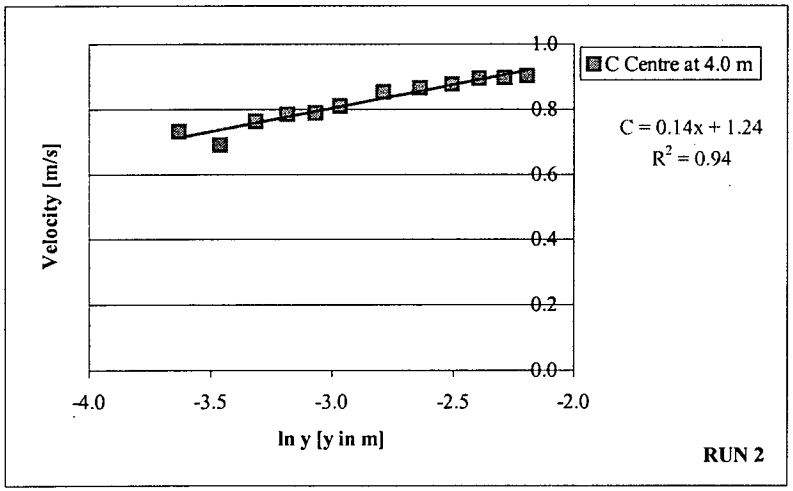

(c)

Figure B-6. *Velocity profiles* ***across*** *the flume for Run 2 without data for bottom 2 cm: (a) cross section A; (b) cross section B; (c) cross section C.*

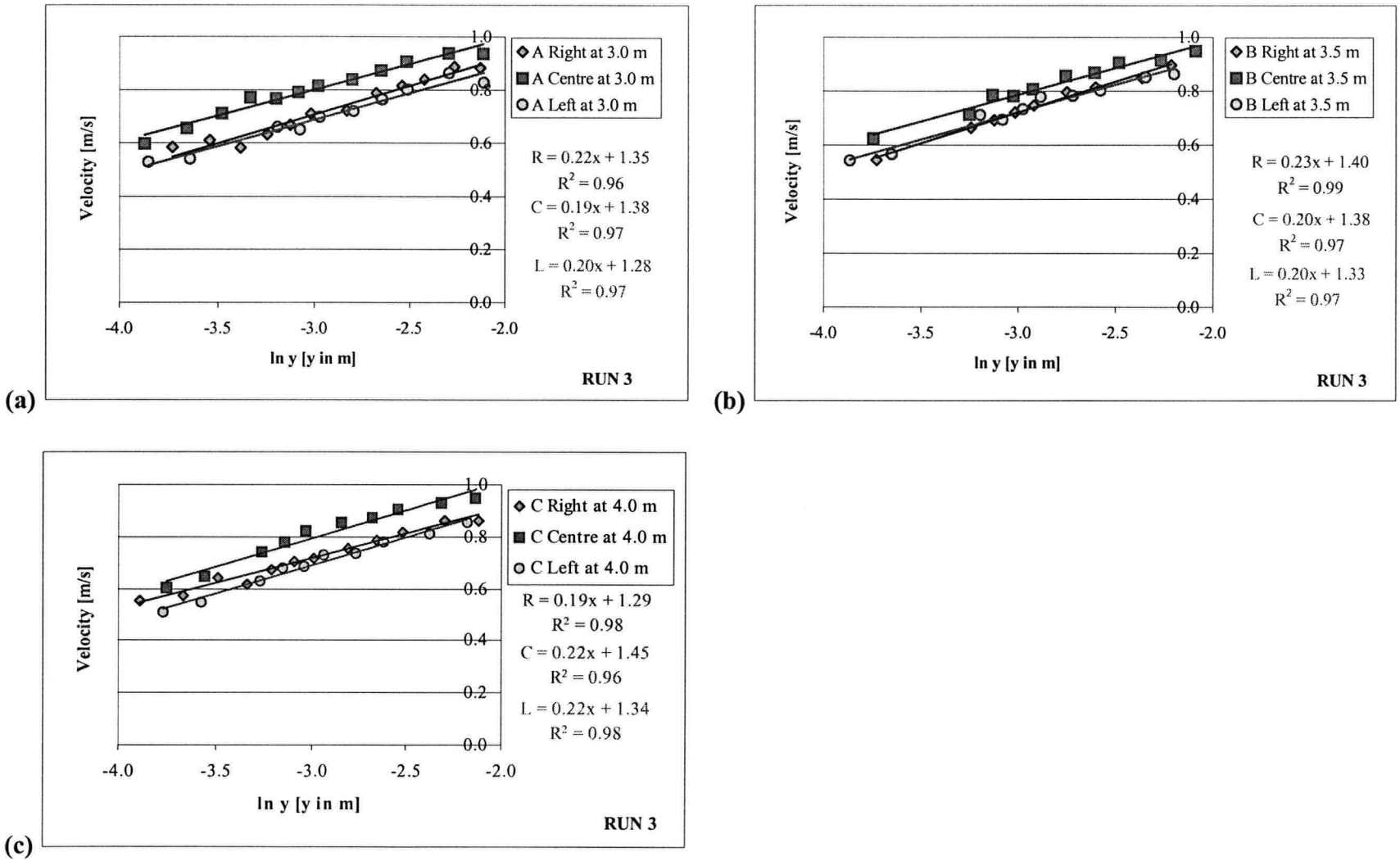

Figure B-7. *Velocity profiles* ***across*** *the flume for Run 3 without data for bottom 2 cm: (a) cross section A; (b) cross section B; (c) cross section C.*

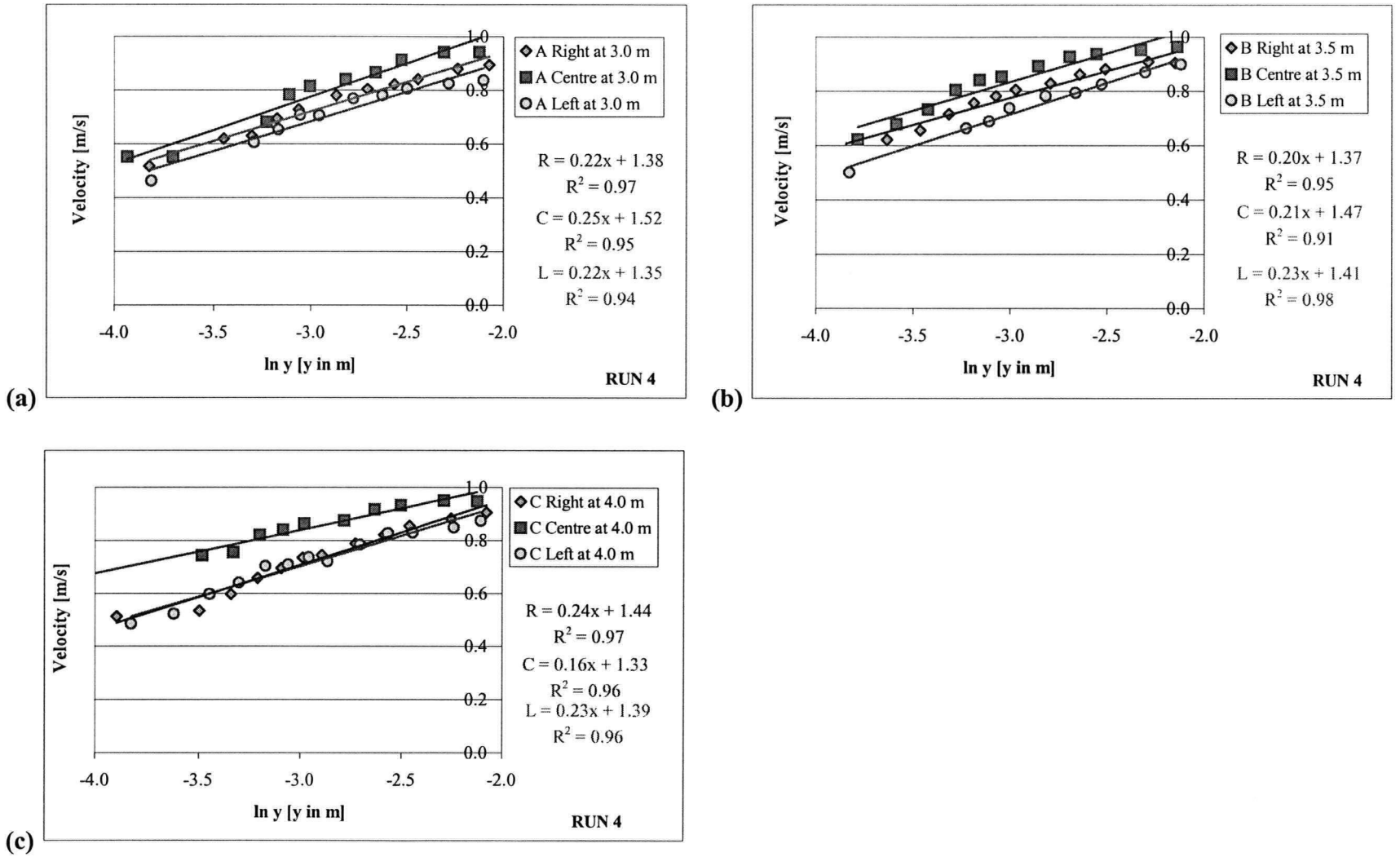

Figure B-8. *Velocity profiles* ***across*** *the flume for Run 4 without data for bottom 2 cm: (a) cross section A; (b) cross section B; (c) cross section C.*

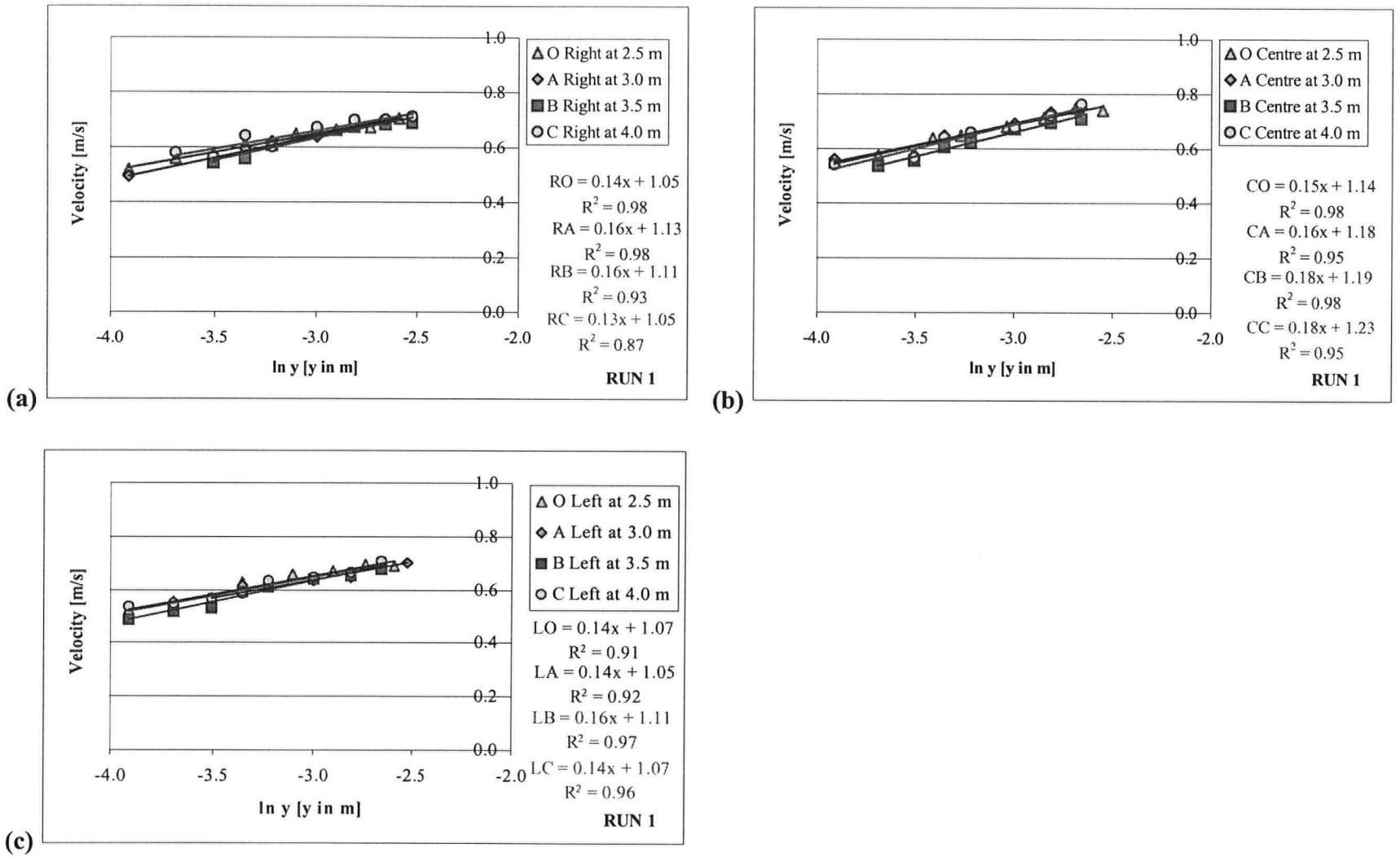

Figure B-9. *Velocity profiles* ***along*** *the flume for Run 1 without data for bottom 2 cm: (a) Right profiles; (b) Centreline profiles; (c) Left profiles.*

(a)

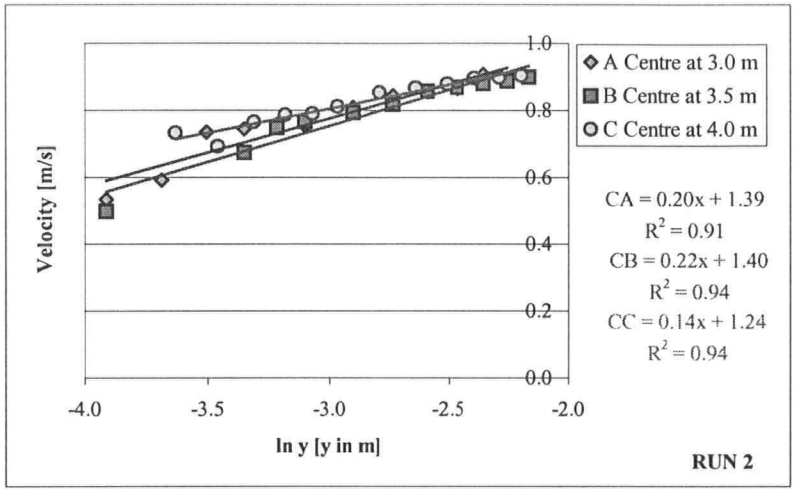

Figure B-10. *Velocity profiles* ***along*** *the flume for Run 2 without data for bottom 2 cm: (a) Centreline profiles.*

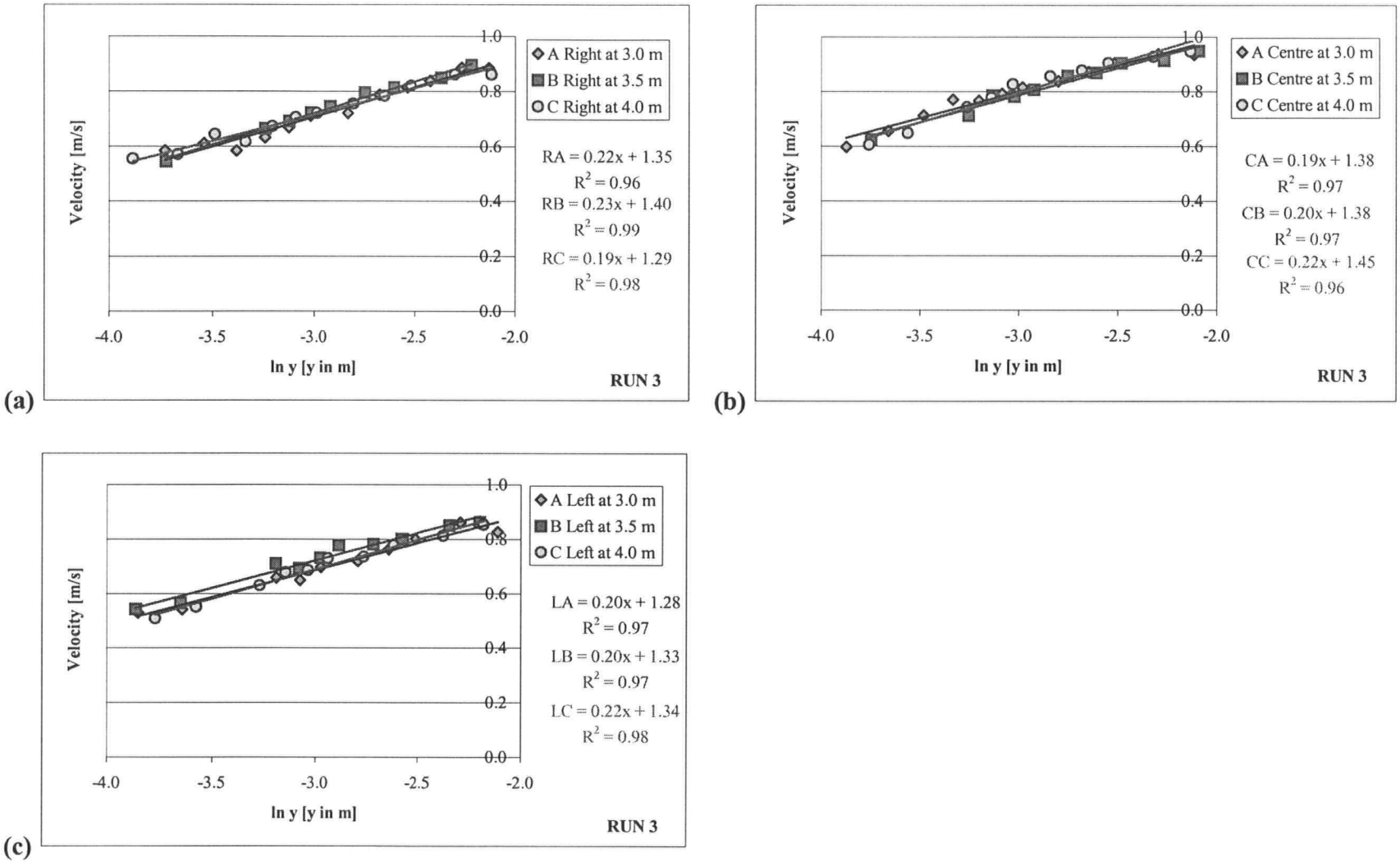

Figure B-11. *Velocity profiles* ***along*** *the flume for Run 3 without data for bottom 2 cm: (a) Right profiles; (b) Centreline profiles; (c) Left profiles.*

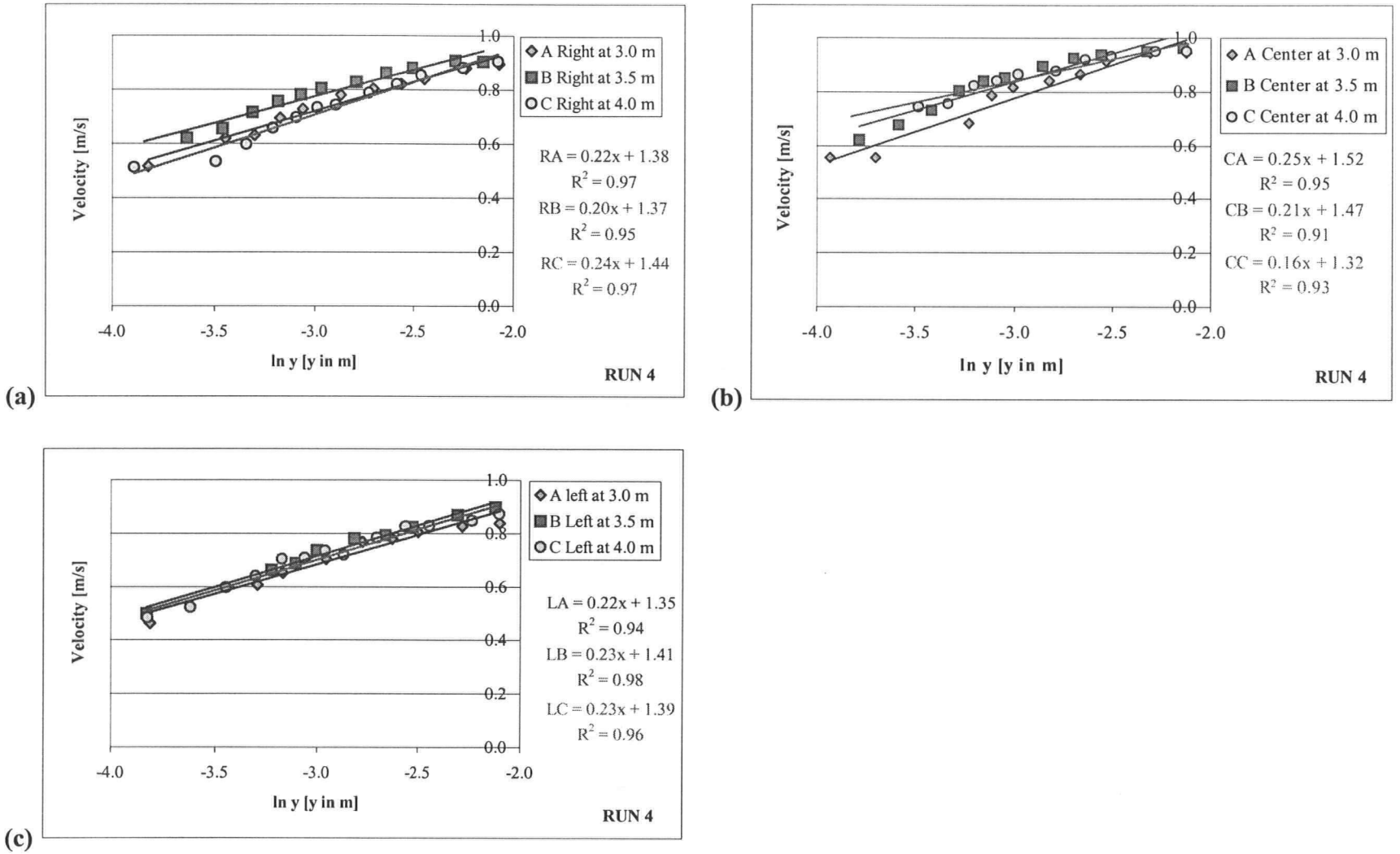

Figure B-12. *Velocity profiles* ***along*** *the flume for Run 4 without data for bottom 2 cm: (a) Right profiles; (b) Centreline profiles; (c) Left profiles.*

APPENDIX C: SEDIMENT SAMPLING CONSIDERATIONS

C.1. Sieving Consistency

One areal sample of Run 5 was sieved twice to test for the sieving consistency, i.e. test whether the shaking time and the amount of material examined was appropriate. Figure C-1 illustrates the grain size distribution curves for both sievings, where the diamond symbols represent the first and the star symbols the second sieving. The two curves virtually overlap with an average difference in retained weight being 0.11%. The largest difference occurred on sieves 18.85 mm and 12.5 mm and these were equal to 0.56% and 0.54%, respectively. This irregularity can be explained if just one more red grain passes through the 18.85 mm sieve during the second sieving.

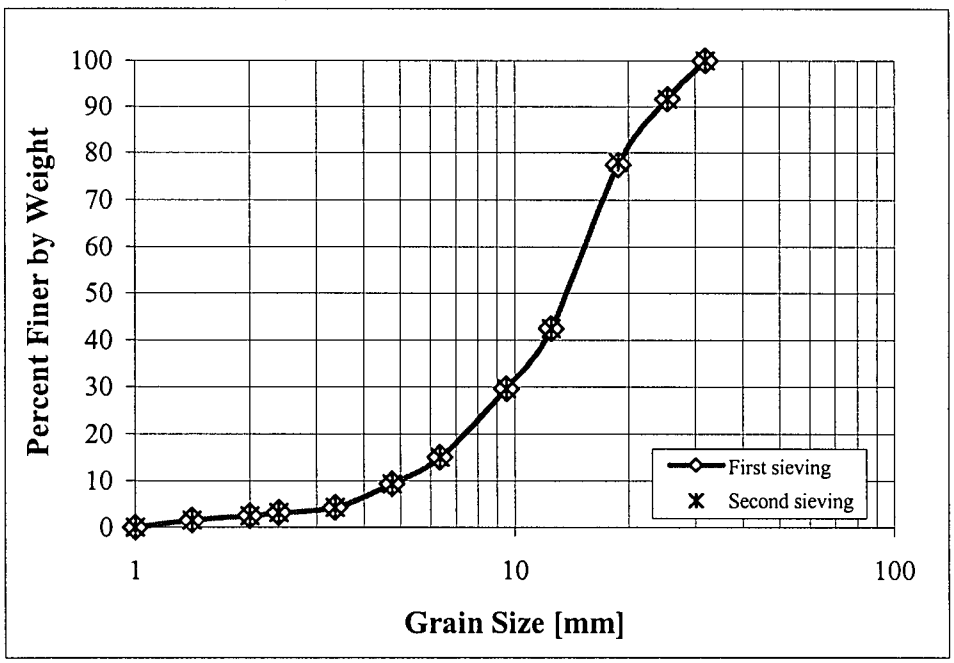

Figure C-1. *Grain size distribution curves for two sieving tests of the same areal sample of Run 5.*

In conclusion, the good agreement indicates that the sieving was repeatable and that the shaking time was chosen properly.

C.2. Splitting consistency

To test the splitting procedure, the volumetric sample of the original material and the volumetric sample of the transported material of Run 5 were split, sieved and analyzed.

For the original material, the total volumetric sample set aside for sieving was split into four sub-samples and each of these was sieved and analyzed separately. The results of this exercise are presented in Table C-1 and Figure C-2. Since the four sub-samples had very similar grain size distributions, the splitting procedure is confirmed to yield satisfactory results. Therefore, the results were combined and the resulting composite curve was plotted in Figure C-2.

The splitting procedure was tested once more on a bigger sample, which represented a part of the transported material for Run 5, and the results can be found in Table C-2 and Figure C-3. It was demonstrated again that the splitting produced similar results. In the column denoted Difference [%], the variation in the retained weight expressed as a percentage of the total amount analyzed was calculated, with the average difference being equal to 0.95%.

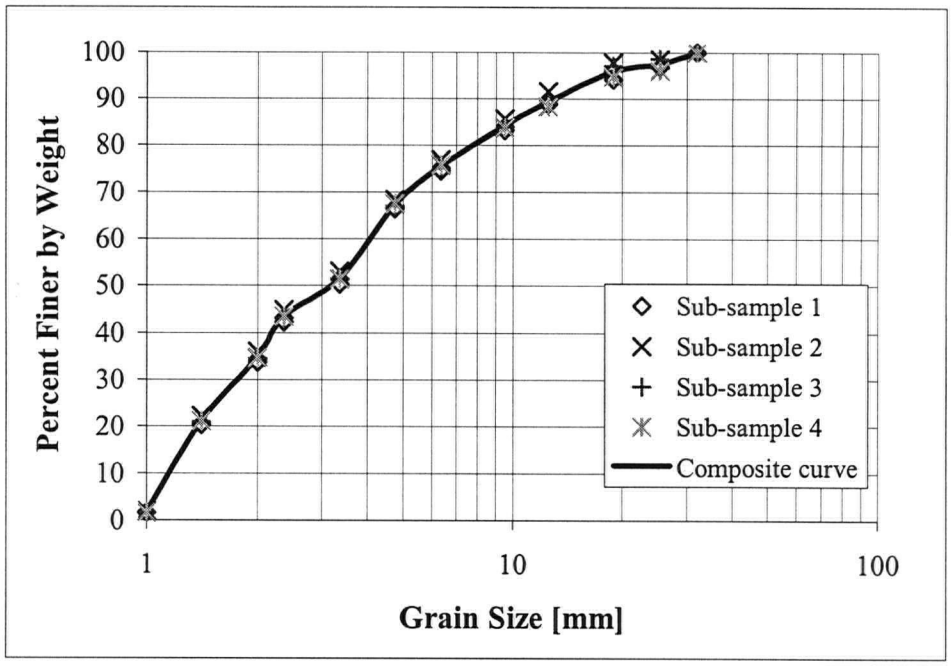

Figure C-2. *Grain size distribution curves for four sub-samples of the original material.*

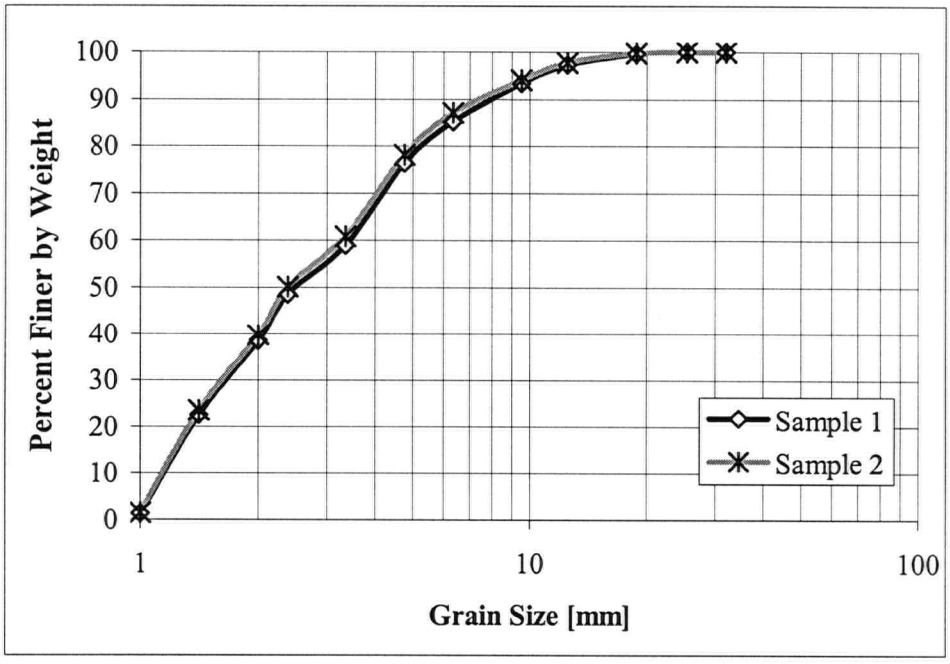

Figure C-3. *Grain size distribution curves for the two transported material samples of Run 5.*

	SUB-SAMPLE 1			SUB-SAMPLE 2			SUB-SAMPLE 3			SUB-SAMPLE 4		
D	**Retained weight**	**Retained weight**	**Cumul. Finer**	**Retained weight**	**Retained weight**	**Cumul. Finer**	**Retained weight**	**Retained weight**	**Cumul. Finer**	**Retained weight**	**Retained weight**	**Cumul. Finer**
[mm]	[g]	[%]	[%]	[g]	[%]	[%]	[g]	[%]	[%]	[g]	[%]	[%]
32.00	0.00	0.00	100.00	0.00	0.00	100.00	0.00	0.00	100.00	0.00	0.00	100.00
25.40	71.07	3.09	96.91	33.77	1.54	98.46	31.06	1.40	98.60	87.15	4.01	95.99
18.85	64.52	2.80	94.11	13.22	0.60	97.85	33.5	1.51	97.08	30.01	1.38	94.62
12.50	123.42	5.36	88.76	137.72	6.29	91.57	179.35	8.10	88.99	138.3	6.36	88.26
9.52	128.28	5.57	83.19	128.85	5.88	85.68	114.96	5.19	83.80	98.18	4.51	83.75
6.35	199.83	8.68	74.51	193.07	8.82	76.87	192.34	8.68	75.11	174.47	8.02	75.73
4.75	184.41	8.01	66.51	184.84	8.44	68.43	178.34	8.05	67.06	178.37	8.20	67.53
3.36	371.92	16.15	50.36	336.9	15.38	53.05	346.31	15.64	51.42	349.23	16.05	51.48
2.36	185.68	8.06	42.30	180.23	8.23	44.82	181.12	8.18	43.24	172.83	7.94	43.54
2.00	198.12	8.60	33.70	192.86	8.81	36.01	193.74	8.75	34.50	193.74	8.90	34.64
1.41	308.54	13.39	20.30	304.22	13.89	22.12	300.03	13.55	20.95	295.56	13.58	21.05
1.00	429.14	18.63	1.67	442.88	20.22	1.90	426.42	19.25	1.69	421.89	19.39	1.66
<1mm	38.51	1.67	0.00	41.60	1.90	0.00	37.52	1.69	0.00	36.22	1.66	0.00
Total:	2303.44			2190.16			2214.69			2175.95		

Table C-1. *Results of sieving for the original material for four sub-samples.*

	SAMPLE 1			SAMPLE 2			
D	**Retained Weight**	**Retained Weight**	**Cumulat. Finer**	**Retained Weight**	**Retained Weight**	**Cumulat. Finer**	**Differen.**
[mm]	[g]	[%]	[%]	[g]	[%]	[%]	[%]
32.00	0.00	0.00	100.00	0.00	0.00	100.00	
25.40	0.00	0.00	100.00	0.00	0.00	100.00	0.00
18.85	30.56	0.42	99.58	15.22	0.21	99.79	0.21
12.50	166.74	2.30	97.28	157.78	2.16	97.64	0.36
9.52	281.09	3.87	93.41	265.04	3.62	94.02	0.61
6.35	591.85	8.16	85.25	507.49	6.93	87.09	1.84
4.75	643.76	8.87	76.37	653.98	8.93	78.15	1.78
3.36	1264.27	17.43	58.95	1269.9	17.34	60.81	1.86
2.38	753.38	10.38	48.56	779.1	10.64	50.17	1.61
2.00	731.94	10.09	38.47	764.23	10.44	39.73	1.26
1.41	1152.76	15.89	22.58	1191.78	16.28	23.45	0.87
1.00	1535.11	21.16	1.42	1606.53	21.94	1.51	0.09
<1	103.13	1.42	0.00	110.4	1.51	0.00	
Total:	7254.59	100.00		7321.45	100.00		Avg: 0.95

Table C-2: *Results of sieving for two samples of the transported material in Run 5.*

C.3. Areal sampling investigations

To assure that the representative section was properly chosen, and that the armour layer was not influenced by the entrance or outlet conditions, the bed surface was sampled just upstream and just downstream from the usual test section (between 3 and 4 m), i.e. between 2 and 3, and 4 and 5 meters for Run 5. The areal samples were converted to volumetric samples (V-V) using Proffitt's conversion coefficient and the characteristic grain sizes can be found in Table C-3, while the areal grain size distributions are plotted in Figure C-4.

V-V	2-3 m	3-4 m	4-5 m
D_{16}	5.26	4.42	4.33
D_{50}	11.23	11.26	10.32
D_{84}	22.25	18.71	19.13
D_{95}	29.37	25.70	29.00
D_G	10.82	9.09	9.10
σ_G	2.06	2.06	2.10

Table C-3. *Characteristic grain sizes for three samples of Run 5.*

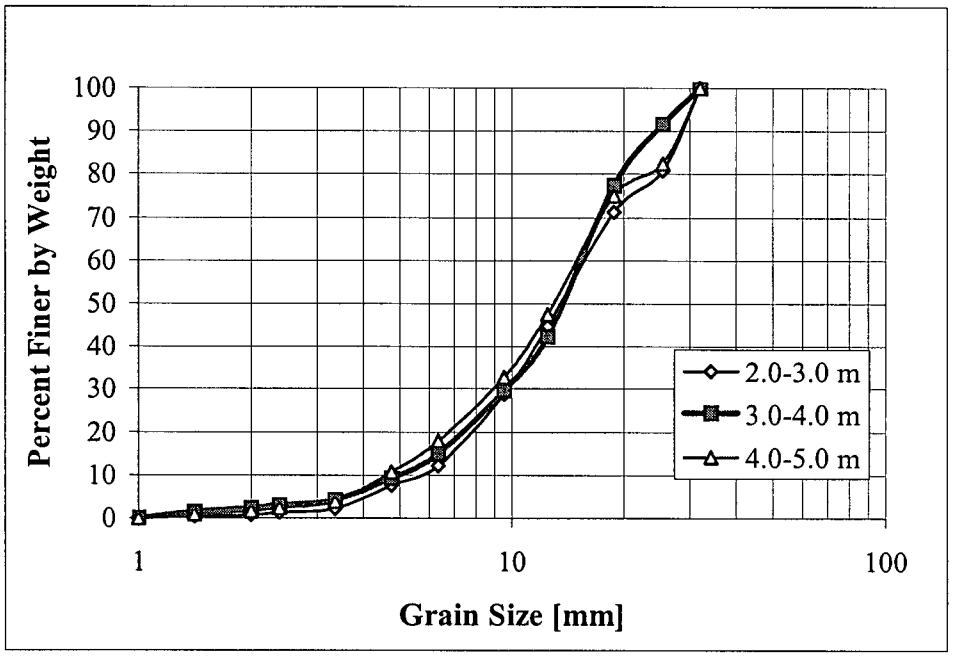

Figure C-4. *Grain size distribution curves for three areal samples of Run 5.*

It can be seen from Figure C-4 that the three samples have a similar distribution, with differences ranging from 0.04 % to 10.80 % (for one sieve size). The average difference for sizes smaller than D_{70} is 1.34 %. The different number of stones in the samples can explain the larger differences, i.e. since each sample size is small, few larger stones contained in a sample will influence the grain size distribution curves quite visibly. The 10.8 % difference

on the coarsest sieve is equivalent to less than 100 g, which is the weight of two to three blue stones.

C.4. Armour layer comparison through time

Another test was performed to investigate how much the armour layer changed during the run after the initial transport phase was over. Run 4 was stopped 45 hours after the initiation of the experiment and an areal sample was obtained. The run was then restarted, the same flow rate and the same depths along the flume were established, and it was continued for another 17 hours, during which velocity measurements were taken. At the end of the run another set of areal samples was taken. However, the two samples were not taken from exactly the same test section, because bed disturbances in the section where the velocity profiles were to be measured had to be avoided. The bed disturbances were due to taking the areal samples, after which the bed level was lowered at these locations, fine particles were uncovered after taking the surface layer off, and the bed had to re-armour when the run was continued. Because of this, the first sample was taken farther upstream (between 1.5 and 2.5 meters), where generally more degradation occurred at the initial stages of the run and more of the largest grains became exposed but were not necessarily transported downstream. Consequently, the grain size distribution for the first sample was somewhat coarser than for the sample taken at the end of the run (Fig. C-5).

At the end of the run, the areal sample was taken at the usual test section (between 3 and 4 meters), and it appears that the bed coarsened somewhat for grain sizes smaller than D_{50}. The differences for this part of the curve are less than 0.5 % though, and can be attributed to

experimental errors rather than to bed coarsening. Larger difference occurred for grain sizes D_{70} and larger (up to 11 %), which is attributed to reasons explained above, namely that a difference of one or two larger grains can significantly change the analysis.

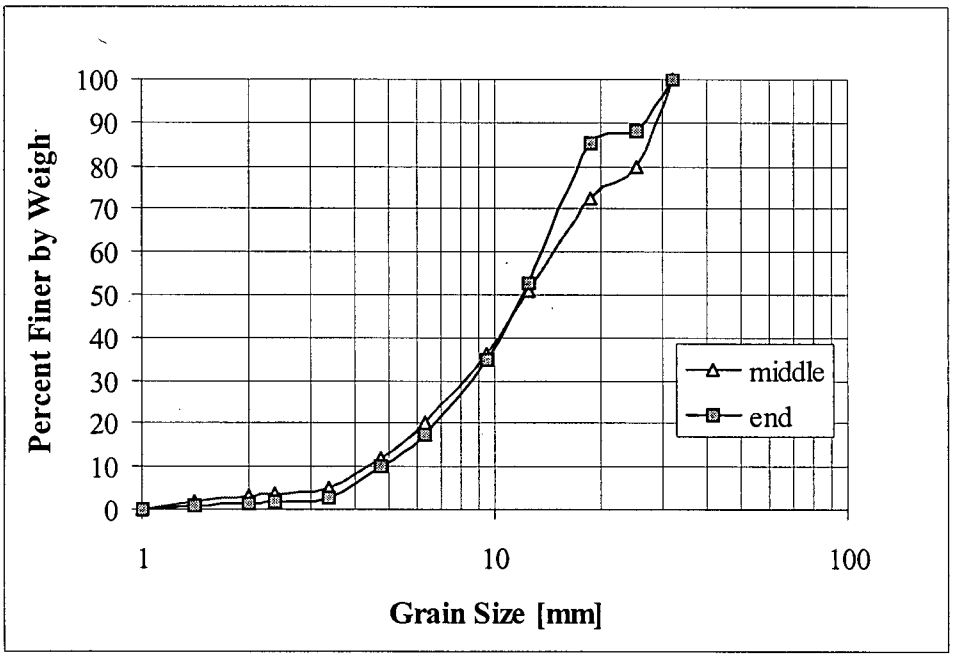

Figure C-5: *Grain size distributions for two areal samples of Run 4 taken after 45 and 62 hours.*

APPENDIX D: GRAIN PROTRUSION MODEL

Sample spreadsheets from the numerical model.

RUN 4

Input

Q =	0.081 m3/s	Solver Error	
S' =	0.003054		0.00
D50 =	0.00995 m		
D100 =	0.032 m		
Ss-1=	1.65		
W=	0.5 m		

Experimental values:

U(meas.)=	0.806 m/s
u*=	0.0776 with sidewall correction
Ymeas=	0.201 m
ks=	0.0347 m
C50=	3.5
n=	0.024 Manning's n

Calculate

Q =	0.081 m3/s	τ (tot)=	5.726 N/m2
Y =	0.191 m	τ*(D50)=	0.036 N/m2
ks =	0.0238 m	τ*(D99)=	0.011 N/m2
C50 =	2.4		
U =	0.848 m/s		
n =	0.022		

S' Friction slope corrected for sidewall effects
Di, Fi input
Hi/Di varied until grain just stable
Hi = height of protrusion above U = 0 datum (= yo + ks/30)
u at 0.4Hi Theoretical drag force velocity
τi = Shear stress for grainsize i
Cd* = 0.54 (1-exp(-2.6 Hi/Di))
τ*c = 0.01+0.45 exp(-11Hi/Di) after Fenton and Abbot

Di	Fi	Hi/Di	Hi	u(0.4Hi)	C_d*	τ_i	Total τ	Cum τ [%]	τ_i*	τ_c*	H/D calc	Error
0.0285	0.070	0.48	0.014	0.390	0.383	29.10	2.023	35.32	0.0124	0.0124 stable	0.48	1.26E-05
0.0219	0.012	0.39	0.009	0.316	0.344	17.18	0.211	39.01	0.0162	0.0161 stable	0.39	2.64E-05
0.0154	0.270	0.32	0.005	0.237	0.306	8.59	2.316	79.47	0.0230	0.0230 stable	0.32	4.61E-05
0.0109	0.174	0.27	0.003	0.174	0.274	4.14	0.719	92.03	0.0324	0.0324 stable	0.27	6.72E-05
0.0078	0.194	0.23	0.002	0.122	0.244	1.83	0.354	98.21	0.0455	0.0454 stable	0.23	9E-05
0.0055	0.103	0.19	0.001	0.081	0.212	0.70	0.072	99.47	0.0644	0.0643 stable	0.19	0.000115
0.0040	0.112	0.16	0.001	0.053	0.183	0.26	0.029	99.97	0.0885	0.0884 stable	0.16	0.000137
0.0028	0.020	0.12	0.000	0.031	0.149	0.07	0.001	100.00	0.1251	0.1249 stable	0.12	0.000157
0.0022	0.011	0.10	0.000	0.020	0.122	0.02	0.000	100.00	0.1621	0.1620 stable	0.10	0.000165
0.0017	0.014	0.07	0.000	0.012	0.094	0.01	0.000	100.00	0.2106	0.2105 stable	0.07	0.000162
0.0012	0.020	0.04	0.000	0.005	0.054	0.00	0.000	100.00	0.2979	0.2978 stable	0.04	0.000129
0.0009	0.001	0.01	0.000	0.002	0.019	0.00	0.000	100.00	0.3955	0.3954 stable	0.01	5.96E-05
Sum=	1.00					Sum=	5.726					

The numbers are taken from flow meter and Vernier measurements (2.5 to 4.5 m).
Degradation = 24.4 mm (between 2.5 and 4.5 m)

RUN 1: overstable grains

Input

Q =	0.05 m3/s	Solver Error	
S' =	0.001176	0.00	
D50 =	0.0047 m		
D100 =	0.032 m		
Ss-1=	1.650		
W=	0.5 m		

Experimental values:

U(meas.)=	0.610 m/s
u*=	0.0435 with sidewall correction
Ymeas=	0.1640 m
ks=	0.0066 m
C50=	1.41
n=	0.017 Manning's n

Calculate

Q =	0.0500 m3/s	τ (tot)=	2.0 N/m2
Y =	0.1765 m	τ*(D50)=	0.027 N/m2
ks =	0.0128 m	τ*(D99)=	0.004 N/m2
C50 =	2.714		
U =	0.567 m/s		
n =	0.019		

S' Friction slope corrected for sidewall effects
Di, Fi input
Hi/Di varied until grain just stable
Hi = height of protrusion above U = 0 datum (= yo + ks/30)
u at 0.4Hi Theoretical drag force velocity
τi = Shear stress for grainsize i
Cd* = 0.54 (1-exp(-2.6 Hi/Di))
τ*c = 0.01+0.45 exp(-11Hi/Di) after Fenton and Abbot

Di	Fi	Hi/Di	Hi	u(0.4Hi)	C_d*	τ_i	Total τ	Cum τ %	τ_i*	τ_c*	H/D calc	Error
0.0285	0.04	*0.12*	0.0034	0.16	0.14	1.91	0.07	3.3	0.0044	0.130 overstable	1.00	-0.1258
0.0219	0.03	*0.16*	0.0035	0.16	0.18	2.49	0.07	6.7	0.0057	0.010 overstable	1.00	-0.0043
0.0154	0.10	*0.23*	0.0035	0.17	0.24	3.32	0.34	23.5	0.0082	0.010 overstable	1.00	-0.0018
0.0109	0.07	0.52	0.0056	0.21	0.40	8.62	0.62	54.0	0.0115	0.012 stable	0.52	0.0000
0.0078	0.12	0.39	0.0030	0.15	0.34	3.99	0.48	77.8	0.0162	0.016 stable	0.39	0.0000
0.0055	0.13	0.32	0.0018	0.11	0.31	1.89	0.25	90.2	0.0229	0.023 stable	0.32	0.0000
0.0040	0.18	0.28	0.0011	0.08	0.28	0.90	0.16	98.2	0.0315	0.031 stable	0.28	0.0001
0.0028	0.06	0.23	0.0007	0.05	0.25	0.37	0.02	99.2	0.0445	0.044 stable	0.23	0.0001
0.0022	0.04	0.20	0.0004	0.04	0.22	0.18	0.01	99.6	0.0577	0.058 stable	0.20	0.0001
0.0017	0.06	0.18	0.0003	0.03	0.20	0.08	0.00	99.8	0.0749	0.075 stable	0.18	0.0001
0.0012	0.16	0.14	0.0002	0.02	0.17	0.02	0.00	100.0	0.1059	0.106 stable	0.14	0.0001
0.0009	0.01	0.11	0.0001	0.01	0.14	0.01	0.00	100.0	0.1406	0.140 stable	0.11	0.0002
Sum=	1.00						2.036					

The numbers are taken from flow meter and Vernier measurements (2.5 to 4.5 m), and not the velocity profiles. Degradation = 6.9 mm.
Protrusion for "overstable" grains is calculated as Degradation (6.9 mm) divided by the grain size (28.5mm) = 0.24, and then divided by 2 to get the mean protrusion (i.e. some grains are protruding 0, others are protruding the whole 6.9 mm).